



HAL
open science

Production optimization of recombinant scorpion antivenom through biotechnological pathway : study of temperature of induction and modeling of biokinetics on *E. coli* strains.

Susana Maria Alonso Villela

► **To cite this version:**

Susana Maria Alonso Villela. Production optimization of recombinant scorpion antivenom through biotechnological pathway : study of temperature of induction and modeling of biokinetics on *E. coli* strains.. Agricultural sciences. INSA de Toulouse, 2020. English. NNT : 2020ISAT0024 . tel-03355989

HAL Id: tel-03355989

<https://theses.hal.science/tel-03355989>

Submitted on 27 Sep 2021

HAL is a multi-disciplinary open access archive for the deposit and dissemination of scientific research documents, whether they are published or not. The documents may come from teaching and research institutions in France or abroad, or from public or private research centers.

L'archive ouverte pluridisciplinaire **HAL**, est destinée au dépôt et à la diffusion de documents scientifiques de niveau recherche, publiés ou non, émanant des établissements d'enseignement et de recherche français ou étrangers, des laboratoires publics ou privés.



THÈSE

En vue de l'obtention du

DOCTORAT DE L'UNIVERSITÉ DE TOULOUSE

Délivré par l'Institut National des Sciences Appliquées de
Toulouse

Présentée et soutenue par

Susana María ALONSO VILLELA

Le 19 Juin 2020

**Optimisation de la production d'antivenin de scorpion
recombinant par voie biotechnologique : étude de la
température d'induction et modélisation de la
biocinétique des souches d'*E. coli*.**

École doctorale : SEVAB – Sciences Ecologiques, Vétérinaires, Agronomiques et
Bioingénieries

Spécialité : Ingénieries microbienne et enzymatique

Unité de recherche :

TBI - Toulouse Biotechnology Institute, Bio & Chemical Engineering

Thèse dirigée par

Luc FILLAUDEAU et César Arturo ACEVES LARA

Jury

Mme Balkiss BOUHAOUALA-ZAHAR, Présidente du jury

M. Alain VANDE WOUWER, Rapporteur

Mme Catherine BÉAL, Rapporteur

M. Luc FILLAUDEAU, Directeur de thèse

M. César Arturo ACEVES LARA, Co-directeur de thèse

M. Jean-Roch MOURET, Examineur

Mme Hazar KRAÏEM, Invitée

Mme Carine BIDEAUX, Invitée

M. Gilles ROUX, Invité

Last name: ALONSO VILLELA**Name:** Susana María**Title:** Production optimization of recombinant scorpion antivenom through biotechnological pathway: study of temperature of induction and modeling of biokinetics on *E. coli* strains.**Year:** 2020**Place:** INSA Toulouse

ABSTRACT

Scorpionism is a serious public health problem in tropical areas, especially in Africa, southern India, the Middle East, and Latin America. There are about 12 species of scorpions that are dangerous to humans and all belong to the *Buthidae* family. In particular, venom on scorpion *Androctonus australis Hector* is particularly toxic to humans. Serotherapy uses antibodies or fragments of antibodies to target the neurotoxins of the scorpion venom. Nanobodies, camelid-derived antibodies, are more effective than the conventional fragments of antibodies due to their low molecular weight (15 kDa). The Laboratoire des Venins et Molécules Thérapeutiques of the Pasteur Institute of Tunis (LVMT-IPT, Tunis, Tunisia) has produced the bispecific nanobodies against the neurotoxins of the *Androctonus australis Hector* scorpion.

In this doctoral project, the production of the bispecific nanobodies NbF12-10 and CH10-12 as recombinant proteins in *Escherichia coli* was studied. Two clones of the NbF12-10 strain were used (NN and NO), and strain *E. coli* WK6 was used as reference. The four strains were characterized in rich medium (TB) and defined minimal medium (MM) in shake-flask cultures. In TB, all strains grow at an average $\mu=0.4\text{h}^{-1}$. The strains WK6 and CH10-12 had a $\mu_{\text{max}}=0.6\text{h}^{-1}$ in MM. The clone NbF12-10 NO could not grow in MM, and the clone NbF12-10 NN had a $\mu_{\text{max}}=0.2\text{h}^{-1}$ in MM. The yield of biomass on glucose, $Y_{X/S}$, was 0.4 g/g in MM for all strains and the yield of acetate on glucose was between 0.06 and 0.14 g/g. The periplasmic extraction of the nanobodies NbF12-10 and CH10-12 was tested in TB, an improvement of 300% in the release of periplasmic proteins was achieved, compared to conventional methods. The strain CH10-12 produced 20-fold higher nanobody than the strain NbF12-10 NN (1.58 vs 0.08 mg/L). The quantification of the nanobody was made through a densitometry protocol developed during this thesis. The protocol uses a processing image program (ImageJ, NIH, USA) to quantify the optical density profiles of electrophoresis gels. The band of 50 kDa of the molecular weight marker was used as reference for 750 ng of recombinant protein.

The production of the nanobodies CH10-12 and NbF12-10 were tested in bioreactor cultures in high cell density cultures in MM ($[X]> 25\text{ g cdw/L}$) through a specific fed-batch strategy. The effect of the temperature (28 – 37°C) during protein expression and the duration of the induction phase (6 – 38 h) were studied. The lower temperatures (28°C, 30°C) produced the highest titer of nanobody CH10-12 (2.3 mg/L) after 10 h and 12 h of induction, respectively. In high temperature cultures (33°C, 37°C) the production of the nanobody was lower (0.4, 0.2 mg/L). In cultures where the induction phase was longer (>30 h), the production of the nanobody CH10-12 was hampered and reached a plateau after 10 h (32°C, 0.7 mg/L) to 25 h (29°C, 1.4 mg/L). The nanobody NbF12-10 also reached a plateau after 10 h of induction (0.7 mg/L). The metabolic burden was lowered by decreasing the temperature of induction, allowing the production of higher titers of recombinant nanobody. The effect of the low specific growth rate (0.02h^{-1}) and the long exposure to the inducer (IPTG, >30 h) could have produced a stringent response in the strain. High maintenance metabolism was found during the induction phase, and the consumption of citrate could hint an inadequate composition of the culture medium for the induction phase, where the microorganism produces internal metabolites to then produce the nanobody. Two non-specific proteins were found in the purified nanobody samples: a low molecular weight (11 kDa), degradation product of the nanobody caused by a high temperature (proteolytic degradation), and a high molecular weight protein (84 kDa), protein aggregate produced as a response to an inadequate medium composition and the low specific growth rate. The generation of unknown proteins in the purified samples of nanobody could be a response of the strain to the low specific growth rate and the long exposure time to the inducer.

Finally, A mathematical model has been proposed to validate the hypothesis of the thermo-dependence of the production of recombinant nanobodies with a Luedeking-Piret kinetics modified with Arrhenius-type kinetic parameters. The model showed that the highest production was obtained at the lowest temperature (28°C), and that the *Escherichia coli* strain NbF12-10 NN showed the same trend as *E. coli* CH10-12 cultures.

Keywords: recombinant protein, biotechnological pathway, *Escherichia coli*, industrialization

Nom : ALONSO VILLELA**Prénom :** Susana María**Titre :** Optimisation de la production d'antivenin de scorpion recombinant par voie biotechnologique : étude de la température d'induction et modélisation de la biocinétique des souches d'*E. coli*.**Année :** 2020**Lieu :** INSA Toulouse

RÉSUMÉ

Le scorpionisme est un grave problème de santé publique dans les zones tropicales, en particulier en Afrique, dans le sud de l'Inde, au Moyen-Orient et en Amérique latine. Il existe environ 12 espèces de scorpions qui sont dangereuses pour l'homme et qui appartiennent toutes à la famille des *Buthidae*. En particulier, le venin du scorpion *Androctonus australis Hector* est particulièrement toxique pour l'homme. La sérothérapie utilise des anticorps ou des fragments d'anticorps pour cibler les neurotoxines du venin de scorpion. Les nanobodies, des anticorps dérivés de camélidés, sont plus efficaces que les fragments d'anticorps classiques en raison de leur faible poids moléculaire (15 kDa). Le Laboratoire des Venins et Molécules Thérapeutiques de l'Institut Pasteur de Tunis (LVMT-IPT, Tunis, Tunisie) a produit les souches productrices de nanobody bispécifiques contre les neurotoxines du scorpion *Androctonus australis Hector*.

Dans ce projet de doctorat, la production des nanobody bispécifiques NbF12-10 et CH10-12 comme protéines recombinantes chez *Escherichia coli* a été étudiée. Deux clones de la souche NbF12-10 ont été utilisés (NN et NO), et la souche *E. coli* WK6 a été utilisée comme référence. Les quatre souches ont été caractérisées en milieu riche (terrific broth, TB) et en milieu minimal défini (MM) dans des cultures en shake-flask. Dans le TB, toutes les souches croissent à une moyenne de $\mu=0,4 \text{ h}^{-1}$. Les souches WK6 et CH10-12 avaient un $\mu_{\max}=0,6 \text{ h}^{-1}$ en MM. Le clone NbF12-10 NO n'a pas eu de croissance en MM, et le clone NbF12-10 NN avait un $\mu_{\max}=0,2 \text{ h}^{-1}$ en MM. Le rendement de la biomasse sur glucose, $Y_{X/S}$, était de 0.4 g/g en MM pour toutes les souches et le rendement d'acétate sur glucose était compris entre 0.06 et 0.14 g/g. L'extraction périplasmique des nanobody NbF12-10 et CH10-12 a été testée dans TB, une amélioration de 300 % de la libération des protéines périplasmiques a été obtenue, par rapport aux méthodes conventionnelles. La souche CH10-12 a produit des 20 fois plus nanobody que la souche NbF12-10 NN (1.58 contre 0.08 mg/L). La quantification du nanobody a été réalisée grâce à un protocole de densitométrie développé au cours de cette thèse. Le protocole utilise un programme de traitement d'images (ImageJ, NIH, USA) pour quantifier les profils de densité optique des gels d'électrophorèse. La bande de 50 kDa du marqueur de poids moléculaire a été utilisée comme référence pour 750 ng de protéine recombinante.

La production des nanobody CH10-12 et NbF12-10 a été testée dans des cultures en bioréacteur dans des cultures à haute densité cellulaire en MM ($> 25 \text{ g cdw/L}$) par une stratégie spécifique de fed-batch. L'effet de la température (28 - 37°C) pendant l'expression des protéines et la durée de la phase d'induction (6 - 38 h) ont été étudiés. Les températures les plus basses (28°C, 30°C) ont produit le titre le plus élevé de nanobody CH10-12 (2.3 mg/L) après 10 h et 12 h d'induction. Dans les cultures à haute température (33°C, 37°C), la production du nanobody était plus faible (0.4, 0.2 mg/L). Dans les cultures de longue durée d'induction ($>30 \text{ h}$), la production du nanobody CH10-12 a atteint un plateau après 10 h (32°C, 0.7 mg/L) à 25 h (29°C, 1.4 mg/L). Le nanobody NbF12-10 a également atteint un plateau après 10 h d'induction (0.7 mg/L). La charge métabolique a été réduite en diminuant la température d'induction, permettant la production de titres plus élevés de nanobody recombinant. L'effet du faible taux de croissance spécifique (0.02 h^{-1}) et de la longue exposition à l'inducteur (IPTG, $>30 \text{ h}$) a pu produire une réponse stringente dans la souche. Un métabolisme de maintenance élevé a été constaté pendant la phase d'induction, et la consommation de citrate pourrait laisser supposer que le micro-organisme produit des métabolites internes pour ensuite produire le nanobody. Deux protéines inconnues ont été trouvées dans les échantillons de nanobody purifiés : une protéine de faible poids moléculaire (11 kDa), produit de dégradation du nanobody causé par une température élevée (dégradation protéolytique), et une protéine de poids moléculaire élevé (84 kDa), agrégat de protéines produit en réponse à une composition inadéquate du milieu et au faible taux de croissance spécifique. La génération de protéines inconnues dans les échantillons purifiés de nanobody pourrait être une réponse de la souche au faible taux de croissance spécifique et à la longue durée d'exposition à l'inducteur.

Pour valider l'hypothèse de la thermo dépendance, un modèle mathématique avec une cinétique de Luedeking-Piret modifiée avec une cinétique Arrhenius a été proposé. Le modèle a montré que la température optimale est à 28°C, et que la souche *Escherichia coli* NbF12-10 NN a montré la même tendance que les cultures de *E. coli* CH10-12.

Mots clés : protéines recombinantes, voie biotechnologique, *Escherichia coli*, industrialisation.

ACKNOWLEDGEMENTS

I would like to thank CONACYT in the first place for giving me the scholarship needed to complete this research work. Without the scholarship to make my master's degree followed by this PhD project, the work made during these 3 years and 3 months would have stayed only in a dream.

I am grateful for the fortune of having had two PhD supervisors with whom I got along very well, without any communication or compatibility problems, and who gave me their support when I felt lost or stuck. Luc and César: I have learned a lot from both of you and both of you are incredibly good teachers. Your availability when I had a doubt, or a question was always appreciated. I really enjoy working with you Luc, we either are on the same page or we have complementing ideas without imposing over each other. You make the relationship PhD student-supervisor seem more like a teamwork rather than like a boss-employee. I love that I can have a one-on-one conversation in Mexican Spanish with you César, where I do not have to think in what the right word would be to describe what I want to say. It always makes me feel close to home.

I want to thank to the people that worked with me in this project: Yannick for giving me that first push during my master and Emna for making it interesting working in the lab and teaching me how to be patient. I am grateful for the Tunisian team in the Pasteur Institute: Hazar for always answering my beginner's questions when I first started, from how to streak a petri dish to how to make highly purified recombinant nanobodies; and Balkiss for always giving constructive criticism during our meetings and providing the insight from the pharmaceutical and the molecular biology point of view.

I very much appreciate the members of the scientific committee and the reviewers of my dissertation for taking an interest in my research and giving me advice on how to improve my works.

I read in an article in Journal of Cell Science about the importance of stupidity in scientific research. And I can confirm. The eagerness to know new things is what motivated me to pursue a PhD, the curiosity about what microbiology had really motivated me. I would like to acknowledge the team FAME for providing me with the tools needed to complete my research and my efforts have come to fruition. With you I learned a little more about endurance and how communication should or should not be made, and the importance of taking a coffee break.

Thank you, Catherine, Yassim and Lucile for accompanying me during (almost) the same stages of a PhD life. You are in the final stretch, freedom is right on the corner, you can do this! Thank you for making the PhD life more bearable, it helped knowing we were on the same boat or on the same side of the battleground.

I wish an exceptionally good luck to Siwar, Arnaud and Ming for finishing their PhD soon and without many problems. You can do it guys! You are doing a great job! *cheerleading pom poms*

I want to acknowledge Carlos, Xiaomin, Asma and Rana for showing me the worst part of a PhD (3rd year/writing stage), and even with their warnings I fell into the same rabbit hole. During that same time, I want to thank the international lunch team Claudio, Jian, Rosie, and Maria for the great lunches we spent together, and for helping me remember how to have a conversation in English.

I'd like to thank the Spanish-speaking wonderful people I met during my journey: Gemma, Lizeth, Pablo, Pablo², and Pepe; speaking my mother-tongue always lifts the spirit and helped me let out some of the frustration encountered in this project and blow out some steam.

Those from the lab at LISBP/TBI: Marine, Huong, Caroline, Cléa, Julie, Nelly, Louna, Berengère, William, Marie-Sarah, Léa, Oumarou, Laure, Florence, Stéphanie, Julie, Eric, Elodie, Elise, Jean-Louis, Céline, Jean-Luc, Alex, Philippe, Fabien, Laurent, and all to whom I once spoke: thank you.

To my big family in Mexico, thank you for your support, even when you did not have any idea of what I was doing. Thank you Ofe, Artu and Izmo for the wonderful summers we spent together while I was in Mexico, it always recharges my batteries.

And a final thank you to Tlotzin for being such a wonderful husband and partner in life, for providing me with Java chip Frappuccinos when I most needed it, for lifting the spirits, for driving me to make the final step even when I did not want to do anything more. This chapter of my life is closing, and a new chapter is opening with new opportunities for emotional and intellectual development.

The North remembers

- George R. R. Martin

INDEX

Abstract.....	i
Résumé	ii
Acknowledgements.....	iii
Index.....	i
Index of tables.....	iv
Index of figures	vi
Abbreviations	xi
Nomenclature	xii
Introduction	1
Chapter I. Literature review.....	3
I.1. SCORPION STINGS AS A HEALTH PROBLEM	3
I.1.1. Scorpion stings around the world.....	4
I.1.1.1. America	5
I.1.1.2. Africa.....	5
I.1.1.3. Asia.....	5
I.1.2. Scorpion venom	6
I.1.3. Global market of therapeutics and treatment cost	6
I.1.3.1. Serotherapy	7
I.1.3.2. Commercially available antivenoms	7
I.1.4. Production of antivenoms	10
I.2. BIBLIOGRAPHY RESEARCH METHODOLOGY	13
I.2.1. Scientific databases	13
I.2.2. Keywords	14
I.2.3. Searching profiles	14
I.2.4. Coupled searching profiles	14
I.3. QUANTITATIVE ANALYSIS OF THE WORKING DATABASE	15
I.4. QUALITATIVE ANALYSIS OF THE WORKING DATABASE	16
I.5. BIOPRODUCTION OF RECOMBINANT PROTEINS	17
I.5.1. Production of recombinant proteins in <i>Escherichia coli</i>	18
I.5.1.1. Protein secretion mechanism	18
I.5.1.1.1. Excretion to medium.....	18
I.5.1.1.2. Periplasmic expression.....	18
I.5.1.1.3. Inclusion bodies.....	19
I.5.1.2. Protein inducer	19
I.5.1.3. Selection marker	19
I.5.1.4. Purification.....	19
I.5.1.5. Culture media	19
I.5.1.6. Culture conditions.....	20
I.5.1.7. Large-scale production.....	20
I.5.1.7.1. Cultivation processes	20
I.5.1.7.2. Downstream process.....	21
I.5.1.8. Emerging pharmaceutical applications of recombinant proteins	22
I.5.2. Bioproduction of scorpion toxins and antivenoms	22
I.5.2.1. Scorpion toxins.....	23
I.5.2.2. Scorpion antivenom	24
I.6. OBJECTIVE OF THIS PHD PROJECT	27
Chapter II. Materials and Methods.....	29
II.1. BACTERIAL STRAINS	29
II.2. BACTERIAL GLYCEROL STOCK	29

II.2.1.	TBI protocol	29
II.2.2.	IPT protocol	30
II.3.	CULTURE MEDIA.....	30
II.3.1.	Inoculum.....	30
II.3.2.	Rich medium (Terrific Broth)	30
II.3.3.	Defined medium (Minimal Medium).....	31
II.3.3.1.	Trace elements.....	31
II.3.3.2.	Salts B.....	31
II.3.3.3.	Thiamine (Vitamin B1)	31
II.3.3.4.	Salts A.....	31
II.3.4.	Glucose solutions	32
II.3.5.	Ampicillin stock.....	32
II.3.6.	IPTG stock	32
II.4.	SHAKE FLASK CULTURES (BATCH MODE).....	32
II.4.1.	Biomass production.....	32
II.4.2.	Protein production	32
II.5.	BIOREACTOR CULTURES (FED BATCH MODE)	33
II.5.1.	Instrumentation	33
II.5.2.	Gas analyzer	36
II.5.3.	Bioreactor feed solution.....	37
II.6.	PHYSICAL AND BIOCHEMICAL ANALYSES	38
II.6.1.	Optical density.....	38
II.6.2.	Biomass cell dry weight	38
II.6.3.	Microscopic analyses.....	39
II.6.4.	Residual glucose	39
II.6.5.	HPLC	39
II.7.	NANOBODY EXTRACTION, PURIFICATION AND QUANTIFICATION	40
II.7.1.	Osmotic shock	40
II.7.2.	IMAC.....	40
II.7.3.	Protein standards	41
II.7.4.	Gel electrophoresis	42
II.7.5.	Nanodrop (Absorbance)	42
II.7.6.	Bradford Assay (Absorbance).....	42
II.7.7.	Image J (Densitometry)	43
II.8.	DATA TREATMENT	43
II.8.1.	Mass and energy balances	43
II.8.1.1.	Volume.....	43
II.8.1.2.	Gas analysis.....	44
II.8.1.2.1.	Balance for Nitrogen.....	44
II.8.1.2.2.	Balance for Oxygen.....	44
II.8.1.2.3.	Balance for Carbon dioxide.....	45
II.8.1.2.4.	Respiratory quotient.....	45
II.8.2.	Carbon balance.....	46
II.8.3.	Redox balance	46
II.8.4.	Data smoothing	46
II.8.5.	Enhancement factor	47
II.8.6.	Microscopic observations.....	47
II.9.	KINETIC MODEL OF THE NANOBODY PRODUCTION	47
Chapter III.	Results.....	49
III.1.	STRAIN SCREENING	50
III.1.1.	Culture study approach	50
III.1.2.	Biomass characterization	50
III.1.2.1.	Correlation coefficient between different biomass measurement methods.....	51
III.1.2.2.	Evolution of the metabolites.....	52
III.1.2.3.	Specific growth rate	54
III.1.2.4.	Biomass yield	55

III.1.2.5.	Acetic acid.....	56
III.1.3.	Protein expression.....	57
III.1.4.	Morphological analysis.....	58
III.1.5.	Conclusion.....	61
III.2.	BIOREACTOR CULTURES.....	63
III.2.1.	Culture strategy.....	63
III.2.2.	Microbial culture.....	64
III.2.2.1.	Presentation of cultures.....	64
III.2.2.1.1.	Reference cultures BR01 and BR09: <i>Escherichia coli</i> WK6.....	65
III.2.2.1.2.	BR02 to BR05: <i>Escherichia coli</i> CH10-12 – short induction times (1 st series).....	67
III.2.2.1.3.	BR06 and BR07: <i>Escherichia coli</i> CH10-12 – longer induction times (2 nd series).....	71
III.2.2.1.4.	BR08: <i>Escherichia coli</i> NbF12-10 NN.....	74
III.2.2.2.	Overall performance of bioreactor cultures.....	76
III.2.2.3.	Oxygen transfer.....	77
III.2.2.3.1.	Abiotic conditions.....	77
III.2.2.3.2.	Biological conditions.....	79
III.2.2.3.3.	Biological enhancement coefficient, E.....	84
III.2.3.	Biotic variables.....	86
III.2.3.1.	Mass and Energy balances.....	86
III.2.3.2.	Biomass.....	86
III.2.3.2.1.	Specific growth rate.....	86
III.2.3.2.2.	Biomass yield.....	89
III.2.3.2.3.	Morphological analysis.....	93
III.2.3.3.	Acetic acid.....	94
III.2.3.4.	Citric acid.....	95
III.2.3.5.	Gas analysis.....	96
III.2.3.6.	Respiratory coefficient.....	102
III.2.4.	Nanobody.....	104
III.2.4.1.	Short induction duration cultures (1 st series).....	104
III.2.4.2.	Long induction duration cultures (2 nd series).....	105
III.2.4.3.	Secondary proteins.....	108
III.2.4.4.	Discussion.....	110
III.2.5.	Conclusion.....	117
III.3.	KINETIC MODEL.....	119
III.3.1.	Kinetic models for recombinant proteins.....	119
III.3.2.	Temperature effect in specific productivity of the nanobody production.....	120
III.3.3.	Conclusion.....	121
	Conclusions and perspectives.....	123
	References.....	127
	Appendix 1. Extended abstract in French.....	139
	Appendix 2. Protein quantification methodology.....	147
	Appendix 3. Kinetic model of recombinant nanobodies.....	157

INDEX OF TABLES

Table I-1. Morbidity and mortality of scorpion stings. N. A.: not available.	5
Table I-2. Antivenoms available in the market. *Accessed October 24, 2019	9
Table I-3. Keywords used for the generation of searching profiles	14
Table I-4. Searching profiles defined for the bibliographic research.....	14
Table I-5. Research axis of the bibliographic research methodology.....	15
Table I-6. Quantitative results of the bibliographic research. WoS: Web of Knowledge (Clarivate Analytics), SD: Science Direct (Elsevier), SU: Sudoc (Theses, France), T: Thèses.fr (Theses, France), N/A: not available.	15
Table I-7. Scope of the articles found on the search queries	17
Table I-8. Recombinant antibody fragments produced in different host cells.....	17
Table I-9. Pharmaceutical applications of venom-derived recombinant proteins. N. A.: not available.	22
Table I-10. Strains producing toxins for antivenom production. N.A.: not available.	23
Table I-11. Recombinant scorpion toxins for therapeutic applications produced in <i>Escherichia coli</i> . N. A.: not available.	24
Table I-12. Antibodies with neutralizing effects against scorpion venoms. N. A.: not available.....	25
Table II-1. Composition of the inoculum media.....	30
Table II-2. Composition of the Terrific Broth	31
Table II-3. Composition of the trace elements	31
Table II-4. Composition of the salts B	31
Table II-5. Composition of the salts A	32
Table II-6. Composition of the bioreactor feed solution	38
Table II-7. Standards prepared and detection by HPLC.....	39
Table II-8. Composition of the PBS 10x stock solution	41
Table II-9. Composition of the elution buffer	41
Table II-10. Henry's law constant parameters	44
Table II-11. Rates of production and consumption of the compounds monitored.....	46
Table III-1. Strategy of study in shake-flask cultures.	50
Table III-2. Average correlation coefficient (α) of strains grown at 37°C in TB, 7.2 and MM, pH 6.8. .	51
Table III-3. Estimation of errors in the biomass measurements.....	52
Table III-4. Specific growth rate for the reference and recombinant strains (μ , h ⁻¹).....	55
Table III-5. Yields of production of biomass in shake-flask cultures grown on MM at 37°C, pH 6.8, 10 g/L glucose.	55
Table III-6. Yields of production of acetate in shake-flask cultures grown on MM at 37°C, pH 6.8, 10 g/L glucose.	56
Table III-7. pH at the start and end of the cultures grown in TB and MM at 37°C.	56

Table III-8. Final concentration and specific yield of the nanobodies NbF12-10 and CH10-12 cultured in TB medium. Protein expression induced at 0.5 g cdw/L with a pulse of 1 mM IPTG and change of temperature to 28°C. Periplasmic protein extracted by different osmotic shock methods after 24 h of induction.	57
Table III-9. Strategy of bioreactor culture conditions.	63
Table III-10. Biomass, acetate, glucose, and citrate at the end of each operating mode.	76
Table III-11. Volumetric mass transfer coefficient (k_{La}) under abiotic conditions.	77
Table III-12. Typical values of the coefficients α and β of the k_{La} correlation of Eq. (III-6).	78
Table III-13. Volumetric mass transfer coefficient for cultures BR01 to BR09 and under abiotic conditions.	84
Table III-14. Typical values of the volumetric oxygen mass transfer coefficient, K_{La} , in biological conditions	85
Table III-15. Average specific growth rates in operating conditions: batch (μ_{max}), fed-batch (μ_{fix}) and induction ($\mu_{induction}$).	88
Table III-16. Average biomass yield on glucose ($Y_{X/S}$) for the operating conditions batch and fed-batch combined.	91
Table III-17. Coefficient of maintenance, m , for various <i>Escherichia coli</i> strains.	92
Table III-18. Yield of acetic acid on glucose ($Y_{Ac/S}$) and on biomass ($Y_{Ac/X}$) for the batch mode. Cultures BR01 – BR09 grown in MM at pH 6.8, 37°C.	95
Table III-19. Antibodies with neutralizing effects against scorpion neurotoxins. N. A.: not available.	112
Table 1-1. Taux de croissance moyen en milieu riche (TB) et maximum en milieu minimum (MM).	139
Table 1-2. Taux de croissance moyen en conditions opératoires : batch (μ_{max}), fed-batch (μ_{fix}) et induction ($\mu_{induction}$).	141
Table 3-1. Average specific growth rates (μ) and average biomass yield on glucose ($Y_{X/S}$) on each culture.	177
Table 3-2. Yield and productivity of antivenom antibodies. $\bar{\mu}_{ind}$: average specific growth rate at induction, MM: defined minimal medium, 2xYT: yeast extract and tryptone medium, TB: terrific broth, N. A.: not available.	178

INDEX OF FIGURES

Figure I-1. Scorpionism around the world [6]	3
Figure I-2. Scorpions of medical importance around the world [9].....	4
Figure I-3. Antibodies and their derivatives. A) Antibodies conventional and camelid. B) Derivatives of antibodies. V: variable, C: constant, L: light-chain, H: heavy-chain, V _H H: variable heavy-chain domain, Fv: variable domain, Fc: crystallizable domain, scFv: single-chain variable domain, Fab: antigen binding domain, F(ab) ₂ : divalent Fab fragments, Nb: nanobody.....	11
Figure I-4. Production of antivenom proteins. A) Equine production systems. B) Camelid systems. C) Microbial production systems.	12
Figure I-5. Strategy of the bibliographic research methodology	13
Figure I-6. Number of articles published per year in the main research axis. A) Articles found in P1 queries on search field "Title", B) Articles found in P2 queries on search field "Topic".	16
Figure I-7. Recombinant protein secretion mechanisms. Image created with Biorender.com.....	18
Figure II-1. A schematic representation of the pHEN6 vector used in the <i>Escherichia coli</i> WK6 strains	29
Figure II-2. Schematic of the fed-batch bioreactor cultures.....	33
Figure II-3. Schematic of the experimental set-up used in fed-batch cultures in 5 L bioreactor. Image created with Biorender.com	34
Figure II-4. A) Configuration of stirrer shaft on the bioreactor. B) Dimensions of the impellers	35
Figure II-5. Experimental set-up: bioreactor with feed solutions	36
Figure II-6. Schematic representation of the measurement system in INNOVA 1313 gas analyzer. ...	37
Figure II-7. Discretization of the glucose feed rate for the fed-batch mode.	38
Figure II-8. Extraction, purification and quantification of the Nanobody. Image created with Biorender.com	40
Figure III-1. Evolution of culture of <i>Escherichia coli</i> WK6 in TB grown at 37°C, pH 7.2. The red arrows show accumulation of the complex medium (TB) in measures taken in micro centrifuge tubes (Eppendorf) compared with measures taken by pre-weighted filters and optical density measures.....	51
Figure III-2. Average correlation coefficient (α) of strains grown in TB (A) and MM (B).....	51
Figure III-3. Evolution of the cultures of the <i>Escherichia coli</i> strains grown in TB at 37°C, pH 7.2 (left) and in MM, pH 6.8 (right). A and B) WK6; C and D) CH10-12; E and F) NbF12-10 NN; G and H) NbF12-10 NO. Triplicates are noted as Exp1, Exp2 and Exp3.....	53
Figure III-4. Specific growth rate in cultures grown in TB (A) and MM (B).	54
Figure III-5. Nanobody expression by different osmotic shock methods. The red arrow marks the band of the nanobody NbF12-10 (29 kDa) and CH10-12 (31 kDa) of the first eluate of IMAC purification on SDS-PAGE gels. The molecular weight marker used was the Precision Plus Protein Unstained Protein Standards (Bio-rad, USA).	57
Figure III-6. Sampling of cultures grown in TB, pH 7.2. Cell culture was imaged at the points selected in the black circles at about 4 h, 6 h and 10.5 h after inoculation. Culture C was induced at an OD of 0.2 with 1 mM IPTG.	58

Figure III-7. Morphological analysis of cultures samples of <i>Escherichia coli</i> CH10-12 grown in TB, pH 7.2, 37°C.....	59
Figure III-8. Dendrogram for cultures of <i>Escherichia coli</i> CH10-12 grown in TB.....	59
Figure III-9. Morphological evolution of <i>Escherichia coli</i> CH10-12 cultures in TB, pH 7.2. A) Pure cell growth at 37°C. B) Pure cell at 37°C and temperature change at 0.5 g cdw/L to 28°C. C) Cell growth at 37°C and induction at 0.5 g cdw/L with change of temperature to 28°C. Images visualized with transillumination and immersion oil, magnification of x100 in a microscope Eclipse E100 (Nikon). The red arrows show the change of operating conditions.	60
Figure III-10. Effect of osmotic shock on <i>Escherichia coli</i> NbF12-10 NN cells. A) Before osmotic shock. B) After osmotic shock. Images visualized with transillumination and immersion oil, magnification of x100 in a microscope Eclipse E100 (Nikon).	61
Figure III-11. Strategy of oxygen transfer during bioreactor cultures	64
Figure III-12. Physico-chemical parameters, operating conditions and biological parameters of the culture of <i>Escherichia coli</i> WK6 (BR01) grown in MM at pH 6.8, 37°C. The dotted lines depict the change in the operating mode.	65
Figure III-13. Physico-chemical parameters, operating conditions and biological parameters of the culture of <i>Escherichia coli</i> WK6 (BR09) grown in MM, pH 6.8, 37°C, induced at 29°C for 28 h. The dotted lines depict the change in the operating mode.	66
Figure III-14. Physico-chemical parameters, operating conditions and biological parameters of the culture of <i>Escherichia coli</i> CH10-12 (BR02) grown in MM, pH 6.8, 37°C, induced at 28°C for 12 h. The dotted lines depict the change in the operating mode.	68
Figure III-15. Physico-chemical parameters, operating conditions and biological parameters of the culture of <i>Escherichia coli</i> CH10-12 (BR03) grown in MM, pH 6.8, 37°C, induced at 30°C for 10 h. The dotted lines depict the change in the operating mode.	69
Figure III-16. Physico-chemical parameters, operating conditions and biological parameters of the culture of <i>Escherichia coli</i> CH10-12 (BR04) grown in MM, pH 6.8, 37°C, induced at 33°C for 6 h. The dotted lines depict the change in the operating mode.	70
Figure III-17. Physico-chemical parameters, operating conditions and biological parameters of the culture of <i>Escherichia coli</i> CH10-12 (BR05) grown in MM, pH 6.8, 37°C, induced at 37°C for 6 h. The dotted lines depict the change in the operating mode.	71
Figure III-18. Physico-chemical parameters, operating conditions and biological parameters of the culture of <i>Escherichia coli</i> CH10-12 (BR06) grown in MM, pH 6.8, 37°C, induced at 29°C for 38 h. The dotted lines depict the change in the operating mode.	72
Figure III-19. Physico-chemical parameters, operating conditions and biological parameters of the culture of <i>Escherichia coli</i> CH10-12 (BR07) grown in MM, pH 6.8, 37°C, induced at 32°C for 35 h. The dotted lines depict the change in the operating mode.	73
Figure III-20. Physico-chemical parameters, operating conditions and biological parameters of the culture of <i>Escherichia coli</i> NbF12-10 NN (BR08) grown in MM, pH 6.8, 37°C, induced at 29°C for 37 h. The dotted lines depict the change in the operating mode.....	75
Figure III-21. Volumetric mass transfer coefficient (k_La) under abiotic conditions for different aeration and agitation conditions in 1.5 L of MM at 37°C, pH 6.8.....	79
Figure III-22. Volumetric mass transfer coefficient (K_La) in culture BR01.....	80
Figure III-23. Volumetric mass transfer coefficient (K_La) in culture BR02 and BR03.	81

Figure III-24. Volumetric mass transfer coefficient (K_La) in culture BR04 and BR05.	81
Figure III-25. Volumetric mass transfer coefficient (K_La) in culture BR06.....	82
Figure III-26. Volumetric mass transfer coefficient (K_La) in culture BR07.....	83
Figure III-27. Volumetric mass transfer coefficient (K_La) in culture BR08.....	83
Figure III-28. Volumetric mass transfer coefficient (K_La) in culture BR09.....	84
Figure III-29. Biological enhancement factor, E, for all cultures (BR01 - BR09).....	85
Figure III-30. Biomass and optical density coefficient (α).....	86
Figure III-31. Biomass evolution of all cultures (BR01 – BR09). Time was normalized to the start of the fed-batch mode.	87
Figure III-32. Average specific growth rate (μ) on each operating condition. Cultures BR01 – BR09 grown on MM at 37°C, pH 6.8.	88
Figure III-33. Specific growth rate after induction of the protein expression.	89
Figure III-34. Evolution of the biomass versus the consumed glucose in cultures BR01 – BR09 from smoothed data. The black circles denote the start of the fed-batch mode and the red squares denote the start of the induction phase.	90
Figure III-35. Average yield of biomass for all cultures (BR01 – BR09).....	91
Figure III-36. Estimation of the maintenance coefficient for strains <i>Escherichia coli</i> WK6, CH10-12 and NbF12-10 NN. In batch and fed-batch modes only the average q_s was used. All data points of the induction phase were plotted.	92
Figure III-37. Morphological analysis of samples taken in fed-batch mode and induction phase of cultures BR02 and BR03. The red arrow shows the shift on the average circle equivalent diameter (CE diameter, μm).	93
Figure III-38. Morphological analysis of samples taken in batch mode and fed-batch mode of cultures BR04 and BR05. The red arrow shows the shift on the average circle equivalent diameter (CE diameter, μm).	94
Figure III-39. Frequency curve of the samples of cultures BR02 – BR05 during the induction phase..	94
Figure III-40. Evolution of citric acid in cultures BR01 to BR09. The dotted lines show the approximate change of operating condition.....	96
Figure III-41. Evolution of carbon dioxide production in cultures BR01 – BR09. The dotted lines show the approximate change of operating mode.....	97
Figure III-42. Evolution of oxygen consumption in cultures BR01 – BR09. The dotted lines show the approximate change of operating mode.	98
Figure III-43. Average yield of carbon dioxide on glucose ($Y_{CO_2/S}$) on each operating condition. Cultures BR01 – BR02 cultured in MM, 37°C, pH 6.8.....	98
Figure III-44. Average yield of oxygen on biomass ($Y_{O_2/X}$) on each operating condition. Cultures BR01 – BR02 cultured in MM, 37°C, pH 6.8.	99
Figure III-45. Rate of consumption of oxygen in cultures BR01 to BR05.	100
Figure III-46. Rate of production of carbon dioxide in cultures BR06 to BR09.	101
Figure III-47. Rate of consumption of oxygen in cultures BR07 to BR09.	101
Figure III-48. Rate of production of carbon dioxide in cultures BR 06 to BR09.	102

Figure III-49. Respiratory quotient (RQ) for cultures BR01 – BR05.....	103
Figure III-50. Respiratory quotient (RQ) for cultures BR06 – BR09.....	103
Figure III-51. Evolution of the concentration of the nanobody CH10-12 in cultures BR02 – BR05.	104
Figure III-52. Specific production rate of the nanobody CH10-12 in cultures BR02 to BR05. Induction made with a pulse of 1 mM of IPTG.	105
Figure III-53. Evolution of the concentration of the nanobody in cultures BR06 to BR09.	106
Figure III-54. Specific production rate of the nanobodies CH10-12 and NbF12-10 in cultures BR06 to BR09. Induction made with a pulse of 1 mM of IPTG.....	107
Figure III-55. SDS-PAGE gels of cultures BR04 and BR08. S: supernatant, S E1: first eluate of purification of supernatant, E1: first eluate of purification of periplasmic extract, PE: periplasmic extract. The red arrows show the presence of the nanobody.....	107
Figure III-56. SDS-PAGE gel of the first eluate of the last sample of cultures BR02 to BR09.....	108
Figure III-57. Graphical comparison of nanobody CH10-12, NbF12-10 and secondary proteins found in the cultures BR02 – BR09. <i>Escherichia coli</i> CH10-12, NbF12-10 NN and WK6 grown in MM at 37°C, pH 6.8, induction at about 25 g cdw/L with 1 mM IPTG and change of temperature as specified in the image.....	109
Figure III-58. Nanobody production in cultures BR02 – BR08 and comparison with the literature...	111
Figure III-59. Production of nanobodies CH10-12 and NbF12-10 in cultures BR02 to BR09.	114
Figure III-60. Specific production rates of nanobodies CH10-12 and NbF12-10 on the bioreactor cultures BR02 to BR07 of <i>Escherichia coli</i> CH10-12 grown on MM.	115
Figure III-61. Simulation of the kinetics for specific production rate of the nanobody.....	120
Figure 1-1. Expression du nanobody par différentes méthodes de choc osmotique. Les flèches rouges indiquent les bandes du nanobody NbF12-10 (29 kDa) et CH10-12 (31 kDa) du premier éluat du purification par IMAC en gels d'électrophorèse. Méthode 1 : incubation en TES (Tris-HCl 200 mM, EDTA 0.5 mM, sucrose 500 mM) pendant 2 h et choc osmotique par addition du TES/4 pendant 2 h ; Méthode 2 : incubation en TES pendant 6 h et choc osmotique par addition du TES/4 pendant 12 h ; Méthode 3 : incubation dans du TES et choc osmotique par addition d'eau distillé froide pendant 2 h. Le marqueur de poids moléculaire utilisé a été le Precision Plus Protein Unstained Protein Standards (Bio-rad, USA).	140
Figure 1-2. Méthodologie de traitement d'images des gels d'électrophorèse. A) Image du gel d'électrophorèse utilisé pour les analyses. BSA : albumine de sérum bovin, OV : ovalbumine, CA : anhydrase carbonique, MW : marqueur du poids moléculaire. B) Profil du puits et détermination de la surface du pic. C) Identification du nanobody CH10-12 en gels d'électrophorèse. La flèche rouge indique la bande du nanobody à un poids moléculaire apparent du 31 kDa. D) Comparaison de la quantification du nanobody par densitométrie et nanodrop.....	141
Figure 1-3. Production du nanobody CH10-12 par de court temps d'induction.	142
Figure 1-4. Production du nanobody CH10-12 et NbF12-10 en cultures de bioréacteur par de longues temps d'induction.	143
Figure 3-1. Schematic of the experimental set-up used in fed-batch cultures in 5 L bioreactor.	172
Figure 3-2. Physico-chemical parameters, operating conditions, and biological parameters of the culture of <i>Escherichia coli</i> CH10-12 grown in MM, pH 6.8, 37°C, induced at 33°C for 6 h. The dotted lines depict the change in the operating mode.	173

Figure 3-3. Evaluation of the temperature and duration of the induction during the production of biomass and recombinant nanobodies. (a) Production of biomass and recombinant nanobody CH10-12 at an induction temperature of 28°C, 30°C, 33°C and 37°C. (b) Production of biomass and recombinant nanobodies CH10-12 and NbF12-10, and the reference strain *E. coli* WK6 at an induction temperature of 29°C. All cultures were grown at 37°C with glucose as carbon source in defined minimal medium and induced at different temperatures. 174

Figure 3-4. Comparison of the recombinant nanobodies CH10-12 and NbF12-10 in bioreactor cultures and the literature. 175

Figure 3-5. Simulation of the kinetics for specific production rate of the nanobody using a growth- and temperature-dependent Luedeking-Piret kinetic model..... 176

ABBREVIATIONS

2xYT	Yeast extract tryptone medium
Aah	<i>Androctonus australis hector</i>
BSA	Bovine serum albumin
CA	Carbonic anhydrase
CHO	Chinese hamster ovary
Cn	<i>Centruroides noxius</i>
DO	Dissolved oxygen
F(ab) ₂	Divalent antigen binding domain
Fab	Antigen binding domain
HCDC	High cell density culture
His ₆ -tag	Hexa-histidine tag
IB	Inclusion bodies
IgG	Immunoglobulin G
IMAC	Immobilized metal affinity chromatography
IPT	Institut Pasteur de Tunis
IPTG	Isopropyl β-D-thiogalactopyranoside
LB	Lysogeny broth
LD ₅₀	Median lethal dose
mAb	Monoclonal antibodies
MBP	Maltose binding protein
mM	Milimolar concentration
MM	Defined minimal medium
Nb	Nanobody
OD	Optical density
px	Pixel
OUR	Oxygen uptake rate
OV	Ovalbumin
scFv	Single-chain variable domain
SDS-PAGE	Sodium dodecyl sulfate polyacrylamide
SUMO	Small ubiquitin-related modifier
TB	Terrific Broth
TBI	Toulouse Biotechnology Institute
V _H H	Variable heavy-chain domain

NOMENCLATURE

a	Volume correction factor, dimensionless
A280	Absorbance at 280 nm, AU
b	Intercept of a linear regression
C	Concentration of protein, mg/mL
c	Constant parameter of Henry's law, K
C*	Oxygen saturation, mol/L
C ₀	Dissolved oxygen at time zero, mol/L
CE	Circle equivalent diameter, μm
C _i ^L	Molar concentration of compound C in the liquid, mol/L
C _p	Dissolved oxygen measured by the dissolved oxygen probe, mol/L
D _i	Diffusion coefficient in the resistance layer, m ² /s
E	Biological enhancement factor, h/h
E _a _i	Activation or inactivation energy for the nanobody production, °C
F _d	Dilution factor, L/L
k _{eq}	Constant of equilibrium of Henry's law, mol/mol
K _H	Henry's law constant, mol/L/atm
k _L a	Volume oxygen mass transfer coefficient, h ⁻¹
MW	Molecular weight, kDa
P	Pressure, mbar
q _i	Specific rate of production or consumption, Cmol/CmolX/h
Q _{in} ^G	Molar air flow entering the bioreactor, mol/L
Q _{out} ^G	Molar air flow leaving the bioreactor, mol/L
R _f	Migration distance of protein band, mm/mm
r _i	Rate of production or consumption of a compound, mol/L/h
rO _{2L}	Rate of consumption of oxygen, mol/h
RQ	Respiratory coefficient or respiratory quotient, dimensionless
S	Glucose, Cmol or g cdw
S _{feed}	Concentration of glucose in the feed solution, g Glc/L
V ₀	Initial volume of the bioreactor, L
V _{equivalent}	Volume of the feed solution without theoretical carbon dioxide conversion, L
V _{evaporation}	Volume of liquid evaporated during a bioreactor culture, L
V _{exp}	Experimental final volume of the bioreactor, L
V _{feed}	Volume added to the bioreactor by the feed solution, L
V _{final}	Theoretical final volume, L

V^G	Gaseous volume of the bioreactor, L
V_{H_2O}	Volume of water in the feed solution, L
V_{pH}	Volume added to the bioreactor by the pH controlling solution, L
V_s	Superficial gas velocity, m/s
V_{sampling}	Volume of samples taken from the bioreactor, L
V_{tip}	Impeller tip velocity, rpm
V_t^L	Theoretical volume in the bioreactor at time t, L
$V_{X/S}$	Volume of glucose converted to biomass, L
X	Biomass, Cmol or g cdw if not stated otherwise
X^+	Plasmid-bearing cells, g/L
X^-	Non-plasmid bearing cells, g/L
X_n	Culturable cells, g/L
x_i^{in}	Molar fraction of the gas, %mol/mol
$Y_{CO_2/S}$	Theoretical yield of glucose converted to carbon dioxide, Cmol/Cmol
z_i	Thickness of the resistance layer, m
α	Biomass correlation coefficient, g cdw/AU
α_{Nb}	Growth associated parameter, mg Nb/g cdw
β	Non-growth associated parameter, mg Nb/g cdw/h
γ	Degree of reduction, dimensionless
γ_i	Pre-exponential constants, mg Nb/g cdw/h
$\epsilon_{1\%}$	Extinction coefficient, mg/mL/AU
μ	Specific growth rate, h^{-1}
ρ_i	Density, g/mL
σ	Non-temperature associated parameter, mg Nb/g cdw/h
τ	Response time of the dissolved oxygen probe, s

INTRODUCTION

Scorpion stings are a serious health problem in tropical and subtropical countries [1]. The most common treatment for scorpion stings is serotherapy. Serotherapy uses antibodies or fragments of antibodies to target the toxic compounds in the scorpion venom, such as neurotoxins. Neurotoxins have a molecular weight of about 7 kDa which accounts for its quick effect in envenomation problems.

The production of new and more efficient therapeutics is a top priority for the pharmaceutical industry. The conventional antivenoms available in the market are a mix of equine antibody fragments, with a molecular weight of about 50 kDa. They are produced by immunization of horses and extracted and purified from blood samples in processes that last from 3 to 15 months.

New antibodies have been discovered. These nanobodies are fragments of camelid antibodies, with a low molecular weight (15 kDa) that enable better tissue penetration [2]. Its production in microbial hosts is a tool frequently used in the biopharmaceutical industry to increase antiserum production [3].

In this doctoral project, the production of nanobodies as recombinant proteins expressed in *Escherichia coli* was studied. The nanobody NbF12-10 [4] was expressed in the two recombinant clones *E. coli* NbF12-10 NN and *E. coli* NbF12-10 NO. The humanized format of the nanobody NbF12-10, called CH10-12 was expressed in the recombinant strain *E. coli* CH10-12. The host strain *E. coli* WK6 was used as reference for comparison purposes. All the strains were prepared by Laboratoire des Venins et Molécules Thérapeutiques of the Pasteur Institute of Tunis (LVMT-IPT, Tunis, Tunisia).

This thesis is divided in 3 main chapters. In the first chapter, a literature review presents the health problem associated with scorpion envenomation and the commercially available antivenoms and alternatives (§I.1). A bibliographic research methodology was followed to prepare a database for the project (§I.2 – §I.4). The state-of-the-art of recombinant proteins in *Escherichia coli* is presented with an emphasis on the production of recombinant venom toxins and antivenoms (§I.5).

The second chapter describes the materials and methods used for the preparation and operation of the cultures in shake-flask and bioreactors (§II.1 – §II.7), as well as the data treatment for the analysis of results (§II.8).

The third chapter corresponds to the results of this work and is subdivided in three main sections. In the first section (§III.1), the screening of the strains and selection of the best nanobody producer will be presented. Performances of the reference and recombinant strains when cultured in rich medium and defined minimal medium will be discussed. In the second section (§III.2), the cultures in bioreactor are presented. The performances of the recombinant strains CH10-12 and NbF12-10 NN are compared during batch and fed-batch modes. The expression of the nanobody CH10-12 was made in high cell density cultures ($[X] > 25$ g cdw/L). The effect of temperature during nanobody expression and the duration of the induction are discussed. The optimal conditions for the expression of the nanobodies CH10-12 and NbF12-10 in bioreactor cultures are proposed. In the third section (§III.3), a kinetic model for the production of the recombinant nanobodies is presented.

Finally, the general conclusions of this doctoral work will be presented, and some perspectives will be proposed.

The results obtained during this project in collaboration with the Pasteur Institute of Tunis (Tunisia) were subject to scientific communications in scientific journals or international congresses.

Published article

Susana María Alonso Villela, Hazar Kraiem, Balkiss Bouhaouala-Zahar, Carine Bideaux, César Arturo Aceves Lara, Luc Fillaudeau. "A protocol for recombinant protein quantification by densitometry". *MicrobiologyOpen*; 9:1175-1182, 2020, doi: 10.1002/MBO3.1027.

Article under preparation

Susana María Alonso Villela, Hazar Kraiem, Balkiss Bouhaouala-Zahar, Carine Bideaux, César Arturo Aceves Lara, Luc Fillaudeau. "Effect of temperature on the production of a recombinant antivenom in fed-batch mode". To be submitted to *Applied Microbiology and Biotechnology* (Springer).

Oral communications and posters

Susana María Alonso Villela, Hazar Kraiem, Balkiss Bouhaouala, Carine Bideaux, Cesar Arturo Aceves Lara, Luc Fillaudeau. "Temperature effect in the production of a recombinant antivenom in fed-batch mode". Lecture presented at: 12th European Congress of Chemical Engineering and 5th European Congress of Applied Biotechnology; 2019 September 15-19; Florence, Italy.

Susana María Alonso Villela, Hazar Kraiem, Balkiss Bouhaouala-Zahar, Emna Ben Khalifa, Rahma Ben Abderrazek, Issam Hmila, Carine Bideaux, César Arturo Aceves Lara, Luc Fillaudeau. "Screening of Bispecific Nanobody-based Antivenom *E. coli* Strains in complex and minimal media". Poster Presented At: Second Mediterranean Congress on Biotechnology; 2019 March 16-20; Hammamet, Tunisia.

Hazar Kraiem, Yannick Manon, Issam Hmila, Rahma Ben Abderrazek, Susana María Alonso Villela, Luc Fillaudeau, Balkiss Bouhaouala-Zahar. "Expression of the recombinant NbF12-10 and its chimeric antibody format in *Escherichia coli*: investigation of fed-batch bioprocess on minimal media". Oral presentation at: Second Mediterranean Congress on Biotechnology; 2019 March 16-20; Hammamet, Tunisia.

Chapter I. LITERATURE REVIEW

The problem addressed by this doctoral project relies on the health problem caused by the scorpion stings around the world. The widespread morbidity in tropical and subtropical zones and limited quantities of antiserum require attention of the pharmaceutical industry [1].

With the limited production of scorpion venoms and the lengthy process to commercially obtain scorpion antiserum, the production of next-generation neutralizing antibodies in microbial hosts rises as a new tool for scorpion antiserum production [3].

This literature review comprises the current status on scorpionism and the antivenom market, followed by the state of the art on the production of recombinant proteins by microbial engineering and cultivation processes. Finally, the most recent publications on the production of scorpion antivenom proteins are addressed with emphasis on nanobodies as next-generation therapeutics.

I.1. Scorpion stings as a health problem

According to the World Health Organization (WHO), scorpionism is a neglected health problem, mainly in underdeveloped tropical and subtropical zones, such as the northern parts of Africa, Middle-East, Central and South America [1]. About 2.5 billion people live in at-risk zones (Figure I-1). Annually, over 1.5 million scorpion stings are reported around the world with a mortality of 0.27% for a total of 3,250 deaths [5]–[7].

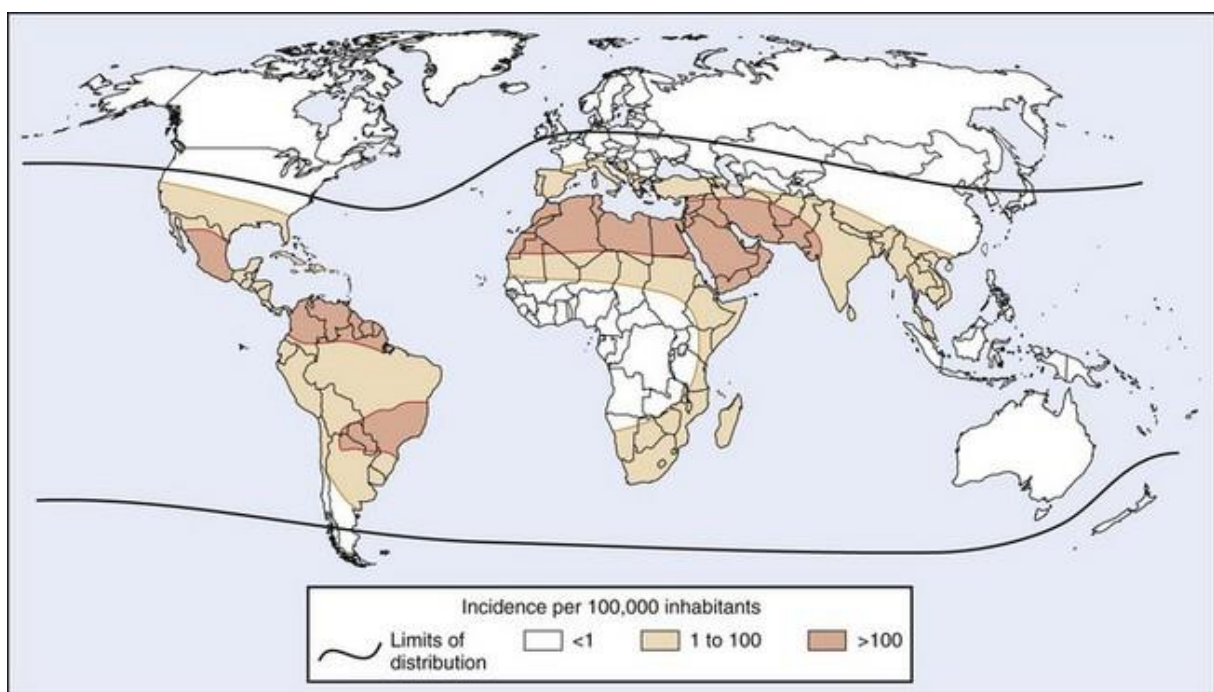


Figure I-1. Scorpionism around the world [6]

Children under seven years old and elders over 60 years old are the most vulnerable to the effects of the scorpion venom [3]. In children, mortality ranges from 3% to 22% [8]. Mortality rates in the whole population can be reduced with the administration of the scorpion antivenom as soon as possible after the sting [1].

The envenomation by scorpion sting is classified in three stages [6], [9]:

- I. Mild: patients present local pain around the sting, usually treated with symptomatic measures.

- II. Moderate: patients present vomiting, abdominal pain, fever, sweats, hypotension and/or bradycardia. Supportive care and symptomatic measures are provided, depending on the severity of the case, antivenom can be administered.
- III. Severe: patients present major respiratory complications and the risk of cardiovascular collapse is the highest, the evolution can be fatal without supportive care and/or administration of the antivenom.

Symptomatic treatment aims to reduce pain on the mild cases, and to maintain vital functions on moderate and severe cases [10]. It often includes analgesics, vasodilators, anticonvulsants, vomiting-preventing drugs, antihistamines, and antipyretics [10]–[12].

I.1.1. Scorpion stings around the world

From the approximately 1500 species of scorpions in the world, less than a dozen are responsible for serious envenomation or death in humans [6]. They belong to the family of *Buthidae*, by example the genera: *Tityus*, *Leiurus*, *Androctonus*, *Centruroides*, and *Buthus*.

Most of the scorpions of medical importance can be found in the continents of America, Africa and Asia (Figure I-2, Table I-1). In Europe and Australia the information regarding epidemiological data is scarce, the scorpions found in these continents are considered not dangerous to the human health [6].

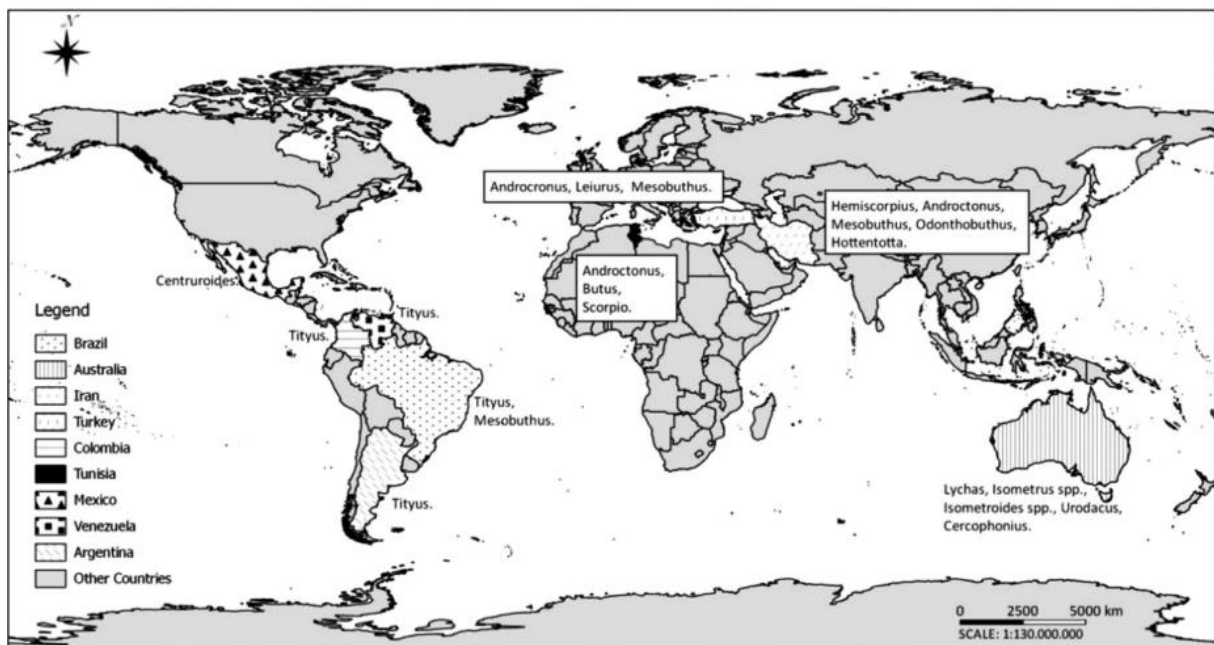


Figure I-2. Scorpions of medical importance around the world [9]

Continent	Country	Stings/year	Deaths/year	Most common genera
America	Mexico	313,000	50	<i>Centruroides</i>
	Brazil	78,000	100	<i>Tityus</i>
	Venezuela	12,000	121	<i>Tityus</i>
Africa	Tunisia	40,000	100	<i>Androctonus</i>
	Algeria	50,000	48	<i>Androctonus</i>
	Morocco	40,000	N. A.	<i>Androctonus</i>
Asia	Saudi Arabia	18,000	N. A.	<i>Leiurus</i>
	Iran	50,000	20	<i>Leiurus</i>
	Israel	200	N. A.	<i>Leiurus</i>

Table I-1. Morbidity and mortality of scorpion stings. N. A.: not available.

I.1.1.1. America

In Mexico, scorpion stings are a big health problem due to the presence of highly venomous *Centruroides* scorpions, such as *C. noxius*, *C. limpidus*, *C. tecomanus* and *C. suffusus* [13]. Envenomation cases have increased from 200,000 cases reported in 1970 to over 310,000 cases reported in 2012 [14]. Mortality has decreased from 310 deaths in 1970 to less than 50 in 2012 due to the availability of the scorpion antivenom in the country [1], [13], [14]. The symptoms of envenomation are more severe in children under 5 years old [15], which is why, at the health facilities, the antivenom is always administered whether the child has symptoms of envenomation or not [16].

In Brazil, the *Tityus serrulatus* scorpion is responsible for most of the cases of envenomation, although other species can be found in the country, such as *T. silvestris*, *T. metuendus*, *T. obscurus* [17]. Morbidity in Brazil has been on increasing in the last two decades, 7,000 cases of scorpion sting were reported in 1995 with 1% of them being fatal, in 2007, 37,000 cases were reported annually with 50 deaths, to over 78,000 cases reported in 2013 and over 100 deaths [1], [17]–[19]. Children under 10 years old represent the largest number of deaths, and antivenom is administered in all children under 7 years old [19].

In Venezuela, the *Tityus discrepans* is the scorpion most studied in the country. In 2013, over 12,000 cases of envenomation were reported, and 121 deaths [20].

I.1.1.2. Africa

In Tunisia, the scorpions *Androctonus australis*, *Buthus occitanus* and *Leiurus quinquestriatus* can be found [21]. An average of 40,000 cases of scorpion stings are reported annually, with 100 deaths by envenomation [1], [8], [22]. All the deaths were in children of less than 15 years old [6].

In Algeria, the scorpions *Androctonus australis* and *Buthus occitanus* are commonly found in the country [23]. Up to 50,000 cases of scorpion stings are reported annually, with 48 deaths, accounting a mortality of 0.1% [24], [25]. Children under 15 years old represent the 73% of the deaths caused by envenomation [23].

In Morocco, the *Australis mauretanicus mauretanicus* scorpion is endemic of the country and it is responsible for about 40,000 cases of envenomation annually [8], [26].

Scorpions of medical interest can be found in Niger, such as the *Leiurus quinquestriatus* scorpion and *Androctonus aeneas* scorpion [27], but the morbidity rates have not been reported.

I.1.1.3. Asia

In Saudi Arabia, the scorpions *Leiurus quinquestriatus* and *Androctonus crassicauda* are responsible for most of the stings reported in the country [28]. With an incidence of over 20,000 cases annually, the mortality rates have decreased from 4.8% in 1995 to less than 0.05% in 2003 due to the use of high doses of antivenom [11], [21], [29].

In Iran, the *Hemiscorpius lepturus* and *Androctonus crassicauda* scorpions are found, the first one being responsible for most of the fatal cases [1], [18], [30]. About 50,000 cases of envenomation and 20 deaths are reported annually, with the children under 10 years old being accounting for up to 16% of the fatal cases [18], [30], [31].

In Israel, the *Leiurus quinquestriatus Hebraeus* yellow scorpion has been used for the production of antivenom [32]. Annually, about 200 cases of envenomation occur in the country [6].

I.1.2. Scorpion venom

The active components of the scorpion venom are the neurotoxins that act on voltage-dependent ionic channels of excitable membranes, such as nervous, glandular and muscular tissue [33]. They have a molecular weight of around 7 kDa [10].

The neurotoxins account for less than 5% of the dry weight of the scorpion venom but are responsible for the symptoms of envenomation in humans [6], [10]. They can be classified in two main classes: alpha (α) and beta (β), according to their activity on the ionic channels. The α -toxins inactivate the closing potential of the sodium channels, inducing paralysis, and the β -toxins affect the voltage of the sodium channels, preventing their activation and resulting in muscular responses [5]–[7], [33].

The ability of the neurotoxins to affect the ionic channels has made them useful for several therapeutic applications, such as for the control of autoimmune diseases and as imaging agent for cancer cells. Their antibacterial effects have also been studied for its use as an alternative to antibiotics and for pest control in agricultural applications [20], [34], [35].

I.1.3. Global market of therapeutics and treatment cost

With an estimated value of 100 billion USD per year, biopharmaceuticals have 20% of the global market of commercial pharmaceuticals [36]–[40]. The therapeutic antibodies market is estimated in 30 billion USD, with an average growth in the last 15 years over 5% [41], [42].

Most of the biopharmaceuticals consist in monoclonal antibodies (mAbs), which are clones of immunoglobulins specific for one antigen. In the market, half of the marketed biopharmaceuticals are monoclonal antibodies [38]. The cost of these therapeutics varies from 2,000 USD per gram of high-dose antibodies to up to 50,000 USD per gram of low-dose antibodies [43].

The cost of antivenoms and envenomation treatment can be very high, taking into account that the cost of developing a new biopharmaceutical is estimated in 1.9 billion USD [44].

In the United States, the scorpion antivenom Anascorp was approved by the FDA in 2011, with a recommended dose of 3 vials for a severe envenomation case [5]. Produced by Bioclon Institute, the retail price of a vial is 3,500 USD, whereas the Mexican version, Alacramyn, is found at a retail price of 100 USD in Mexico.

A case study in the United States estimated the treatment of a scorpion sting in up to 11,000 USD, including the cost of antivenom and supportive care, and the treatment without the antivenom in up to 5,200 USD [45]. The case study suggested that the use of antivenom was not cost-effective at the current price and that antivenom should be reserved only for the highly severe cases of envenomation.

In North Africa, the economic burden due to envenomation was calculated using the disability adjusted life year (DALY) and the cost of averted deaths. Depending on the country, the DALY varied from 2,000 to 6,000 USD, and the cost of averted deaths in 100 to 300 USD [46].

In Tunisia, envenomation treatments cost about 1 million USD to the Health Ministry of Tunisia, and about 80% goes only to the antivenom [47].

I.1.3.1. Serotherapy

Serotherapy for the treatment of scorpion stings consists in antivenom, or scorpion antiserum, that targets the neurotoxins of the scorpion venom. Antivenoms are in the list of essential medicines of the World Health Organization (WHO) which contains the minimum drug needs for the basic health-care system. It is the generalized treatment measure for moderate and severe envenomation cases.

The antivenom should be administered within the first hour after the sting [47]–[49]. The initial dose consists on one to three vials of 5 mL of serum. The vials are diluted in 50 mL of saline solution and administered intravenously. Depending on the severity of the envenomation, additional vials can be used [45].

As symptomatic treatment, the use of drugs to reduce pain, anxiety and fever are often administered with or without the antivenom, and in the cases of mild envenomation [9], [16]. It has been found that drugs as heparin, EDTA, aristolochic acid and 1,10-phenanthroline can inhibit various venom toxins, although they are not clinically used [50].

In the 80's, the use of antivenoms or serotherapy as treatment for the scorpion stings was often discouraged due to the side effects of the serum on the patients and their ineffectiveness against the scorpion venom [51], [52].

Nowadays, antivenoms consist in highly purified antibodies, and the doses of administration in the health facilities have been ameliorated to increase their effectiveness and reduce the mortality due to envenomation [7].

Despite the existence of these highly purified antivenoms, their availability is limited, for example in Africa or Asia. In Iran and Saudi Arabia, 12% and 19.4% of the patients, respectively, are not treated with the antivenom due to its unavailability; in Libya, many patients are treated of envenomation with traditional medicine [1], [6], [11], [31]. In traditional medicine, the use of medicinal plants and the application of steam on the area of the sting is recommended [8], [12].

I.1.3.2. Commercially available antivenoms

There are 20 research institutes that produce antivenom for human use distributed in 15 countries around the world (Table I-2). Among the scorpions targeted by the antivenoms, the African scorpion species (*A. australis*, *B. occitanus*) and the Asian scorpion species (*A. crassicauda*, *L. quinquestriatus*) are highly represented. Others, like the *Centruroides spp.* and *Tityus spp.* have been thoroughly studied in Mexico and Brazil, respectively. The antivenoms for these American species are distributed by several research institutes in these countries: Bioclon Institute and Birmex in Mexico, and Butantan Institute, Ezequiel Dias Foundations and Vital Brazil Institute in Brazil. The doses of neutralized scorpion venom per mL of serum vary from 10 to 500 of median lethal dose (LD₅₀).

Country	Manufacturer	Specificity	Neutralized venom per mL of serum	Type of antibody	Reference
Mexico	Bioclon Institute Birmex	<i>Centruroides noxius</i> <i>Centruroides limpidus limpidus</i> <i>Centruroides limpidus tecomanus</i> <i>Centruroides suffusus suffusus</i>	30 LD ₅₀	Equine F(ab) ₂ '	[53], [54]
Brazil	Butantan Institute Ezequiel Dias Foundation Vital Brazil Institute	<i>Tityus serrulatus</i>	1 mg of venom	Equine F(ab) ₂ '	[17], [19], [55], [56]
Venezuela	Central University of Venezuela	<i>Tityus discrepans</i>	1 mg of venom	Equine F(ab) ₂ '	[20], [57]
Argentina	ANLIS Dr. Carlos Malbrán	<i>Tityus trivittatus</i>	200 LD ₅₀	Equine F(ab) ₂ '	[7]
Tunisia	Pasteur Institute of Tunis	<i>Androctonus australis</i> <i>Buthus occitanus</i>	10 LD ₅₀	Equine F(ab) ₂ '	[47]
Algeria	Pasteur Institute of Algeria	<i>Androctonus australis hector</i>	20 LD ₅₀	Equine F(ab) ₂ '	[24]
Morocco	Pasteur Institute of Morocco	<i>Buthus occitanus</i> <i>Androctonus mauritanicus</i>	12.5 LD ₅₀	Equine F(ab) ₂ '	[26]
Egypt	VACSERA	<i>Leiurus quinquestriatus</i> <i>Scorpio maurus</i> <i>Androctonus crassicauda</i> <i>Buthus occitanus</i>	N. A.	Equine F(ab) ₂ '	[50]
North Africa	Sanofi-Pasteur	<i>Buthus occitanus</i> <i>Androctonus australis</i> <i>Leiurus quinquestriatus</i>	50 LD ₅₀	Equine F(ab) ₂ '	[7] http://www.toxinfo.org/antivenoms/ *
North Africa	Pasteur Institute of Tunis	<i>Androctonus australis</i> <i>Buthus occitanus</i> <i>Leiurus quinquestriatus</i>	N. A.	Equine F(ab) ₂ '	[50]
South Africa	South African Vaccine Producer	<i>Parabuthus transvaalicus</i>	N. A.	Equine IgG	[50]

Saudi Arabia	National Antivenom and Vaccine Production Center	<i>Leiurus quinquestriatus</i> <i>Androctonus crassicauda</i>	50 LD ₅₀	Equine F(ab) ₂	http://www.toxinfo.org/antivenoms/ *
Iran	Razi Vaccine and Serum Production and Research Institute	<i>Androctonus crassicauda</i> <i>Buthotus (Hottentota) saulcyi</i> <i>Buthotus (Hottentota) schach</i> <i>Odontobunthus doriae</i> <i>Mesobuthus eupeus</i> <i>Hemiscorpius lepturus</i>	26 LD ₅₀	Equine F(ab) ₂	[30]
India	Haffkine Bio-Pharmaceutical Corporation LTD	<i>Buthus tamulus</i>	25 LD ₅₀	Equine F(ab) ₂	[7]
India	Vins Bioproducts	<i>Leiurus quinquestriatus</i> <i>Androctonus amoreuxi</i>	50 LD ₅₀ L. <i>quinquestriatus</i> 35 LD ₅₀ A. <i>amoreuxi</i>	Equine IgG	http://www.toxinfo.org/antivenoms/ *
Turkey	Refik Saydam Hygiene Center	<i>Androctonus crassicauda</i>	500 LD ₅₀	Equine F(ab) ₂	[7], [50]
Israel	Central Laboratories of the Ministry of Health	<i>Leiurus quinquestriatus</i> <i>Hebraeus</i>	80 LD ₅₀	Unspecified donkey antibodies	[32]

Table I-2. Antivenoms available in the market. *Accessed October 24, 2019

There is scientific evidence that some antivenoms can be used to neutralize the venom of other scorpion species, which is called cross-reactivity [1]. Cross-reactivity occurs when an antibody raised against an antigen shows high affinity to a different antigen. The neurotoxins (α and β toxins) have similar primary sequences, tertiary structures and pattern of disulfide bonds, therefore an antivenom created against one type of toxin may cross-react and neutralize other toxic components of the scorpion venom [3].

The efficacy of the Mexican, Brazilian and Venezuelan antivenoms were tested against the venom of the *Tityus pachyurus* scorpion of Colombia. Pre-incubation of venom and antivenom was injected in mice. The Mexican and Brazilian antivenoms successfully neutralized the LD₅₀ of the venom, while the Venezuelan did not, although it increased the survival time of the subjects [33].

Clinical studies and experimental data have proven the efficacy of the Venezuelan antivenom against the venom of *T. neoespartanus*, *T. falconensis*, *T. nororientalis* and *T. zulianus* scorpions, with the disappearance of the symptoms in 8 to 24 h after the administration of the antivenom [20].

The Moroccan antivenom against *A. mauretanicus* was tested on patients stung by *B. occitanus* successfully. The equine F(ab)₂ antivenom reduced the clinical symptoms on the patients and did not produced allergic reactions [26].

In a similar note, the bispecific nanobody NbF12-10 V_HH produced against the toxins of *A. australis hector* was tested against the toxins of the *A. mauretanicus* venom. Pre-incubation of the nanobody with the toxic fractions of the venom was injected in mice, resulting in the survival of 50% of the animals that did not exhibit symptoms of envenomation [58].

I.1.4. Production of antivenoms

Antibodies are proteins produced by the immune system to neutralize foreign biologicals or chemical substances, in this context known as antigens. They recognize the antigens and bind to them to alter their characteristics [59].

A conventional antibody (Figure I-3), also known as immunoglobulin G, is a Y-shaped protein of about 150 kDa of molecular weight; it comprises an antigen-binding domain (Fab) and a crystallizable domain (Fc). The domains are constituted of four polypeptides: constant heavy-chain domain (CH), light heavy-chain domain (CL), variable heavy-chain domain (VH) and variable light-chain domain (VL) [39], [59], [60]. In most cases, the antibody is fragmented to obtain the antigen-binding sites, obtaining single-chain variable domain (scFv), antigen-binding domain (Fab) and divalent Fab fragments (F(ab)₂).

Recently, the antibodies found in camelids (llamas, camels or alpacas) are gaining interest due to their antigen-binding domain. Comprising on only heavy-chain domains, the antigen-binding domain (V_HH) has a molecular weight of about 15 kDa, enabling effective tissue penetration [2], [61]. Also known as Nanobody, the V_HH has better solubility and higher thermostability than the conventional antibody derivatives (Fab, F(ab)₂, scFv) [62]. As therapeutics, nanobodies can be used in medical applications as anti-inflammatories and drug carriers to deliver therapy to diseased tissue [37], [59], [61]. Nanobodies induce a mild immune response to humans, but it can be reduced by humanizing the nanobody [37], [61], [63].

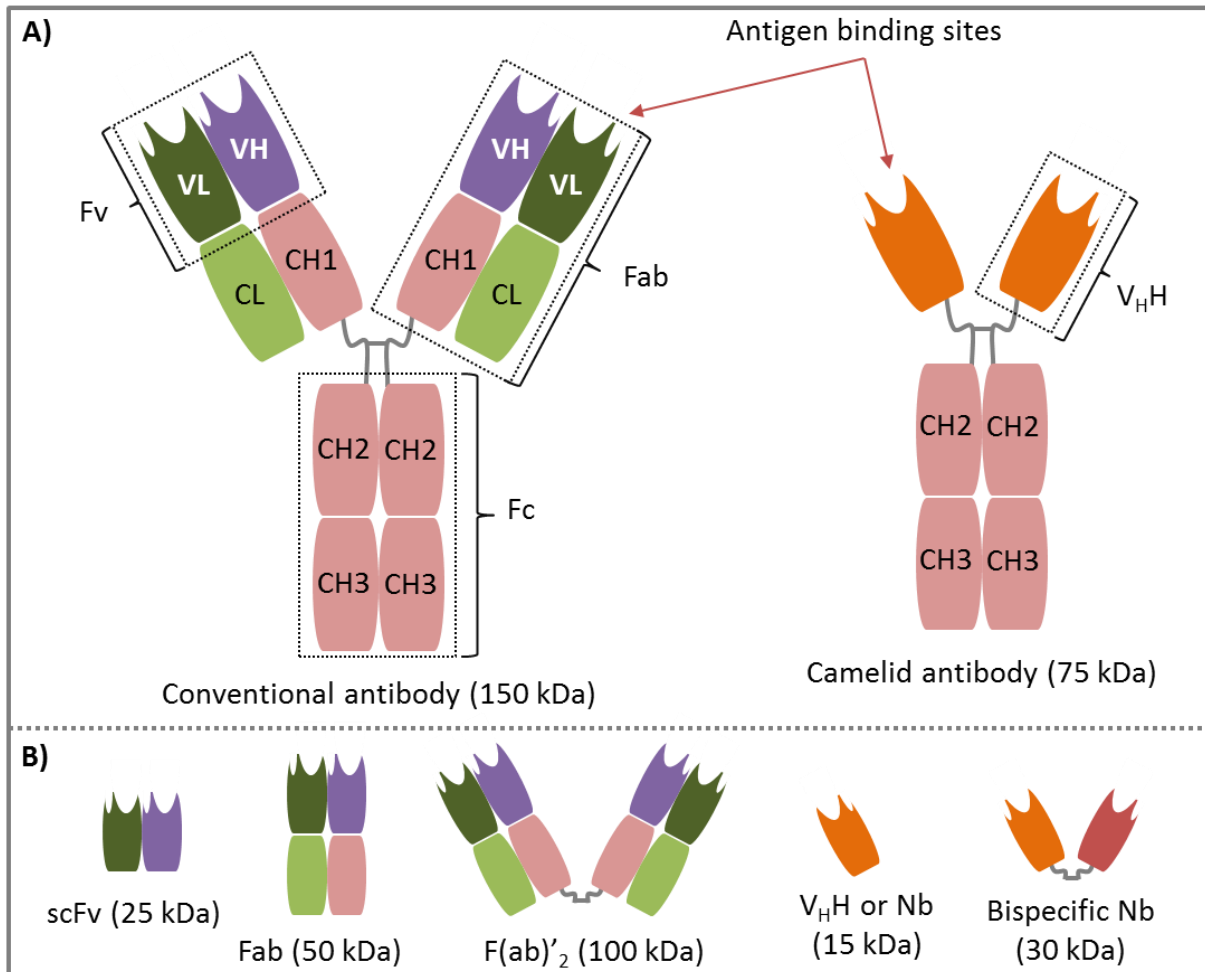


Figure I-3. Antibodies and their derivatives. A) Antibodies conventional and camelid. B) Derivatives of antibodies. V: variable, C: constant, L: light-chain, H: heavy-chain, V_HH: variable heavy-chain domain, Fv: variable domain, Fc: crystallizable domain, scFv: single-chain variable domain, Fab: antigen binding domain, F(ab)₂: divalent Fab fragments, Nb: nanobody.

Most of the scorpion antivenoms in the market consist of fragments F(ab)₂ of equine antibodies. The horses are injected with small doses of the crude venom or the toxic fraction to induce the production of the antibodies (Figure I-4). The antibodies are purified from the plasma and fractionated by enzymatic digestion into Fab or F(ab)₂, removing the Fc domain [5]. It has been proven that the deletion of the Fc domain reduces the adverse reactions of the patients to the antivenom [26], [64].

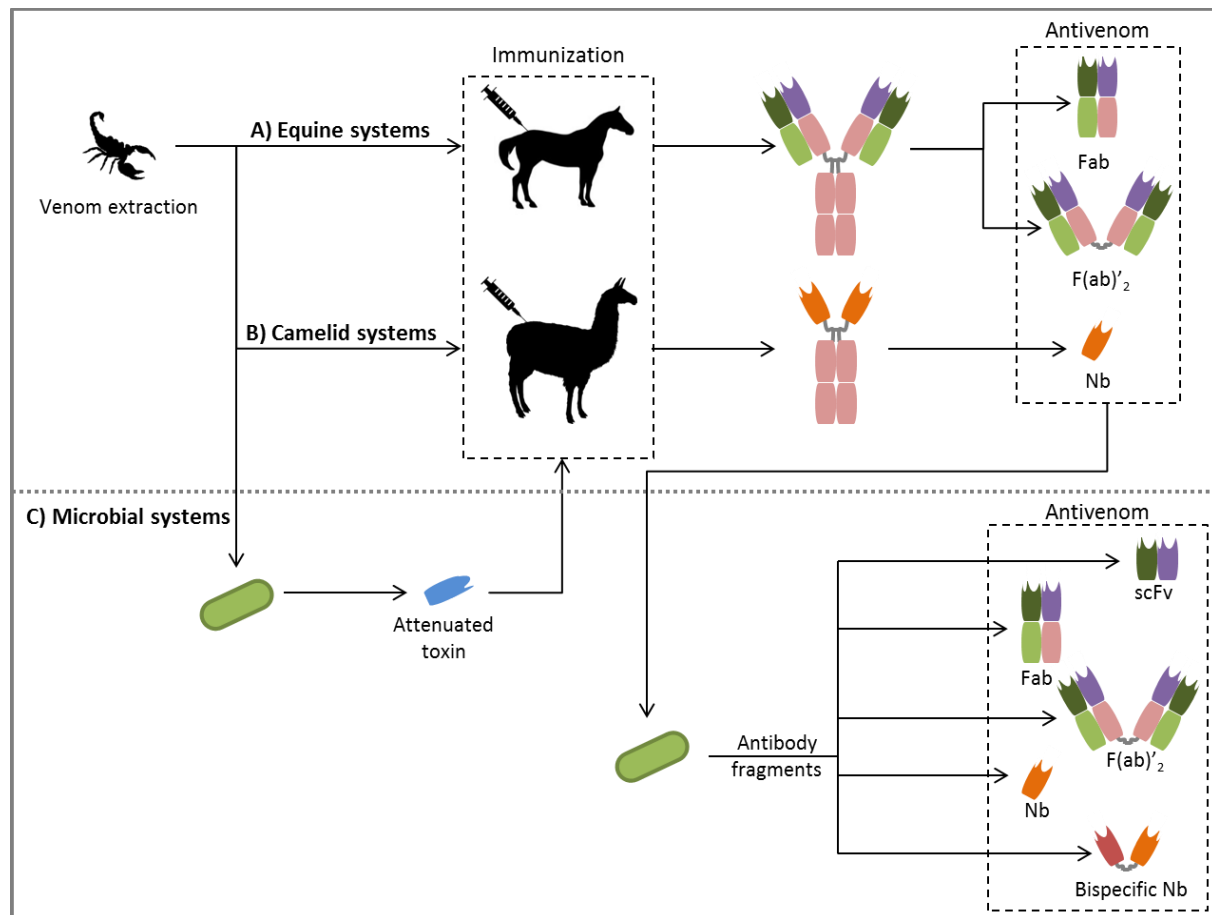


Figure I-4. Production of antivenom proteins. A) Equine production systems. B) Camelid systems. C) Microbial production systems.

Scorpion venom is obtained by manually or electrically milking the scorpion, obtaining up to 10 μL of venom per session and 0.4 mg of venom per month [65], [66]. Alternatively, the telson of the scorpion, commonly known as a stinger, can be macerated in a saline solution to obtain a venom solution. The disadvantage of this method is that for the hyper immunization of one horse up to 2,000 stingers can be needed and scorpions have to be killed [67].

Horses aged from 3 to 10 years are preferred for immunization [68]. Hyper immunization of the horses can take from 3 to 15 months, the venom is administered in increasing doses until a desirable titer of antibody is reached [69]. Depending on the size of the horse, 3 to 6 L of blood can be drawn in a session, with rests of 4 to 8 weeks between sessions [68]. The antibody IgG obtained after centrifugation of the blood plasma is around 13% v/v [67].

Immunization of the animal can be made with: attenuated crude venom to increase the life expectancy of the animal; venom toxins, to obtain better neutralizing antibodies; anatoxins, which are not toxic to mammals but induce the same immune response than toxins, and with recombinant toxins or synthetic peptides conjugated with a carrier protein, produced in *E. coli* [3].

The antibodies are extracted from the plasma by centrifugation and fractionated by enzymatic digestion with pepsin to obtain F(ab)₂ fragments or papain to obtain Fab fragments. The fragments of equine antibodies requires several steps to control the purity of the antibodies, the risk of viral and biological contamination and the antivenom efficacy *in vitro* and *in vivo* [68], [70].

Alternatively to the production in equines, the production of nanobodies can be done in camelids in a similar process than for equines; but it takes only 6 weeks for hyper immunization while using around 1 mg of functional toxin [71].

The nanobody fragments (V_HH) obtained by enzymatic digestion are of a smaller size (15 kDa) than Fab (50 kDa) or F(ab)₂ fragments (100 kDa). The nanobodies also have a better pharmacokinetic in the bloodstream and are low immunogenic due to the resemblance of the V_HH to the human VH gene family [37].

To avoid the use of mammals, the antibodies can be also expressed in a host cell. The expression as a recombinant protein can be coded into the DNA of the host cell to produce high quantities of the protein in a short period of time in high cell density cultures [72].

In this PhD project, the production of the recombinant nanobodies in *Escherichia coli* will be studied. *Escherichia coli* can be grown and cultivated easily and inexpensively in a laboratory setting obtaining high productivities and has been intensively investigated in molecular biology laboratories. It has a high facility to be metabolically modified to obtain overproducer strains and to modify the profile of the molecules targeted.

1.2. Bibliography research methodology

A bibliographic database was constructed following five steps of the methodology shown here below (Figure I-5). The methodology uses searching profiles composed of the keywords in the title of this PhD thesis to interrogate scientific databases and obtain a broad scope of the articles. The selection of relevant articles was based on the analysis of the title, abstract and the article itself.

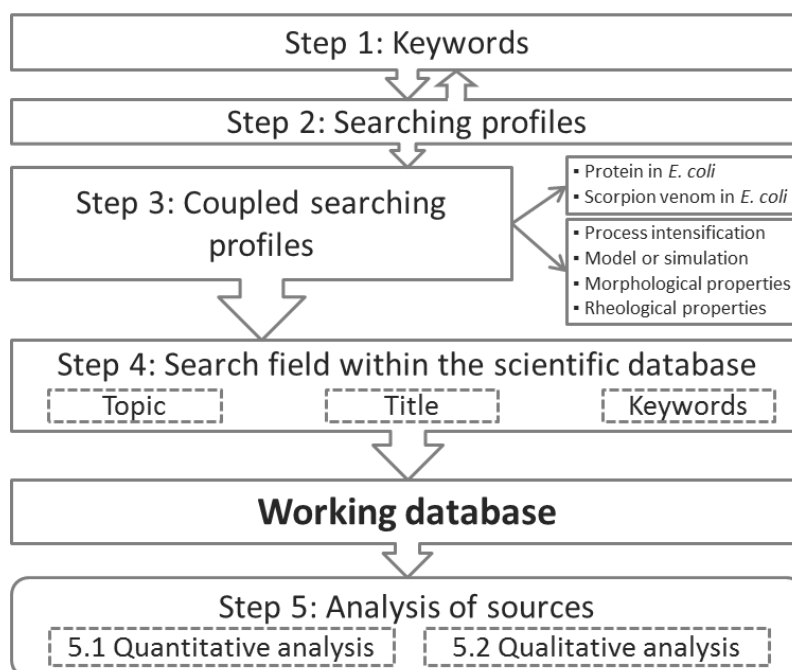


Figure I-5. Strategy of the bibliographic research methodology

1.2.1. Scientific databases

The scientific databases consulted were the Web of Science Core Collection (<http://apps.webofknowledge.com>, Clarivate Analytics) and Science Direct (<http://www.sciencedirect.com/>, Elsevier).

The doctoral dissertation databases accessed were the University Documentation System (<http://www.sudoc.abes.fr/>, Système Universitaire de Documentation, SUDOC) and the database of French doctoral dissertations defended since 1985 (<http://www.theses.fr/>), both databases belong to the Bibliographic Agency of Higher Education of France (Agence Bibliographique de l'Enseignement Supérieur, ABES). The EBSCO Open dissertations library (<https://biblioboard.com/opensdissertations/>) including doctoral dissertation accepted in American Universities and the Open Access Theses and Dissertations (OATD, <https://oatd.org/>) including over

3.5 million of electronic theses and dissertations were consulted but not used for quantitative purposes.

1.2.2. Keywords

The keywords selected for the interrogation of the scientific databases were carefully chosen from the title of this thesis and some supporting articles related to our research. Table I-3 shows the chosen keywords were some synonyms or related words are assembled within the same search string with the Boolean operator "OR". The quotation marks (" ") is used to find the exact words. The star (*) is used for truncated words that often have different endings or form composed words, for example *process* matches: process, bioprocess, processes, processing, and so on.

Search string ID	Keywords
S0	coli OR escherichia
S1	recombinant OR protein OR nanobody OR antibody OR biosimilar
S2	antivenom OR "anti venom" OR "anti-venom" OR venom OR scorpion
S3	*process* OR intensification OR *kinetic*
S4	prod* OR optim*
S5	"silico" OR model* OR simulat*
S6	granulo* OR morpho* OR size OR shape
S7	rheo* OR visco* OR newt*

Table I-3. Keywords used for the generation of searching profiles

1.2.3. Searching profiles

The searching profiles were constructed with the searching strings of Table I-3, using the operator "AND". Table I-4 shows the searching profile defined from the search strings.

The search strings P3 and P4 were simplified and separated into new search profiles after the preliminary searches showed a low count of articles due to the restricted search criteria.

Searching profile	Keywords
P1	(coli OR escherichia) AND (recombinant OR protein OR nanobody OR antibody OR biosimilar)
P2	(coli OR escherichia) AND (venom OR scorpion)
P3	(*process* OR intensification OR *kinetic*) AND (prod* OR optim*) AND ("silico" OR model* OR simulat*)
P3a	(*process* OR intensification OR *kinetic*)
P3b	(model* OR simulat*)
P4	(granulo* OR morpho* OR size OR shape) AND (rheo* OR visco* OR newt*)
P4a	(granulo* OR morpho* OR size OR shape)
P4b	(rheo* OR visco* OR newt*)

Table I-4. Searching profiles defined for the bibliographic research

1.2.4. Coupled searching profiles

The coupled searching profiles were constructed around the research objectives of our research, taking as pivot points: (P1) antibodies or recombinant proteins in *Escherichia coli* and (P2) scorpion antivenoms in *Escherichia coli*. The secondary points were: (P3a) process intensification, (P3b) modeling or simulation, (P4a) morphological properties or changes, and (P4b) rheological properties. The searching profiles were coupled as shown in Table I-5.

Research axis	P1	P2
Main axis	Protein in <i>Escherichia coli</i>	Scorpion antivenom in <i>Escherichia coli</i>
Process intensification	P1 + P3a	P2 + P3a

Research axis	P1	P2
Model or simulation	P1 + P3b	P2 + P3b
Morphological properties	P1 + P4a	P2 + P4a
Rheological properties	P1 + P4b	P2 + P4b

Table I-5. Research axis of the bibliographic research methodology

The coupled searching profiles were placed in the advanced search query of each database. The search was made within the fields “Topic”, “Title” and “Keywords” of the database records. The papers published between 1975 and 2019 are comprised in the search. The languages preferred were English, French and Spanish. All the publications within the search queries were subject to quantitative and qualitative analysis to determine their relevance to our research.

I.3. Quantitative analysis of the working database

The search queries were subject to a quantitative analysis, shown in Table I-6. The difference between the searching profile P1 and P2 is notable, where only in the “Topic” field there are over 200,000 articles concerning the production of proteins or antibodies in *E. coli*, compared with only over 800 of articles published concerning the production of venom or antivenom in *E. coli*. This confirms the importance of the bacteria *E. coli* as a workhorse to produce recombinant proteins via biotechnological pathway. The limited amount of publications surrounding the production of venoms or antivenoms in *E. coli* supports the importance of our research.

Main axes	Protein in <i>E. coli</i>				Scorpion venom in <i>E. coli</i>			
	P1				P2			
	WoS	SD	SU	T	WoS	SD	SU	T
Topic	222 101	39 880	268	406	841	332	4	4
Title	19 029	5 329	127	114	46	32	0	0
Keywords	N/A	5 155	N/A	114	N/A	22	N/A	0
Process	P1+P3a				P2+P3a			
intensification	WoS	SD	SU	T	WoS	SD	SU	T
Topic	17 101	6 112	23	131	47	38	0	0
Title	111	77	6	4	0	0	0	0
Keywords	N/A	100	N/A	1	N/A	0	N/A	1
Model or simulation	P1+P3b				P2+P3b			
	WoS	SD	SU	T	WoS	SD	SU	T
Topic	35 461	4 245	7	147	129	17	0	0
Title	269	73	4	8	0	0	0	0
Keywords	N/A	88	N/A	0	N/A	0	N/A	0
Morphological properties	P1+P4a				P2+P4a			
	WoS	SD	SU	T	WoS	SD	SU	T
Topic	18 263	3 306	31	36	55	23	0	1
Title	179	30	0	0	0	0	0	0
Keywords	N/A	N/A	N/A	0	N/A	3	N/A	0
Rheological properties	P1+P4b				P2+P4b			
	WoS	SD	SU	T	WoS	SD	SU	T
Topic	667	93	1	343	0	0	0	0
Title	1	0	0	3	0	0	0	0
Keywords	N/A	0	N/A	2	N/A	0	N/A	3

Table I-6. Quantitative results of the bibliographic research. WoS: Web of Knowledge (Clarivate Analytics), SD: Science Direct (Elsevier), SU: Sudoc (Theses, France), T: Thèses.fr (Theses, France), N/A: not available.

The query results were classified according to the number of articles on the query: queries with over 300 papers were not analyzed due to its large scope, the articles on the remaining of the queries (yellow and green dots in Table I-6) were analyzed and duplicated papers were eliminated.

In average for the P2 queries, P3a, P3b and P4a represent about 25% of the total articles found in Web of Knowledge and Science Direct, this set out interesting points to be explored. The search query P2 + P4b did not show any results, which could indicate that during the production of venoms there is not a limitation in the transfer of oxygen, or it is not a priority for its production.

The evolution of each research axis over the years is shown in Figure I-6. The coupled searching profiles of P1 is represented only on the “Title” field, the coupled searching profiles of P2 are represented over the field “Topic”.

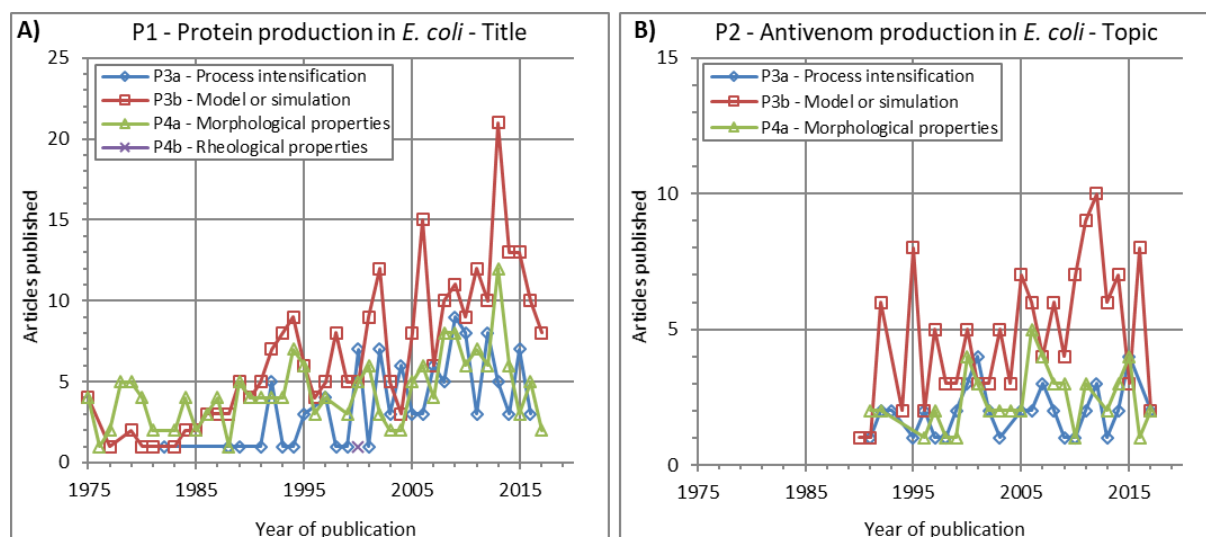


Figure I-6. Number of articles published per year in the main research axis. A) Articles found in P1 queries on search field “Title”, B) Articles found in P2 queries on search field “Topic”.

The tendency of both main research axes is the same but limited in number for the query P2; the focus of the published research is on the modelling or simulation of proteins, followed by the morphological properties of proteins and process intensification. The rheological properties do not appear highly represented on the queries.

The interest in the production of proteins in *E. coli* has increased in the last 15 years and coupled with the few articles published regarding the process intensification of antivenom proteins confirms the importance of our research project.

I.4. Qualitative analysis of the working database

Title, abstract and, in most cases, the article itself was analyzed to determine their relevance to the research axis, and their pertinence to our project. The summary of the relevant articles found in the search queries is shown in Table I-7.

Research axis	P1	P2
Main axis	Antibodies and recombinant proteins in <i>Escherichia coli</i> .	Purification of antivenom/toxins/enzymes in shake flask. Activity and folding of proteins in <i>Escherichia coli</i> .
Process intensification	Enzymes or human proteins produced in shake flasks and bioreactors from 1 to 12 L. Model and/or control for biomass maximization in fed-batch cultures.	Purification of antivenom/toxins/enzymes in shake flask. Activity and folding of proteins.
Model or simulation	Production of enzymes or peptides in bioreactors from 1 to 10 L. 3D models of proteins.	Purification of toxins in shake flask and 3D models.
Morphological properties	Formation of inclusion bodies and changes in <i>E. coli</i> due to changes in culture medium.	Purification of antivenom/toxins/enzymes in shake flask and formation of inclusion bodies.
Rheological properties	Motility of <i>E. coli</i> .	No articles found.

Table I-7. Scope of the articles found on the search queries

For the doctoral dissertations found on the French doctoral databases, only the abstract was analyzed but the document was not available online and they were not further used as reference. The doctoral dissertations found on the American databases cover only the production of scorpion peptides for antimicrobial applications.

The resulting working database used for the project consists of 101 articles pivoting the production of recombinant proteins produced in *Escherichia coli*. 59 articles explore the production of recombinant proteins in the periplasm of the cell; in 9 of them the protein has potential antivenom properties for scorpion toxins and is produced in batch mode. 37 articles explore the model and/or control of the culture for the maximization of protein or biomass.

The database was expanded as needed with small search queries in Web of Science, but the core of the research was done using the database obtained from this research methodology.

I.5. Bioproduction of recombinant proteins

Recombinant proteins can be produced in different types of host cells (Table I-8). In the biopharmaceutical industry, mammalian cells (50%), the bacteria *Escherichia coli* (30%) and the yeast *Saccharomyces cerevisiae* (18%) are used as host cells for the expression of recombinant proteins [36], [40].

Strain	Protein	Concentration	Production scale	Reference
<i>Escherichia coli</i>	Fab	0.1 – 100 mg/L	Shake-flask	[73]
<i>Escherichia coli</i>	Nb	1 – 10 mg/L	Shake-flask	[74]
<i>Escherichia coli</i>	Nb	10 mg/L	Shake-flask	[2]
<i>Escherichia coli</i>	F(ab)' ₂	2 g/L	Bioreactor	[73]
<i>Escherichia coli</i>	Fab	60 mg/L	Bioreactor 300 L	[75]
<i>Bacillus megaterium</i>	scFv	4 mg/L	Bioreactor 3 L	[36]
<i>Bacillus subtilis</i>	scFv	9 mg/L	Shake-flask	[36]
<i>Bacillus subtilis</i>	scFv	56 mg/L	Bioreactor 3 L	[36]
<i>Saccharomyces cerevisiae</i>	Nb	100 mg/L	Shake-flask	[2]
<i>Saccharomyces cerevisiae</i>	Nb	1 g/L	Bioreactor 10 L	[2]
<i>Pichia pastoris</i>	Nb	8 – 18 mg/L	Shake-flask	[74]
<i>Pichia pastoris</i>	scFv	1.2 g/L	Shake-flask	[73]
<i>Pichia pastoris</i>	Nb	1 g/L	Bioreactor 1500 L	[74]
Chinese hamster ovary (CHO)	Nb	100 mg/L	Shake-flask	[74]
Chinese hamster ovary (CHO)	mAb	10 g/L	Bioreactor 25 m ³	[43]

Table I-8. Recombinant antibody fragments produced in different host cells.

Mammalian cells, such as CHO, are widely used as expression systems due to their ability to produce correctly folded proteins with low immune response [76]. Unfortunately, the scale-up is difficult and their production is expensive, with the downstream process accounting for about 75% of the total downstream process [43]. They require complex and expensive media, they have low specific growth rates and its genetic manipulation is challenging [41], [76].

Yeast and bacteria hosts are most commonly used due to their low production costs and their ease of genetic manipulation [39]. The yeasts are better for producing correctly folded proteins, performing posttranslational modifications while secreting extracellularly to the medium [77]. Overexpression of proteins in *Saccharomyces cerevisiae* may however cause intracellular accumulation and reduced yields [78].

The gram-positive bacteria *Bacillus* strains have the ability to produce recombinant proteins extracellularly, which allows a cost-effective purification process [36], [60]. However, the

degradation of the membrane can be produced by proteases due to inefficient and slow protein folding [36].

Thus the gram-negative bacteria *Escherichia coli* is the preferred host for microbial expression systems for the production of recombinant proteins [60]. *E. coli* has its entire genome sequenced and it is recognized by drug regulatory authorities for the production of recombinant proteins [79].

I.5.1. Production of recombinant proteins in *Escherichia coli*

The production of recombinant proteins in *Escherichia coli* requires the definition of several key properties of the plasmid and culture conditions to produce a stable protein within the microorganism.

I.5.1.1. Protein secretion mechanism

There are two secretion mechanisms frequently used in *Escherichia coli* strains for the production of recombinant proteins: Type I and Type II (Figure I-7). Type I transports the recombinant proteins in a one-step process through the cytoplasmic and periplasmic membranes and into the culture medium [80]. Type II is a two-step process of secretion of recombinant proteins to the periplasm of the bacteria, in the first step the protein is fully synthesized in the cytoplasm and in the second step the protein is transported through the cytoplasmic membrane into the periplasm, where the protein is folded [81]. The use of each secretion mechanism depends on the type of recombinant protein to be produced and the desired purification method.

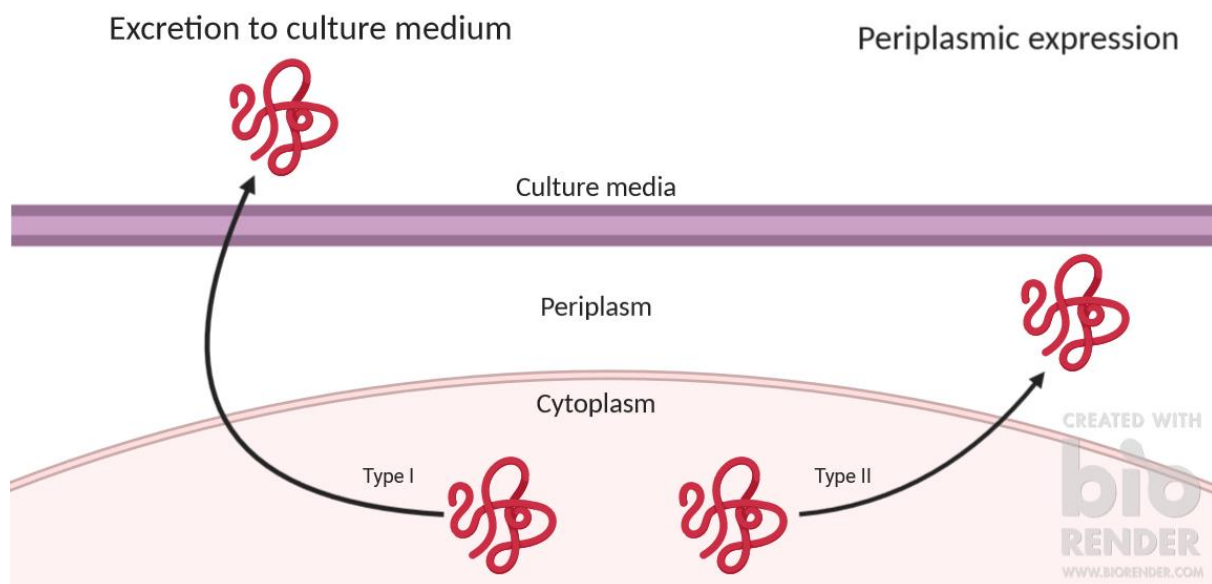


Figure I-7. Recombinant protein secretion mechanisms. Image created with Biorender.com.

I.5.1.1.1. Excretion to medium

Excretion to the culture medium (type I) is used for high-molecular-weight toxins or enzymes, it produces partially folded molecules with low protein translation [81]. This mechanism can produce recombinant protein up to 5% of total cell protein [80].

Although the secretion of proteins to the medium is an advantage for the downstream process, it has been reported that in large-scale production antibody fragments become unstable in solution, rendering critical the downstream process to minimize product loss [82].

I.5.1.1.2. Periplasmic expression

Excretion to the periplasm (type II) is most commonly used for recombinant proteins, where the disulfide bonds can be formed properly in the oxidizing environment of the periplasm [42], [83]. This mechanism allows recombinant protein yields from 0.3% to 3.8% of total cell protein [80].

Permeation of the outer membrane by osmotic shock allows the recovery of the periplasmic proteins without the cytoplasmic proteins [84]. The release of periplasmic proteins can occur accidentally by difference of osmotic pressure due to the accumulation of protein in the periplasm or by lysis in older cultures [81].

I.5.1.1.3. Inclusion bodies

The overexpression of recombinant proteins in *E. coli* can induce the formation of inclusion bodies [80]. Inclusion bodies (IB) are composed of aggregates of unfolded or misfolded proteins [75]. IB are formed in the cytoplasm of the microorganism due to limited solubility and lack of appropriate folding systems [77], although it has been reported the formation of IB in the periplasm [83].

At industrial scale, IB can be isolated after cell disruption and centrifugation, and stored frozen for several months [77]. The IB require re-solubilization and refolding of the target protein to achieve biological activity for therapeutic applications [40].

I.5.1.1.2. Protein inducer

Protein expression can be enabled with the use of promoters. In *E. coli* the well-known *lac* promoter is the most commonly used to regulate the expression of recombinant proteins [85].

Induction under the *lac* promoter can be done using lactose [86]–[89]. If glucose and lactose are present in the medium, the *lac* promoter will not enable the expression of the protein until depletion of glucose [90]. The induction is usually triggered with isopropyl β -D-thiogalactopyranoside (IPTG), a non-hydrolyzable analog to lactose which is not metabolized by the cell [85], [90].

IPTG is commonly used at a rate of 1 mmol/L for intracellular recombinant proteins, and between 0.01 and 0.1 mmol/L for proteins excreted to the culture medium [85]. Metabolic burden can result when using high concentrations of inducer, and care should be taken when trying to optimize product yield of the recombinant protein [40], [85].

Expression can be enabled with other kind of promoters, such as arabinose-induced [91], [92], temperature-induced [93]–[95], methanol-induced [96] and anhydrotetracycline-induced [97] promoters.

I.5.1.1.3. Selection marker

To avoid the presence of plasmid-free cells, the use of an antibiotic and the corresponding resistance gene is coded into the plasmid [79]. The ampicillin-resistance gene is most commonly used in *E. coli* strains [90]. Other antibiotics used in *E. coli* strains as selection markers are: kanamycin [98]–[107] and chloramphenicol [108]–[110].

I.5.1.1.4. Purification

The purification of recombinant proteins for biopharmaceutical applications includes the removal of impurities, for example: compounds of culture media, host cell components and product variants or isoforms [111].

Recombinant proteins can be produced with an affinity tag, which will allow the recovery of the protein in a one-step process [90]. The use of the hexa-histidine tag (His₆-tag) is widely used in proteins produced in *E. coli*. His₆-tagged proteins can be readily purified by immobilized metal affinity chromatography (IMAC) using Cu²⁺, Ni²⁺ or Zn²⁺ metal ions [112].

To increase the solubility of the protein, fusion partners are used, such as: maltose binding protein (MBP) [107], [113], [114] and small ubiquitin-related modifier (SUMO) [99], [106].

I.5.1.1.5. Culture media

The cultivation of *Escherichia coli* for production of recombinant proteins requires several nutrients to sustain the cell growth, such as carbon source, nitrogen source, essential salts and minerals to reach optimal cell density [75]. Typically, there are three types of culture media: rich medium, semi-defined medium and defined minimal medium.

Lysogeny Broth (LB) is a rich medium used frequently in lab-scale experiments [94], [107], [115]–[118]. It is rich in nutrients and optimal for growth at early log phase, but low cell densities are obtained due to the scarce amount of carbohydrates it contains [90].

To maintain the growth of the microorganism past the log phase and obtain high cell densities, other kind of rich media can be used for the growth of plasmid-bearing cells: Terrific Broth (TB) [4], [119]–[121], circle growth media [114], [122] and 2xYT medium [123]–[125].

Semi-defined media contains a mix of rich components (yeast extract, peptone, tryptone) and chemicals of known identities and concentrations [89], [95], [126]–[130]. Complex and semi-defined media are used in large-scale manufacturing processes for the production of different antibodies [90].

The disadvantage of using complex and semi-defined media lies on the variation batch-to-batch due to the use of complex ingredients [75]. In this case, the use of defined minimal medium becomes an alternative.

Defined minimal medium is composed of known chemicals. M9 medium is a simple defined medium used in lab-scale experiments, but it yields low biomass concentrations [131], [132]. Riesenbergl medium is richer in nitrogen source and yields higher protein concentrations [133]–[135].

The optimization of defined medium components is required to contain all necessary components for the microorganism at the optimal concentrations to avoid growth inhibition [75]. Nitrogen sources, minerals and trace elements are essential for cell growth and are present in most defined minimal media [88], [91], [136]–[140].

I.5.1.6. Culture conditions

To assure optimal production and in addition to the choice of culture medium, physical parameters, such as aeration, pH and temperature should be taken into account. The production of recombinant proteins is made nearly entirely under aerated conditions [141]. In small scale, the use of baffled shake flasks ensures oxygen availability, and agitation speeds range from 100 to 350 rpm [90]. For *E. coli*, protein expression is made at pH around 7, ranging from 6.5 to 7.5 [40].

The optimal growth temperature for *E. coli* is 37°C [85]. For protein expression, this temperature could favor protein aggregation due to hydrophobic interactions inter- and intramolecular [40], [142]. Lowering the induction temperature to 25°C – 30°C could reduce proteolytic degradation and improve the stability of recombinant proteins [75], [85], [142]. Improved folding is also obtained at low temperatures, thus improving the solubility and quality of the recombinant protein [75], [79], [85], [142], [143].

The optimum combination of expression temperature and induction time is still a trial-and-error process [40].

I.5.1.7. Large-scale production

Production of recombinant proteins at industrial scale involves not only knowledge from lab- and pilot-scale cultures for the scale-up, but also knowledge of the purification and downstream processes involved when working with highly engineered proteins.

In the biopharmaceutical industry, yields of 2 – 6 g/L of monoclonal antibodies for cancer treatment and inflammatory diseases are routinely achieved in 25 m³ bioreactor cultures of mammalian cells [41], [43], [78]. Up to 10 g/L of V_HH can be produced in 1.5 m³ bioreactors of *Pichia pastoris*, used for bone-related diseases (www.ablynx.com).

I.5.1.7.1. Cultivation processes

Fed-batch cultures is used to achieve high cell density cultures (HCDC, >40 g cdw/L) by maintaining the nutrients to control the cell growth and reach high protein productivity [72]. Cell growth can be

optimized by controlling the carbon source and physical parameters, such as temperature, pH and dissolved oxygen (DO), at minimum [77].

To achieve HCDC, different feeding strategies have been developed: pH-stat control [134], DO-stat control, constant feeding [135], [144] and specific growth rate controlled feeding [145]–[148].

In pH-stat control, the substrate feed is coupled with the ammonia feed used for pH control and activated at the same time. In DO-stat control, the DO is used as the parameter to control the substrate feed and keep strict aerobic conditions [72], keeping the DO above or at a desired value.

The substrate feed can be kept constant or be exponential to impose a fixed specific growth rate. Ideally, with a constant feed, the total biomass will grow linearly and specific growth rate will decrease during the culture, whereas with an exponential substrate feeding high productivities can be achieved in less process time [72]. However, specific growth rate during fed-batch cultures should be kept lower than a specific critical growth rate to avoid the production of inhibitory sub-products, such as acetate [75], in the case of *E. coli* cultures.

In aerated cultures, additional to the feed strategy, oxygen transfer from the culture medium to the microorganism plays a critical role. The maximal biomass achievable of the culture depends on an optimal oxygen transfer in the bioreactor.

Scale-up of bioprocesses starts from lab-scale fermentations (1 – 20 L) and increased in a ratio 1:10 to pilot scale (30 – 500 L) and then industrial scale (>1000 L), optimizing conditions in each scale [40]. The common criterion for scale-up bioprocesses is to keep some parameters constant. The parameters used are impeller tip velocity (V_{tip}), oxygen transfer rate (OUR), oxygen volumetric mass transfer coefficient (k_La), power input per unit volume (P/V) and impeller's Reynolds number [40]. For *E. coli* fermentations, the best criteria is to keep constant the volumetric mass transfer coefficient (k_La) or the oxygen transfer rate [149].

1.5.1.7.2. Downstream process

Downstream processing accounts for 50% to 90% of the overall processing costs and it plays a big role for the economic viability of some recombinant protein production processes [82], [144]. For pharmaceuticals, the development of up- and downstream processes is generally conducted in parallel due to the tight speed to market timelines [111].

Downstream process involves primarily three steps: cell recovery, protein recovery and refolding, and purification. Each process depends on the nature of the recombinant protein, the production host and mechanism of production and affect the recovery yield and purity [126].

During cell recovery, the cells are separated from the fermentation broth by centrifugation, depth filtration, tangential flow filtration or microfiltration [43].

In general, at industrial scale, proteins are produced either in the periplasm of the microorganism or as inclusion bodies. Osmotic shock is used for the recovery of periplasmic proteins and cell disruption by high pressure homogenization and bead mill is used to recover the inclusion bodies [40], [77].

Inclusion bodies need to be solubilized and refolded to obtain biologically active proteins for pharmaceutical applications [126]. Denaturing and reducing agents are commonly used to solubilize the inclusion bodies [40]. The formation of disulfide bonds in IB can be initiated with oxygen or a mixture of reducing and oxidizing agents [77]. Protein refolding is not needed for periplasmic recombinant proteins [81].

Affinity chromatography is the method of choice to obtain high purity recombinant antibodies [82]. The tags and fusion partners need to be eliminated from the recombinant protein by enzymatic or chemical cleavage [90].

Further purification is made by polishing of the protein with size exclusion chromatography, where trace impurities are removed, such as host cell proteins and solubilizing and refolding agents. Finally, virus clearance and pharmaceutical formulation assures long stability and preserves bioactivity of the protein [43].

I.5.1.8. Emerging pharmaceutical applications of recombinant proteins

Recombinant proteins produced for the biopharmaceutical process have multiple applications; in our research we came across some emerging venom-derived proteins produced in *Escherichia coli*, a few of them are shown in Table I-9.

Some recombinant toxins and enzymes are produced in shake-flasks via the periplasm of the cell [99], [115], [150] or most commonly as inclusion bodies [98], [100], [117], [151]–[153] with high yields.

The snake venom toxins have been investigated to create new anticoagulating agents, or to use the damaging properties of some toxins for tumor treatment [109], [150].

The production of antivenoms and anti-allergens from the venom toxins has also been investigated for treatment of snake bites and bee's and wasp's stings [100], [115], [117].

Strain	Protein	Concentration, mg/L	Application	Reference
<i>E. coli</i> BL21 (DE3)	7 kDa cardiotoxin of <i>Naja naja atra</i> snake	40	Hemolytic activity	[151]
<i>E. coli</i> BL21	14 kDa toxin of <i>Crotalus adamanteus</i> snake	1	Antitumor	[150]
<i>E. coli</i> BL21 (DE3)	14 kDa toxin of <i>Bothrops jararacussu</i> snake	5	Membrane-damaging activity	[109]
<i>E. coli</i> BL21 (DE3)	27 kDa enzyme of <i>Gloydius shedaoensis</i> snake	N. A.	Anticoagulating agent	[153]
<i>E. coli</i> BL21 (DE3)	30 kDa enzyme of <i>Gloydius halys</i> Pallas snake	46	Anticoagulating agent	[152]
<i>E. coli</i> BL21 (DE3)	48 kDa enzyme of <i>Agkistrodon contortrix laticinctus</i> snake	16	Anticoagulating agent	[98]
<i>E. coli</i> BL21	20 kDa enzyme of <i>Deinagkistrodon acutus</i> snake	57	Snake antivenom	[100]
<i>E. coli</i> BL21	25 kDa toxin of <i>Vespa vulgaris</i> wasp	15	Wasp antivenom	[117]
<i>E. coli</i> XL-1 Blue	55 kDa enzyme of <i>Apis mellifera</i> bee	50	Bee antivenom	[115]
<i>E. coli</i> BL21 (DE3)	24 kDa enzyme of <i>Loxosceles intermedia</i> spider	2	Anticoagulating agent	[99]
<i>E. coli</i> BL21 (DE3)	4.7 kDa toxin of <i>Conus marmoreus</i> snail	5.9	Analgesic	[154]

Table I-9. Pharmaceutical applications of venom-derived recombinant proteins. N. A.: not available.

I.5.2. Bioproduction of scorpion toxins and antivenoms

Recombinant toxins and toxin-neutralizing antibodies produced in microbial hosts give new options to the biopharmaceutical industry. Providing better bioactivity, higher efficacy or alternate delivery route, these new pharmaceuticals contribute to the next-generation pharmaceuticals.

I.5.2.1. Scorpion toxins

The production of scorpion venom through the conventional route requires either a lot of time or a high quantity of scorpions removed from their ecosystem to obtain high quantities of venom [65]–[67].

Scorpion toxins used for immunization purposes can be produced in *Escherichia coli* with little to no effect of toxicity on the immunized animal (Table I-10).

Strain	Scale	Concentration, mg/L	Protein	Specificity	Reference
<i>E. coli</i> HB101	Bioreactor 5L, fed-batch 0.3 h ⁻¹	1	24 kDa IgG-fusion toxin of BotI, BotII, BotIII and BotXI	<i>Buthus occitanus tunetanus</i> BotI toxin and BotG-50	[155]
<i>E. coli</i> HB101	Bioreactor 5L, fed-batch 0.3 h ⁻¹	16-18	7 kDa IgG-fusion toxin of BotXIV and LqhαIT	<i>Buthus occitanus tunetanus</i> and <i>Leiurus quinquestriatus hebraeus</i>	[156]
<i>E. coli</i> DH5α	Shake-flask	40	47 kDa MBP-fusion toxin of AahI, AahII and AahIII	<i>Androctonus australis hector</i>	[114]
<i>E. coli</i> BL21	Shake-flask	N. A.	21 kDa Cn2 and Css2 toxins	<i>Centruroides noxius</i> and <i>Centruroides suffusus</i>	[157]

Table I-10. Strains producing toxins for antivenom production. N.A.: not available.

The recombinant toxin BotXIV can be used to produce an anti-BotXIV serum, capable of neutralizing *Buthus occitanus tunetanus* scorpion venom in the same capacity than the commercially available equine-derived antivenom without inducing toxic effects in mice [155]. Furthermore, the chimera BotXIVM8-10, produced from BotXIV and the LqhαIT *Leiurus quinquestriatus hebraeus* scorpion toxin, showed properties comparable to α-toxins [156].

Fusion proteins of the toxins Aah I, Aah II and Aah III of the *Androctonus australis hector* scorpion and MBP were able to recognize and neutralize the native toxins in rabbits, and the immunization in rabbits conferred protection against the *Androctonus australis hector* venom without toxic symptoms [114].

The toxins Cn2 and Css2 of the *Centruroides noxius* and *Centruroides suffusus*, respectively, were used on rabbits without showing symptoms of envenomation while producing the antigens against the respective whole venom [157]. Their cross-reactivity was tested against the *Centruroides limpidus* venom resulting in partial protection.

The ability of the scorpion toxins to activate or deactivate the sodium and potassium channels has raised the interest on the extent of their biological activity for therapeutic applications, for example as an anti-tumor, analgesic and anti-inflammatory therapeutic applications, among others (Table I-11).

Strain	Protein	Application	Concentration, mg/L	Reference
<i>E. coli</i> DH5α	4 kDa toxin of <i>Androctonus mauretanicus</i>	K-channel related applications	0.3	[122]
<i>E. coli</i> DH5α	Toxin of <i>Buthus eupeus</i>	Antimicrobial	N. A.	[158]
<i>E. coli</i> BL21 (DE3)	22 kDa toxin of <i>Buthus martensii</i> Karsch	Na-channel related diseases	1.6	[159]

Strain	Protein	Application	Concentration, mg/L	Reference
<i>E. coli</i> BL21 (DE3)	80 kDa toxin of <i>Buthus martensii</i> Karsch	Anti-tumor and analgesic	2.5	[104]
<i>E. coli</i> BL21 (DE3)	7 kDa SUMO-fusion toxin of <i>Buthus martensii</i> Karsch	Anti-tumor and analgesic	24	[106]
<i>E. coli</i> BL21 (DE3)	Toxin of <i>Buthus martensii</i> Karsch	Analgesic and antimicrobial	4.2	[103]
<i>E. coli</i> BL21 (DE3)	27 kDa toxin of <i>Buthus martensii</i> Karsch	Analgesic	5	[107]
<i>E. coli</i> BL21 (DE3)	19 kDa enzyme of <i>Mesobuthus tamulus</i>	Anti-inflammatory	2.8	[160]
<i>E. coli</i> AD494 (DE3)	7.5 kDa β -toxin Cssl of <i>Centruroides suffusus suffusus</i>	Research tool	2	[102]
<i>E. coli</i> KRX	11 kDa peptide of <i>Hottentotta judaicus</i>	Cardiac pharmaceutical	4.5	[161]
<i>E. coli</i> BL21 (DE3)	10 kDa β -toxin of <i>Hottentotta judaicus</i>	Paralysis pharmaceutical	0.3	[97]
<i>E. coli</i> DH5 α	6.5 kDa toxin of <i>Leiurus quinquestriatus hebraeus</i>	Paralysis pharmaceutical	0.5	[105]
<i>E. coli</i> AD494 (DE3)	7.7 kDa toxin of <i>Leiurus quinquestriatus quinquestriatus</i>	Na-channel related diseases	1.5	[110]
<i>E. coli</i> XL1-Blue	30 kDa toxin of <i>Tityus discrepans</i>	Anti-cancer	3.5	[162]

Table I-11. Recombinant scorpion toxins for therapeutic applications produced in *Escherichia coli*. N. A.: not available.

Most of the toxins are produced in *E. coli* with little modification, usually with the addition of the His₆-tag for purification. Some studies analyzed the activity of the expressed toxins to determine their similarity with the native toxin with positive results but without a defined application [110], [122], [159].

The recombinant production of the *Buthus martensii* Karsch scorpion toxins is widely studied for their applications as analgesic and antitumoral bioactivity [103], [104], [106], [107], [159]. It was found that fusing the toxin with a SUMO-tag increased the productivity of the toxin, obtaining up to 40% of the total cellular protein [106].

I.5.2.2. Scorpion antivenom

As shown earlier (Section I.1.4.), the production of antivenoms by the equine system can take up to 15 months without taking into consideration the purification steps required to obtain a functional pharmaceutical.

The production of fully-matured scorpion antibodies can be possible by coding the expression of the antibody in *Escherichia coli*. The model antibodies used for the codification can be obtained from immunization of horses (scFv, Fab) or camelids (V_HH), with the latter being the most used in recent years (Table I-12).

Antibody	Specificity	Concentration, mg/L	Strain	Reference
30 kDa scFv	Subunit Aa1 of the Hemocyanin of <i>Androctonus australis garzonii</i>	N. A.	<i>E. coli</i> HB2151	[125]

Antibody	Specificity	Concentration, mg/L	Strain	Reference
29 kDa scFv 9C2	Aahl toxins of <i>Androctonus australis hector</i>	1-2	<i>E. coli</i> HB2151	[124]
50 kDa scFv-scFv	Aahl toxins of <i>Androctonus australis hector</i>	0.5 – 0.8	<i>E. coli</i> HB2151	[123]
14 kDa V _H H, 29 kDa V _H H-V _H H and 78.5 kDa V _H H	Aahl' toxin of <i>Androctonus australis hector</i>	3, 2 and 1.5	<i>E. coli</i> WK6	[163]
29 kDa V _H H-V _H H	Aahl' toxin of <i>Androctonus australis hector</i>	3.75	<i>E. coli</i> WK6	[4]
29 kDa V _H H-V _H H	Aahl' toxin of <i>Androctonus australis hector</i> and F3 fraction of <i>Australis mauretanicus</i>	N. A.	<i>E. coli</i> WK6	[58]
48 kDa chFab	Cn2 toxin of <i>Centruroides noxius</i> Hoffmann	1	<i>E. coli</i> TOPP2	[101]
14 kDa V _H H	Crude venom of <i>Hottentotta saulcyi</i>	2	<i>E. coli</i> WK6	[121]

Table I-12. Antibodies with neutralizing effects against scorpion venoms. N. A.: not available.

Among the recent antibodies produced by *E. coli*, the antibodies targeting *Androctonus australis hector* toxins are noteworthy and two research groups work actively on it: the Parasitic Immunology and Vaccinology department of Tours University and the Pasteur Institute of Tunisia.

The mouse-derived scFv 9C2 was produced by immunization with the Aahl fraction of the *Androctonus australis hector* scorpion. It had a protective capacity of 0.36 mmol of Aahl toxins per nmol of purified scFv in mice [124]. The production of a diabody scFv-scFv derived from the scFv 9C2 allowed a protective capacity between 102 and 205 LD₅₀ per milligram of diabody in mice, its larger size allows the persistence of the antibody in the host but reduced the ability of the antibody to reach the toxin before it binds to the receptor [123].

Nanobodies have higher neutralization ability than scFv or full antibodies and have easy-folding mechanisms [5]. Their small size and the absence of the Fc region enables a high diffusivity in the body [59]. The nanobodies are the best candidate to produce bi-specific antibodies, defined as next-generation therapeutics [2].

The production of nanobodies in the periplasm of *E. coli* allows the formation of the disulfide bonds in the protein and the cytoplasmic proteins can be avoided during purification steps [63], [74].

The dromedary-derived nanobody NbAahl'22 was obtained after immunization with the AahG50 toxic fraction of the *Androctonus australis hector* scorpion. In mice, the nanobody NbAahl'22, its bivalent format and the parent camelid antibody showed a neutralization capacity of 3 LD₅₀ [163].

The bispecific nanobody NbF12-10 obtained after immunization of dromedaries with AahG50 and Aahl' toxic fractions of the *Androctonus australis hector* scorpion displayed neutralizing abilities against the whole venom. In mice, the NbF12-10 was able to neutralize 13 LD₅₀ of the AahG50 toxic fraction and 5 LD₅₀ of the whole venom. In repeated challenge rescue experiments, full protection was obtained after administering 1.5 LD₅₀ of the venom and no immune response was raised against the therapeutic [4].

The nanobody NbF12-10 showed cross-reactivity when challenged with the *Androctonus mauretanicus* scorpion venom and its toxic fractions F2 and F3 [58]. In a recent conference proceeding this nanobody was produced in a 5 L bioreactor achieving 0.3 mg/L after 4 h of induction at 37°C in minimal medium [164]. The nanobody NbF12-10 shows promising properties as new therapeutic antivenom for treatment of the North African scorpion stings.

The chFab is a mouse-derived Fab, it was able to neutralize the toxin Cn2 of the *Centruroides* scorpion in 90% of the mice tested, and showed total protection against the crude venom of the *Centruroides noxius* scorpion [101].

The nanobody Nb12 was obtained from the camel immunization with the crude venom of *Hottentotta saulcyi* scorpions. Neutralization experiments in mice showed the Nb12 fully neutralized 2 LD₅₀ in mice after incubation with the venom, and in challenge rescue experiments full protection was achieved even when the Nb12 was administered 20 min after toxin injection [121].

The production of all the scorpion antibodies investigated as today is in shake-flask scale with rich medium as culture media, with only one study of bioreactor cultures in MM. The expression on the periplasm of the cell seems to be the best for the production of nanobodies to accomplish active biomolecules. The production of neutralizing-venom antibodies has not been studied at bioreactor scale and further research is needed to increase the production yields in the host *Escherichia coli*.

I.6. Objective of this PhD project

This literature review highlighted the importance of scorpion sting as a public health problem, the difficulties associated with the production of commercial scorpion antivenoms and its limited availability in the neediest areas.

In the biopharmaceutical industry, nanobodies show promising properties for its application in serotherapy for serums targeting the most toxic components of scorpion venom. Nevertheless, the limited number of scientific publications on the production of nanobodies for antivenom productions poses a challenge. The reported final concentration is low (< 4 mg/L [4]), biomass production is not reported, and the production in high cell density cultures has not been studied. Production conditions (temperature of induction and induction time) are still a trial-and-error problem and biokinetics has not been addressed.

The aim of this PhD is to identify the optimal conditions to produce bispecific nanobodies for its application in the pharmaceutical industry as antivenom against scorpion stings of the *Androctonus australis hector* species. The nanobodies are produced as a His₆-tagged periplasmic protein in *Escherichia coli*, and induced by the *lac* promoter.

The scientific strategy lays on the switch of a complex culture medium (Terrific broth) to a defined minimal medium and an identified carbon source (glucose). With this new medium we will be able to draw up mass balances and analyze the biokinetics of the process in batch and fed-batch culture conditions within a strategy of industrial development.

This strategy will allow us to obtain the scientific objectives of this project:

- To select the best strain for cultures in defined minimal medium (MM) and production of the nanobody in defined minimal medium (MM) cultures.
- To accurately quantify the protein produced in the periplasmic space of the strain.
- To study and combine high cell density cultures (~40 g cdw/L) with different protein induction conditions (time, temperature) in 5 L bioreactors.
- To model the production of the nanobody as function of the induction temperature.
- To define a kinetic model to estimate the recombinant nanobody production.

Chapter II. MATERIALS AND METHODS

II.1. Bacterial strains

In our project, three derivatives of the *Escherichia coli* K12 strain, the *Escherichia coli* WK6 were used:

- *Escherichia coli* WK6 wild-type: WK6 wild-type *Escherichia coli* K12 strain { Δ (lac-pro), galE, strA, nal; F' lacIq Δ M15, pro+}.
- *Escherichia coli* WK6/pHEN6/NbF12-10: a clone harboring the recombinant plasmid pHEN6 with cDNA fragment encoding the fragment of the bispecific VHHF12-VHH10 of the NbF12-10 nanobody coming from a VH domain bank of dromedary lymphocytes [4].
- *Escherichia coli* WK6/pHEN6/CH10-12: a clone harboring the recombinant plasmid pHEN6 with cDNA fragment encoding the humanized form of the bispecific VHH10-VHH12 of the CH10-12 nanobody coming from a VH domain bank of dromedary lymphocytes [165].

The strains were obtained from the Therapeutic Molecules and Venom Laboratory of the Pasteur Institute of Tunisia (Laboratoire de Venins et Biomolécules Thérapeutiques, IPT). The recombinant strains produce the nanobody NbF12-10 and its chimeric format, the nanobody CH10-12. The wild-type strain, WK6, is used as a reference on the kinetic analysis of biomass production. For the NbF12-10 strain we used two clones, named NbF12-10 NN and NbF12-10 NO. The difference between the clones is the date of transformation, which were 24/02/2015 and 15/03/2016 for NO and NN, respectively. The second transformation was made due to the suspicion of the loss of the recombinant plasmid in the strain NbF12-10 NO.

The pHEN6 vector derived from the pBR322 (Figure II-1) uses the *lac* promoter to induce the production of the Nanobodies in the periplasmic space of the bacteria as the soluble format and with a hexa-Histidine (His₆) tag. The pHEN6 vector also gives to the strain the resistance to a specific antibiotic (ampicillin).

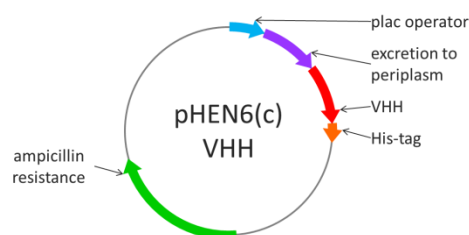


Figure II-1. A schematic representation of the pHEN6 vector used in the *Escherichia coli* WK6 strains

II.2. Bacterial glycerol stock

A bacterial stock was prepared from the strains of the Pasteur Institute of Tunisia (IPT) for their storage at -80°C in single-dose cryovials containing glycerol as cryoprotectant. Two different methods were used, the first using the protocol of the hosting laboratory (Toulouse Biotechnology Institute, TBI), and the second following the instructions of the IPT.

The bacterial stock primarily used was the one prepared following the TBI protocol, the stock prepared with the IPT protocol was stocked as back-up.

II.2.1. TBI protocol

Under sterile conditions, a 100 mL baffled shake-flask containing 15 mL of LB broth and final concentration of 100 µg/mL of ampicillin was prepared and inoculated with a single colony picked up from the LB agar plates using a sterile tip and grown at 37°C and 150 rpm for 12 h in a shaking incubator.

A 500 mL baffled shake-flask containing 45 mL of LB broth and final concentration of 100 µg/mL of ampicillin was inoculated with 5 mL of the inoculum and grown at 37°C and 120 rpm for 12 h in a shaking incubator.

After the incubation, 20 mL of pure glycerol was added to the culture attaining 30% of final concentration of glycerol; 30 sterile Cryotube® vials of 1.8 mL of final volume were filled with the glycerol stock and stored at -80°C.

For each strain this procedure was followed, except for the *Escherichia coli* wild-type were ampicillin was not added to the culture.

II.2.2. IPT protocol

Under sterile conditions, a 100 mL baffled shake-flask containing 15 mL of LB broth and final concentration of 100 µg/mL of ampicillin was prepared and inoculated with a single colony picked up from the LB agar plates using a sterile tip and grown at 37°C and 150 rpm for 12 h in a shaking incubator.

A 1 L baffled shake-flask containing 99 mL of LB broth and final concentration of 100 µg/mL of ampicillin was inoculated with 1 mL of the inoculum and grown at 37°C and 120 rpm for 12 h in a shaking incubator.

After the incubation, 45 mL of the culture were mixed with 15 mL of pure glycerol, attaining 25% of final concentration of glycerol; 27 sterile Cryotube® vials of 1.8 mL of final volume were filled with the glycerol stock and stored at -80°C.

For each strain this procedure was followed, except for the *Escherichia coli* wild-type were ampicillin was not added to the culture.

II.3. Culture media

II.3.1. Inoculum

The inoculum was prepared in a solid phase first in LB agar, and then a liquid phase in LB broth. The compounds in Table II-1, with exception of the ampicillin, were dissolved in distilled water and autoclaved at 121°C for 20 min. Ampicillin was added to a final concentration of 100 µg/mL to the LB agar plates before pouring, and to the LB broth just before inoculation.

Compound	Concentration (g/L)	
	LB agar	LB liquid
Yeast extract	5	5
Tryptone or Peptone	10	10
NaCl	10	10
Agar	15	0
Ampicillin (100 g/L)	0.1	0.1

Table II-1. Composition of the inoculum media

A cryovial was thawed and, using a sterile tip, streaks were made on a LB agar plate with one drop of the cryostock. The plates were incubated at 37°C for 12 h. A 100 mL baffled shake-flask containing 15 mL of LB broth was inoculated with a single colony of the LB agar plate and grown at 37°C and 120 rpm for 12 h in a shaking incubator.

II.3.2. Rich medium (Terrific Broth)

Terrific Broth (TB) was used as the Rich or complex medium (Table II-2). The TB was designed especially for the recombinant *Escherichia coli* strains, allowing for a high plasmid yield and extending the growth phase of the culture [166]. The tryptone and the yeast extract are the source of nutrients, the potassium phosphates act as a pH buffer and the glycerol is added as an additional carbon source.

Compound	Quantity
K ₂ HPO ₄	2.3 g/L
K ₂ HPO ₄ ·3H ₂ O	16.4 g/L
Tryptone or Peptone	12 g/L
Yeast extract	24 g/L
Glycerol (100%)	4 mL/L

Table II-2. Composition of the Terrific Broth

The dry components were dissolved in 900 mL of distilled water. Glycerol was added and distilled water was added to a final volume of 1 L. The solution was autoclaved at 121°C for 20 min.

II.3.3. Defined medium (Minimal Medium)

The defined culture medium or Minimal Medium (MM) was developed especially for the culture of *Escherichia coli* strains by the TBI and up to 30 g/L of biomass can be obtained [167]. The MM must be done in several steps to avoid the precipitation of mineral ions.

II.3.3.1. Trace elements

Each trace element is prepared in a 1000-fold concentrated stock solution (Table II-3). The stock solution was sterilized with a 0.22 µm filter (Sartorius) into a 100 mL penicillin vial crimped and previously autoclaved.

Compound	Concentration (g/L)
MnSO ₄ ·H ₂ O	20
Na ₂ MoO ₄ ·2H ₂ O	4
CoCl ₂ ·6H ₂ O	8
CuCl ₂ ·2H ₂ O	2
ZnSO ₄ ·7H ₂ O	4
H ₃ BO ₃	1

Table II-3. Composition of the trace elements

II.3.3.2. Salts B

The salts B (Table II-4) were prepared in stock solution 1000-fold concentrated, except for the Magnesium sulfate (MgSO₄·7H₂O) which was 500-fold concentrated [167]. The stock solution was sterilized with a 0.22 µm filter (Sartorius) into a crimped 100 mL penicillin vial previous autoclaved.

Compound	Concentration (g/L)
MgSO ₄ ·7H ₂ O	500
CaCl ₂ ·2H ₂ O	40
FeSO ₄ ·7H ₂ O (pH 2)	40

Table II-4. Composition of the salts B

The pH of the Iron sulfate (FeSO₄·7H₂O) solution was adjusted to 2.0 with HCl before filter sterilization.

II.3.3.3. Thiamine (Vitamin B1)

A stock solution of 10 g/L of thiamine (C₁₂H₁₇N₄OS⁺, vitamin B1) was sterilized with a 0.22 µm filter (Sartorius) into a 100 mL penicillin vial crimped and previously autoclaved. The thiamine solution was stored protected from light at 4°C.

II.3.3.4. Salts A

The salts A (Table II-5) were dissolved in distilled water in approximately 75% of the final desired volume [167].

Compound	Concentration (g/L)
----------	---------------------

Compound	Concentration (g/L)
$(\text{NH}_4)_2\text{HPO}_4$	8
K_2HPO_4	8
$\text{Na}_2\text{HPO}_4 \cdot 12\text{H}_2\text{O}$	5.046
NH_4Cl	0.13
$(\text{NH}_4)_2\text{SO}_4$	0.75

Table II-5. Composition of the salts A

A solution of 100 g/L of citric acid was prepared in a volume equivalent to 3/50 of the final desired volume. The trace elements and the salts B were added at 1 mL per liter of final volume in the order shown in Table II-3 and Table II-4. Magnesium sulfate was added at 2 mL per liter.

The citric solution was added to the salts A and pH was adjusted at 6.8 with 28% ammonia. The solution was brought to the final desired volume and autoclaved 20 min at 121°C. Thiamine was added at 1 mL per liter before inoculation.

II.3.4. Glucose solutions

Glucose was used as a carbon source for the cultures in minimal medium (MM) in shake flask and on the batch mode in the bioreactor cultures. A solution of glucose at 300 g/L was prepared in distilled water and autoclaved at 121°C for 20 min. The concentration of the solution was determined after autoclaving by enzymatic analyzer and HPLC. The density of the solution was measured by a densitometer (DE40 density meter, Mettler Toledo) and used for the mass calculations [168].

II.3.5. Ampicillin stock

Due to their antibiotic resistance, recombinant strain cultures were supplemented with ampicillin. A solution of 100 g/L of ampicillin was prepared with 70% ethanol and filter sterilized with a 0.22 μm filter under the laminar flux hood. The solution was stored in 1 mL aliquots at -20°C.

II.3.6. IPTG stock

Isopropyl β -D-1-thiogalactopyranoside (IPTG) was used as the inducer of the *lac* operon for the expression of periplasmic proteins. A solution of 1 M of IPTG was prepared with distilled water and filter sterilized with a 0.22 μm filter (Sartorius) under the laminar flux hood. The solution was stored in 2 mL aliquots at -20°C.

II.4. Shake flask cultures (Batch mode)

The cultures in shake flask were carried out with either rich medium (TB) or defined medium (MM). Biomass production was monitored during cell growth and during protein expression. Protein production was checked at the end of the culture.

TB was supplemented with 1 g/L of glucose, and MM with 10 g/L of glucose. The cultures with the recombinant strains were supplemented with 100 $\mu\text{g}/\text{mL}$ of ampicillin. All cultures were performed in 2 L baffled shake flasks containing 330 mL of culture medium.

II.4.1. Biomass production

The cultures in TB and MM were inoculated with 1 mL of inoculum and carried out at 37°C and 120 rpm in a shaking incubator (Infors HT). Optical density, biomass cell dry weight and residual glucose were monitored until stationary phase was attained.

II.4.2. Protein production

The cultures in TB and MM were inoculated with 1 mL of inoculum and kept at 37°C and 120 rpm in a shaking incubator (Infors HT). Protein expression was induced with 1 mM of IPTG when the cultures reached 0.6 AU in a 10 mm cuvette (or 0.12 AU in a 2 mm cuvette) in TB. Temperature was modified to 28°C in a step change and cultures were kept under agitation for 12 to 16 h.

II.5. Bioreactor cultures (Fed batch mode)

The cultures carried out in a fully instrumented bioreactor and followed three phases: cell growth in batch mode, cell growth in fed batch mode, and induction. Batch and fed-batch mode were conducted at 37°C, induction was carried out at a range of 28 to 37°C, depending on the experiment.

Batch mode was started with 1.5 L of MM at 7.5 to 12.5 g/L of glucose; the inoculation of the bioreactor was made with 100 to 200 mL of inoculum in MM at 5 g/L of glucose. At depletion of glucose, an exponential feed was started, imposing a specific growth rate of 0.38 h⁻¹, which is about half the maximum specific growth rate of *Escherichia coli* WK6 when grown in rich medium.

The production of the recombinant protein started when IPTG was added to the culture during a second fed-batch phase. Protein expression was made with 1 mM of IPTG when biomass reached 21 to 30 g cdw/L (Figure II-2). At induction, temperature was modified (28 to 37°C) and the feed solution rate was set to 4.5 g/h of glucose, which imposed a specific growth rate inferior to 0.05 h⁻¹.

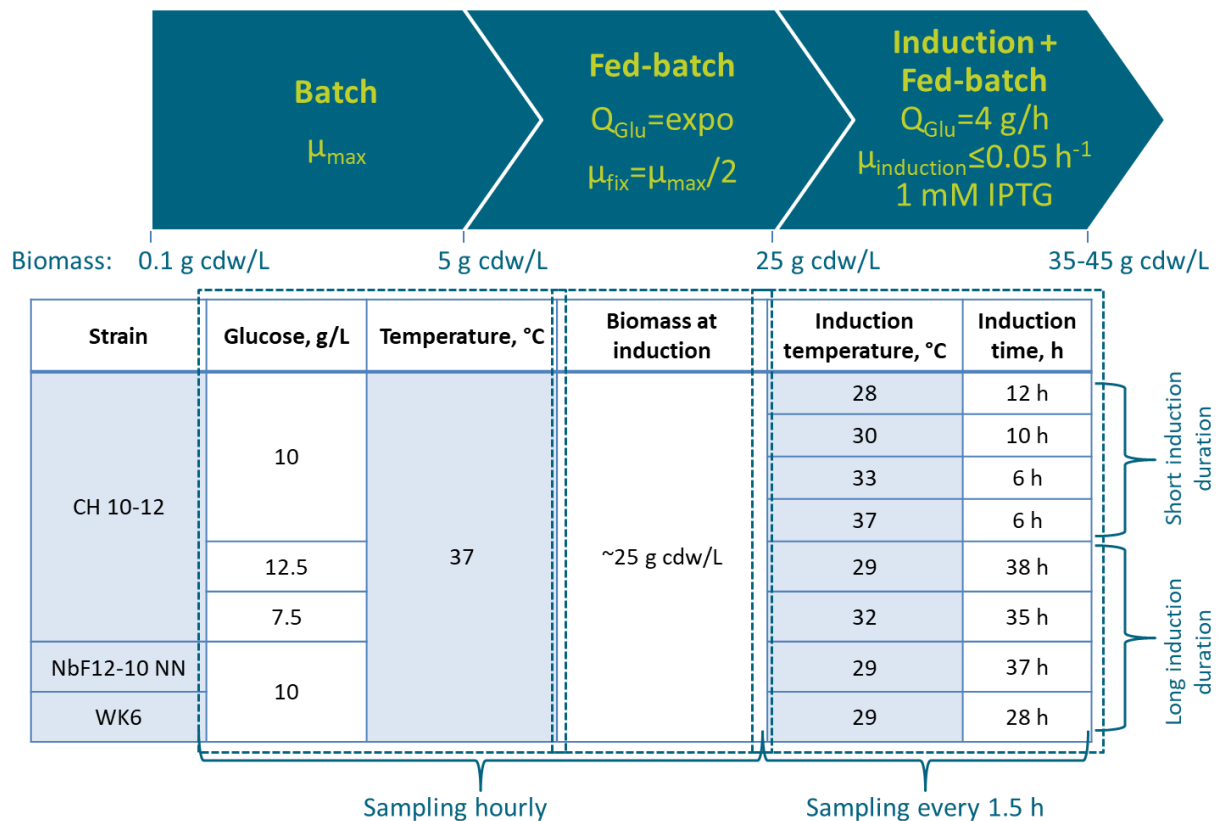


Figure II-2. Schematic of the fed-batch bioreactor cultures.

II.5.1. Instrumentation

The experimental set-up of the cultures in bioreactor is represented in Figure II-3. The bioreactor used in the experiments is a Biostat B-DCU (Sartorius) in borosilicate glass and stainless steel, of 5 L of working volume. The bioreactor is fully instrumented with sensors of dissolved oxygen, pH, temperature, and pressure. The control and monitoring of these parameters are made by the BioPAT MFCS (Sartorius) acquisition system.

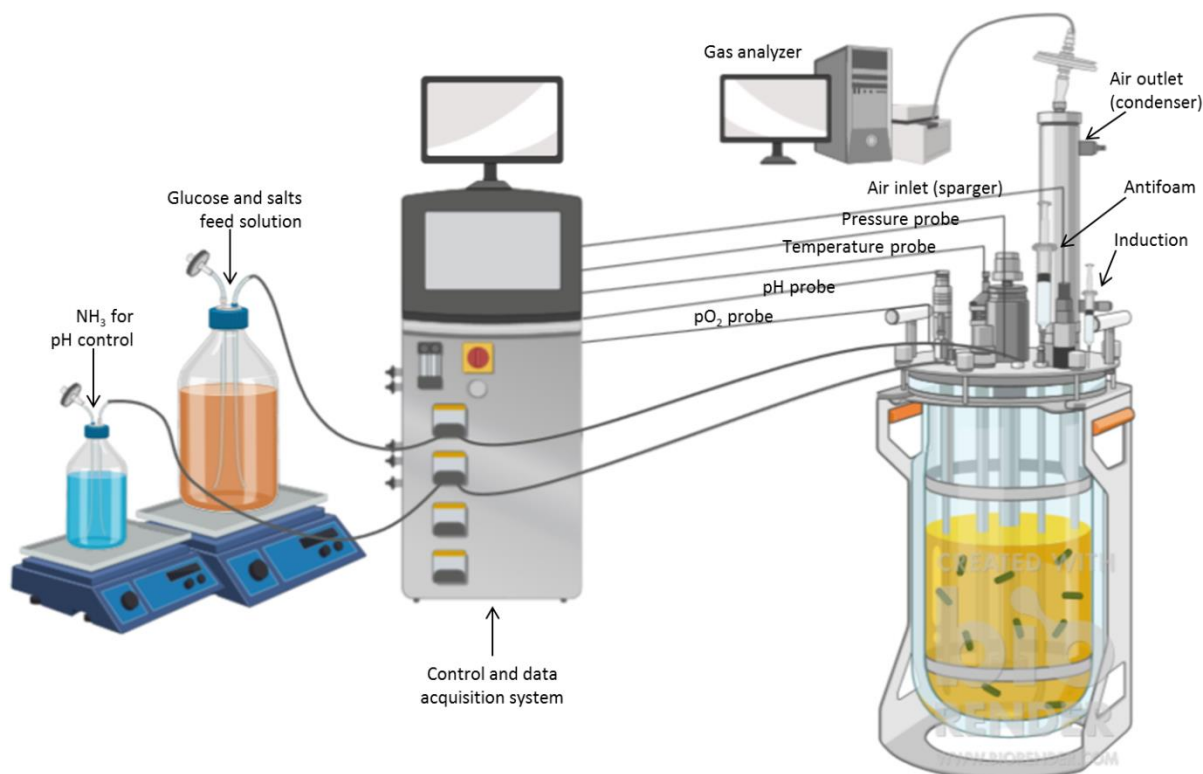


Figure II-3. Schematic of the experimental set-up used in fed-batch cultures in 5 L bioreactor. Image created with Biorender.com

Temperature, pH and inlet gas are controlled by the acquisition system. Temperature was controlled to 37°C for the batch and fed-batch mode by the circulation of water in the external double-wall of the bioreactor. The pH probe (pH 405-DPAS-SC-K8S/325, pH 0-12, 0-130°C, Mettler Toledo) was calibrated with buffer solutions of 4.00 and 7.01 pH (Sigma-Aldrich) before sterilization of bioreactor.

During cultures, the pH was controlled to 6.8 by addition of a solution of 14% w/v ammonia by a peristaltic pump (102R, 1-10 rpm Watson Marlow). The pressure probe was used only to monitor pressure in case of overpressure. The inlet gas was connected to a sparger (maximum 30 NL/min), which injected the air at the bottom of the bioreactor. The outlet gas was passed through a condenser to avoid high rates of evaporation and sent to a gas analyzer.

The stirrer of the bioreactor has a range from 10 to 3000 rpm. The impellers were distributed as shown in Figure II-4. Two six-flat-blade Rushton turbines and a three-blade marine impeller were used in the configuration. During the batch phase the first two impellers are submerged and during fed-batch phase the third impeller is gradually used with the change of volume in the bioreactor.

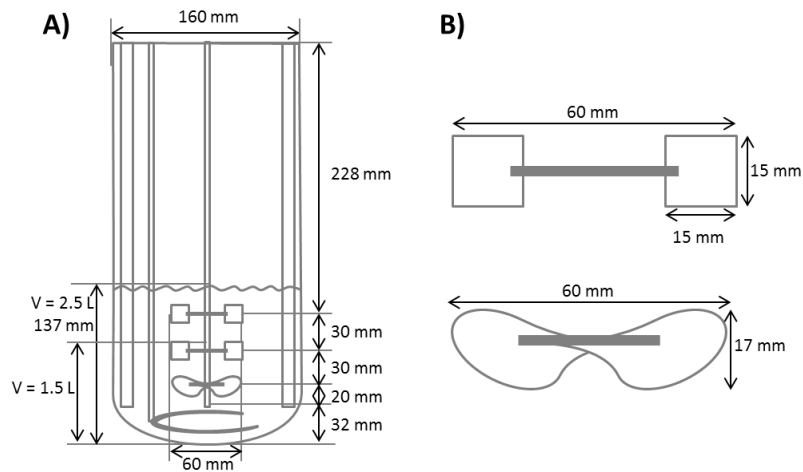


Figure II-4. A) Configuration of stirrer shaft on the bioreactor. B) Dimensions of the impellers

The optical oxygen sensor (InPro 6860i/320, precision 1%, 0-60°C Mettler Toledo) was calibrated before sterilization of the bioreactor with pure nitrogen and air for the 0% and 100%, respectively. To maintain strict aerobic conditions, air inlet and/or agitation were adjusted to increase the transfer of oxygen in the bioreactor when the dissolved oxygen was close to 15%.

The feeding of glucose solution was controlled with the acquisition system (MFCS) and a previously calibrated peristaltic pump (102R, 5-50 rpm, Watson Marlow). An exponential control was programmed in the acquisition system and started at depletion of glucose on the batch phase. During the induction phase, a constant feed was set, equivalent to 4 g/h of glucose.

Antifoam (100% polypropylene glycol P2000, Sigma-Aldrich) and inducer were installed on the top plate of the bioreactor with a sterile syringe. A few drops of antifoam were injected whenever foam was close to the top of the bioreactor to avoid the fouling of the pressure sensor and of the exhaust gas exit. The inducer was taken in a sterile syringe and injected under sterile conditions to the bioreactor at the moment of the induction of protein.

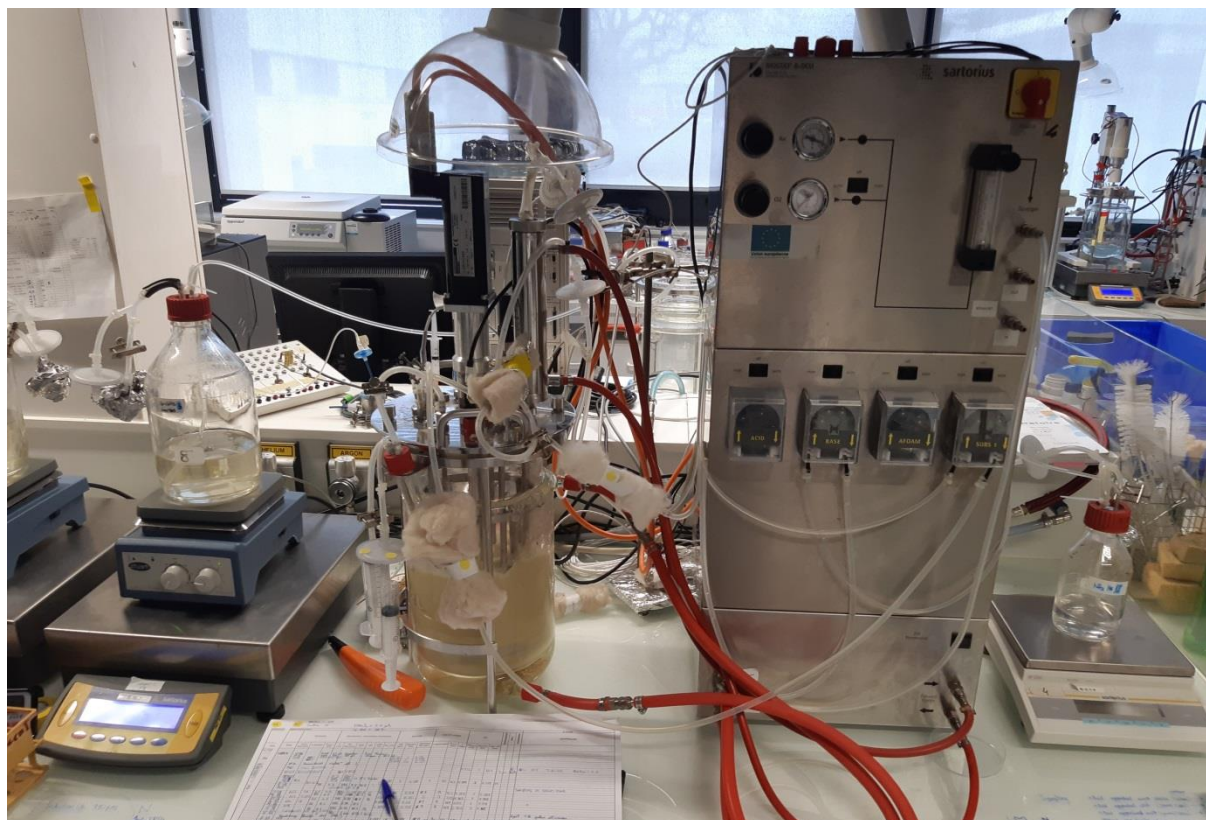


Figure II-5. Experimental set-up: bioreactor with feed solutions

II.5.2. Gas analyzer

In the gas analyzer (INNOVA 1313, Lumasense Technologies) inlet and outlet gas were analyzed for carbon dioxide and oxygen by photoacoustic spectroscopy and magneto acoustic spectroscopy, respectively.

Acoustic techniques for gas measurement are based on the principle that if energy is applied to a gas it will expand and increase pressure. When energy is applied in pulses; pressure will manifest itself as a sound wave, which can be listened by a microphone. The microphone will give an electrical output proportional to the intensity of the pressure fluctuations, which in turn are proportional to the concentration of the gas present.

Carbon dioxide absorbs infra-red light, which is used in the photoacoustic spectroscopy (Figure II-6). Oxygen is not affected by infra-red light, so a magnetic field is used to give pressure fluctuations.

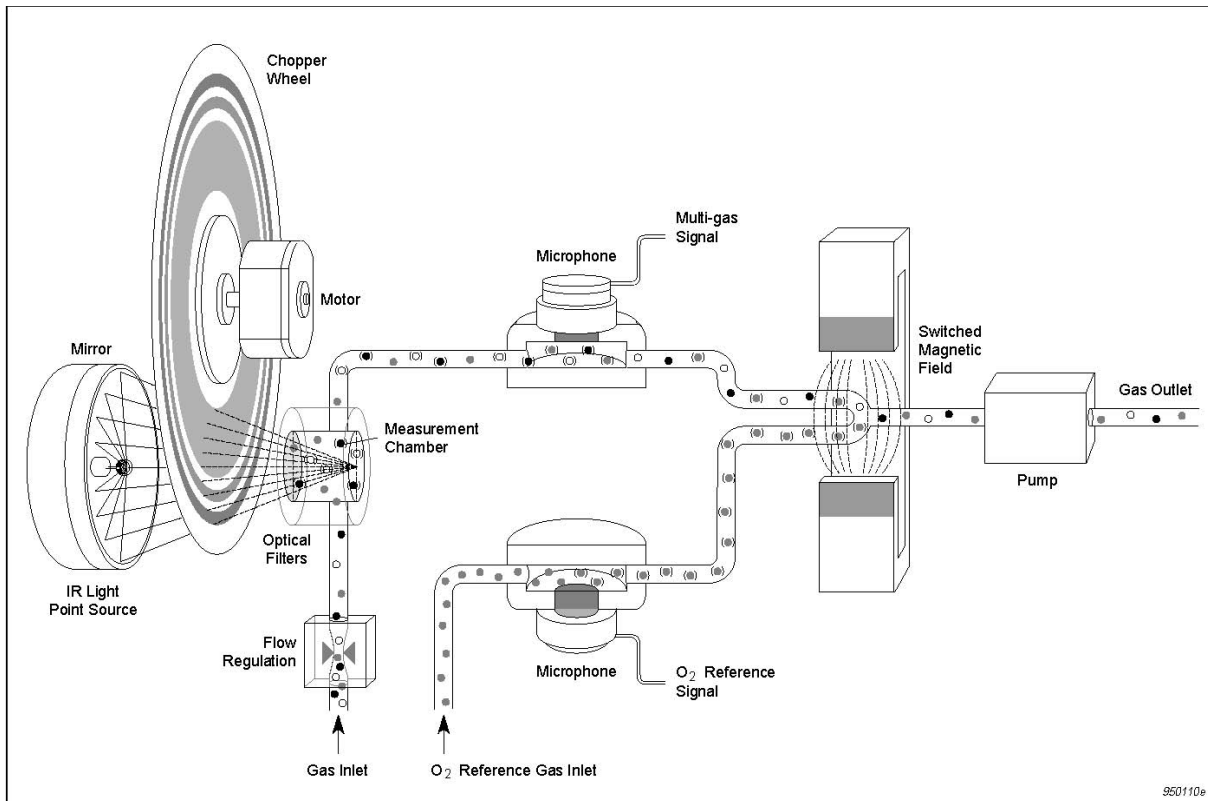


Figure II-6. Schematic representation of the measurement system in INNOVA 1313 gas analyzer.

The gas analyzer requires a minimal flow of 130 mL/min to make the analysis; it was calibrated with a gas of known composition (5% mol/mol CO₂, 10% mol/mol O₂, 85% mol/mol N₂, Air liquide). Carbon dioxide was measured within a range of 0 to 10% mol/mol, and oxygen within the range of 0 to 100% mol/mol.

II.5.3. Bioreactor feed solution

During the fed-batch phase of the bioreactor cultures, the feed solution contained glucose, salts and trace elements to maintain the metabolic needs of the strain. The composition of the feed solution was based on the works of Manon [167], but the concentrations of salts and trace elements were modified to adapt them to a glucose solution of 300 g/L.

For the feed solution preparation, salts and trace elements (from concentrated stock solutions) were added as shown in Table II-6, with exception of thiamine in a glucose solution of 300 g/L. The solution was autoclaved at 121°C for 20 min. Thiamine was added to the feed solution before fed-batch phase was started. The pH was not adjusted to avoid the precipitation of metal ions, and final pH of the solution was 2.4.

Compound	Quantity
Glucose	300 g/L
H ₃ PO ₄ (85%)	0.96 mL/L
K ₂ HPO ₄	3.2143 g/L
Na ₂ HPO ₄ ·12H ₂ O	0.3857 g/L
MgSO ₄ ·7H ₂ O	2.0143 g/L
CaCl ₂ ·2H ₂ O	0.1586 g/L
FeSO ₄ ·7H ₂ O	0.1586 g/L
1000x MnSO ₄ ·H ₂ O	0.45 mL/L
1000x Na ₂ MoO ₄ ·2H ₂ O	0.24 mL/L

Compound	Quantity
1000x CoCl ₂ ·6H ₂ O	0.19 mL/L
1000x CuCl ₂ ·2H ₂ O	1.37 mL/L
ZnSO ₄ ·7H ₂ O	0.031 g/L
1000x H ₃ BO ₃	0.98 mL/L
1000x Thiamine	3.42 mL/L

Table II-6. Composition of the bioreactor feed solution

The feed was controlled by the discretization of the exponential specific growth rate equivalent to 0.38 h^{-1} . It was programmed as a series of linear feeds over 4.5 h (Figure II-7).

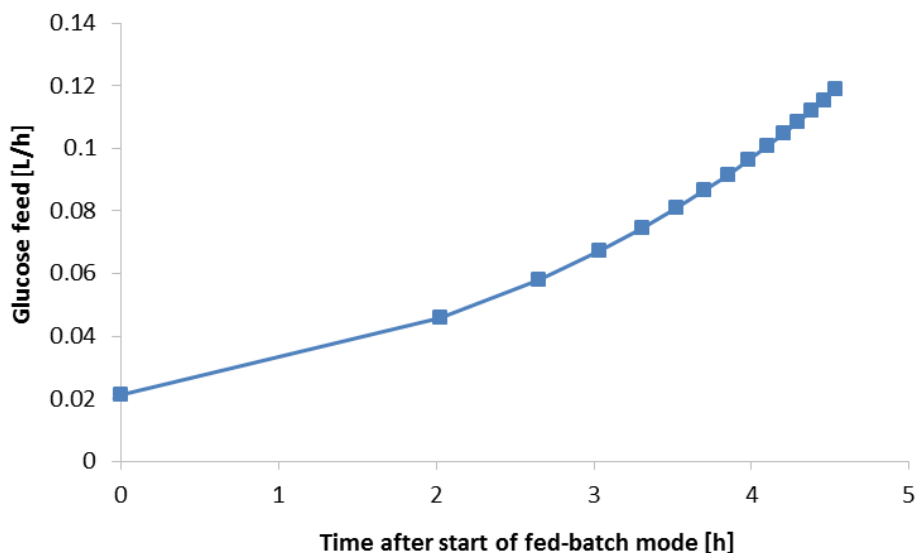


Figure II-7. Discretization of the glucose feed rate for the fed-batch mode.

II.6. Physical and biochemical analyses

II.6.1. Optical density

The spectroscopic absorbance of the cell culture was measured with a spectrophotometer (Biochrom Libra S4) at a wavelength of 600 nm. The readings were made with High quality disposable cells of a light path of 10 mm or with a High precision cell (Hellma Analytics) of 2 mm of light path. Cell culture was diluted with a Microlab 500 (Hamilton) diluter in order to keep the absorbance under 0.5 AU.

II.6.2. Biomass cell dry weight

The biomass in the cell culture was measured by two methods of weight difference: pre-weighted filters and micro centrifuge tubes. Membrane filters of polyamide (Sartolon, Sartorius) of 0.2 μm pore size were dried at 60°C and 266 mbar for 2 days and weighted prior utilization. A defined volume of cell culture (5 to 10 mL) was filtered on the pre-weighted filters and put to dry in an oven at 60°C and 266 mbar for 4 days. Difference of weight of the filter was used for the calculation of cell dry weight.

Micro centrifuge tubes (Eppendorf) of 1.7 mL of total volume were punctured with a needle in the top cap, put to dry in an oven at 60°C and 266 mbar for 2 days and weighted prior utilization. A defined volume of the cell culture (1.4 mL) was put in the pre-weighted micro centrifuge tube and spun down at 12 000 g for 5 min; the cell residue was washed thrice with distilled water. The micro centrifuge tubes were put to dry in the oven at 60°C and 266 mbar for 4 days. Difference of weight of the micro centrifuge tube was used for the calculation of cell dry weight.

II.6.3. Microscopic analyses

Escherichia coli morphology was analyzed through microscopic observations during biomass production and protein expression. The Morphologi G3S Image analyzer (Malvern Panalytical) was used to observe particle size and shape of the bacteria and thus to characterize its morphology.

Samples of the cell culture with an optical absorbance under 0.5 UA were prepared by dilution. One drop was put between a microscope slide and a coverslip and preserved at 4°C. Each microscope slide was analyzed with a Standard Operating Procedure (SOP). The SOP was defined with a threshold of 80, imaged in dark field (episcopic illumination), an exposure of 1000 ms, 100% of the lamp power, magnification with a 20x lens over a surface of 1 mm².

Optical observations of the same samples were made with an optical microscope Eclipse E100 (Nikon). The slides were visualized in bright field (trans-illumination) and a magnification with a 100x lens.

II.6.4. Residual glucose

The residual glucose in the cell culture was measured with an enzymatic analyzer (YSI Model 2700, Yellow Springs Instruments Life Sciences). The enzymatic analyzer uses immobilized oxidase enzymes that in contact with the glucose produce hydrogen peroxide (H₂O₂). The hydrogen peroxide is oxidized at the probe producing a signal current proportional to the concentration of glucose. The range of linearity of the enzymatic analyzer is between 0 and 2.5 g/L of glucose and precision of 0.01 g/L. Samples were kept within this range with the aid of a Microlab 500 (Hamilton) diluter.

II.6.5. HPLC

The residual glucose and organic acid concentrations in the supernatant were quantified by a high-performance liquid chromatography coupled with a photodiode array (UV) and a refractive index (RI) detector (Waters Alliance 2690 HPLC, Waters 996 PDA detector, Waters 2414 RI detector). The retention of glucose and organic acids was made with a column Aminex HPX-87H (Biorad). Glucose can be detected from 0.5 to 50 g/L in the RI detector, and organic acids can be detected from 0.1 to 10 g/L in the RI and UV detectors.

Two standard solutions were prepared containing glucose and acetate at 5 g/L and 20 g/L, and other organic acids at 1 g/L and 2 g/L (Table II-7). The standards were successively diluted to obtain a range from 0.1 g/L up to 20 g/L. Standard solutions and supernatant samples were filtered with a filter 0.22 µm (Minisart, Sartorius) into a vial type 13 x 32 mm with an insert, and put in the sampling chamber of the HPLC at 4°C.

Compound	Standards (g/L)	RI detection	UV detection
Glucose	5, 10, 20	X	
Acetate	1, 2, 5, 20	X	X
Lactate	1, 2	X	X
Succinate	1, 2	X	X
Citrate	1, 2	X	X
Pyruvate	1, 2	X	X

Table II-7. Standards prepared and detection by HPLC.

The mobile phase of the HPLC was a solution of 5 mM H₂SO₄ in deionized water (18.2 MΩ) and filtered with a 0.22 µm filter (Sartorius). The temperature of the column was set to 50°C. The PDA was set at 210 nm and the RI used the mobile phase as reference.

Each analysis took 10 µL of sample and was run for 30 min at a rate of 0.5 mL/min. Samples of filtered deionized water were used at the start, end and every 10 samples to check the baseline of the analysis. The standard solutions were run first to determine the calibration curves and every 20 samples one standard sample was run to check the stability of the analysis.

II.7. Nanobody extraction, purification and quantification

The expression of the protein was induced using IPTG at a final concentration of 1 mM in the culture. Induction was carried out at temperatures from 28 to 37°C for up to 38 h. Periplasmic proteins were obtained by osmotic shock and purification of His₆-tagged proteins was made with affinity chromatography. The purity of the protein of interest was checked with SDS-PAGE. Quantification was made by Nanodrop, Bradford and image densitometry (Figure II-8).

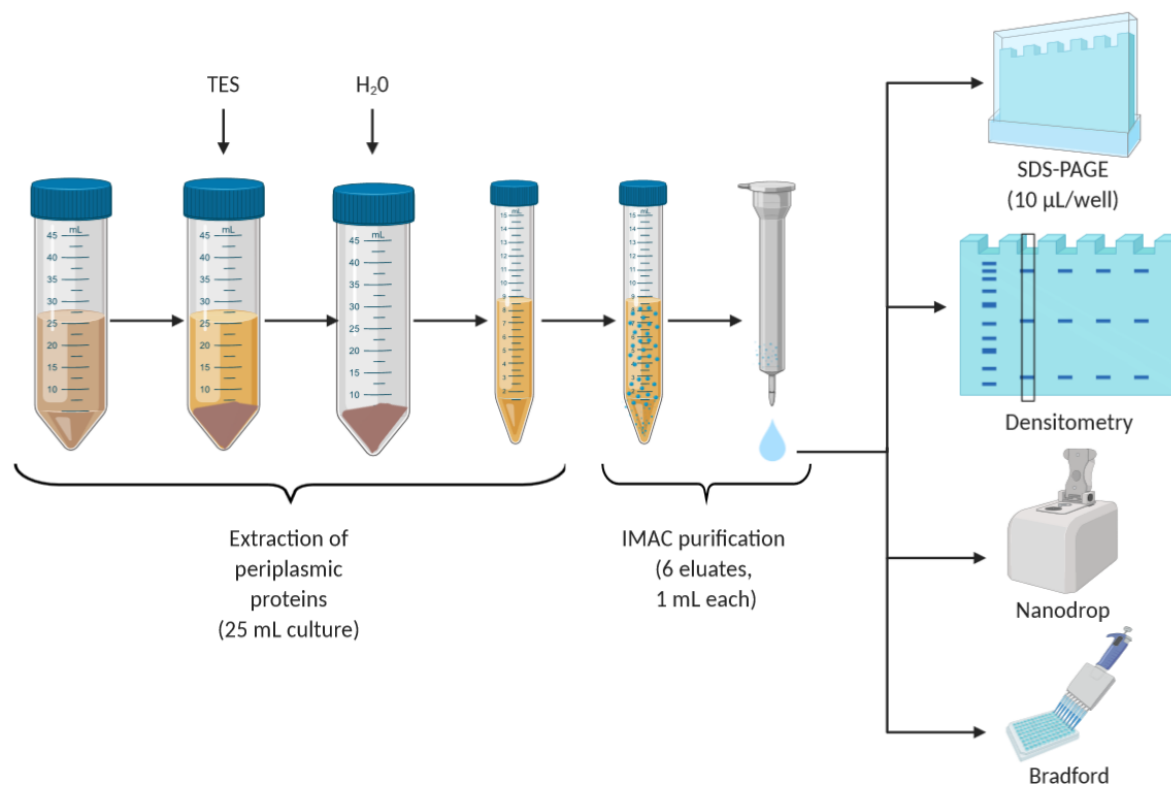


Figure II-8. Extraction, purification and quantification of the Nanobody. Image created with Biorender.com

II.7.1. Osmotic shock

Osmotic shock is used as process for the liberation of the periplasmic proteins [169]. The cells were suspended in a concentrated solution of Sucrose (0.5 M, Merck), EDTA (0.5 mM, VWR Chemicals) and Tris-HCl (0.2 M, Sigma-Aldrich) and incubated for 2 h at 4°C under agitation. Distilled cold water was added to the cells and incubated for 2 h at 4°C under agitation at 350 rpm (Thermomixer confort, Eppendorf, USA). Cells were spun down at 8228 g for 30 min at 4°C and periplasmic extract was obtained.

II.7.2. IMAC

Purification of periplasmic proteins was made with Immobilized Metal Affinity Chromatography (IMAC). Gravity flow PD-10 empty columns (GE Healthcare) were used for the IMAC and the chromatography resin used was the His-select nickel affinity gel (Sigma-Aldrich), with a binding capacity of up to 15 mg/mL of His-tagged protein.

A stock solution of phosphate buffered saline (PBS 10x) was prepared as the mobile phase [71]. The compounds in Table II-8 were dissolved in distilled water and autoclaved at 121°C for 20 min. The mobile phase (PBS 1x) was prepared diluting the PBS 10x in ten parts of distilled water and filtering through a 0.22 µm filter (Sartorius).

Compound	Concentration (g/L)
NaCl	80
KCl	2
KH ₂ PO ₄	2.4

Compound	Concentration (g/L)
Na ₂ HPO ₄ ·2H ₂ O	18

Table II-8. Composition of the PBS 10x stock solution

Imidazole was used as competing agent for the elution of His-tagged proteins [170]. The elution buffer was freshly prepared dissolving the imidazole in the PBS 1x and adjusting the pH to 7.54 with HCl. The solution was filtered through a 0.22 µm filter (Sartorius).

Compound	Quantity
Imidazole	1.7 g
PBS 1x	100 mL

Table II-9. Composition of the elution buffer

The PD-10 columns and the frit were washed with 20% ethanol before assembly of the column. The resin was equilibrated in with three (3) washes of 10 mL of PBS 1x solution, between washes the column was kept in vertical position until decantation of the resin. The washes were discarded.

After the equilibration of the column, the periplasmic proteins were added to the column and incubated under gentle agitation at 4°C for 2 h in a Thermomixer confort (Eppendorf, USA). After incubation, the resin was decanted, the supernatant was recovered and passed a second time to the column until decantation. The supernatant or flow-through obtained after incubation on the column does contain only non-specific proteins.

The column was washed three (3) times with 10 mL of PBS 1x. After the washes, the specific proteins were eluted with 1 mL of PBS + 250 mM imidazole, the resin was decanted, and eluate was recovered. The elution of specific proteins was repeated until 6 elute fractions were recovered.

II.7.3. Protein standards

Three proteins were used as standards for Bradford and densitometry assays: Bovine Serum Albumin (BSA, Sigma-Aldrich, USA) lyophilized powder for gel electrophoresis with a molecular weight of 66 kDa; Albumin from Chicken egg white or Ovalbumin (OV, Sigma-Aldrich, USA) lyophilized powder for gel electrophoresis with a molecular weight of 45 kDa, and Carbonic Anhydrase from bovine erythrocytes (CA, Sigma-Aldrich, USA) lyophilized powder for enzyme analysis with a molecular weight of 30 kDa. The BSA is a cheap, well-known protein commonly used in protein quantification. The ovalbumin (OV) and the carbonic anhydrase (CA) have a molecular weight close to that of the Nanobody.

A protein standard of 10 mg/mL of each protein was prepared by diluting 10 mg of protein in 1 mL of distilled water. A mixture of the proteins was prepared by combining 100 µL of each protein standard in a microcentrifuge tube (Eppendorf, USA) for a final concentration of each protein of 3.3 mg/mL. Successive dilutions were made from this protein mixture and five concentrations were prepared: 0.01 mg/mL, 0.03 mg/mL, 0.06 mg/mL, 0.1 mg/mL and 0.3 mg/mL per protein mixture. All protein standards were stored in aliquots at -20°C until use.

For the SDS-PAGE, the ready-to-use Precision Plus Protein Unstained Protein Standards (Bio-rad, USA) were used as molecular weight marker. The marker contains ten recombinant protein bands of 250, 150, 100, 75, 50, 37, 25, 20, 15 and 10 kDa.

According to the manufacturer, the protein bands of 75, 50 and 25 kDa are reference markers within the molecular weight marker, as they are three times the intensity of the other bands. Similarly, for a 10 µL lane of molecular weight marker, the band of 50 kDa has 750 ng of protein, and the bands of 20 kDa and 100 kDa have 150 ng of protein, each. The nature of the recombinant proteins in the molecular weight marker is not described by the manufacturer.

II.7.4. Gel electrophoresis

Sodium Dodecyl Sulfate Polyacrylamide Gel Electrophoresis (SDS-PAGE) was used for the identification and determination of molecular weight of the protein of interest. The samples are prepared using Laemmli buffer (Biorad) with β -mercaptoethanol (Sigma-Aldrich) as a denaturing agent. The samples were prepared a ratio of 1:1 of sample and Laemmli buffer solution and heated for 5 min at 90°C. Precast Mini PROTEAN TGX Stain Free gels Any kD (Biorad) were loaded with 10 μ L of loading sample per well and Unstained Precision Plus Protein Standards (Biorad) were used as molecular weight markers.

SDS-PAGE was performed at 200 V for 30 min using TGX 1x running buffer (Biorad). After the electrophoresis, the gels were stained for 1 h in Instant Blue (Expedeon) and imaged with a Quantity One image analyzer (Biorad) on bright field and on Hi sensitivity UV light.

For each gel, a calibration curve was prepared correlating the molecular weight of each protein standard band versus the migration distance of each band (R_f), according to the method described by Biorad.

$$R_f = \frac{\text{distance to the band}}{\text{distance to the migration bottom}} \quad (\text{II-1})$$

The molecular weight (MW) of the protein of interest was determined using the linear correlation between the relative mobility of the proteins and the molecular weight.

$$\log MW = \text{slope} * R_f + b \quad (\text{II-2})$$

II.7.5. Nanodrop (Absorbance)

The NanoDrop 1000 Spectrophotometer (Thermo Scientific) was used for the measure of spectroscopic absorbance of 2 μ L protein samples. The detection limit of the Nanodrop is 0.10 mg/mL to 100 mg/mL, and an accuracy of ± 0.10 mg/mL in the range from 0.1 to 10 mg/mL, and 2% for samples above 10 mg/mL.

The absorbance was measured at a wavelength of 280 nm and expressed at an equivalent path length of 10 mm. Protein concentration was calculated from the Beer-Lambert law using the percent extinction coefficient ($\epsilon_{1\%}$).

$$C = \frac{A_{280}}{\epsilon_{1\%} l} \quad (\text{II-3})$$

The extinction coefficient of the Nanobody NbF12-10 was calculated from its amino acid content and equal to 1.62 [165]. Depending on the analyzed sample, RNA-free water, PBS 1x or PBS + 250 mM imidazole were used as blank.

II.7.6. Bradford Assay (Absorbance)

The Bradford Assay is a colorimetric analysis that uses the Coomassie Brilliant Blue G-250 dye as a reagent to measure the quantity of protein present in the sample. The Coomassie blue binds to the protein, turning blue and causing a shift in the absorption of the dye at 595 nm [171]. The assay can be prepared for two detection limits: from 1 to 10 μ g/mL with the micro assay, and 0.1 to 1.4 mg/mL with the standard assay.

The protein used as standards were bovine serum albumin (BSA), carbonic anhydrase (CA) and ovalbumin (OV). Two protein standards were prepared for micro and standard assays, using as diluent distilled water, PBS 1x or PBS + 250 mM imidazole.

For the standard assay, 4 μ L of protein standard or sample were poured per well in a 96-well plate, and 200 μ L of Bradford reagent (Sigma-Aldrich) were added. For the micro assay, 100 μ L of protein standard or sample were poured per well in a 96-well plate, and 100 μ L of Bradford reagent (Sigma-Aldrich) were added.

Each sample was made by triplicate and absorbance was read in a microplate reader (Synergy HT) at 595 nm after 20 min of incubation at room temperature. The net absorbance of the protein standards was calculated using as blank the corresponding diluent. A linear correlation between the protein concentration and the net absorbance gave as result calibration curves of $R^2 \approx 0.9$.

The protein concentration of unknown samples was calculated from the calibration curves and multiplying by the dilution factor of the sample.

II.7.7. Image J (Densitometry)

Images of the SDS-PAGE were analyzed with the ImageJ processing program (v151r Java 1.8.0_131, 64-bit, NIH) with the objective to quantify the protein in the gels by densitometry. The methodology was the subject of an article published on MicrobiologyOpen [172], and it is described in Appendix 2.

II.8. Data treatment

The evolution of any microbial culture is governed by the following set of equations:

$$\frac{dX}{dt} = \mu X - \frac{dV}{dt} \frac{X}{V} \quad (\text{II-4})$$

$$\frac{dS}{dt} = -\frac{\mu X}{Y_{X/S}} + \frac{dV}{dt} \frac{(S_{feed} - S)}{V} \quad (\text{II-5})$$

$$\frac{dV}{dt} = F_S \quad (\text{II-6})$$

Where X is the biomass in Cmol, μ is the specific growth rate in h^{-1} , V is the volume of the bioreactor in L, S is the substrate in Cmol, $Y_{X/S}$ is the yield of biomass on glucose, S_{feed} is the glucose concentration on the feed in g/L, and F_S is the feed rate in L/h.

These equations were used to obtain the kinetic parameters in the batch and fed-batch cultures.

II.8.1. Mass and energy balances

The global mass balance was made over the Carbon element, hence considering substrates and products with Carbon only: biomass, organic acids and carbon dioxide. The global energy balance was determined by the oxydo-reduction (redox) balances over the production and consumption of compounds containing the following elements: carbon, oxygen, nitrogen, and hydrogen.

II.8.1.1. Volume

In a fed-batch culture, volume is a changing parameter dependent of the addition of substrates and removal of samples and evaporation. The reconstitution of volume was made in several steps. First, the theoretical final volume (V_{final} , L) was calculated.

$$V_{final} = V_0 + V_{equivalent} + V_{pH} - V_{sampling} \quad (\text{II-7})$$

Where V_0 is the initial volume in the bioreactor at inoculation, $V_{sampling}$ (L) is the volume of the samples taken during the culture, V_{pH} (L) is the volume added by the pH controlling solution (NH_3) and $V_{equivalent}$ (L) is calculated with the following formulae:

$$V_{equivalent} = V_{H_2O} + V_{X/S} \quad (\text{II-8})$$

$$V_{H_2O} \cdot \rho_{H_2O} = V_{feed} (\rho_{feed} - S_{feed}) \quad (\text{II-9})$$

$$V_{X/S} = a(V_{feed} - V_{H_2O})(1 - Y_{CO_2/S}) \quad (\text{II-10})$$

Where ρ_{feed} (g/mL) is the density of the feed solution, S_{feed} (g/L) is the concentration of glucose in the feed solution, a (l) is the volume correction factor, $Y_{CO_2/S}$ (Cmol CO_2 /Cmol S) is the theoretic yield of glucose converted to CO_2 .

Secondly, Evaporation ($V_{evaporation}$, L) is calculated from the difference between the theoretical final value and the experimental final volume (V_{exp} , L).

$$V_{evaporation} = V_{final} - V_{exp} \quad (II-11)$$

Finally, the theoretical volume (volume without sampling, V^L , L) is calculated for each data point using a dilution factor (Fd) for the correction of volume, using as first value the initial volume of the bioreactor (V_0 , L).

$$Fd = 1 + \frac{dV_{pH} + dV_{equivalent} - dV_{evaporation}}{V_{t-1}^L} \quad (II-12)$$

$$V_t^L = Fd * V_{t-1}^L \quad (II-13)$$

II.8.1.2. Gas analysis

The global balance per gaseous compound can be described by:

$$\frac{d(x^L V_t^L)}{dt} + \frac{d(x^G V^G)}{dt} = Q_{in}^G x_{in} - Q_{out}^G x_{out} + r_i V_t^L \quad (II-14)$$

Where x is the gaseous compound, V_t^L and V^G are the liquid and gaseous volume of the bioreactor in L, Q_{in}^G (mol/h) and Q_{out}^G (mol/h) are the molar air flow entering and leaving the bioreactor, x_2^{in} and x_i^{out} are the molar fractions (%mol/mol) entering and leaving the bioreactor, and r_i (mol/L/h) is the rate of production or consumption of the compound.

II.8.1.2.1. Balance for Nitrogen

Nitrogen is an inert gas, not consumed during the culture and not soluble in water, therefore the accumulation and the rate terms are. So, for the global balance in Nitrogen we have:

$$\underbrace{\frac{d(N_2^L V_t^L)}{dt}}_0 + \frac{d(N_2^G V^G)}{dt} = Q_{in}^G N_2^{in} - Q_{out}^G N_2^{out} + \underbrace{r_{N_2}^L V_t^L}_0 \quad (II-15)$$

This equation allows us to calculate the molar air flow leaving the bioreactor (Q_{out}^G).

II.8.1.2.2. Balance for Oxygen

Oxygen is consumed by the microorganisms on the liquid phase, and its global mass balance is defined by:

$$\frac{d(O_2^L V_t^L)}{dt} + \frac{d(O_2^G V^G)}{dt} = Q_{in}^G O_2^{in} - Q_{out}^G O_2^{out} + r_{O_2}^L V_t^L \quad (II-16)$$

The solubility of oxygen is temperature dependent and it can be obtained through the Henry's law:

$$k_H = \frac{C_i^L}{P x_i} \quad (II-17)$$

Where C_i^L (mol/L) is the concentration of the compound in the liquid phase, P (atm) is the total pressure in the bioreactor and x_i (%mol/mol) is the molar concentration of the compound in the gas phase. Henry's constant, k_H (mol/L/atm), can be calculated from the following formula:

$$k_H = k_H^* e^{c\left(\frac{1}{T} - \frac{1}{T^*}\right)} \quad (II-18)$$

Where k_H^* , T^* and c are constant parameters are described in Table II-10 [173].

Compound	k_H^* (mol/L/atm)	T^* (K)	c (K)
O ₂	1/770	298.15	1700
CO ₂	1/29	298.15	2400

Table II-10. Henry's law constant parameters

The oxygen in the liquid phase can be obtained by:

$$O_2^L = k_H O_2^{*L} P \quad (II-19)$$

Where O_2^L (mol/L) is the concentration of oxygen in the liquid phase and O_2^{*L} (mol/L) is the concentration of oxygen in the liquid phase at saturation, ergo 100% dissolved oxygen.

The rate of consumption of oxygen can be calculated as follows:

$$r_{O_2}^L = \left[\frac{d(O_2^L V_t^L)}{dt} + \frac{d(O_2^G V^G)}{dt} - Q_{in}^G O_2^{in} + Q_{out}^G O_2^{out} \right] * \frac{1}{V_t^L} \quad (II-20)$$

From the oxygen mass balance in the liquid phase, the coefficient of transfer of oxygen can be easily obtained by:

$$K_L a = \frac{r_{O_2}^L}{(O_2^* - O_2^L)} \quad (II-21)$$

II.8.1.2.3. Balance for Carbon dioxide

Carbon dioxide is produced by the microorganisms on the liquid phase; its global mass balance is defined by:

$$\frac{d(CO_2^L V_t^L)}{dt} + \frac{d(CO_2^G V^G)}{dt} = Q_{in}^G CO_2^G - Q_{out}^G CO_2^G + r_{CO_2}^L V_t^L \quad (II-22)$$

The gas is dissociated into carbonic acid in water, and the dissociation is pH dependent. At working culture conditions, the reversible reaction is:



The equilibrium constant of the carbon dioxide (K_{eq}) in water is defined by:

$$K_{eq} = \frac{[HCO_3^-][H^+]}{[CO_2]} \quad (II-24)$$

With $[CO_2]$ (mol/L) being the molar concentration of the carbon dioxide in the liquid phase, obtained through the Henry's law (Table II-10); and $[H^+]$ is the molar concentration of the hydrogen ions in the liquid phase, obtained from the definition of pH (II-26).

$$[CO_2] = k_H P x_{CO_2} \quad (II-25)$$

$$[H^+] = 10^{-pH} \quad (II-26)$$

Therefore, the total concentration of CO_2 in the liquid phase can be defined as:

$$CO_2^L = [CO_2]_{liquid} + [HCO_3^-]_{dissociated} \quad (II-27)$$

$$CO_2^L = [CO_2] + \frac{K_{eq}[CO_2]}{[H^+]} \quad (II-28)$$

$$CO_2^L = k_H P x_{CO_2} \left(1 + \frac{4.45 * 10^{-7}}{10^{-pH}} \right) \quad (II-29)$$

The rate of production of carbon dioxide can be calculated as follows:

$$r_{CO_2}^L = \left[\frac{d(CO_2^L V_t^L)}{dt} + \frac{d(CO_2^G V^G)}{dt} - Q_{in}^G CO_2^G + Q_{out}^G CO_2^G \right] * \frac{1}{V_t^L} \quad (II-30)$$

II.8.1.2.4. Respiratory quotient

The respiratory quotient, or respiratory coefficient, RQ is a dimensionless number that describes the metabolism of a microorganism. In the case of cultures of *Escherichia coli* grown with glucose as carbon source, the respiratory coefficient is expected to be around 1 for biomass production, and

inferior to 1 for production of proteins. It is the ratio of instantaneous rate of production of carbon dioxide to the instantaneous rate of oxygen consumed and is given by:

$$RQ = \left| \frac{r_{CO_2}^L}{r_{O_2}^L} \right| \quad (\text{II-31})$$

II.8.2. Carbon balance

The carbon balance is calculated on each experimental point of the bioreactor cultures. The masses of biomass (X, Cmol) and organic acids (OA, Cmol) produced were calculated as follows:

$$i = C_i V_t^L \quad (\text{II-32})$$

Where i is the mass of the compound in Cmol, C_i is the concentration of the compound in Cmol/L and V_t^L is the theoretical volume of liquid in the bioreactor. The mass of protein is very small and was not taken into account for the mass balances.

The consumption of glucose was calculated as follows:

$$\frac{d(S * V_t^L)}{dt} = r_S V_t^L + F_S S^{feed} \quad (\text{II-33})$$

$$S V_{t_0}^L - S V_t^L = S_{consumed} + S_{added} \quad (\text{II-34})$$

Finally, the global mass balance was verified as:

$$r_S + r_X + r_{CO_2}^L + \sum r_{OA} = 0 \quad (\text{II-35})$$

$$S_{consumed} - X - CO_2^{produced} - \sum OA = 0 \quad (\text{II-36})$$

II.8.3. Redox balance

For the redox balance, the masses produced and consumed are multiplied by the degree of reduction of each compound (γ). The degree of reduction is defined as the number of available electrons per gram atom C. The global redox balance is calculated with:

$$\gamma_S S + \gamma_X X + \gamma_{CO_2} CO_2^{produced} + \gamma_{O_2} O_2^{consumed} - \sum \gamma_{OA} OA = 0 \quad (\text{II-37})$$

II.8.4. Data smoothing

Data smoothing of the glucose consumed, oxygen consumed and carbon dioxide produced was made using a program called LIREC (FAME team, TBI) that fits a polynomial regression in a subset of data using the Savitzky-Golay filter [174]. The result is a series of polynomials that describes the data and provides easy derivatives and integrals. The polynomial fit is degree 3 or 4. Between the polynomial sets, the first and second derivatives are set to be equal to ensure the continuity of the smoothed data.

Biomass and glucose were smoothed with a series of polynomials on subsets of data, usually the different phases of the culture: batch, fed batch and induction. Acetate was smoothed with a series of polynomials over the batch phase.

The objective of the data smoothing is to have access to the rate of reaction of each compound analyzed Table II-11.

C	Variables	Biotic			Abiotic	
	Variable	S	X	P	O ₂	CO ₂
dC/dt	Rate of production/consumption	r _S	r _X	r _P	r _{O2}	r _{CO2}
dC/dt/X	Specific rate	q _S	μ	q _P	q _{O2}	q _{CO2}

Table II-11. Rates of production and consumption of the compounds monitored

II.8.5. Enhancement factor

In a biological process, the oxygen transfer in the liquid phase can be enhanced as a result of the oxygen consumption by the microorganism.

The biological enhancement factor, E , is defined as the ratio of the absorption flux of oxygen in the presence of the microorganism, $K_L a$, to the absorption flux in abiotic conditions under the same hydrodynamic conditions, $k_L a$, and driving force for mass transfer [149], [175].

$$E = \frac{J}{J^0} = \frac{K_L a}{k_L a} \quad (\text{II-38})$$

García Ochoa and Gómez [149], [175], [176] proposed a model to estimate the biological enhancement factor as a function of the mass transfer resistances that describe the oxygen transport in bioreactors (II-39). The model takes into account the resistances by the coefficients of diffusion (D_i) in each layer thickness (z_i) in the layers relative to the cell membrane layer (m) and the liquid layer (L).

$$E = \left[1 + \frac{q_{O_2}[X]_m z_m^2}{2D_m(C^* - C_L)} \cdot \left(1 + 2 \cdot \frac{z_L D_m}{z_m D_L} \right) + \frac{1}{3} \cdot \frac{q_{O_2}[X]_L z_L^2}{2D_L(C^* - C_L)} \right] \cdot \left[\frac{z_L/D_L}{\sum_i z_i/D_i} \right] \quad (\text{II-39})$$

II.8.6. Microscopic observations

The characterization of each microscopic slide was subject to a data analysis on the Morphologi G3S Image analyzer to determine particle size and shape ratios of *Escherichia coli*. To avoid quantification of unwanted particles, exclusion filters were applied to the data set after the measurement was completed. The Morphologi software (version 8.21, Malvern Instruments) was used to apply the exclusion filters.

The physical limitation of the camera resolution was considered as a first filter for the data. The camera of the microscope has a resolution of 2.78 μm per pixel, for the magnification used that leads to a size of 0.14 μm per pixel. Particles with insufficient pixel resolution were excluded using a filter on the Area parameter, to have particles of at least 50 pixels.

The removal of touching particles or agglomerates was taken as the second filter. The parameter of Solidity was used, which is the object area divided by the area enclosed by the convex hull. The convex hull is the border created by an imaginary rubber band wrapped around the object. Touching particles with solidity under 0.9 were excluded.

After filtration of the data, each slide was composed of around 1000 particles, and the statistical analysis of size and shape was done with the Morphologi software.

II.9. Kinetic model of the nanobody production

The kinetics of the specific production rate of the nanobody were established mathematically to study the effect of the temperature. A modified Luedeking-Piret kinetics described the specific production rate of the nanobody, dependent on the specific growth rate and a decoupling factor as a function of the temperature in an Arrhenius-like kinetics as follows:

$$q_{Nb} = -\alpha_{Nb} * \mu_{ind} + \beta \quad (\text{II-40})$$

Where:

$$\beta = \gamma_1 * e^{-Ea_1/T} - \gamma_2 * e^{-Ea_2/T} + \sigma \quad (\text{II-41})$$

With q_{Nb} as the specific productivity rate of the nanobody (mg Nb/(g cdw*h)), μ_{ind} as the specific growth rate at induction (h^{-1}), α_{Nb} as the growth associated parameter (mg Nb/g cdw) and β as the non-growth associated parameter (mg Nb/(g cdw*h)), β as function of the temperature with γ_1 and γ_2 as the pre-exponential constants (mg Nb/(g cdw*h)), Ea_1 and Ea_2 as the activation and inactivation energy for the nanobody production ($^\circ\text{C}$), respectively, and σ as the non-temperature associated parameter (mg Nb/(g cdw*h)).

All parameters were estimated using the function *fmincon* of MATLAB® software (MATLAB® R2019, MathWorks) and experimental data of the strain CH10-12. The objective function used to minimize the sum of the least squares [177] was defined as follows:

$$J(\varphi) = 10 * \min \sum_{i=1}^N \left(\frac{(y_{exp} - y_{model})}{\max(y_{exp})} \right)^2 \quad (II-42)$$

Chapter III. RESULTS

The efficacy of the nanobody NbF12-10 against the neurotoxins present in the venom of the scorpion *Androctonus australis Hector* has been proven at shake-flask scale in rich medium (TB, 28°C, 16 h, [4]). The nature of the nanobody NbF12-10, a 29 kDa camelid V_HH antibody with a size comparable to the scorpion venom toxins makes it the best candidate for serotherapy treatment of scorpion stings [4].

In this work, the two clones of *Escherichia coli* NbF12-10 NN and NbF12-10 NO were cultured in defined minimal medium and rich medium. Their performance was compared with the strain *Escherichia coli* CH10-12 that produces the humanized chimeric format of the nanobody NbF12-10. The unmodified strain *Escherichia coli* WK6 was used as reference strain for comparison of performances.

The production of the recombinant nanobodies NbF12-10 and CH10-12 in *Escherichia coli* was studied to determine the optimal conditions for their production at shake-flask (§III.1) scale and bioreactor scale (§III.3). The effect of the temperature during the induction of the nanobody CH10-12 was studied to obtain the optimal production conditions (§III.2.4). Finally, a kinetic model was proposed to estimate the specific production of the recombinant nanobodies CH10-12 and NbF12-10 (§III.3).

In this study, the following scientific questions will be answered:

- What is the best strain to produce recombinant nanobodies?
- What is the dynamic response of *Escherichia coli* WK6 to a scale-up strategy (from shake flask to 5L bioreactor, from rich medium to defined minimal medium)?
- What are the best culture conditions to achieve maximum protein production in a high cell density culture ($[X] > 25$ g cdw/L)?
- What is the effect of the induction temperature and the induction duration in the production of the nanobody?
- Can the production of the nanobody be indicated by physico-chemical *ex-* and *in-situ* measurements?
- Is there a morphological change in the microorganism during nanobody production?
- Can the effect of the temperature in the nanobody production be mathematically modeled?

III.1. Strain screening

The performances of the reference strain *Escherichia coli* WK6 and the recombinant strains (CH10-12, NbF12-10 NN, NbF12-10 NO) were studied through different approaches:

- (i) The characterization of their specific growth rate in complex (TB) and mineral minimal media (MM) (§III.2.1 – §III.1.2.3).
- (ii) The effect of the different culture media in the yields of biomass and by-products (§III.1.2.4 and §III.1.2.5).
- (iii) The production of the recombinant nanobodies NbF12-10 and CH10-12 in the periplasm of the cell in TB medium (§III.1.3).
- (iv) The study of the shape and size of the cell of the recombinant strains during protein expression (§III.1.4).

III.1.1. Culture study approach

In order to characterize the performance of the strains during biomass production and protein production, a study strategy was defined (Table III-1). Firstly, the characterization of the kinetic parameters in shake-flask is made in both culture media: terrific broth and defined minimal medium. Secondly, the protocol of periplasmic protein extraction was optimized in cultures in terrific broth.

Objective	Culture medium	Strain
Characterization the kinetic parameters at 37°C	Terrific Broth	<i>E. coli</i> WK6
	Defined minimal medium	<i>E. coli</i> CH10-12
		<i>E. coli</i> NbF12-10 NN
		<i>E. coli</i> NbF12-10 NO
Evaluation of osmotic shock protocols for better release of periplasmic proteins	Terrific Broth	<i>E. coli</i> CH10-12 <i>E. coli</i> NbF12-10 NN
Comparison of strains for recombinant nanobody production	Terrific Broth	<i>E. coli</i> CH10-12 <i>E. coli</i> NbF12-10 NN
Characterization the morphology at 37°C, 28°C and during induction	Terrific Broth	<i>E. coli</i> CH10-12

Table III-1. Strategy of study in shake-flask cultures.

Thirdly, the production of the nanobodies CH10-12 and NbF12-10 was compared in cultures in terrific broth. Finally, the effect of the change of temperature on the specific growth rate and the morphology was studied. Each experiment cultured on TB was made by duplicate; the experiments cultured on MM were made by triplicate.

III.1.2. Biomass characterization

The reference strain *Escherichia coli* WK6, the recombinant strains *Escherichia coli* CH10-12 and the recombinant clones *Escherichia coli* NbF12-10 NN and NbF12-10 NO were cultured in terrific broth (TB) and defined minimal medium (MM) as described in §II.4.

The estimation of an accurate concentration of biomass is critical for the calculation of most kinetic parameters. In this project, the biomass was measured by an optical method (§II.6.1) and by difference of cell dry weight (§II.6.2).

In the measure of biomass by micro centrifuge tubes (Eppendorf) of cultures grown in TB, the accumulation of the complex medium could be noted at low biomass concentrations (Figure III-1), even after three washes with distilled water were made. The high concentration of yeast extract (24 g/L) and the low precision of measurement are presumed to be the responsible of these data points.

In the cultures grown in MM, there was no accumulation of the culture medium in the filter or the eppendorf.

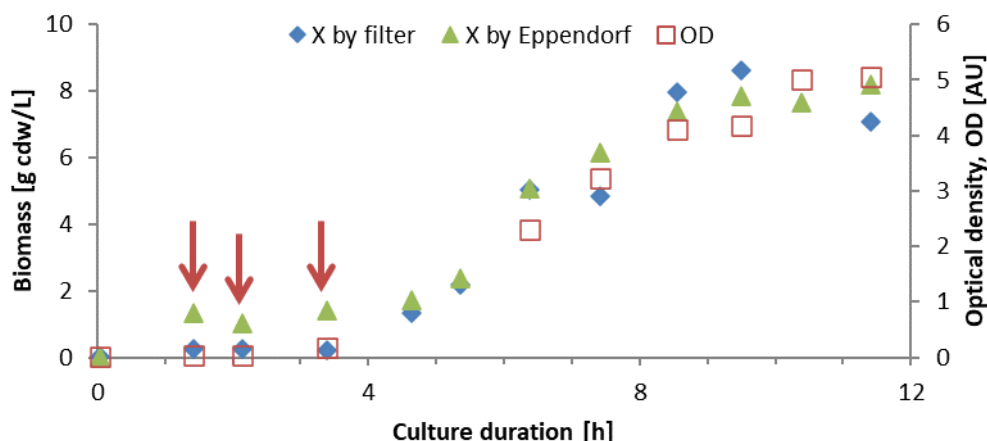


Figure III-1. Evolution of culture of *Escherichia coli* WK6 in TB grown at 37°C, pH 7.2. The red arrows show accumulation of the complex medium (TB) in measures taken in micro centrifuge tubes (Eppendorf) compared with measures taken by pre-weighted filters and optical density measures.

III.1.2.1. Correlation coefficient between different biomass measurement methods

The optical density and the cell dry weight were correlated in the form of the Beer-Lambert law:

$$X = \alpha \cdot OD_{600nm} \quad (\text{III-1})$$

Where X is the biomass cell dry weight in g cdw/L, α is the correlation coefficient in g cdw/L/AU and OD_{600nm} is the optical density in absorbance units (AU).

In average, the correlation coefficient, α , was about 2 g cdw/L/AU for cultures grown in TB and MM (Figure III-2, Table III-2). The cultures of the clone of *Escherichia coli* NbF12-10 NO did not grow in MM, as it will be shown in §III.1.2.2, and the correlation coefficient could not be calculated.

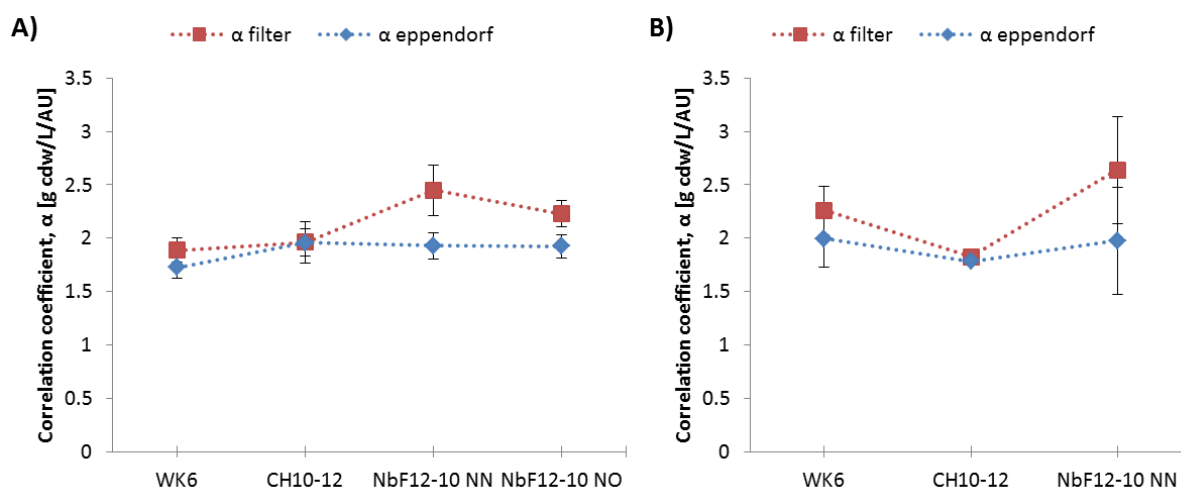


Figure III-2. Average correlation coefficient (α) of strains grown in TB (A) and MM (B).

Strain	Terrific Broth (TB)		Defined minimal medium (MM)	
	α -filter	α -eppendorf	α -filter	α -eppendorf
<i>E. coli</i> WK6	1.89 ± 0.11	1.72 ± 0.10	2.26 ± 0.23	1.99 ± 0.26
<i>E. coli</i> CH10-12	1.96 ± 0.12	1.96 ± 0.13	1.83 ± 0.01	1.78 ± 0.01
<i>E. coli</i> NbF12-10 NN	2.45 ± 0.23	1.93 ± 0.12	2.64 ± 0.50	1.98 ± 0.50
<i>E. coli</i> NbF12-10 NO	2.23 ± 0.12	1.92 ± 0.11	/	/

Table III-2. Average correlation coefficient (α) of strains grown at 37°C in TB, 7.2 and MM, pH 6.8.

The correlation coefficient can be used to determine an equivalent of biomass concentration from the optical density, and vice versa. The lower limit of detection of the biomass measures depends on the precision of the measures. The linearity of the optical density is from 0.05 AU to 0.5 AU (§II.6.1), equivalent to 0.1 g cdw/L at the lower limit, and dilutions of the sample can be made to be always under the upper limit.

In the case of the biomass measures by filter and eppendorf, the precision of the scale and the volume of the sample determine the relative error, and the number of measurements determine the experimental errors. Each error was calculated for both methods (Table III-3), both human errors.

Biomass measurement method	Relative error (scale)	Absolute error (measurements)
Biomass range [g cdw/L]	0.1 → 1 → 10	0.1 → 1 → 10
Filter	4.6% → 1% → 0.6%	80.6% → 9.5% → 1.4%
Eppendorf	15.8% → 2.9% → 1.6%	73% → 11.7% → 2.2 %

Table III-3. Estimation of errors in the biomass measurements

The relative error is rather low compared with the absolute error. The use of biomass concentrations of under 1 g cdw/L measured by cell dry weight was avoided when possible for the calculations of specific growth rates and yields. The correlation coefficient was used to determine an equivalent of biomass concentration when needed.

III.1.2.2. Evolution of the metabolites

In the cultures grown in TB the optical density and cell dry weight were used to quantify the biomass (§II.6.1 and §II.6.2), and residual glucose was measured by an enzymatic analyzer (§II.6.4). In cultures grown in MM, in addition to the methods used for TB cultures, the residual glucose and organic acids were quantified by HPLC (§II.6.5).

The evolution of the metabolites is shown in Figure III-3 for the TB cultures (left) and MM cultures (right). The main difference between the two culture media is the carbon source in the medium, leading to the difference in the maximum biomass production. In TB, a concentration of 1 g/L of glucose is used to start the culture, and glycerol, yeast extract and peptone are used as secondary carbon sources (§II.3.2). In MM the only carbon source is glucose at a concentration of 10 g/L.

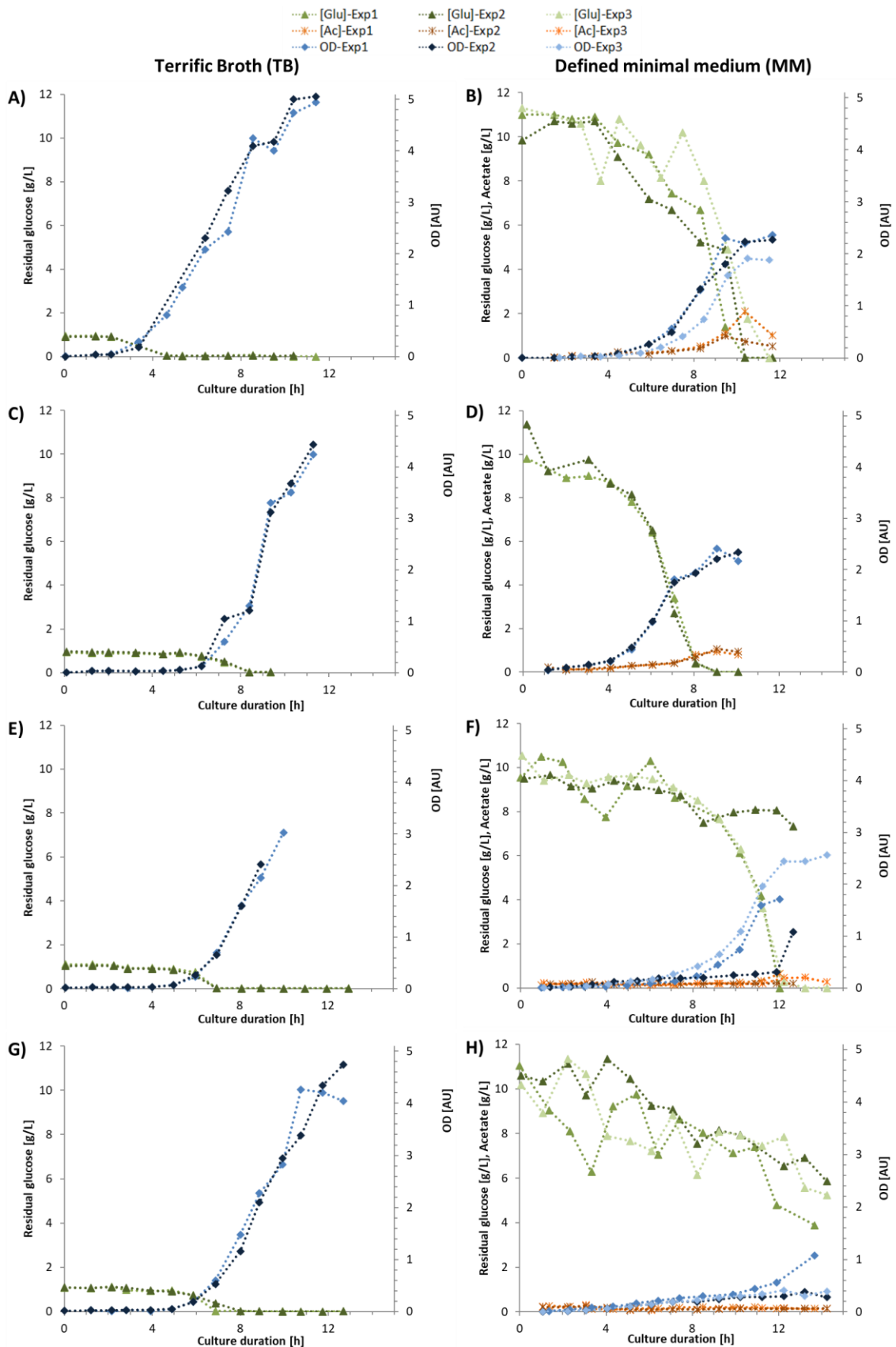


Figure III-3. Evolution of the cultures of the *Escherichia coli* strains grown in TB at 37°C, pH 7.2 (left) and in MM, pH 6.8 (right). A and B) WK6; C and D) CH10-12; E and F) NbF12-10 NN; G and H) NbF12-10 NO. Triplicates are noted as Exp1, Exp2 and Exp3.

At the end of the cultures the biomass produced in TB was about 8 g cdw/L, double than the 4 g cdw/L of biomass obtained in MM. The culture of the clone NbF12-10 NO had almost no growth in MM (Figure III-3H), as compared with its good performance in TB (Figure III-3G).

The difference in the performance of the strain NbF12-10 NO compared to the other strains could be explained by three main hypotheses: 1) nutritional limitation caused by the composition in the MM, compared with the richness of the TB medium; 2) the loss of ampicillin resistance due to the loss of the vector pHEN6, hence the low growth during the culture; 3) adaptation of the strain to the MM, where only the pre-exponential phase was observed.

For the cultures grown in MM, a same batch of MM was prepared and used for cultures of the clones NbF12-10 NN and NbF12-10 NO. Both clones NbF12-10 NN and NbF12-10 NO were constructed with the same vector (§II.1), and their nutritional needs should have been the same. In this way, hypothesis 1 can be ruled out. For the 2nd hypothesis, the loss of the vector during replication of the strain NbF12-10 NO is a feasible explanation to the low biomass production [178]. The 3rd hypothesis is that the strain had a latency phase due to the adaptation of the strain to the MM and culture should have been monitored during a longer period of time to evaluate the eventual exponential growth.

As the cultures of the strain *Escherichia coli* NbF12-10 NO in MM presented a problem of growth, no further effort was made to improve its performance and the screening of the biomass and protein production was conducted only with the recombinant clone NbF12-10 NN and the strain CH10-12. The strain WK6 was used as reference.

III.1.2.3. Specific growth rate

The variety of the carbon sources in the complex medium (TB, §II.3.2) does not allow to determine a maximum specific growth rate. The average maximum specific growth rate ($\bar{\mu}$) was determined for these cultures by a regression in the exponential zone at cell growth.

The maximum specific growth rate (μ_{\max}) was determined on the exponential phase of cultures grown in defined minimal medium (MM) at 37°C, which contain glucose as the only carbon source. Figure III-4 shows that the reference strain *Escherichia coli* WK6 has the highest average maximum specific growth rate in TB medium, whereas in MM *Escherichia coli* WK6 and CH10-12 have the same maximum specific growth rate. In TB medium, the recombinant strains CH10-12, NbF12-10 NN and NO had similar growth performances, but lower than those of the strain WK6.

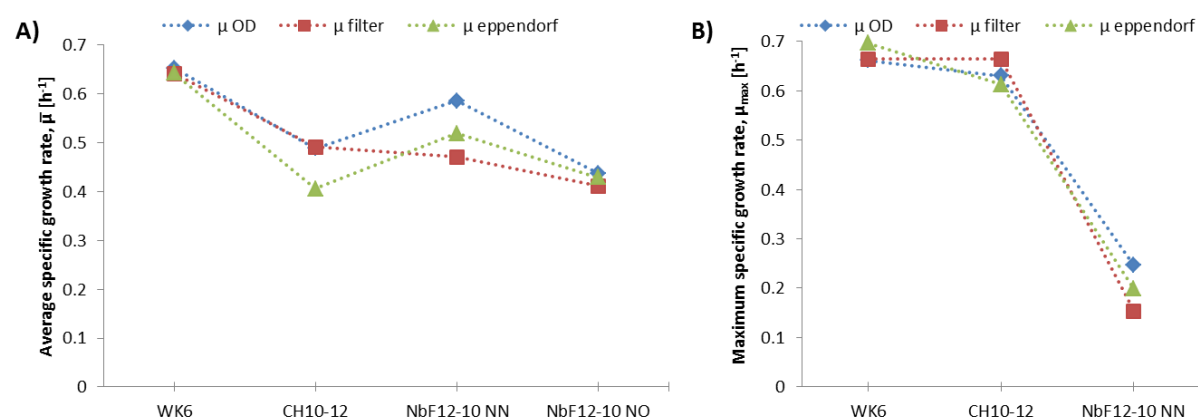


Figure III-4. Specific growth rate in cultures grown in TB (A) and MM (B).

The strain NbF12-10 NN had a two-fold lower specific growth rate on MM (Table III-4) than on TB. The hypothesis proposed in §III.1.2.2 of the lack of nutrients on the MM compared with the richness of TB medium could partially explain this difference. In the complex medium, the different substrates provide, not only a carbon source to the microorganism, but also the release of basic amino acids, peptides and/or fatty acids to the medium due to the catabolism of the substrates. In

MM, with only the glucose as carbon source, the strain is bound to anabolize the needed metabolites for its growth, hence the lower specific growth rate.

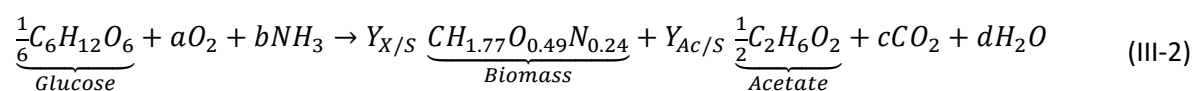
Strain	Terrific Broth (TB)			Defined minimal medium (MM)		
	OD	Filter	Eppendorf	OD	Filter	Eppendorf
<i>E. coli</i> WK6	0.65 ± 0.05	0.64 ± 0.04	0.64 ± 0.05	0.66 ± 0.02	0.66 ± 0.06	0.70 ± 0.08
<i>E. coli</i> CH10-12	0.49 ± 0.01	0.49 ± 0.04	0.41 ± 0.01	0.63 ± 0.02	0.66 ± 0.04	0.61 ± 0.05
<i>E. coli</i> NbF12-10 NN	0.59 ± 0.08	0.52 ± 0.01	0.47 ± 0.01	0.26 ± 0.03	0.15 ± 0.08	0.20 ± 0.16
<i>E. coli</i> NbF12-10 NO	0.44 ± 0.01	0.41 ± 0.05	0.43 ± 0.01	/	/	/

Table III-4. Specific growth rate for the reference and recombinant strains (μ , h^{-1}).

The cultures grown on TB had no problem of adaptability, with an average specific growth rate of over $0.4 h^{-1}$ and slightly over other values of the literature for other recombinant strains in rich medium ($0.41 h^{-1}$, shake-flask, 200 rpm, $30^{\circ}C$, [179]). When challenged with a defined mineral medium (MM), the strain CH10-12 matched the maximum specific growth rate of the reference strain WK6 at $0.66 h^{-1}$, which is higher than the values of the literature for other recombinant strains ($0.48 h^{-1}$, shake-flask, 250 rpm, $30^{\circ}C$, [180]). The clone NbF12-10 NN had a lower maximum specific growth rate in MM ($0.2 h^{-1}$) than in TB ($0.5 h^{-1}$). The clone NbF12-10 NO grew well in TB ($0.4 h^{-1}$) but in MM it could not adapt and growth was almost negligible (Figure III-3H).

III.1.2.4. Biomass yield

In the cultures grown in MM, glucose is the only carbon source available for the microorganism. The consumption of glucose can be defined by the overall mass balance in Eq. (III-2).



Where the coefficients a, b, c and d are molar stoichiometric coefficients; $Y_{X/S}$ is the yield of production of biomass on glucose in Cmol/Cmol, and $Y_{Ac/S}$ is the yield of production of acetate on glucose in Cmol/Cmol. The elemental composition of the biomass is assumed to be constant during all the culture [167], [181].

The yield of biomass production on glucose, $Y_{X/S}$, was calculated for the cultures grown in MM according to Eq. (III-3).

$$Y_{X/S} = \frac{X_f - X_0}{S_0 - S_f} \quad (\text{III-3})$$

Where $Y_{X/S}$ is the yield of production of biomass on glucose in g cdw/g glucose, X_f and X_0 are the final and initial biomass concentration in g cdw/L, and S_0 and S_f are the initial and final glucose concentrations in g/L.

Strain	$Y_{X/S}$ [g cdw/g glucose]	$Y_{X/S}$ [Cmol X/Cmol S]
<i>E. coli</i> WK6	0.37 ± 0.02	0.44 ± 0.02
<i>E. coli</i> CH10-12	0.40 ± 0.04	0.48 ± 0.05
<i>E. coli</i> NbF12-10 NN	0.36 ± 0.04	0.43 ± 0.04

Table III-5. Yields of production of biomass in shake-flask cultures grown on MM at $37^{\circ}C$, pH 6.8, 10 g/L glucose.

From the stoichiometric balance (Eq. (III-2)), $Y_{X/S}$ is expected to be around 0.5 g/g on pure cell growth cultures, without acetic acid production [167]. For all strains the yield of production, $Y_{X/S}$, was around 0.4 g/g. These values are consistent with the literature, the yield of biomass on glucose ($Y_{X/S}$) varies from 0.52 to 0.29 g/g for other recombinant *Escherichia coli* strains cultured in shake-flask (250 rpm, $30^{\circ}C$, [179], [180]).

III.1.2.5. Acetic acid

Acetic acid can be produced by *Escherichia coli* in an excess of glucose, such that the specific growth rate exceeds the growth rate at which acetate is formed, under oxygen limitation or anaerobic conditions and when culture has a high partial pressure of CO₂ [182]. On the shake-flask cultures grown in MM, acetate is produced as a by-product due to the excess of glucose in the medium as defined by Eq. (III-2). In bioreactor cultures, the production of acetate can be avoided with the control of the glucose feed in a fed-batch mode.

The yields were not calculated from the cultures on TB, since the composition of the main carbon source, yeast extract, remains an unknown.

Strain	$Y_{Ac/S}$ [g Ac/g X] and [Cmol Ac/Cmol S]	$Y_{Ac/X}$ [g Ac/ g X]	$Y_{Ac/X}$ [Cmol Ac/Cmol X]
<i>E. coli</i> WK6	0.14 ± 0.07	0.37 ± 0.18	0.42 ± 0.21
<i>E. coli</i> CH10-12	0.10 ± 0.01	0.25 ± 0.03	0.29 ± 0.03
<i>E. coli</i> NbF12-10 NN	0.06 ± 0.03	0.12 ± 0.05	0.13 ± 0.05

Table III-6. Yields of production of acetate in shake-flask cultures grown on MM at 37°C, pH 6.8, 10 g/L glucose.

The yield of acetic acid on glucose, $Y_{Ac/S}$, was 0.14 g/g for the reference strain WK6, followed by the strain CH10-12 with 0.1 g/g, and finally the clone NbF12-10 NN with a yield of 0.06 g/g (Table III-6). These yields are consisted compared with the values reported by the literature, of 0.05 g/g to 0.1 g/g for cultures of *Escherichia coli* grown in minimal medium (5 g/L glucose, 250 rpm, M9 medium, [180]).

The pH at the start of the cultures TB and MM were 7.2 and 6.8, respectively. There is a change in the pH during the cultures grown in MM. The pH was measured at the end of the culture as shown in Table III-7.

Strain	Terrific Broth (TB)		Defined minimal medium (MM)	
	Start of culture	End of culture	Start of culture	End of culture
<i>E. coli</i> WK6	7.2	7.6	6.8	5.4
<i>E. coli</i> CH10-12	7.2	7.3	6.8	5.6
<i>E. coli</i> NbF12-10 NN	7.2	7.4	6.8	6.5
<i>E. coli</i> NbF12-10 NO	7.2	7.5	/	/

Table III-7. pH at the start and end of the cultures grown in TB and MM at 37°C.

The pH for the cultures grown in TB changed in a maximum of 5%. The high concentration of phosphates in the medium (Table II.2, §II.3.2) acted as a pH buffer and kept the pH stable during all the cultures. The slight increase in the pH can be due possibly to the release of ammonium ions (NH₄⁺) in the consumption of amino acids or peptides present in the carbon source (yeast extract, peptone).

In the case of cultures grown in MM, an average reduction of 24% was observed for strains WK6 and CH10-12, and 5% for strain NbF12-10 NN (Table III-7). The defined minimal medium does not contain salts that act as a buffer, and two phenomena can explain the decrease of the pH during culture: 1) the consumption of ammonium ions during the culture, and 2) the production of acetic acid in the culture.

The ammonium ions of the culture medium are consumed to produce the amino acids needed in the production of the biomass. Its removal from the medium will reduce the pH of the culture medium. At the end of the cultures in MM, the same biomass concentration was attained for all strains but the pH value for the strain NbF12-10 NN is one pH unit higher than for the other strains. As the consumption of ammonium ions will be the same for all the strains, this consumption will not explain the totality of the pH change.

On the other hand, the greater production of acetic acid in the case of strains WK6 and CH10-12 (Figure III-1A and Figure III-1B) seems responsible for the higher decrease of pH. For the case of strain NbF12-10 NN, the acetic acid present in the medium was very low (Figure III-1C), therefore the pH changed in a small amount.

III.1.3. Protein expression

In shake-flask cultures grown in TB, periplasmic extraction was performed by osmotic shock after 24 h of induction at 28°C. Three different methods of osmotic shock were tested: (1) incubation in TES for 2 h and addition of TES/4 for other 2 h, (2) incubation in TES for 6 h and addition of TES/4 for 12 h, and (3) incubation in TES for 2 h and addition of cold distilled water for 2 h.

After extraction of the periplasmic proteins, purification by IMAC was made and the first and second eluted fractions were checked by SDS-PAGE. The osmotic shock methods were tested on the recombinant strains NbF12-10 NN and CH10-12 (Figure III-5). The nanobodies NbF12-10 and CH10-12 were found at an apparent molecular weight of 29 kDa and 31 kDa, respectively.

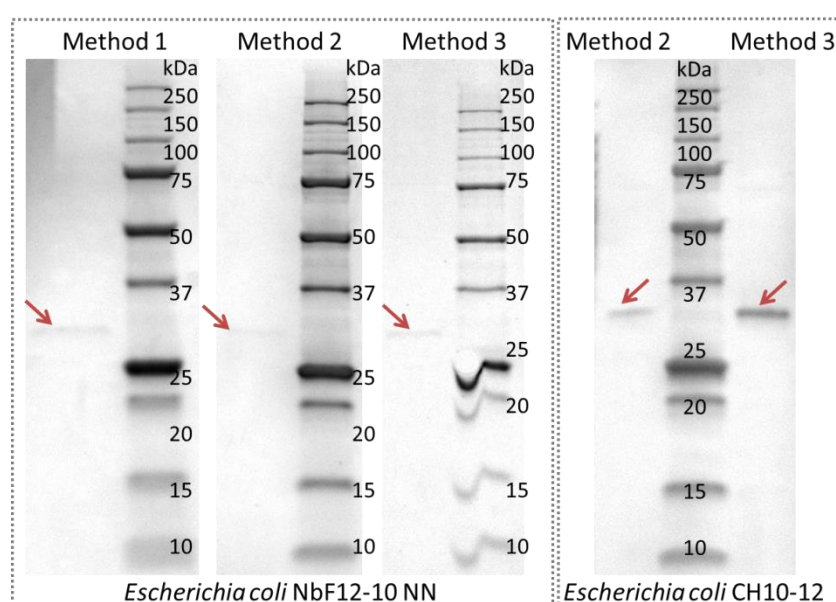


Figure III-5. Nanobody expression by different osmotic shock methods. The red arrow marks the band of the nanobody NbF12-10 (29 kDa) and CH10-12 (31 kDa) of the first eluate of IMAC purification on SDS-PAGE gels. The molecular weight marker used was the Precision Plus Protein Unstained Protein Standards (Bio-rad, USA).

The second eluted fraction did not show a band on the SDS-PAGE gel of the clone NbF12-10 NN, but it did appear on the gels from the strain CH10-12. The three methods were tested on the clone NbF12-10 NN, and the second and third methods were tested on strain CH10-12.

Strain	Method 1	Method 2	Method 3	Method 1	Method 2	Method 3
	$\mu\text{g Nb/L culture}$			$\mu\text{g Nb/g cdw}$		
<i>E. coli</i> NbF12-10 NN	36.7 ± 2.3	25.9 ± 2.8	76.3 ± 1.1	5.4 ± 0.3	3.1 ± 0.3	8.8 ± 1.3
<i>E. coli</i> CH10-12	/	579 ± 112	1575 ± 159	/	71 ± 14	199 ± 20

Table III-8. Final concentration and specific yield of the nanobodies NbF12-10 and CH10-12 cultured in TB medium. Protein expression induced at 0.5 g cdw/L with a pulse of 1 mM IPTG and change of temperature to 28°C. Periplasmic protein extracted by different osmotic shock methods after 24 h of induction.

The clone NbF12-10 NN produced an amount of target protein one order of magnitude lower than the strain CH10-12 (Table III-8). The strain CH10-12 had a final concentration of nanobody 20-fold higher than the strain NbF12-10 NN. It was noticeable that the third method resulted in the release of periplasmic proteins 300% higher than the second method for both strains.

From these results, the optimization of the periplasmic extraction was obtained for the nanobodies NbF12-10 and CH10-12. The method 3: incubation 2 h in TES and addition of cold distilled water and incubation for 2 h was kept for the next experiments.

III.1.4. Morphological analysis

The effect of temperature and induction in the morphology of the *Escherichia coli* strain CH10-12 was studied. Three cultures (A, B and C) grown in TB were sampled at three different culture times, corresponding at biomass concentrations of 0.2 g cdw/L, 1 g cdw/L and 8 g cdw/L, approximately (Figure III-6). Culture A was conducted at 37°C; culture B and C were started at 37°C, and temperature was changed to 28°C at 0.4 g cdw/L of biomass; protein induction was made only for culture C at 0.4 g cdw/L of biomass with 1 mM of IPTG.

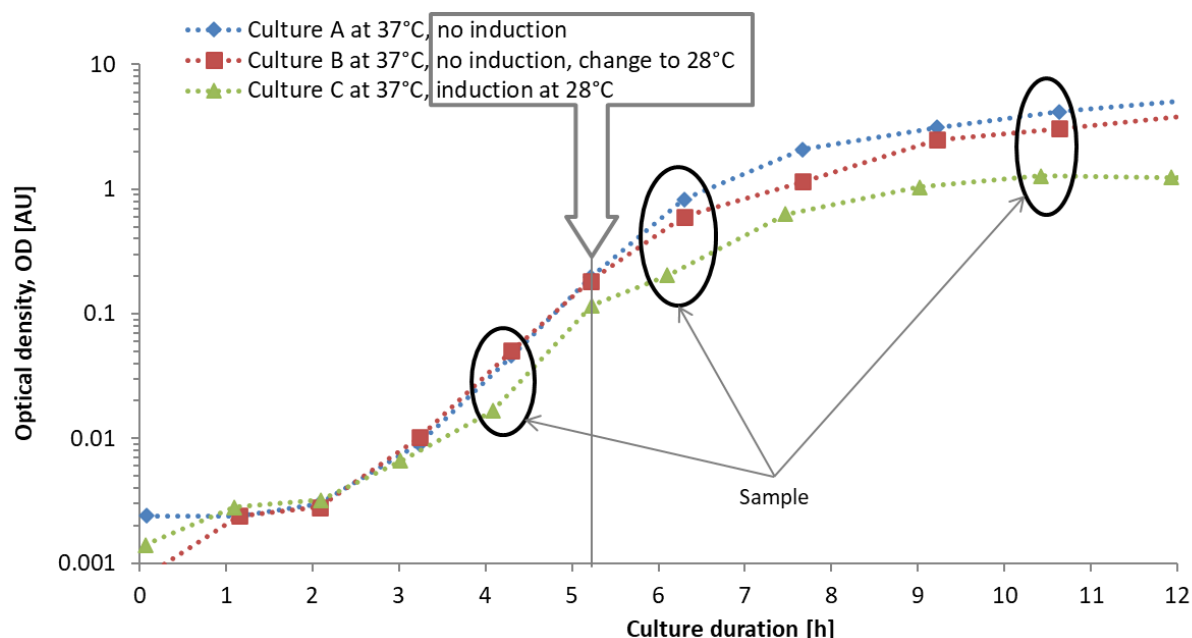


Figure III-6. Sampling of cultures grown in TB, pH 7.2. Cell culture was imaged at the points selected in the black circles at about 4 h, 6 h and 10.5 h after inoculation. Culture C was induced at an OD of 0.2 with 1 mM IPTG.

Samples of the cultures A, B and C were visualized on an optical microscope as described in §II.6.3 and images were analyzed as described in §II.8.6. After filtration, the samples had between 300 and 1000 particles. The parameter used to compare the samples was the circle equivalent diameter (CE diameter), which is defined in the Morphologi G3 software as the diameter of a circle of the same area than the particle. The CE diameter will get larger or smaller as the particle does.

First, the low biomass concentrations (0.2 – 1 g cdw/L) were analyzed in the Morphologi software (Malvern Panalytical, Figure III-7). At low biomass concentration, the statistical analysis is not accurate, as it can be seen by the ragged frequency curves. The low quantity of particles used for the analysis (300-700) does not allow for a reliable statistical analysis. The analysis could have been improved by taking an image larger than 1 mm² for the low biomass concentrations to obtain a higher number of particles.

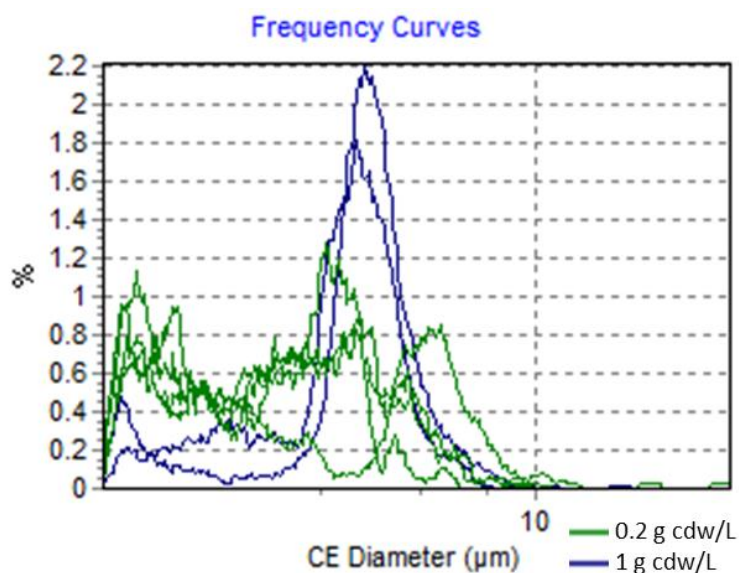


Figure III-7. Morphological analysis of cultures samples of *Escherichia coli* CH10-12 grown in TB, pH 7.2, 37°C.

Secondly, the higher biomass concentrations (1 – 8 g cdw/L) were compared. The result of the comparison is showed in a dendrogram in Figure III-8. The modification of temperature from 37°C to 28°C in the culture B (Figure III-6) does not lead to a morphological difference compared to the culture A that remained at 37°C, at both biomass concentrations (1 g cdw/L and 8 g cdw/L). In contrast, the samples of culture C induced with IPTG at 28°C were significantly different from the non-induced samples.

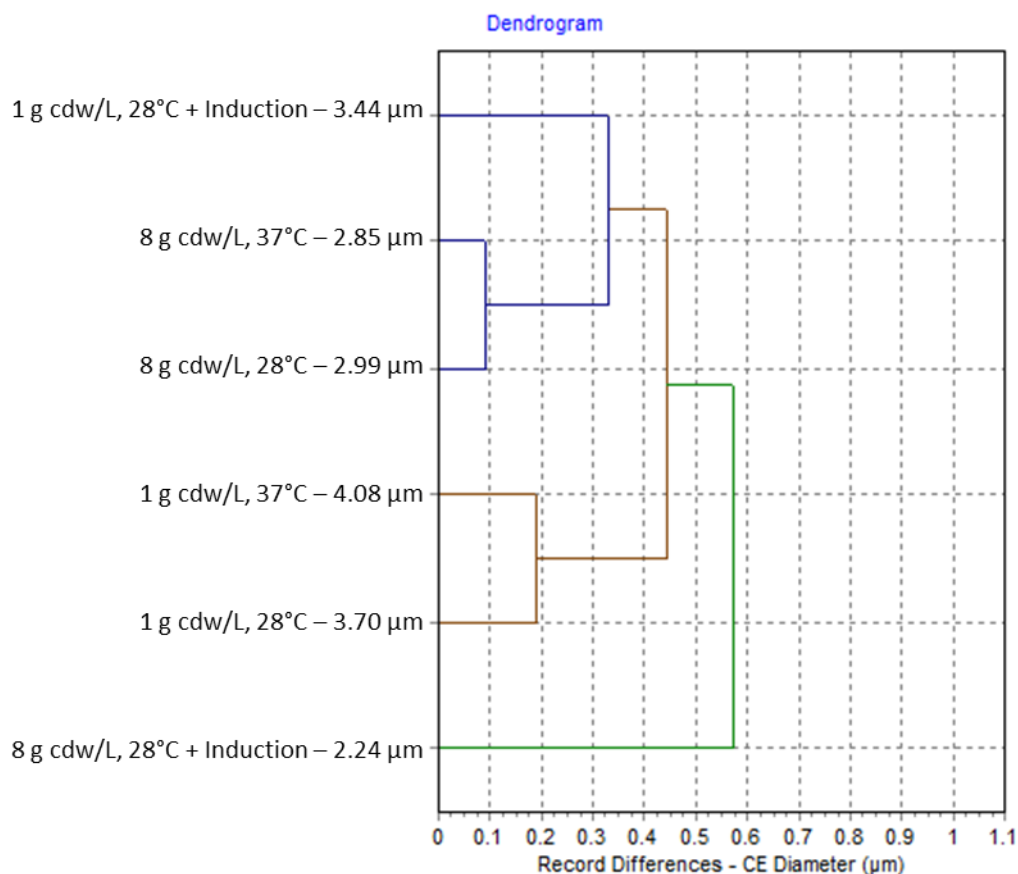


Figure III-8. Dendrogram for cultures of *Escherichia coli* CH10-12 grown in TB.

Figure III-9 shows that the optical microscope images of the cells. An apparent reduction of cell size was noted for culture C after protein induction (Figure III-9C), but as the statistical analysis showed, not statistically significant. The size of the cell at the end of the cultures A, B and C was relatively the same, whether the cultures were in pure cell growth or in protein production.

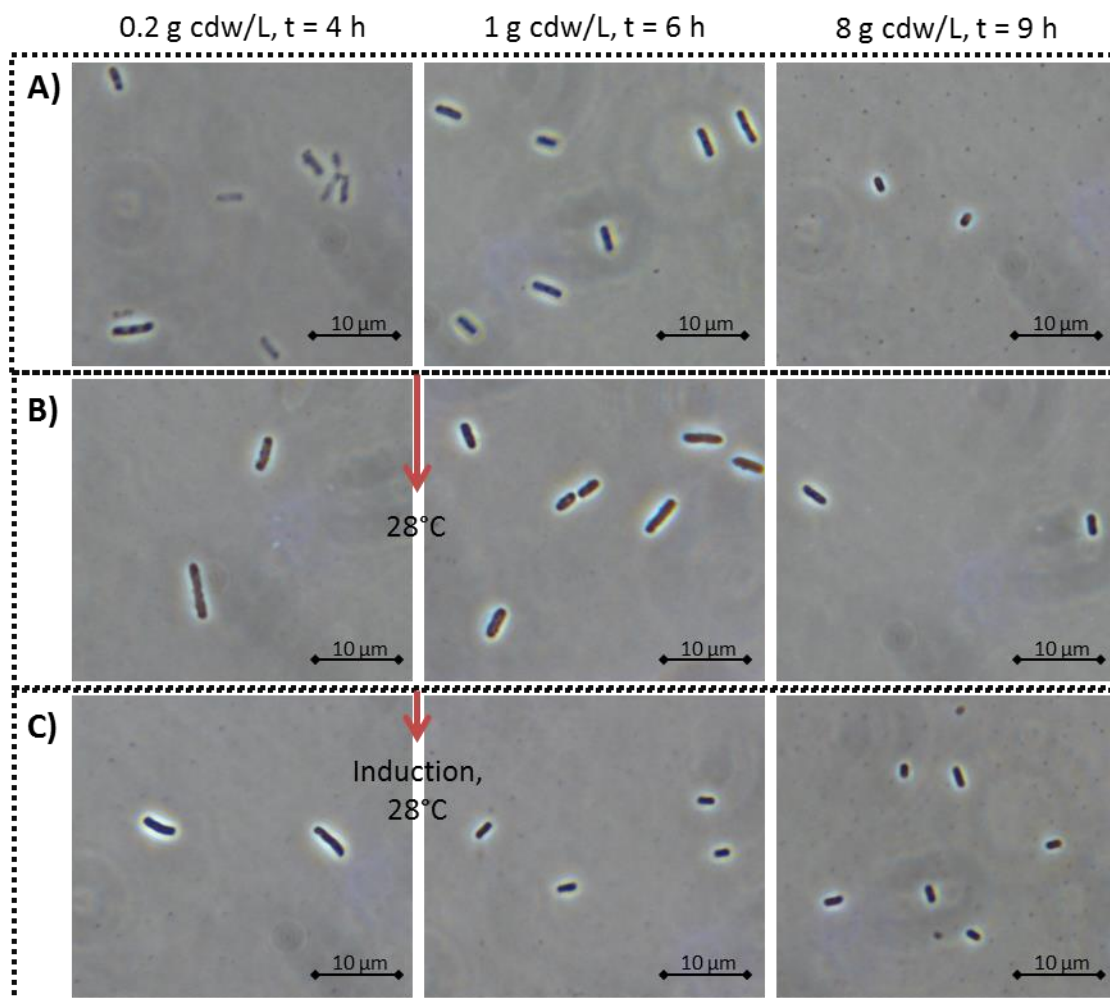


Figure III-9. Morphological evolution of *Escherichia coli* CH10-12 cultures in TB, pH 7.2. A) Pure cell growth at 37°C. B) Pure cell at 37°C and temperature change at 0.5 g cdw/L to 28°C. C) Cell growth at 37°C and induction at 0.5 g cdw/L with change of temperature to 28°C. Images visualized with transillumination and immersion oil, magnification of x100 in a microscope Eclipse E100 (Nikon). The red arrows show the change of operating conditions.

One hypothesis to explain the morphological change was the availability of nutrients in the complex medium. The microorganism metabolizes first the small metabolites such as glucose and glycerol and follows to the next available nutrients found in TB: yeast extract and peptone.

The second hypothesis considered was that the morphological change was temperature-dependent, and not a response to the protein expression [183]. This hypothesis was rejected, since the modification of temperature from 37°C to 28°C had no effect on the size of the bacteria as can be seen in Figure III-9A and Figure III-9B, and the statistical analyses in the Morphologi software (Figure III-8).

The cells subject to the periplasmic extraction were visualized on an optical microscope to evaluate the damage of the osmotic shock (Figure III-10). The osmotic shock causes the burst of the periplasmic membrane, and no effect in the morphology of the cell should be seen.

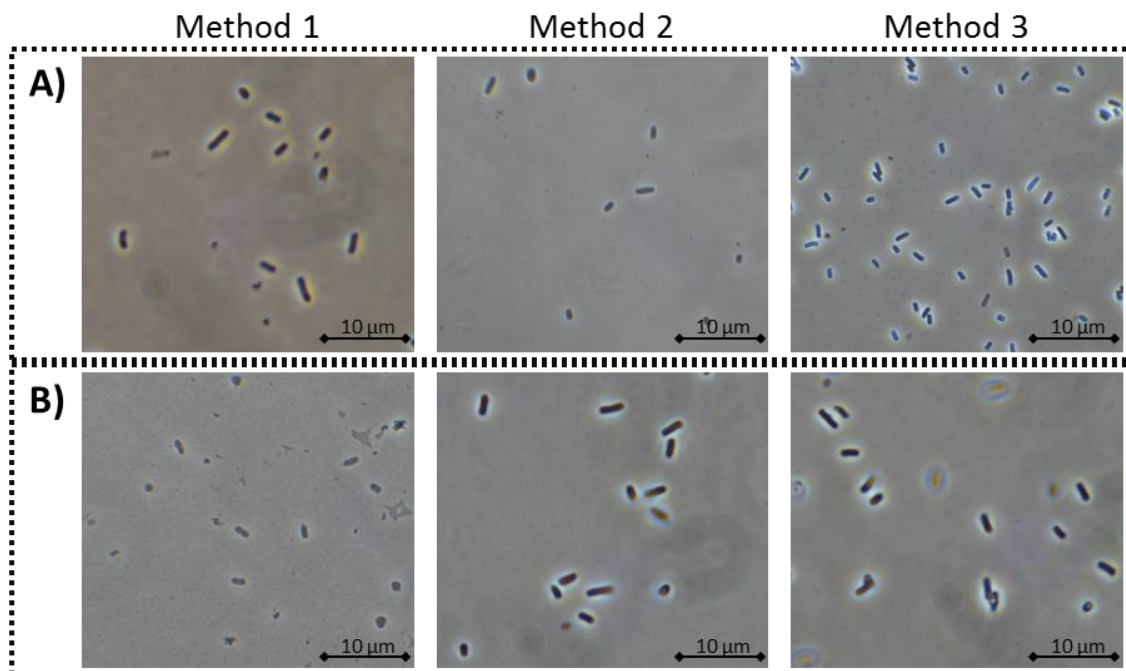


Figure III-10. Effect of osmotic shock on *Escherichia coli* NbF12-10 NN cells. A) Before osmotic shock. B) After osmotic shock. Images visualized with transillumination and immersion oil, magnification of x100 in a microscope Eclipse E100 (Nikon).

After osmotic shock, cells did not show visual damage, indicating that the osmotic shock only permeated the outer membrane of the cells, as expected for the extraction of periplasmic proteins [81]. The cells were later cultured on LB plates, after 12 h at 37°C, colonies were found, showing that the cells were cultivable after osmotic shock, but no further analyses were made for its quantification. The viability of the cells subjected to osmotic shock has been demonstrated in the literature, where survival is reported to be above up to 70% [169].

III.1.5. Conclusion

The adaptation of the strains *Escherichia coli* WK6, CH10-12, NbF12-10 NN and NbF12-10 NO to different culture media was studied in shake-flask cultures. The strain *Escherichia coli* NbF12-10 NO grew well in rich medium (TB) but no growth was observed in the defined minimal medium (MM). The kinetic parameters of the strain NbF12-10 NO in MM were not exploited. The biomass and optical density coefficient, α , was equivalent to 2 g cdw/AU for all strains in both culture media.

All strains had an average maximum specific growth rate superior to 0.4 h⁻¹ in the TB medium: 0.64 h⁻¹ for WK6, 0.5 h⁻¹ for CH10-12 and NbF12-10 NN, and 0.4 h⁻¹ for NbF12-10 NO. When cultured in MM, strains WK6 and CH10-12 adapted without problems, both achieving a maximum specific growth rate of 0.6 h⁻¹. The clone NbF12-10 NN had problems for adapting to the defined minimal medium (MM), with a maximum specific growth rate of 0.2 h⁻¹.

The yield of biomass on glucose, $Y_{x/s}$, was in average 0.4 g cdw/ g glucose for all strain in MM. the yield of acetic acid on glucose was 0.14, 0.1 and 0.06 g acetic acid/g glucose for strains WK6, CH10-12 and NbF12-10 NN, respectively.

The methodology of periplasmic protein extraction was optimized in shake-flask scale. The release of periplasmic proteins was studied in strains NbF12-10 NN and CH10-12. An improvement of over 300% was obtained with a change in the protocol for both strains.

The strain CH10-12 showed to be the most competent for bispecific nanobody production in TB, producing 20-fold more nanobody than strain NbF12-10 NN. At the end of 24 h of induction at 28°C, a yield of 1.575 mg/L (0.009 mg/g cdw) and 0.076 mg/L (0.2 mg/g cdw) was obtained at for strains CH10-12 and NbF12-10 NN, respectively.

In shake-flask cultures, the change in the morphology of the cell during protein expression cannot be taken as an indicator of the production of the protein. Further analyses with larger samples were studied in the bioreactor cultures in §III.2.3.2.3 to assess the significance of the cell shape change.

III.2. Bioreactor cultures

The cultures in bioreactor were made to study different aspects of the expression of the nanobodies CH10-12 and NbF12-10: culture medium, induction temperature and induction duration. Firstly, the effect of the induction temperature during the protein expression was studied. The strain CH10-12 was cultured at 37°C, and then temperature was modified to a value between 28°C to 37°C with different induction duration and a specific feed strategy to maintain a residual growth while producing the nanobody.

Secondly, the yields of biomass, acetic acid, carbon dioxide, and nanobody were determined through mass and oxydo-reduction balances.

Finally, the evolution of the biological enhancement factor was studied during microbial cultures.

III.2.1. Culture strategy

The effect of the induction temperature was studied on the strain *Escherichia coli* CH10-12 over a range of temperatures from 28°C to 37°C, with different induction duration (Table III-9). The strain *Escherichia coli* NbF12-10 NN was cultured and protein expression was made at 29°C. The reference strain *Escherichia coli* WK6 was used as the control and induced with IPTG at 29°C.

Cultures BR02 to BR05 are referred in this manuscript as cultures with “short induction duration” (series 1), varying from 6 h to 12 h. Cultures BR06 to BR09 are referred as cultures with “long induction duration” (series 2), varying from 28 h to 38 h.

Batch ref.	Objectives	Strain	Culture medium	Induction conditions (Temperature – duration)	[Glc] at the start of batch mode	[Glc] in feed solution
BR01	Control for sampling strategy and feed profiles	<i>E. coli</i> WK6	Defined minimal medium	/	10 g/L	286 g/L
BR02	Induction of protein at 25 g cdw/L at different temperatures	<i>E. coli</i>	Defined	28°C – 12 h	10 g/L	298 g/L
BR03		CH10-12	minimal	30°C – 10 h	10 g/L	298 g/L
BR04			medium	33°C – 6 h	10 g/L	326 g/L
BR05				37°C – 6 h	10 g/L	326 g/L
BR06	Induction of protein at 30 g cdw/L for long induction times	<i>E. coli</i>	Defined	29°C – 38 h	12.5 g/L	305 g/L
BR07		CH10-12	minimal	32°C – 35 h	7.5 g/L	305 g/L
BR08	Induction of protein at 25 g cdw/L	<i>E. coli</i> NbF12-10 NN	Defined minimal medium	29°C – 37 h	10 g/L	305 g/L
BR09	Control with induction	<i>E. coli</i> WK6	Defined minimal medium	29°C – 28 h	10 g/L	305 g/L

Table III-9. Strategy of bioreactor culture conditions.

The cultures in bioreactor of 5 L were made under strict aerobic conditions. Four conditions of agitation and air flow were chosen (500 rpm – 1 NL/min; 1000 rpm – 2 NL/min; 1500 rpm – 3 NL/min; 1500 rpm – 1 NL/min), corresponding to the three different culture modes and phases (batch, fed-batch and induction; Figure III-11). Each condition allows a time window of 2 to 4 h of culture in which the dissolved oxygen is kept over 15%. This strategy will allow the analysis and comparison of the oxygen transfer for all cultures under similar conditions.

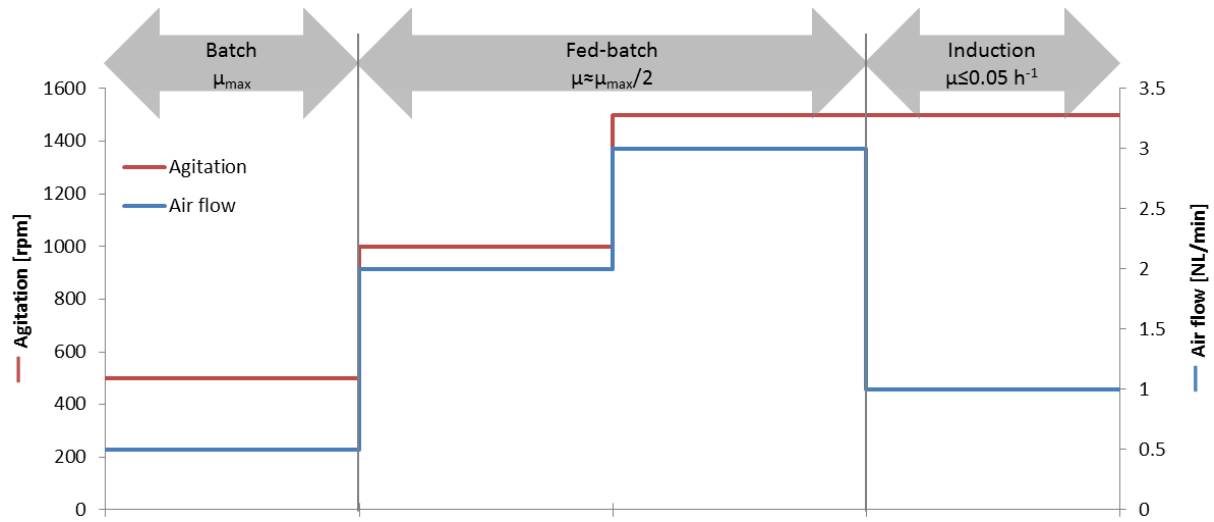


Figure III-11. Strategy of oxygen transfer during bioreactor cultures

III.2.2. Microbial culture

III.2.2.1. Presentation of cultures

In this section, each bioreactor culture will be described through the evolution of the physico-chemical parameters (pH, pO_2 , T, P) and operating conditions (air flow, agitation, substrate feed setup, glucose added), as well as their biological parameters (biomass, glucose, acetate, and citrate).

The citrate was an organic acid usually kept constant during the culture but during the analysis of the cultures we found that during the induction the mass changed, that is why an increased interest in citrate surfaced and it was monitored during all the cultures.

III.2.2.1.1. Reference cultures BR01 and BR09: *Escherichia coli* WK6

The objective of the culture BR01 was to get hold of the sampling strategy and define the agitation and aeration conditions for cell growth with the strain *Escherichia coli* WK6 in MM at 37°C and pH 6.8. Batch mode started with the inoculation of 100 mL of a culture grown at 37°C for 12 h in MM. At the time of the inoculation the aeration was stopped to allow the inlet of the inoculum, but agitation was kept. The decrease in the dissolved oxygen was an indicator of the microbial activity and aeration was started to obtain the measure of outlet gas.

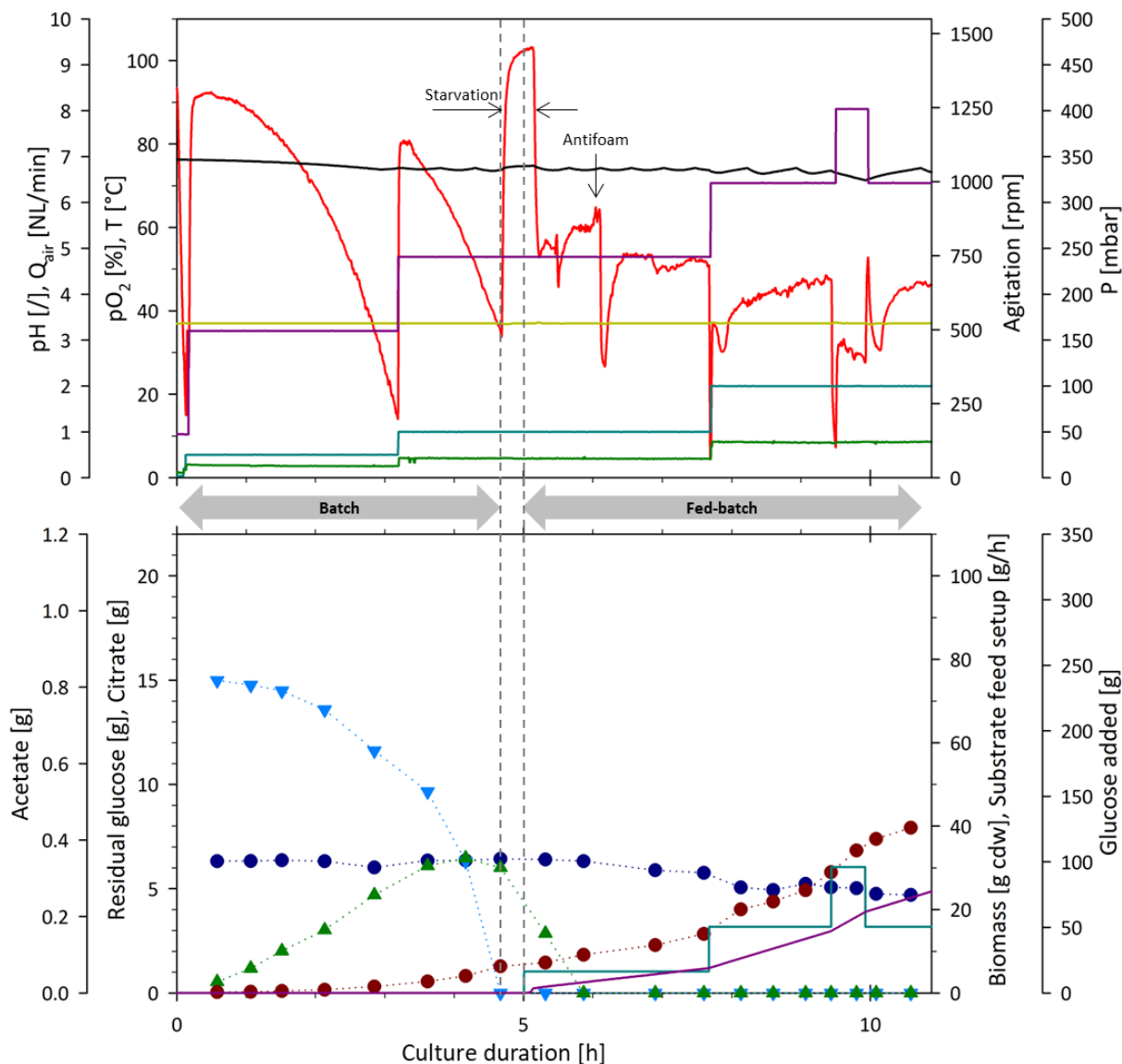


Figure III-12. Physico-chemical parameters, operating conditions and biological parameters of the culture of *Escherichia coli* WK6 (BR01) grown in MM at pH 6.8, 37°C. The dotted lines depict the change in the operating mode.

During the culture BR01, glucose was supplied at different constant rate feedings (Figure III-12). The feed solution was supplied when a sudden increase on dissolved oxygen was observed, which corresponded to the depletion of the initial 10 g/L of glucose. A few drops of antifoam were supplied only once when foam was formed in the bioreactor. The addition of antifoam caused a severe decrease in the dissolved oxygen (Figure III-12).

For the calculations of the volumetric mass transfer coefficient, k_{La} , and data smoothing, the perturbations by the antifoam, and the change of agitation and aerating conditions were excluded. Also, for the k_{La} , the zones where starvation was observed were excluded from the calculations and interpretation. The exclusion of these zones and perturbations was applied for all cultures.

In the culture BR01, 6.5 g cdw of biomass and 0.3 g of acetate were produced from 14.5 g of glucose in the batch mode. During the fed-batch mode, the acetate was consumed, and 40 g cdw of biomass were attained, with the consumption of 87 g of glucose by the end of the culture. Dissolved oxygen was always kept over 15% and there was no accumulation of glucose during the fed-batch mode.

The objective of the culture BR09 was to have a negative control over the production of the protein with the reference strain *Escherichia coli* WK6. The culture was inoculated with 200 mL of cultures grown at 37°C for 12 h in MM. Batch mode was conducted with an initial titer of glucose of 10 g/L and fed-batch mode was conducted as described in §II.5. When culture reached 21 g cdw/L of biomass IPTG was added in one pulse and temperature was modified to 29°C.

Pressure started to increase after 33 h of culture and, despite the change of the outlet filters and aeration rates, the pressure did not decrease (~400 mbar, Figure III-13). The culture was stopped 37 h after the inoculation.

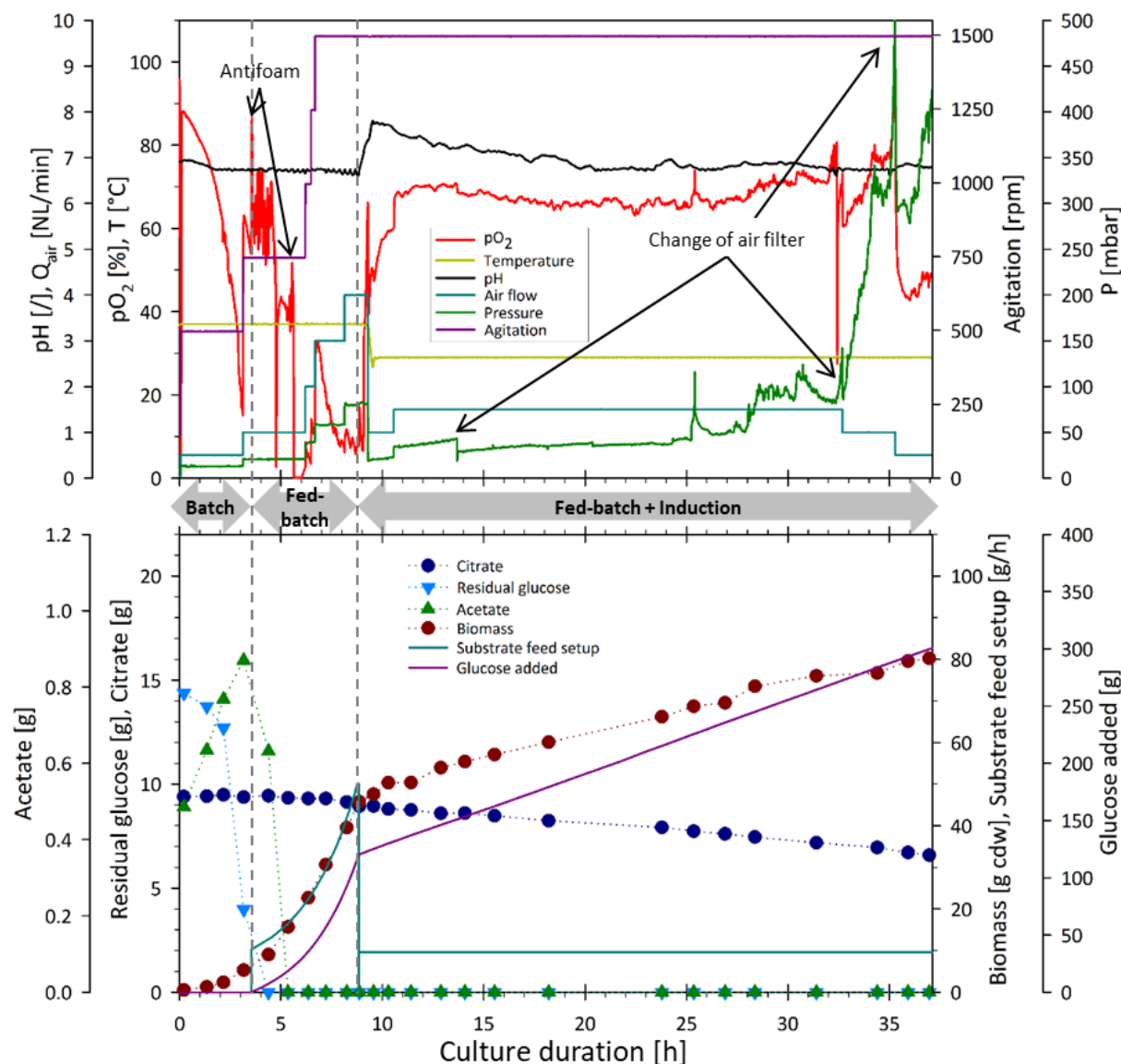


Figure III-13. Physico-chemical parameters, operating conditions and biological parameters of the culture of *Escherichia coli* WK6 (BR09) grown in MM, pH 6.8, 37°C, induced at 29°C for 28 h. The dotted lines depict the change in the operating mode.

In the culture BR09, 7 g cdw of biomass and 0.9 g of acetate were produced from 14.9 g of glucose in the batch mode. During the fed-batch mode, the acetate was consumed within the first hour after

the fed-batch mode was started, and 47 g cdw of biomass were attained, with the consumption of 133 g of glucose at the end of the fed-batch mode. During the induction phase, a total biomass of 80 g cdw was attained and a total of 312 g of glucose were consumed at the end of the culture. Dissolved oxygen was kept over 10% during the growth phases (batch and fed-batch) and over 65% during the induction phase. There was no accumulation of glucose during the fed-batch mode with the exponential feed. The final citrate mass was 6.6 g at the end of the culture, from the starting 9 g at the start of the culture.

III.2.2.1.2. BR02 to BR05: *Escherichia coli* CH10-12 – short induction times (1st series)

The cultures of *Escherichia coli* CH10-12 BR02 (Figure III-14) and BR03 (Figure III-15) were inoculated with 100 mL of an inoculum cultured for 12 h at 37°C in MM. The inoculum had a low biomass concentration. At the depletion of the initial 10 g/L of glucose, 12 h after the inoculation, feeding was started.

Protein expression was induced at approximately 17 h of culture when biomass reached 23 g cdw/L for BR02 and 25 g cdw/L for BR03, and feed was set to 4 g/h of glucose. Temperature was modified to 28°C and 30°C, in BR02 and BR03, respectively. During the induction phase, the dissolved oxygen was over 60%.

In culture BR02, the antifoam solution was added at big quantities (more than a few drops), which disturbed the dissolved oxygen measure ($pO_2=0\%$). The effect of the antifoam was completely overcome 1 h after its addition and dissolved oxygen was about 15% until the induction phase was started.

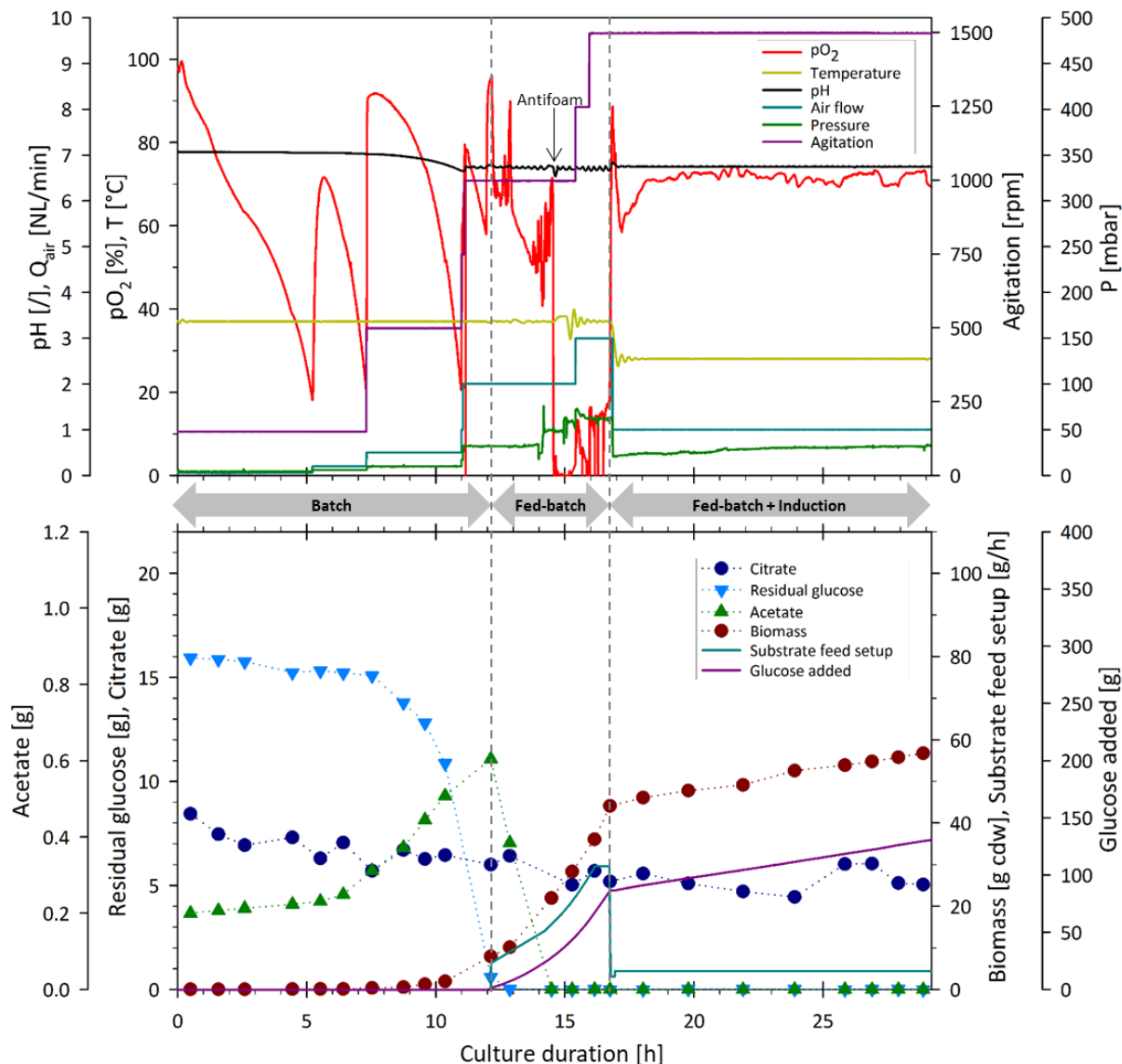


Figure III-14. Physico-chemical parameters, operating conditions and biological parameters of the culture of *Escherichia coli* CH10-12 (BR02) grown in MM, pH 6.8, 37°C, induced at 28°C for 12 h. The dotted lines depict the change in the operating mode.

In culture BR02, 6.5 g cdw of biomass and 0.6 g of acetate were produced from 13.7 g of glucose in the batch mode. During the fed-batch mode, the acetate was consumed, and 44.7 g cdw of biomass were attained, with the consumption of 103 g of glucose at the end of the fed-batch mode. During the induction phase, a total biomass of 57 g cdw was attained and a total of 145 g of glucose were consumed. Dissolved oxygen was kept over 10% during growth phases and over 70% during the induction phase. There was no accumulation of glucose during the fed-batch mode with the exponential glucose feed. The final citrate mass was 5 g at the end of the culture, from the starting 8 g.

For the culture BR03 (Figure III-15), as the pump (Watson-Marlow) feeding the bioreactor did not turn with the minimum speed (5 rpm) equivalent to the desired glucose feeding value, the control was changed to 6 rpm, and furthermore at 7 rpm, equivalent to 5 g/h of glucose. This is delimited in Figure III-15 as starvation zones, where glucose was not assured, and the dissolved oxygen increased to 100%. Once the feed was restarted, dissolved oxygen decreased to a value about 65%.

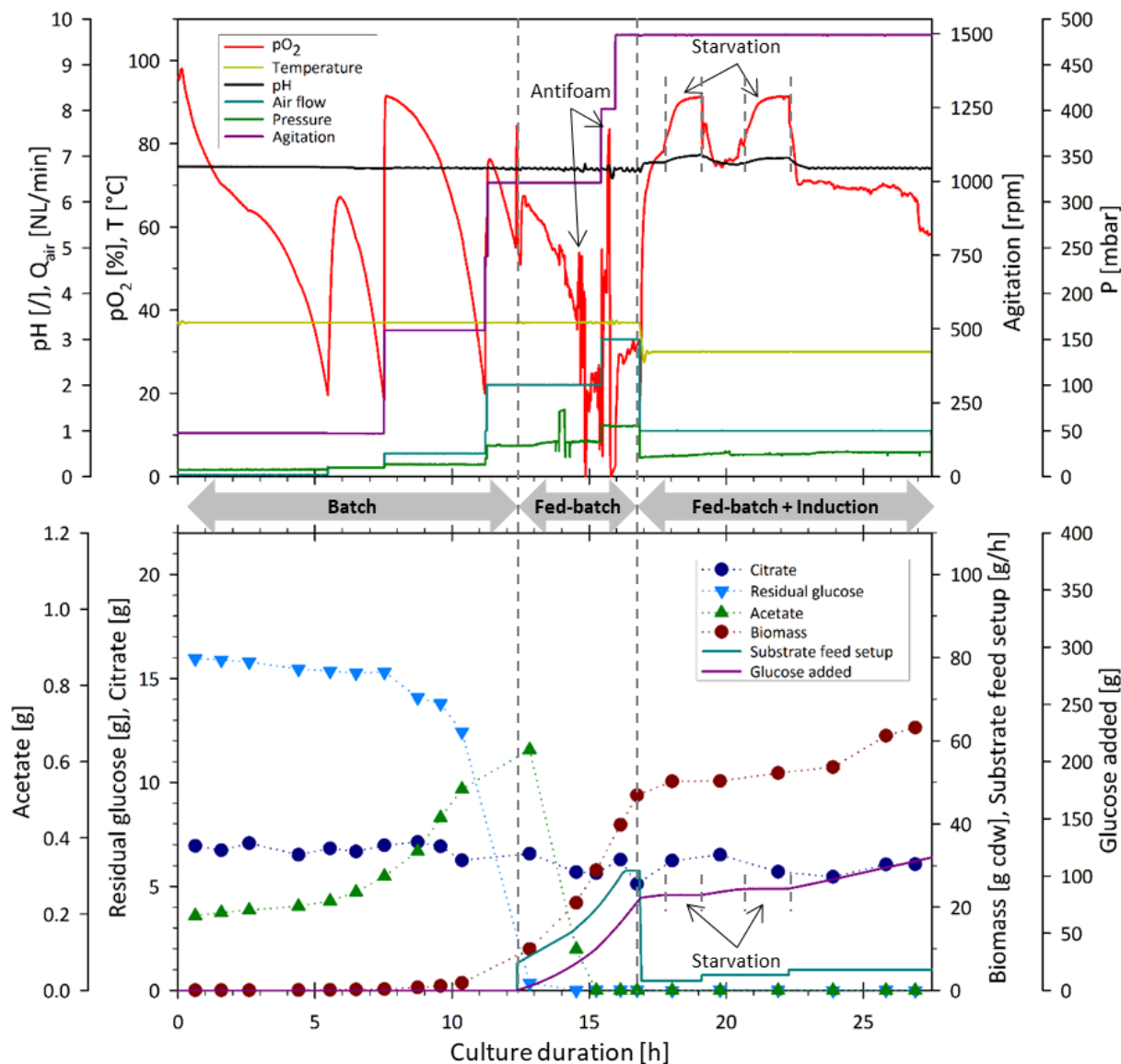


Figure III-15. Physico-chemical parameters, operating conditions and biological parameters of the culture of *Escherichia coli* CH10-12 (BR03) grown in MM, pH 6.8, 37°C, induced at 30°C for 10 h. The dotted lines depict the change in the operating mode.

In the culture BR03, 6.6 g cdw of biomass and 0.6 g of acetate were produced from 11.2 g of glucose in the batch mode. During the fed-batch mode, the acetate was consumed, and 47 g cdw of biomass were attained, with the consumption of 97 g of glucose at the end of the fed-batch mode. During the induction phase, a total biomass of 63 g cdw was attained and a total of 129 g of glucose were consumed. Dissolved oxygen was kept over 10% during growth phases and over 65% during the induction phase. There was no accumulation of glucose during the fed-batch mode and during the induction. The final citrate mass was 6 g at the end of the culture, from the starting 7 g at the start of the culture.

The cultures of *Escherichia coli* CH10-12 BR04 (Figure III-16) and BR05 (Figure III-17) were inoculated with 100 mL of cultures grown at 37°C for 15 h in MM, with the objective of shortening the batch mode. Initial glucose was 10 g/L. Fed-batch mode was started at 6 h after inoculation and conducted as described for BR02 and BR03. Protein expression was induced after 10 h of culture corresponding to 29.5 g cdw/L and 28 g cdw/L for BR04 and BR05, respectively. During the induction phase, temperature was modified to 33°C for BR04 and the induction phase lasted 6 h for both cultures.

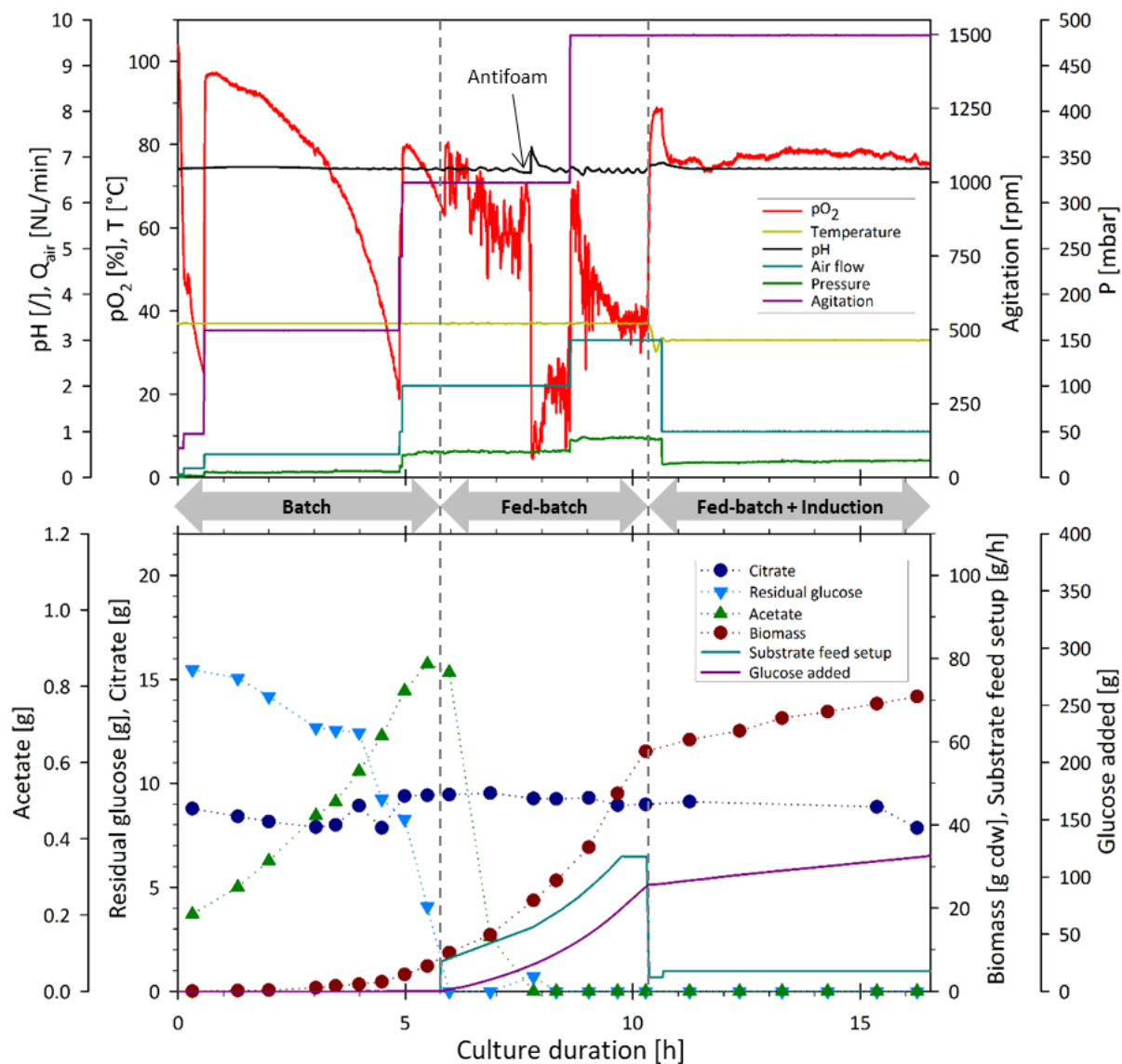


Figure III-16. Physico-chemical parameters, operating conditions and biological parameters of the culture of *Escherichia coli* CH10-12 (BR04) grown in MM, pH 6.8, 37°C, induced at 33°C for 6 h. The dotted lines depict the change in the operating mode.

In culture BR04, 7.6 g cdw of biomass and 0.9 g of acetate were produced from 14 g of glucose in the batch mode. During the fed-batch mode, the acetate was consumed, and 58 g cdw of biomass were attained, with the consumption of 109 g of glucose at the end of the fed-batch mode. During the induction phase, a total biomass of 71 g cdw was attained and a total of 133 g of glucose were consumed. Dissolved oxygen was kept over 10% during growth phases and over 70% during the induction phase. There was no accumulation of glucose during the fed-batch mode with the exponential glucose feed. The final citrate mass was 8 g at the end of the culture, from the starting 9 g.

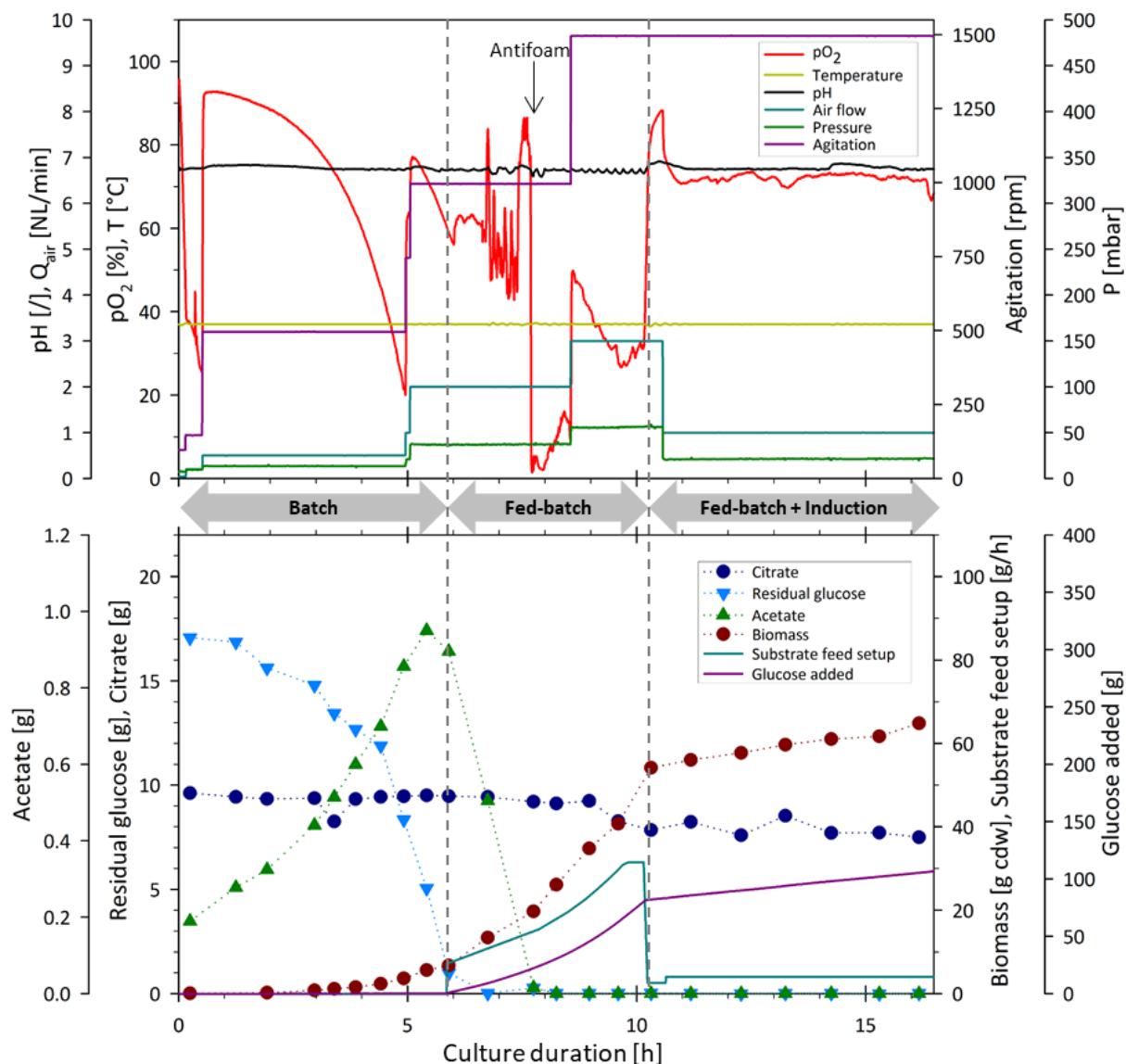


Figure III-17. Physico-chemical parameters, operating conditions and biological parameters of the culture of *Escherichia coli* CH10-12 (BR05) grown in MM, pH 6.8, 37°C, induced at 37°C for 6 h. The dotted lines depict the change in the operating mode.

In the culture BR05, 7 g cdw of biomass and 0.9 g of acetate were produced from 15.4 g of glucose in the batch mode. During the fed-batch mode, the acetate was consumed, and 55 g cdw of biomass were attained, with the consumption of 99 g of glucose at the end of the fed-batch mode. During the induction phase, a total biomass of 65 g cdw was attained and a total of 124 g of glucose were consumed. Dissolved oxygen was kept over 10% and over 70% during the induction phase. There was no accumulation of glucose during the fed-batch mode or during the induction with the exponential feed. The final citrate mass was 7.5 g at the end of the culture, from the starting 9.6 g at the start of the culture.

III.2.2.1.3. BR06 and BR07: *Escherichia coli* CH10-12 – longer induction times (2nd series)

The cultures of *Escherichia coli* CH10-12 BR06 (Figure III-18) and BR07 (Figure III-19) were inoculated with 200 mL of a culture grown at 37°C for 15 h in MM, with the objective of shortening the batch mode. The initial glucose titer was 12.5 g/L and 7.5 g/L for BR06 and BR07, respectively. Fed-batch mode was started after depletion of the initial glucose and conducted as described for culture BR02. Induction was made after 9 h and 12 h of inoculation, corresponding to 30.8 g cdw/L and 23.5 g cdw/L for BR06 and BR07, respectively. On these cultures, induction durations of over 35 h (long

duration) were tested and temperature was controlled during the induction phase at a temperature 29°C and 32°C for BR06 and BR07, respectively.

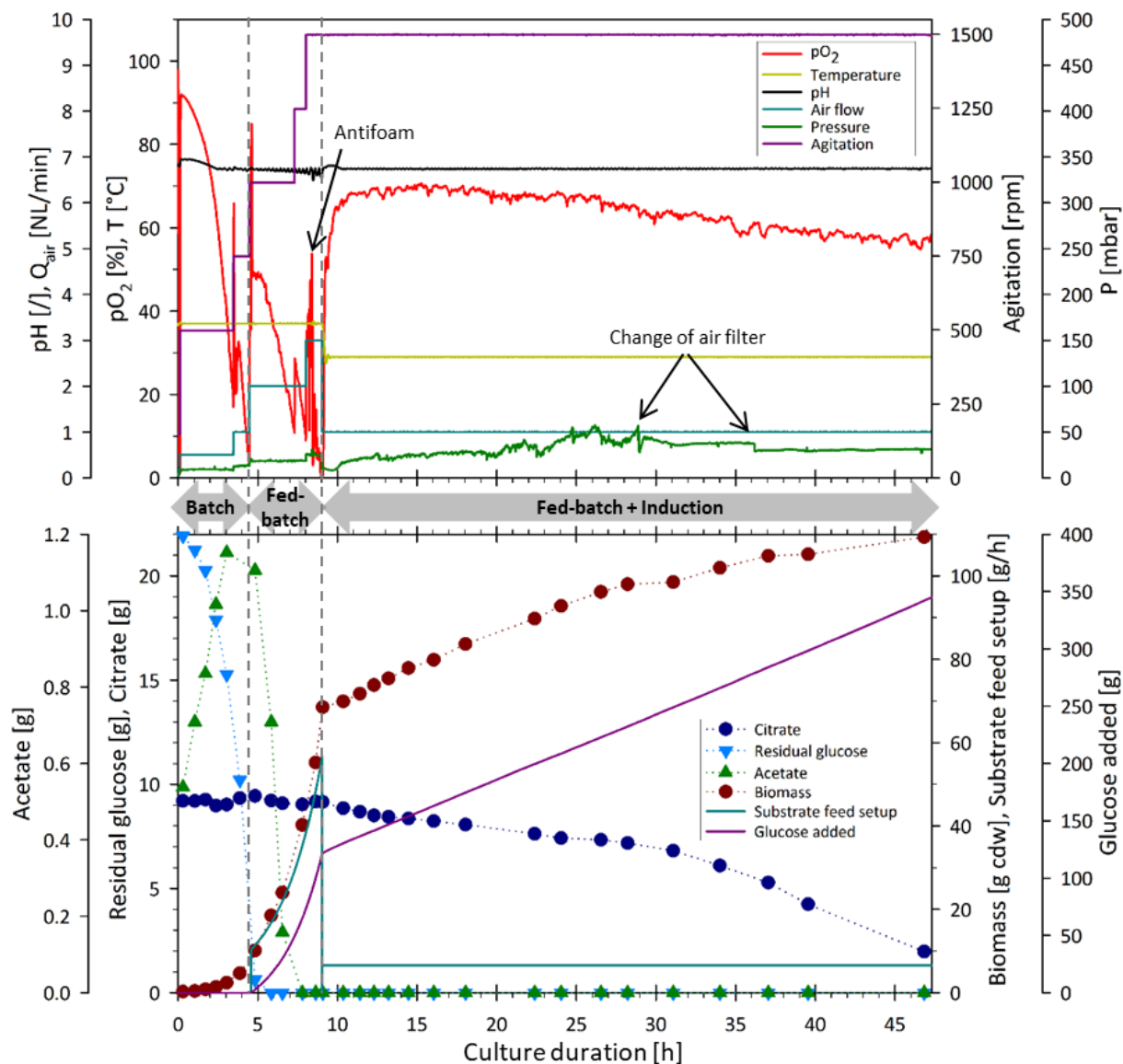


Figure III-18. Physico-chemical parameters, operating conditions and biological parameters of the culture of *Escherichia coli* CH10-12 (BR06) grown in MM, pH 6.8, 37°C, induced at 29°C for 38 h. The dotted lines depict the change in the operating mode.

In the culture BR06, 10 g cdw of biomass and 1.2 g of acetate were produced from 23 g of glucose in the batch mode. During the fed-batch mode, the acetate was consumed after the first two hours after the glucose feed started, and 67 g cdw of biomass were attained, with the consumption of 145 g of glucose at the end of the fed-batch mode. During the induction phase, a total biomass of 109 g cdw was attained and a total of 365 g of glucose were consumed. Dissolved oxygen was kept over 15% during the growth phases and over 60% during the induction phase. No accumulation of glucose was observed during the fed-batch mode or the induction. The final citrate mass was 2 g at the end of the culture, from the starting 9 g at the start of the culture.

In the culture BR07 (Figure III-19) there were some problems with the agitation shaft of the bioreactor, which made noises over 1,000 rpm, and agitation was not further increased. The strategy of aeration was changed from that used in all the other cultures (Figure III-11). Air flow was gradually increased up to 5 NL/min to maintain the oxygen needs of the microorganism due to the exponential glucose feed. Foam was formed in the bioreactor due to the high aeration rates and an increase of

pressure was noted (~300 mbar). High quantities of antifoam were added after 8 h of inoculation and consumed over a period of 6.5 h, where the dissolved oxygen measure remained close to zero. The increase of the pressure was caused by the clogging of the outlet filters (biomass particles, humidity, etc.).

To reduce the overpressure on the bioreactor, the aeration was reduced and set to 3 NL/min. The glucose feed was also reduced to a constant feed equivalent to a specific growth rate of 0.2 h^{-1} at the start of the feed, until biomass reached 23.5 g cdw/L . The decrease in biological activity resolved the oxygen transfer problem due to the inability to increase agitation over 1,000 rpm. Induction phase was conducted at 1,000 rpm and 1 NL/min, and pressure was stabilized at around 20 mbar.

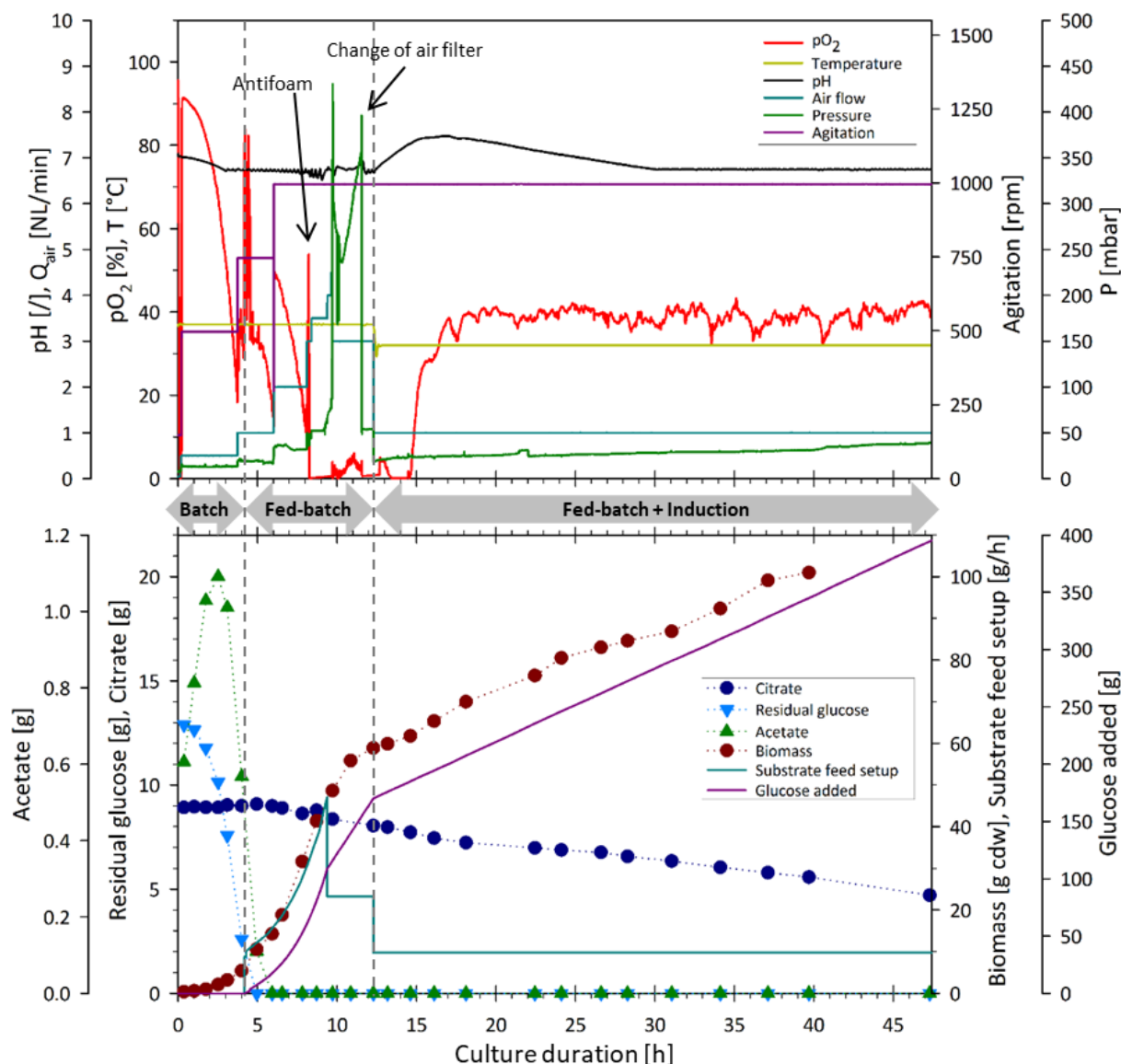


Figure III-19. Physico-chemical parameters, operating conditions and biological parameters of the culture of *Escherichia coli* CH10-12 (BR07) grown in MM, pH 6.8, 37°C, induced at 32°C for 35 h. The dotted lines depict the change in the operating mode.

In the culture BR07, 8 g cdw of biomass and 1.1 g of acetate were produced from 16 g of glucose in the batch mode. During the fed-batch mode, the acetate was consumed within the first two hours after the start of the fed-batch mode, and 60 g cdw of biomass were attained, with the consumption of 184 g of glucose at the end of the fed-batch mode. During the induction phase, a total biomass of 113 g cdw was attained and a total of 408 g of glucose were consumed. Dissolved oxygen was kept over 15% during the growth phases and over 35% during the induction phase. There was no

accumulation of glucose during the fed-batch mode with the exponential feed. The final citrate mass was 4.7 g at the end of the culture, from the starting 9 g at the start of the culture.

III.2.2.1.4. BR08: *Escherichia coli* NbF12-10 NN

The culture of *Escherichia coli* NbF12-10 NN (BR08) was inoculated with 200 mL of a culture grown at 37°C for 15 h in MM. The initial glucose titer was 10 g/L and the exponential phase was conducted for 5 h as previously described, after 4 h of batch mode.

In the shake-flask cultures, the strain *E. coli* NbF12-10 NN had a maximum specific growth rate (μ_{\max}) of 0.2 h⁻¹ in MM. During the batch mode in the bioreactor, the maximum specific growth rate of the strain was found to be over 0.7 h⁻¹, for which the feed strategy for an exponential feed equivalent to 0.38 h⁻¹ could be applied. This was confirmed when, during fed-batch mode, there was no accumulation of glucose.

The supply of ammoniac solution was stopped by accident during the start of the fed-batch mode and pH decreased gradually from 6.8 to 5.5 in a lapse of 2 h, at which point the ammoniac solution supply was restored and pH was controlled at 6.8. Protein expression was induced at 25.5 g cdw/L of biomass at 29°C. Outlet air filters were changed at about 13 h of culture to reduce the pressure of the bioreactor (Figure III-20). Culture was stopped after 47 h of culture and 37 h of induction.

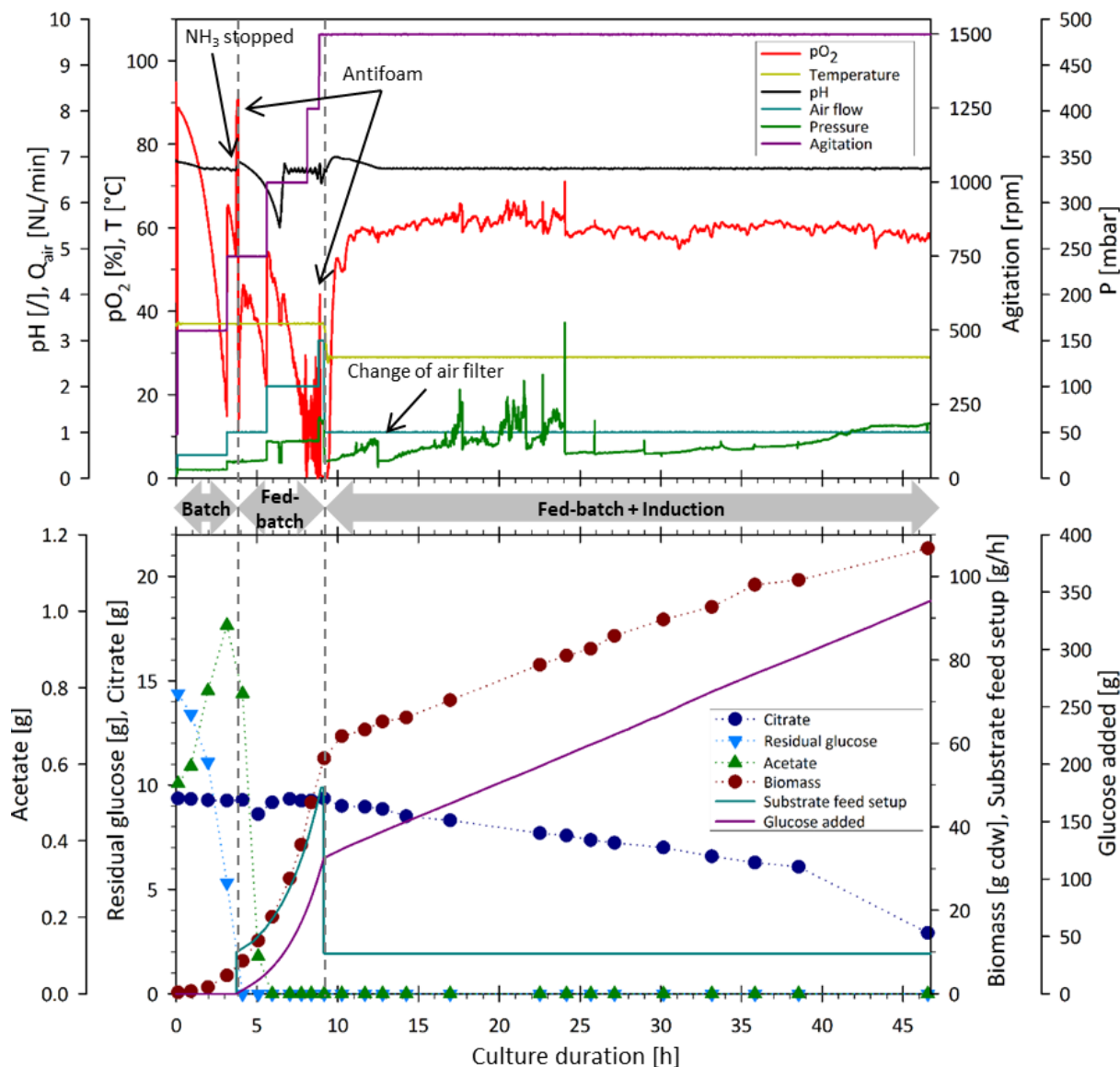


Figure III-20. Physico-chemical parameters, operating conditions and biological parameters of the culture of *Escherichia coli* NbF12-10 NN (BR08) grown in MM, pH 6.8, 37°C, induced at 29°C for 37 h. The dotted lines depict the change in the operating mode.

In the culture BR08, 7.3 g cdw of biomass and 0.9 g of acetate were produced from 14.5 g of glucose in the batch mode. During the fed-batch mode, the acetate was consumed during the first two hours after the start of the fed-batch mode, and 58 g cdw of biomass were attained, with the consumption of 135 g of glucose at the end of the fed-batch mode. During the induction phase, a total biomass of 107 g cdw was produced and a total of 358 g of glucose were consumed. Dissolved oxygen was kept over 15% during the growth phases and over 55% during the induction phase. There was no accumulation of glucose during the fed-batch mode with the exponential feed. The final citrate mass was 3 g at the end of the culture, from the starting 9.3 g at the start of the culture.

III.2.2.2. Overall performance of bioreactor cultures

During the batch mode of all cultures, dissolved oxygen was kept over 15%. Acetate was produced at a maximum titer of 1.2 g, and 7 g cdw of biomass were produced in average from 14.5 g of glucose (Table III-10).

Culture	Batch mode				Fed-batch mode			Induction phase		
	X [g cdw]	S [g]	Acetate [g]	Citrate [g]	X [g cdw]	S [g]	Citrate [g]	X [g cdw]	S [g]	Citrate [g]
BR01	6.5	14.5	0.3	6.4	40	87	6.4	/	/	4.7
BR02	6.5	13.7	0.6	8	45	103	6	57	145	5
BR03	6.6	11.2	0.6	7	48	97	5	63	129	6
BR04	7.6	14	0.9	9	58	109	9	71	133	8
BR05	7	15.4	0.9	9.6	55	99	8	65	124	7.5
BR06	10	23	1.2	9	67	145	9	109	365	2
BR07	8	16	1.1	9	60	184	8	113	408	4.7
BR08	7.3	14.5	1	9.3	58	135	9	107	358	3
BR09	7	14.9	0.9	9.2	47	133	9	80	312	6.6

Table III-10. Biomass, acetate, glucose, and citrate at the end of each operating mode.

During the fed-batch mode, an exponential feed was successfully applied, and equivalent to a specific growth rate of 0.38 h^{-1} . There was no accumulation of glucose, and the acetate was consumed during the first hours of the fed-batch mode. About 50 g cdw of biomass were produced at the end of the fed-batch mode.

The induction phase lasted between 6 h and 38 h after the pulse of 1 mM IPTG, depending on the culture. The dissolved oxygen was always kept over 55% during the induction phase, without accumulation of glucose or production of acetate. In the cultures with longer induction duration, the citrate in the culture medium decreased, which indicates its unexpected consumption.

III.2.2.3. Oxygen transfer

In aerobic cultures, it is important to remain in non-limiting oxygen transfer conditions to achieve acceptable biomass productivities. The couple of aeration and agitation will assure an adequate oxygen transfer from the inlet gas to the liquid medium, from which the microorganism will consume the oxygen.

III.2.2.3.1. Abiotic conditions

The transfer of oxygen in the defined minimal medium (MM) was characterized in the bioreactor under abiotic conditions. As a first step, the response time of the oxygen probes was determined. The probe lag was modeled as a first order lag [149], [175], [184].

$$\frac{dC_p}{dt} = \frac{C - C_p}{\tau} \quad (\text{III-4})$$

Where C_p is the dissolved oxygen measured by the probe, C is the dissolved oxygen concentration in the liquid and τ the response time of the probe. The response time was determined from equation (III-4) from the step change from 0% to 100% of dissolved oxygen. Measurements were made by quintuplicate in the probes of the two bioreactors used.

The manufacturer assures a response time of less than 70 s from a step change from air to nitrogen at 25°C (InPro 6860i/320, Mettler Toledo). In accordance with this manufacturer, a response time of about 40 s (39.7 ± 2.4 s and 44.5 ± 2.4 s) was measured for the oxygen probes in the bioreactor.

After the measurement of the oxygen probes in the bioreactor, the oxygen transfer was measured in the bioreactor filled with 1.5 L with defined minimal medium (MM). The Dynamic Method, also known as Gassing out-Gassing in method, was used for the measurements [185]–[187]. It consisted in measuring the change in the concentration of the dissolved oxygen when facing a step change in the inlet gas. The reactor was gassed with pure nitrogen, displacing the oxygen dissolved in the system, and when concentration reached zero, a step change was made to introduce air to the bioreactor [149], [175], [185], [187]–[190]. The volumetric oxygen mass transfer coefficient (k_La) was calculated using equation (III-5).

$$\ln \frac{C^* - C_p}{C^* - C_0} = \frac{t}{\left(\frac{1}{k_La} + \tau\right)} \quad (\text{III-5})$$

Where C^* is the oxygen saturation concentration in the liquid phase and C_0 is the dissolved oxygen concentration at time zero. The transfer of oxygen was measured by duplicate at the four conditions (Table III-11).

Aeration – Agitation conditions	k_La [h^{-1}]
0.5 NL/min – 500 rpm	10.5
1 NL/min – 1500 rpm	14.6
2 NL/min – 1000 rpm	27.4
3 NL/min – 1500 rpm	47.9

Table III-11. Volumetric mass transfer coefficient (k_La) under abiotic conditions.

Typical values of k_La in water vary from $24 h^{-1}$ to $300 h^{-1}$ for 2 L bioreactors [191], [192], and from $12 h^{-1}$ to $426 h^{-1}$ in 30 L bioreactors [193], [194]. The values of k_La depend highly on the configuration of the bioreactor, the number and type of agitation impellers and aeration conditions.

Semi-empirical correlations for the estimation of the k_La can be obtained (Eq. (III-6)), taking into account the dissipated power of the impeller (P/V in W/m^3) and the superficial gas velocity of the gas (V_s in m/s).

$$k_L a = c \left(\frac{P}{V} \right)^\alpha (V_S)^\beta \quad (\text{III-6})$$

Where α and β are the dimensionless correlation coefficients for the dissipated power and superficial gas velocity, respectively. Some typical values for the parameters α and β of can be found in Table III-12.

α	β	Impeller type	Bioreactor volume	Reference
0.4 – 0.95	0.2 – 0.64	Rushton	5 – 50 L	[149], [175], [188], [195]–[198]
0.58 – 1.23	0.27 – 0.7	2 Rushton	5 – 20 L	[188], [199], [200]
0.59 – 1.24	0.34 – 0.56	3 Rushton	2 – 20 L	[188], [192], [200], [201]

Table III-12. Typical values of the coefficients α and β of the $k_L a$ correlation of Eq. (III-6).

The volumetric mass transfer coefficient can also be expressed in terms of the agitation and the aeration rates. Considering the relation between the dissipated power and the mixing rate (Eq. (III-7)), a second correlation can be deduced in function of the working parameters (N , Q_{air} , V), according to the following demonstration:

$$P = N_P \rho N^3 D_i^5 \quad (\text{III-7})$$

$$k_L a = c \left(\frac{N_P \rho N^3 D_i^5}{V} \right)^\alpha \left(\frac{Q_{air}}{S_R} \right)^\beta \quad (\text{III-8})$$

$$k_L a = \frac{c (N_P \rho D_i^5)^\alpha}{S_R^\beta} N^{3\alpha} Q_{air}^\beta V^{-\alpha} \quad (\text{III-9})$$

$$k_L a = c' N^{3\alpha} Q_{air}^\beta V^{-\alpha} \quad (\text{III-10})$$

Where N_P is the power number of the impeller, ρ is the density of the liquid, N is the agitation rate, D_i is the diameter of the impeller, and S_R is the cross-sectional area of the bioreactor. N_P , ρ , D_i and S_R are assumed constant in (III-10).

Using the correlation in Eq. (III-10), a semi-empirical correlation could be found for the abiotic volumetric mass coefficient and function of the aeration and agitation parameters in 5 L bioreactors with the configuration used in Figure II-4 :

$$k_L a = 8.72 * N^{0.14} * \left(\frac{Q_{air}}{V_t} \right)^{0.99} \quad (\text{III-11})$$

The coefficient of the aeration is higher than the coefficient of the agitation (0.99 vs 0.14). This suggests that at the working conditions, the transfer of oxygen is made mainly by the aeration and the rising bubbles than for the dissipated power of the mixing system, and increasing only the aeration will have a higher impact than only increasing the agitation (Figure III-21).

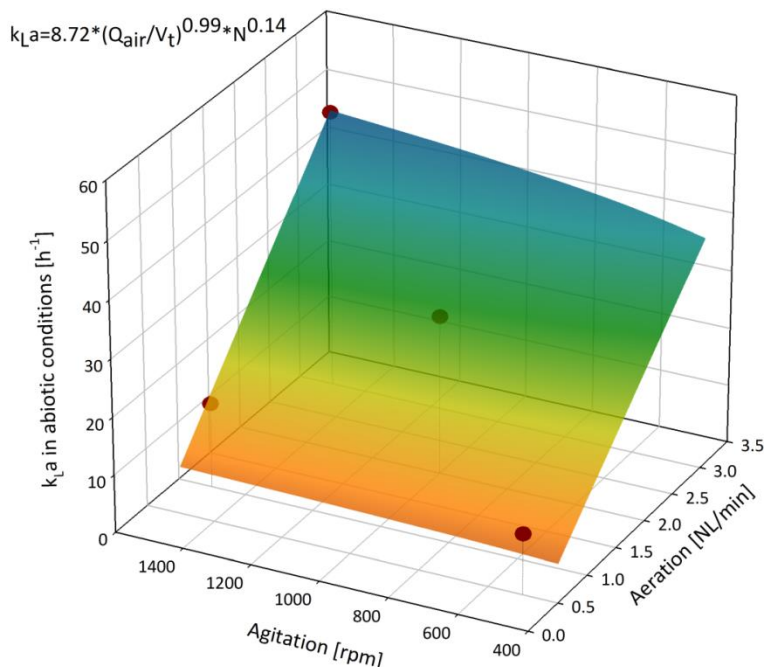


Figure III-21. Volumetric mass transfer coefficient (k_{La}) under abiotic conditions for different aeration and agitation conditions in 1.5 L of MM at 37°C, pH 6.8.

III.2.2.3.2. Biological conditions

The oxygen transfer rate was used to obtain the volumetric mass transfer coefficient in the cultures BR01 to BR09 as defined by equation (III-12).

$$K_L a = \frac{r_{O_2}^L}{(C^* - C)} \quad (III-12)$$

Where $K_L a$ is the volumetric mass transfer coefficient in h^{-1} , r_{O_2} is the rate of consumption of oxygen in mol/h, C^* and C are the dissolved oxygen concentration at saturation and in the liquid, respectively, in mol/L, and V_t^L is the volume of the liquid in the bioreactor in L.

The transition zones, after the change of aeration and agitation conditions were not taken into consideration for the $K_L a$ calculations. The perturbations due to the addition of the antifoam, as shown in §III.2.2.1, and the starvation zones, were also not taken into consideration.

The aeration and agitation conditions defined in §III.2.1 were applied for cultures BR02 to BR09 in the following order: during batch mode 0.5 NL/min – 500 rpm, during fed-batch mode 2 NL/min – 1,000 rpm and 3 NL/min – 1,500 rpm. For culture BR01, different conditions were used (0.5 – 2 NL/min, 500 – 1,250 rpm).

In the culture BR01 the $K_L a$ reached values of about 130 h^{-1} in the batch mode and values of up to 800 h^{-1} and 1200 h^{-1} in the fed-batch mode, where aeration and agitation were higher (Figure III-22).

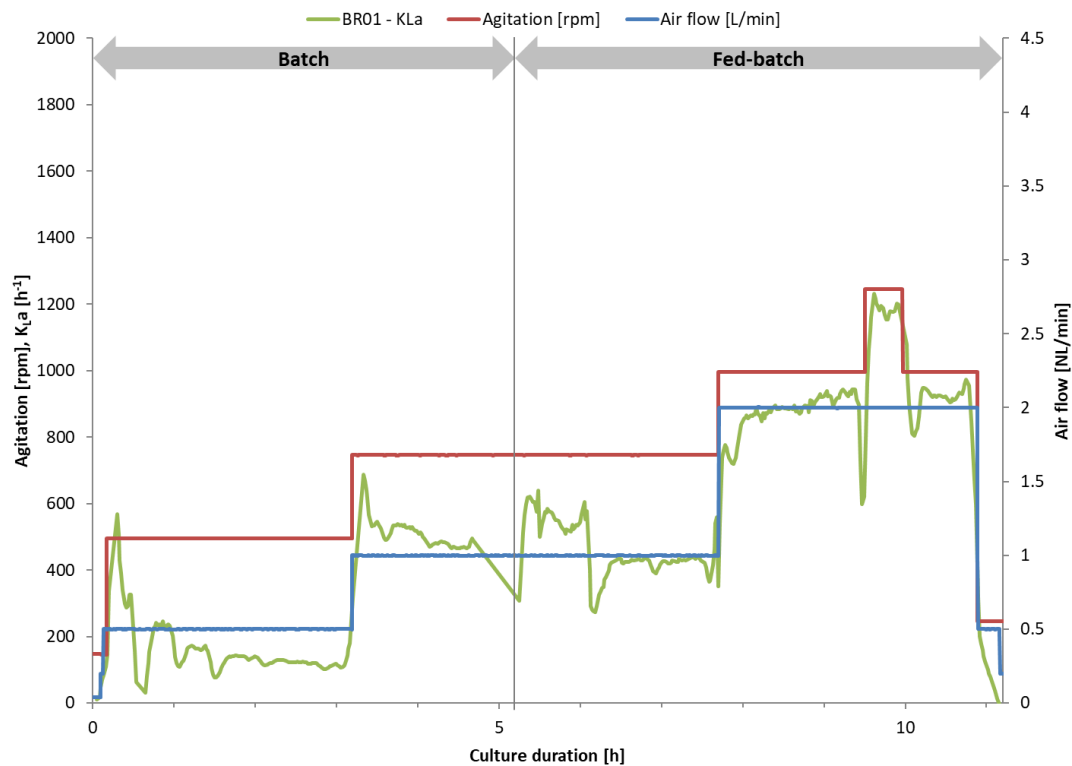


Figure III-22. Volumetric mass transfer coefficient (K_La) in culture BR01.

In the cultures BR02 and BR03 the volumetric mass transfer coefficient, K_La , was about 200 h^{-1} at the batch mode in both cultures at $0.5 \text{ NL/min} - 500 \text{ rpm}$ (Figure III-23). In the fed-batch mode values of about 800 h^{-1} for both strains were obtained at 2 NL/min and $1,000 \text{ rpm}$. The same values were achieved for the culture BR01 at the same aeration and agitation conditions. At the end of the fed-batch mode, at higher aeration and agitation conditions ($3 \text{ NL/min} - 1,500 \text{ rpm}$) the K_La reached values close to 1600 h^{-1} and $1,400 \text{ h}^{-1}$ for BR02 and BR03, respectively. For the induction phase ($1 \text{ NL/min} - 1,500 \text{ rpm}$), the K_La was almost constant at 300 h^{-1} for culture BR02, but for culture BR03 values of about 700 h^{-1} were achieved.

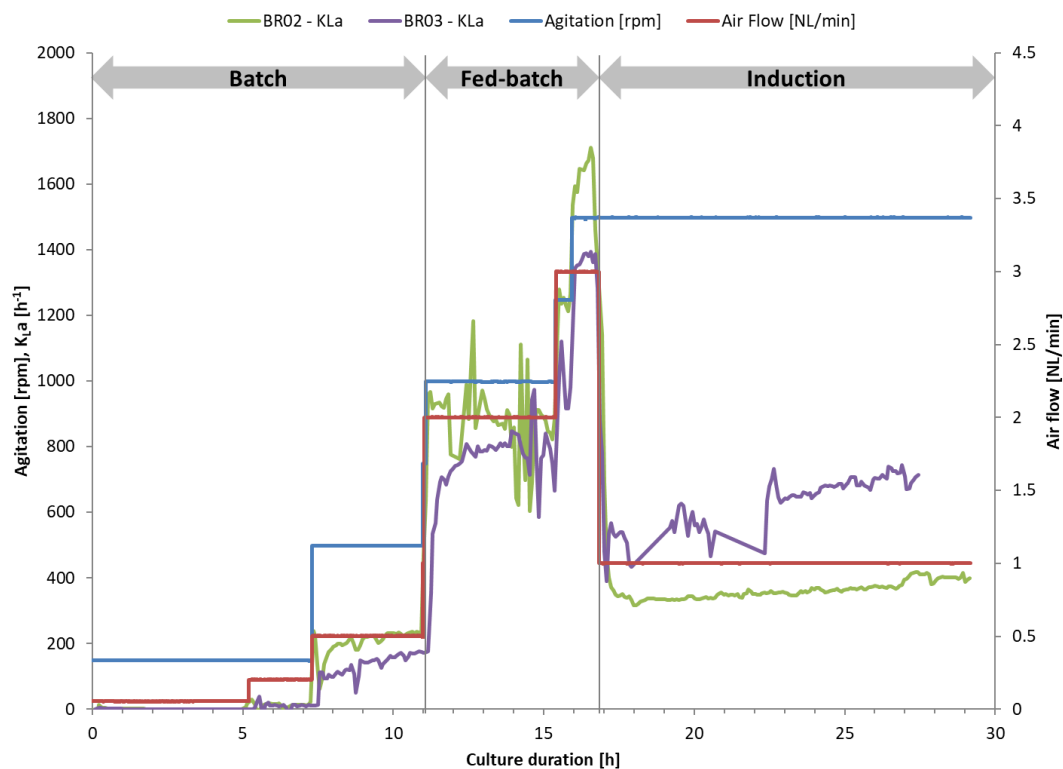


Figure III-23. Volumetric mass transfer coefficient (K_{La}) in culture BR02 and BR03.

Similar results were found in the cultures BR04 and BR05 (Figure III-24). In batch mode (0.5 NL/min – 500 rpm), the K_{La} was about 200 h^{-1} in both cultures and increased during the start of the fed-batch mode (2 NL/min – 1,000 rpm) to 900 h^{-1} and 700 h^{-1} for BR04 and BR05, respectively. At the end of the fed-batch mode (3 NL/min – 1,500 rpm), values of 1,650 h^{-1} and 1,100 h^{-1} were obtained for BR04 and BR05, respectively. During the induction phase and nanobody production (1 NL/min – 1,500 rpm), values of 750 h^{-1} and 600 h^{-1} were obtained for BR04 and BR05, respectively.

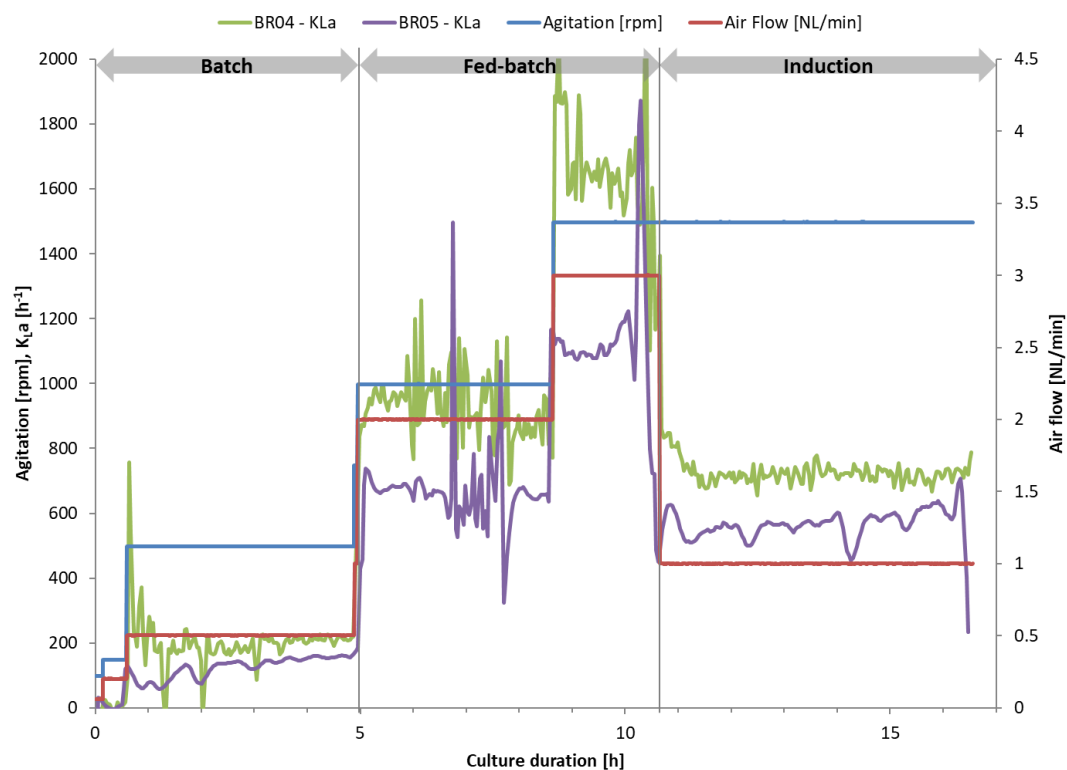


Figure III-24. Volumetric mass transfer coefficient (K_{La}) in culture BR04 and BR05.

In the culture BR06 the K_{La} was about 120 h^{-1} in the batch mode (0.5 NL/min – 500 rpm) and between 600 h^{-1} and 1200 h^{-1} in the fed-batch mode (Figure III-25). During the induction phase and nanobody production, K_{La} remained almost constant during the over 36 h of induction at 600 h^{-1} at the aeration and agitation conditions of 1 NL/min – 1,500 rpm.

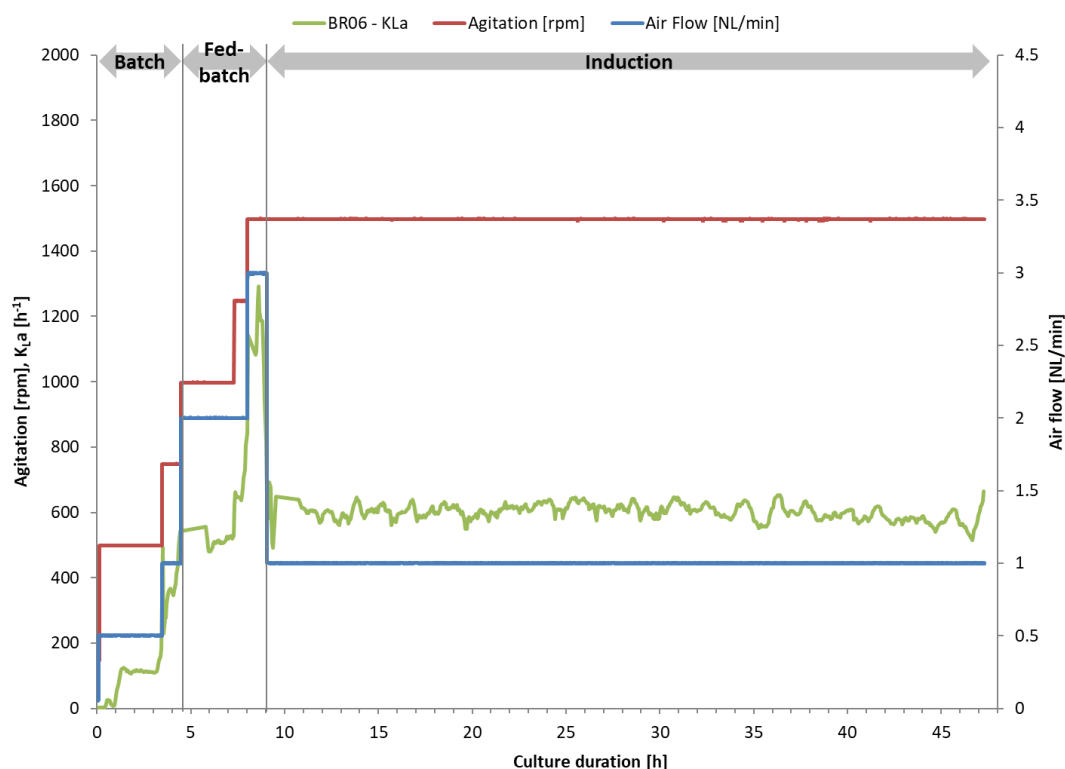


Figure III-25. Volumetric mass transfer coefficient (K_{La}) in culture BR06.

In the culture BR07 the K_{La} was about 160 h^{-1} during the batch mode (0.5 NL/min, 500 rpm, Figure III-26). The K_{La} was highly perturbed by the changes of aeration made to maintain the dissolved oxygen above 15%, and values varied from 220 h^{-1} to 1000 h^{-1} . During induction and production of the nanobody, the K_{La} was about 600 h^{-1} with an aeration of 1 NL/min and 1000 rpm.

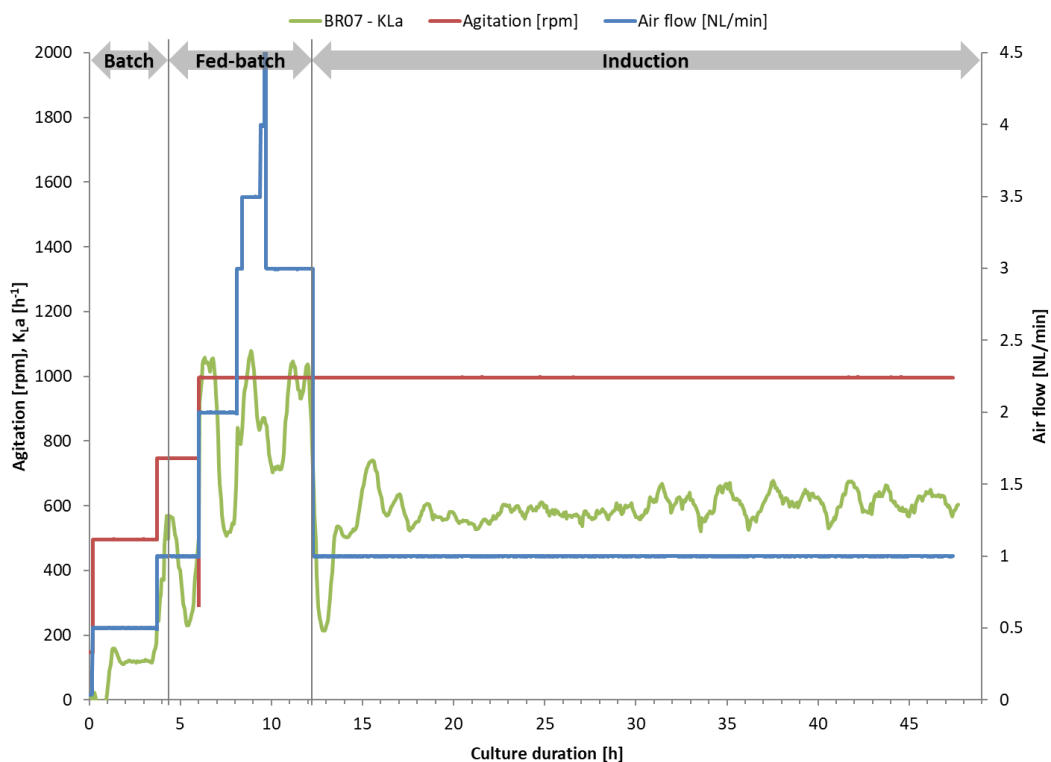


Figure III-26. Volumetric mass transfer coefficient (K_{La}) in culture BR07.

For the culture of *Escherichia coli* NbF12-10 in the culture BR08 the K_{La} was about 210 h^{-1} (0.5 NL/min, 500 rpm, Figure III-27), similar to the values obtained for cultures of *Escherichia coli* CH10-12 (BR02 – BR07). In the fed-batch mode, the K_{La} values obtained were lower than for the strain CH10-12, with values between 500 h^{-1} and $1,100 \text{ h}^{-1}$ at the end of the fed-batch mode. During the induction and production of the nanobody, the K_{La} remained constant at 600 h^{-1} and equal than for the other strains (1 NL/min, 1,500 rpm).

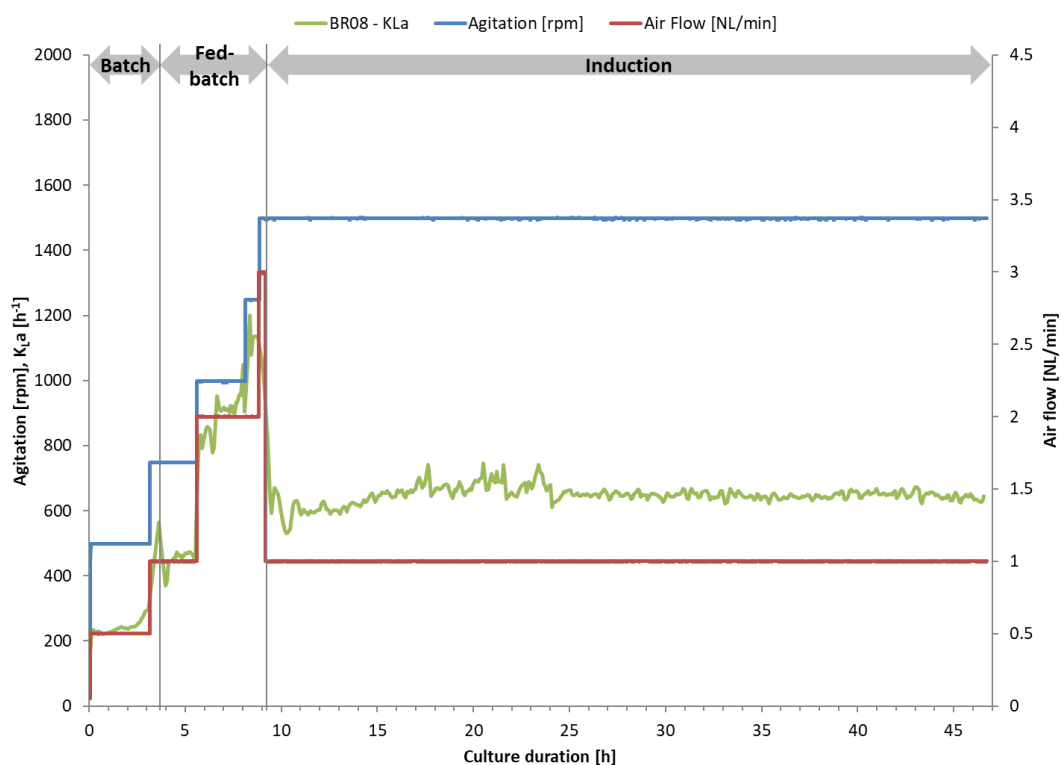


Figure III-27. Volumetric mass transfer coefficient (K_{La}) in culture BR08.

In the culture of *Escherichia coli* WK6 used as negative control (BR09), the K_La during the batch mode was close to 250 h^{-1} (0.5 NL/min, 500 rpm, Figure III-28). In the fed-batch mode, the K_La reached values from 650 h^{-1} at 2 NL/min – 1,000 rpm to 1500 h^{-1} at the end of the fed-batch mode (3 NL/min – 1,500 rpm) and comparable with the cultures of strain CH10-12. During the induction, the K_La was kept almost constant at 710 h^{-1} , the highest found for all cultures and strains.

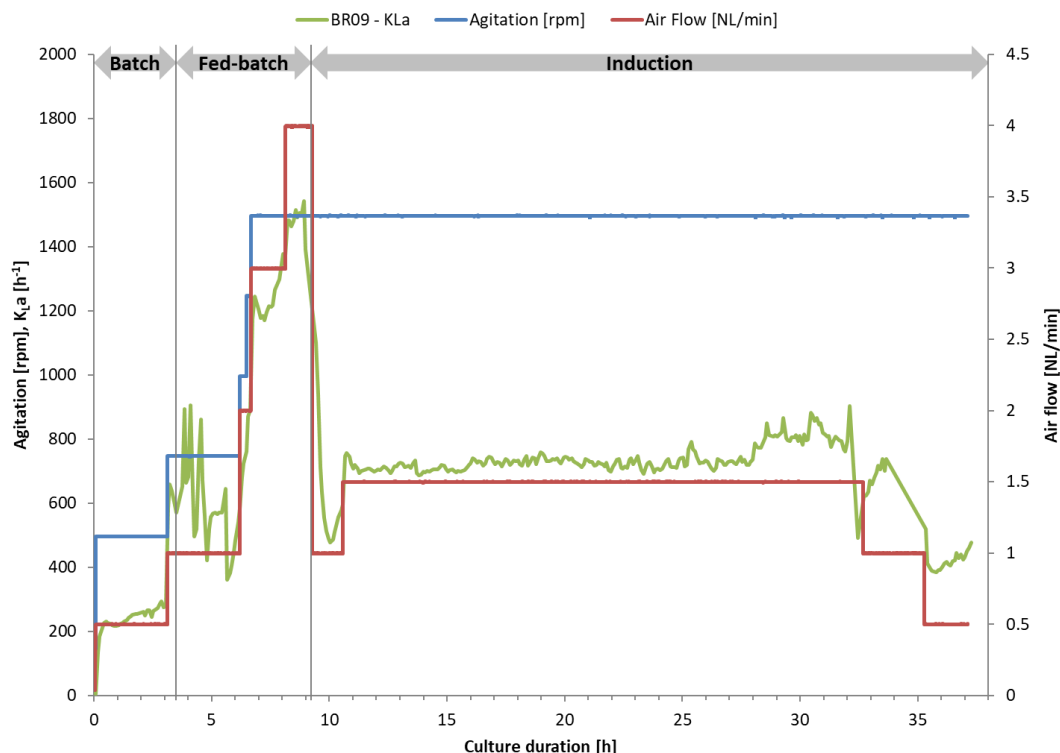


Figure III-28. Volumetric mass transfer coefficient (K_La) in culture BR09.

III.2.2.3.3. Biological enhancement coefficient, E

The biological enhancement factor, E, is defined as the ratio of the oxygen transfer in abiotic conditions to the oxygen transfer in biotic conditions as defined by equation (III-13).

$$E = \frac{K_L a}{k_L a_0} \quad (\text{III-13})$$

The average volumetric oxygen mass transfer coefficient in abiotic conditions, $k_L a_0$, was obtained as described in §III.2.2.3.1. The average volumetric oxygen mass transfer coefficient in biological conditions, $K_L a$, was obtained from the oxygen transfer in cultures BR01 to BR09 (Table III-13).

Volumetric oxygen mass coefficient, $K_L a$ [h^{-1}]	500 rpm	1000 rpm	1500 rpm	
	0.5 NL/min	2 NL/min	3 NL/min	1 NL/min
Abiotic conditions	10.53 ± 0.7	27 ± 0	47.86 ± 0	15 ± 1
BR01 - WK6	164.1 ± 4.4	877 ± 7	/	/
BR02 - CH10-12	173.4 ± 7	867 ± 7	1653 ± 3	354 ± 13
BR03 - CH10-12	132.7 ± 4.2	748 ± 12	1339 ± 41	521 ± 17
BR04 - CH10-12	138.6 ± 1.6	723 ± 19	1257 ± 32	643 ± 8
BR05 - CH10-12	129.9 ± 2.6	654 ± 11	1138 ± 13	576 ± 3
BR06 - CH10-12	90.74 ± 5.9	782 ± 53	1255 ± 50	609 ± 3
BR07 - CH10-12	96.7 ± 7.5	757 ± 38	/	/
BR08 - NbF12-10 NN	234.3 ± 5.9	888 ± 5	1068 ± 2	642 ± 21
BR09 - WK6	249.6 ± 5.9	719 ± 2	1255 ± 4	780 ± 6

Table III-13. Volumetric mass transfer coefficient for cultures BR01 to BR09 and under abiotic conditions.

The volumetric oxygen mass transfer coefficient, K_La , under biological conditions varies from 90 h^{-1} to 1650 h^{-1} at the high aeration and agitation conditions. These values are consistent with the literature (Table III-14).

Strain	$k_La \text{ [h}^{-1}\text{]}$	Culture conditions	Reference
<i>Escherichia coli</i>	180 – 2340	25 NL/min, 800 rpm, 20 L bioreactor	[202]
<i>Rhodotorula glutinis</i>	1200	10 NL/min, 1000 rpm, 20 L bioreactor	[203]
<i>Yarrowia lipolytica</i>	120 – 700	5 → 20 NL/min, 500 → 1200 rpm, 20 L bioreactor	[204]
<i>Saccharomyces cerevisiae</i>	24 – 540	5 NL/min, 600 rpm, 5 L bioreactor	[187]
<i>Aspergillus awamori</i>	100 – 450	2 → 10 NL/min, 300 → 700 rpm, 10 L bioreactor	[198]

Table III-14. Typical values of the volumetric oxygen mass transfer coefficient, K_La , in biological conditions

The biological enhancement factor varied from 15 to 40 in the fed-batch mode to values close to 40 for the induction (Figure III-29). The biological enhancement factor increases from 5 to 30 in the batch mode and slightly during the fed-batch mode.

The enhancement due to the microbial growth was higher than the values found in the literature, ranging from 0.85 to 1.5 in other microbial cultures of biomass concentration of up to 25 g cdw/L [149], [175]. The methods of quantification of the biological enhancement factor found in the literature are made through mass transfer resistances, and not from the volumetric mass transfer coefficient under the biotic and abiotic conditions used in our analysis.

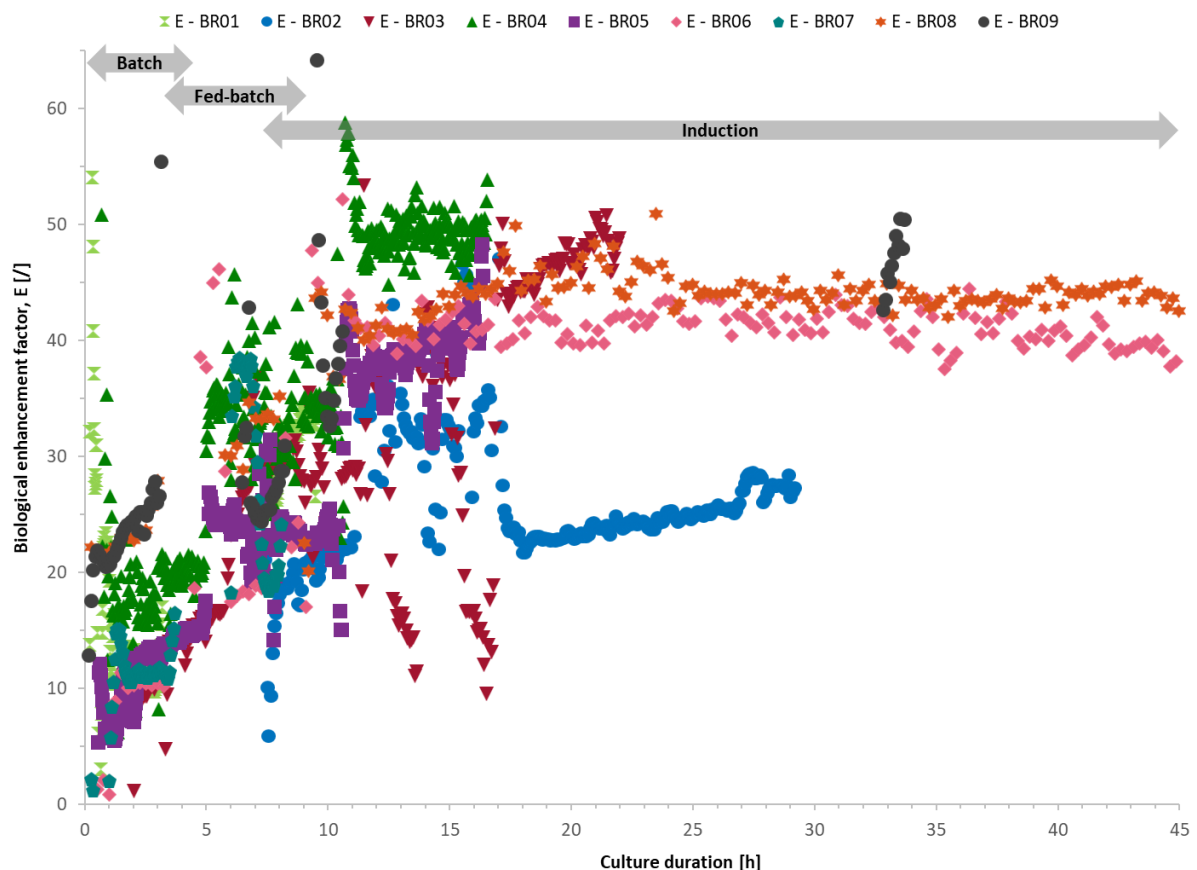


Figure III-29. Biological enhancement factor, E , for all cultures (BR01 - BR09).

In the short induction duration cultures, during protein expression the biological enhancement factor increased from 20 to about 50, depending on the culture. In the long induction duration

cultures, the protein expression in the induction phase did not affect the biological enhancement factor.

III.2.3. Biotic variables

During the aerobic culture of *Escherichia coli* with glucose as carbon source, biomass and carbon dioxide are formed as the main products, acetic acid is formed when glucose is present in excess, and the nanobody is produced when the protein expression is induced by the IPTG pulse.

III.2.3.1. Mass and Energy balances

The carbon and degree of reduction (redox) balances were calculated at the final points from the raw data, according to §II.8.2 and §II.8.3. The carbon and the redox recoveries at the final points were 95% and 92%, respectively for all cultures.

III.2.3.2. Biomass

The biomass was quantified by two methods: the optical density (§II.6.1) and the cell dry weight (§II.6.2). Both methods were correlated with the Beer-Lambert law as defined by equation (III-1). The correlation coefficient was determined along all the culture modes within the precision range defined in §III.1.2.1. It was around 2 for all culture modes in all strains (Figure III-30), regarding of the method of quantification.

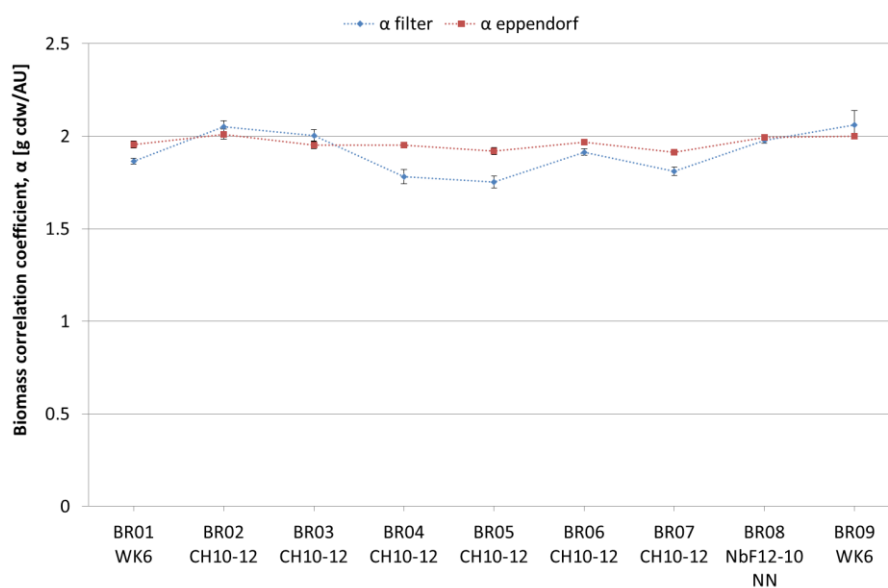


Figure III-30. Biomass and optical density coefficient (α).

III.2.3.2.1. Specific growth rate

All cultures show high repeatability using the strategies defined for the oxygen transfer (Figure III-11) and the glucose feed. Biomass was produced exponentially during batch and fed-batch modes, at different rates shown by the slope discontinuity between the batch and fed-batch modes in the logarithmic scale (Figure III-31).

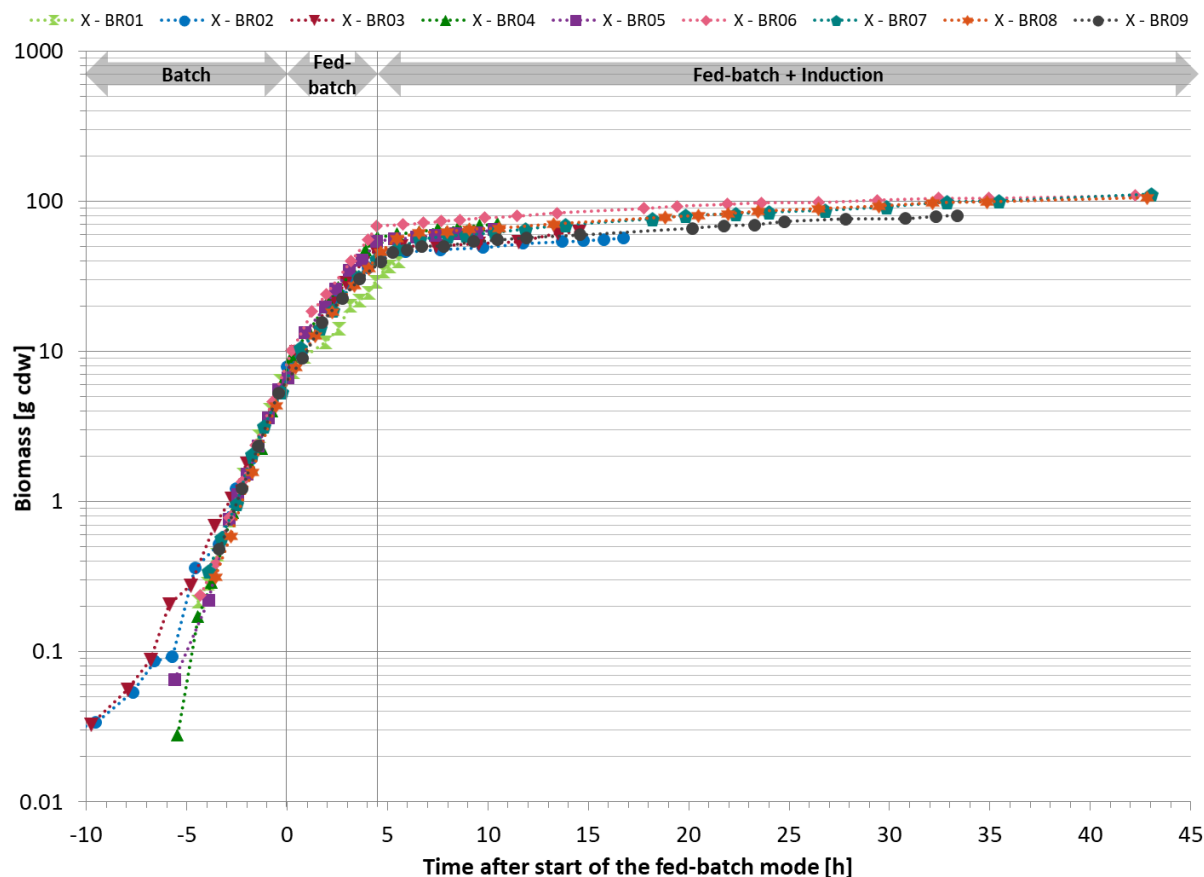


Figure III-31. Biomass evolution of all cultures (BR01 – BR09). Time was normalized to the start of the fed-batch mode.

The maximum specific growth rates were determined for batch mode and the average specific growth rates were determined in fed-batch mode and the induction phase (Figure III-32). At the batch mode all cultures were grown at 37°C, pH of 6.8 and dissolved oxygen was kept over 15%. The maximum specific growth rate was in average 0.8 h^{-1} for most cultures, cultures BR02 and BR03 had an average specific growth rate of 0.7 h^{-1} . The difference between the batch mode of the cultures BR02 and BR03 and the rest of the cultures is the low biomass in which the bioreactors were inoculated and the adaptation of the microorganism to the culture medium in the first 5 h of the cultures (Figure III-14, Figure III-15). Despite this minor difference, the maximum specific growth rate of all strains was virtually the same under the controlled optimal conditions: 37°C, pH 6.8, good oxygen transfer. The maximum specific growth rates found in bioreactor cultures were higher than those of shake flask cultures due to the controlled culture conditions (§III.1.2.3).

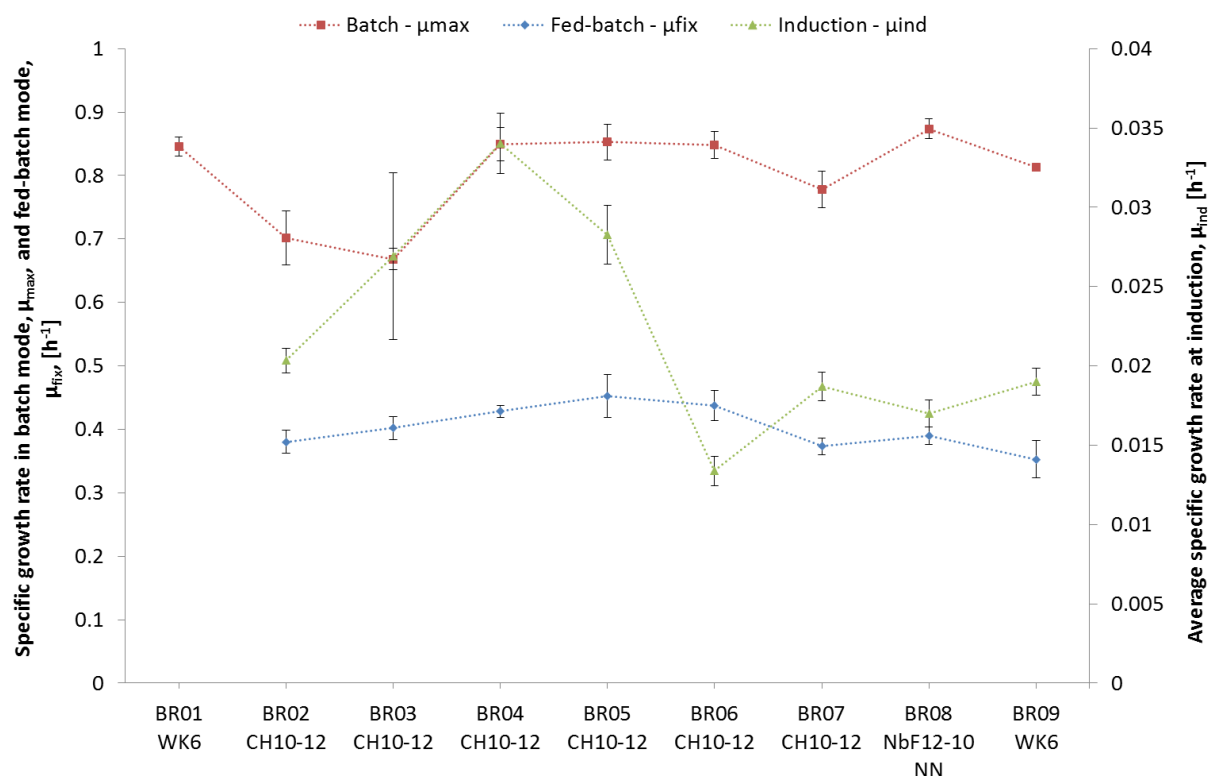


Figure III-32. Average specific growth rate (μ) on each operating condition. Cultures BR01 – BR09 grown on MM at 37°C, pH 6.8.

During the fed-batch mode, the average specific growth rate was 0.4 h^{-1} for cultures BR02 to BR09, and it was consistent with the feed of glucose imposed a specific growth rate of 0.38 h^{-1} . The fed-batch mode of the culture BR01 was controlled at different constant glucose feeds and the specific growth rate decreased with the production of the biomass. In culture BR01 the specific growth rate during fed-batch varied from 0.52 h^{-1} to 0.13 h^{-1} (Table III-15).

Culture	$\mu_{\max} [\text{h}^{-1}]$	$\mu_{\text{fix}} [\text{h}^{-1}]$	$\mu_{\text{ind max} \rightarrow \text{min}} [\text{h}^{-1}]$	Induction temperature [°C]	Induction duration [h]
BR01 – WK6	0.85 ± 0.02	0.52 to 0.13	/	/	/
BR02 – CH10-12	0.70 ± 0.04	0.38 ± 0.02	$0.023 \rightarrow 0.018$	28	12
BR03 – CH10-12	0.67 ± 0.02	0.40 ± 0.03	$0.074 \rightarrow 0.014$	30	10
BR04 – CH10-12	0.85 ± 0.03	0.43 ± 0.03	$0.048 \rightarrow 0.022$	33	6
BR05 – CH10-12	0.85 ± 0.03	0.45 ± 0.03	$0.031 \rightarrow 0.003$	37	6
BR06 – CH10-12	0.85 ± 0.02	0.44 ± 0.02	$0.029 \rightarrow 0.002$	29	38
BR07 – CH10-12	0.78 ± 0.03	0.37 ± 0.01	$0.025 \rightarrow 0.013$	32	35
BR08 – NbF12-10 NN	0.87 ± 0.02	0.39 ± 0.01	$0.029 \rightarrow 0.008$	29	37
BR09 – WK6	0.81 ± 0.01	0.35 ± 0.03	$0.033 \rightarrow 0.001$	29	28

Table III-15. Average specific growth rates in operating conditions: batch (μ_{\max}), fed-batch (μ_{fix}) and induction ($\mu_{\text{induction}}$).

During the induction phase of the cultures BR02 to BR09, the specific growth rate decreased because of the constant substrate flow rate (Figure III-33). In the case of culture BR03, where there were problems with the glucose feed, the specific growth rate was null in the periods of starvation; with the increase of the glucose feed the specific growth rate was slightly higher than the other cultures near the end of the culture. The evolution of the specific growth rate of culture BR03 is not shown in Figure III-33.

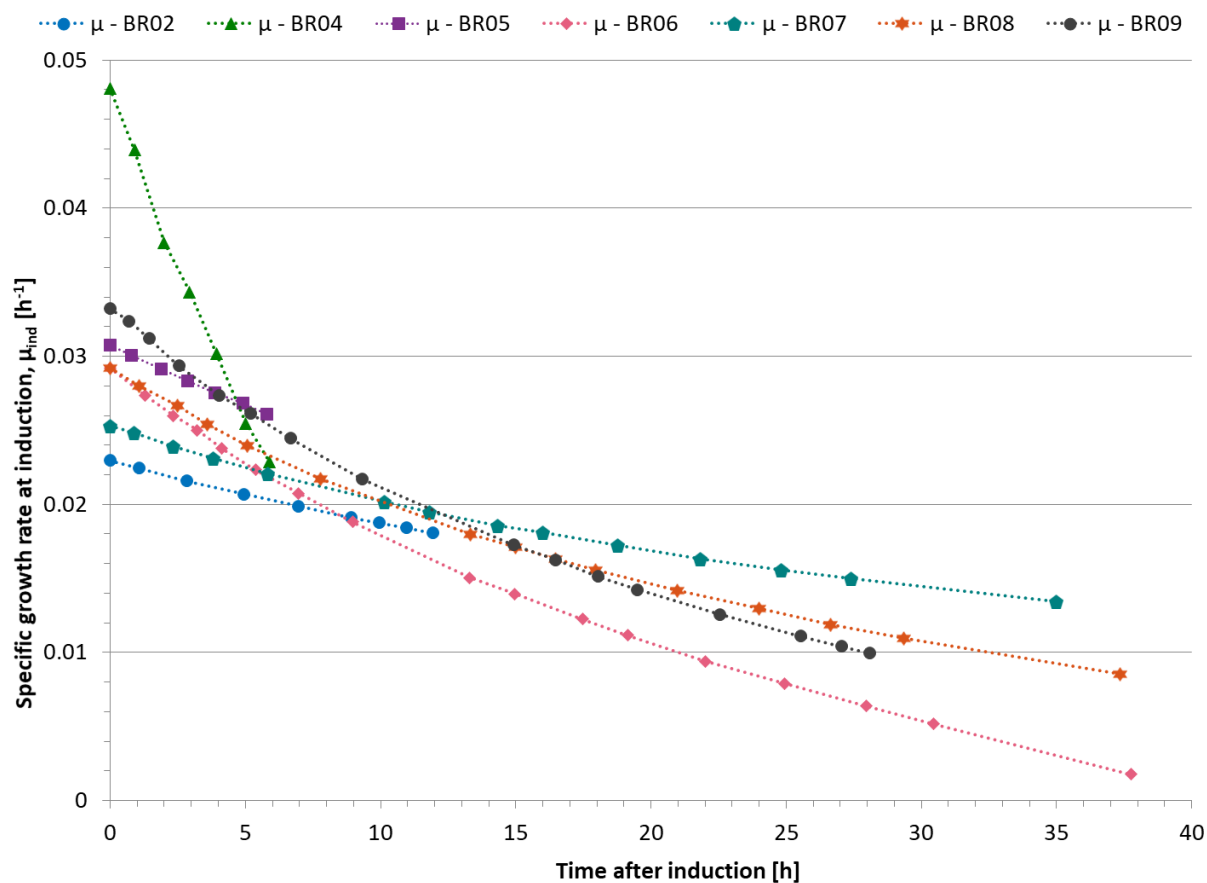


Figure III-33. Specific growth rate after induction of the protein expression.

III.2.3.2.2. Biomass yield

The evolution of the yield of biomass on glucose, $Y_{X/S}$, reflects the carbon utilization during the cultures. These yields were calculated for each operating condition as the slope on the representation of biomass versus glucose (Figure III-34).

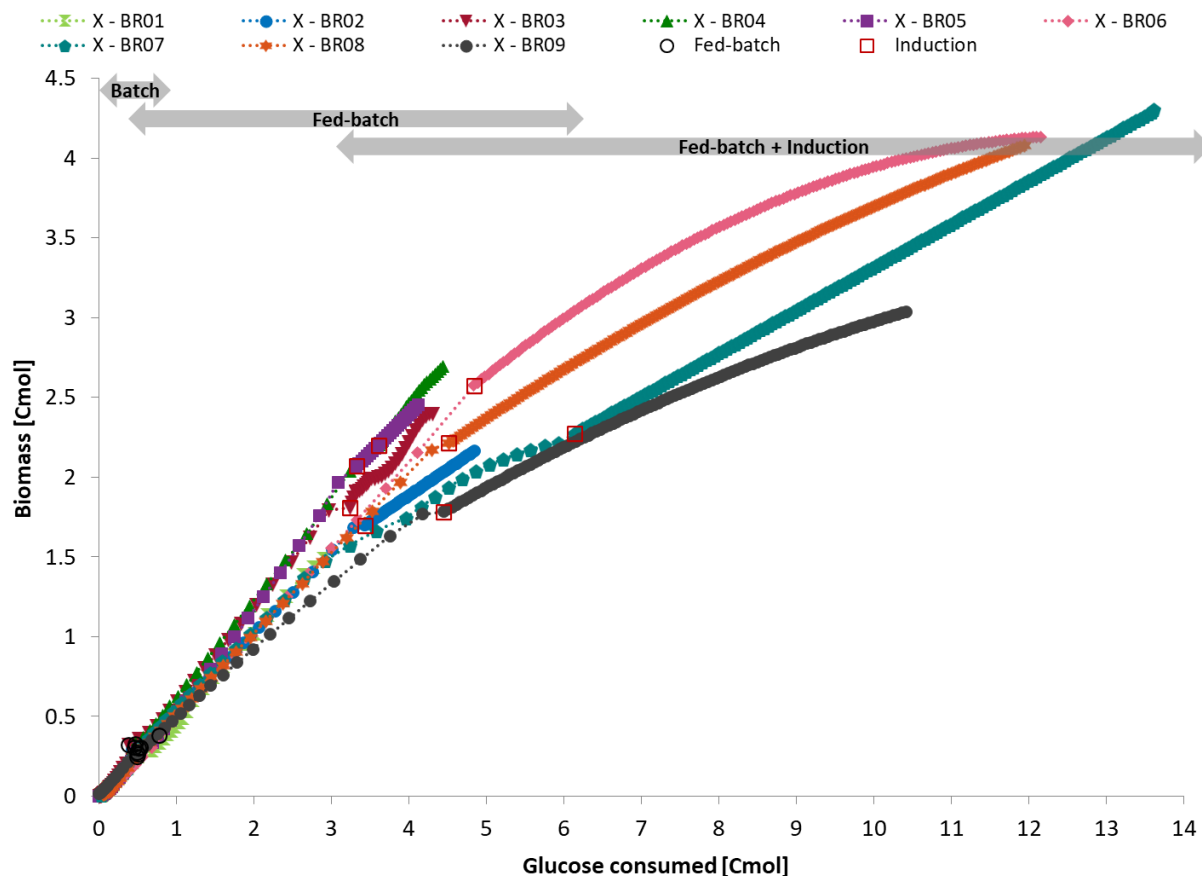


Figure III-34. Evolution of the biomass versus the consumed glucose in cultures BR01 – BR09 from smoothed data. The black circles denote the start of the fed-batch mode and the red squares denote the start of the induction phase.

The yields for each operating condition of the cultures are presented in Table III-16. Generally, the yields are higher in the fed-batch mode than in the batch mode, which is expected taking into consideration the production of acetic acid as a by-product in the batch mode due to the excess of glucose.

Culture	Batch mode		Fed-batch mode		Induction	
	$Y_{x/s}$ [Cmol/Cmol]	$Y_{x/s}$ [g/g]	$Y_{x/s}$ [Cmol/Cmol]	$Y_{x/s}$ [g/g]	$Y_{x/s}$ [Cmol/Cmol]	$Y_{x/s}$ [g/g]
BR01 – WK6	0.50 ± 0.01	0.42 ± 0.01	0.54 ± 0.01	0.45 ± 0.01	/	/
BR02 – CH10-12	0.54 ± 0.01	0.45 ± 0.01	0.50 ± 0.01	0.42 ± 0.01	0.33 ± 0.01	0.27 ± 0.01
BR03 – CH10-12	0.61 ± 0.02	0.50 ± 0.01	0.58 ± 0.01	0.48 ± 0.01	0.50 ± 0.01	0.42 ± 0.01
BR04 – CH10-12	0.64 ± 0.01	0.53 ± 0.01	0.62 ± 0.01	0.51 ± 0.01	0.61 ± 0.01	0.51 ± 0.01
BR05 – CH10-12	0.55 ± 0.01	0.46 ± 0.01	0.66 ± 0.01	0.55 ± 0.01	0.48 ± 0.01	0.40 ± 0.01
BR06 – CH10-12	0.45 ± 0.01	0.37 ± 0.01	0.53 ± 0.01	0.44 ± 0.01	0.21 ± 0.01	0.18 ± 0.01
BR07 – CH10-12	0.59 ± 0.01	0.49 ± 0.01	0.48 ± 0.01	0.40 ± 0.01	0.27 ± 0.01	0.23 ± 0.01
BR08 – NbF12-	0.60 ± 0.02	0.50 ± 0.02	0.50 ± 0.01	0.42 ± 0.01	0.25 ± 0.01	0.21 ± 0.01

Culture	Batch mode		Fed-batch mode		Induction	
	$Y_{X/S}$ [Cmol/Cmol]	$Y_{X/S}$ [g/g]	$Y_{X/S}$ [Cmol/Cmol]	$Y_{X/S}$ [g/g]	$Y_{X/S}$ [Cmol/Cmol]	$Y_{X/S}$ [g/g]
10 NN						
BR09 – WK6	0.55 ± 0.01	0.46 ± 0.01	0.41 ± 0.01	0.35 ± 0.01	0.21 ± 0.01	0.17 ± 0.01

Table III-16. Average biomass yield on glucose ($Y_{X/S}$) for the operating conditions batch and fed-batch combined.

In the literature, a yield of 0.42 g/g was found for another recombinant strain of *E. coli* grown in a continuous culture with our same defined minimal medium (§II.3.3, [205]). In defined minimal medium, values between 0.38 g/g to 0.47 g/g can be found for other recombinant strains of *Escherichia coli* in batch cultures [148], [182], and a yield of 0.42 g/g to 0.51 g/g can be found for fed-batch cultures [95], [205]. In our case, we found the yield is around 0.4 g/g and 0.5 g/g, for batch mode and fed-batch mode, respectively (Figure III-35).

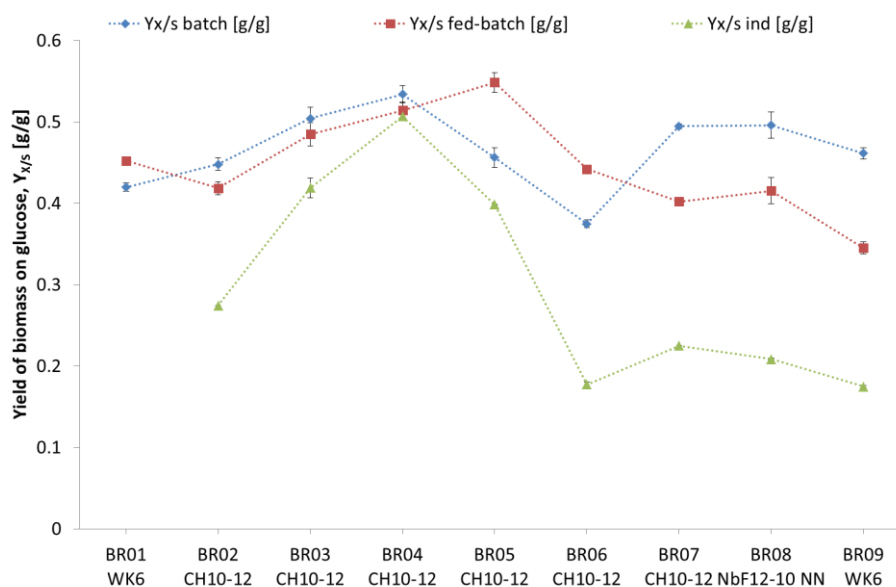


Figure III-35. Average yield of biomass for all cultures (BR01 – BR09).

During the induction phase, the yield of biomass on glucose, $Y_{X/S}$, was significantly lower than in batch and fed-batch modes, especially for the cultures with long induction times (BR06 – BR09). The yield of biomass on glucose decreased with time, as it can be seen in Figure III-34.

The induction of the protein expression caused by the pulse of IPTG induced the production of the nanobody in the recombinant strains. A shift on the metabolism is expected, which would cause the glucose to be converted to either carbon dioxide or the recombinant nanobody.

The maintenance of a microorganism includes several complex phenomena, physiological and non-growth associated, and can be defined as the consumption of apparently non-finalized substrate [206], [207]. To obtain the maintenance coefficient, m , the specific glucose consumption, q_S , was plotted against the specific growth rate, μ , as defined by Eq. (III-14).

$$q_S = \frac{\mu}{Y_{X/S}} + m \quad (\text{III-14})$$

With q_S in Cmol S/Cmol X/h, μ in h^{-1} , $Y_{X/S}$ in Cmol S/CmolX and m in Cmol S/Cmol X/h.

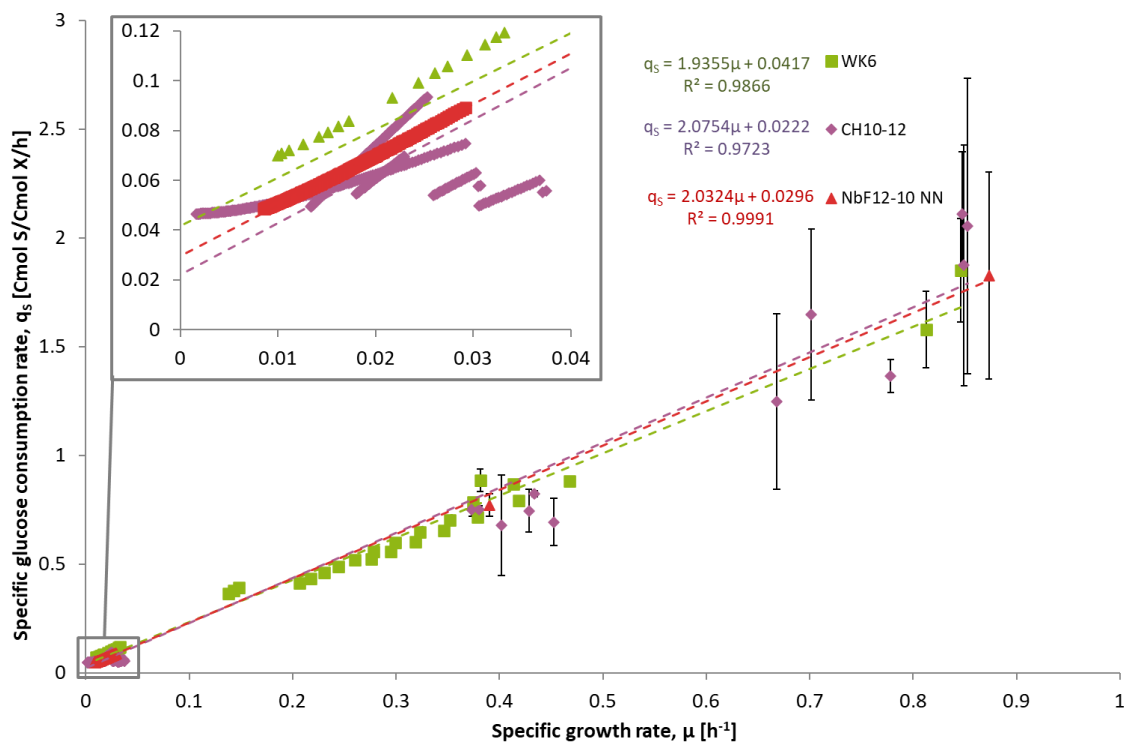


Figure III-36. Estimation of the maintenance coefficient for strains *Escherichia coli* WK6, CH10-12 and NbF12-10 NN. In batch and fed-batch modes only the average q_s was used. All data points of the induction phase were plotted.

The specific glucose consumption rate, q_s , in batch and fed-batch mode was represented as the average in each mode and error bars show the range in which the q_s varies. The maintenance coefficient was 0.04, 0.02 and 0.03 Cmol S/Cmol X/h for strains WK6, CH10-12 and NbF12-10 NN, respectively (Figure III-36).

At the low specific growth rates, corresponding to the induction phase, the values of q_s for the CH10-12 strain tend to converge at around 0.04 Cmol S/Cmol X/h. A hypothesis of thermo-dependency of the maintenance coefficient was checked at the low specific growth rates for cultures BR02 to BR07, but no relationship between the maintenance coefficient and the induction temperature was found (data not shown). The values of maintenance found for each strain were consistent with those found in the literature (Table III-17).

Strain	m [CmolS/CmolX/h]	m [gS/gX/h]	Reference
<i>E. coli</i> WK6	0.0417 ± 0.0108	0.0476	This work
<i>E. coli</i> CH10-12	0.0222 ± 0.0019	0.0253	This work
<i>E. coli</i> NbF12-10 NN	0.0296 ± 0.0004	0.0338	This work
<i>E. coli</i> BL21	/	0.024	[136]
<i>E. coli</i> recombinant	/	0.046	[95]
<i>E. coli</i> RV304	/	0.03	[93]

Table III-17. Coefficient of maintenance, m , for various *Escherichia coli* strains.

The maintenance metabolism has been reported to increase at low specific growth rates ($<0.06 \text{ h}^{-1}$) [208], with stress proteins formed during glucose limitation, and producing a response similar to the observed during complete glucose starvation [209].

During the induction phase of the cultures BR02 to BR09, low specific growth rates were attained due to the limiting substrate ($\leq 0.04 \text{ h}^{-1}$). In this phase, glucose was mostly utilized in the energy of maintenance, which is the production of internal metabolites, instead than for the production of biomass, therefore the low biomass yields during the induction phase.

In the case of the culture BR09 where the inducer was added to the culture of the reference strain *E. coli* WK6, no change of metabolism was expected. Despite that, the change of the average molar yield of biomass to glucose from 0.42 to 0.21 indicates that the IPTG had a negative effect in the production of the biomass. From this result, the main hypothesis proposed is that the IPTG could possibly change the metabolism to produce other metabolites instead of biomass as a defense mechanism in the wild type strain. Since the culture is under glucose limitation, the carbon dioxide is the other metabolite produced during induction and most likely, its production was enhanced.

Our results are consistent with the literature. Thus, some studies have shown that the induction of non-recombinant strains with IPTG results in a variety of stress responses in the cell: from the production of heat-shock-like protein and proteases, to the degradation of metabolic pathways [85], [210]. In either case, the flux of glucose is diverted from the production of biomass to the production of energy of maintenance and the production of other proteins or proteases.

III.2.3.2.3. Morphological analysis

The cultures were sampled during the three phases of culture: maximum exponential cell growth, fixed exponential growth, and expression of the protein. The microscopic visualizations were made as described in §II.6.3 and the statistical analysis were made as described in §II.8.6. Samples taken on the batch mode had an average of 3000 particles after filters were applied. For the samples taken on the fed-batch mode, the average of particles after filtration was 10,000.

Figure III-37 and Figure III-38 show the frequency curves of cultures BR02-BR05 for the circle equivalent diameter (CE diameter). The CE diameter is a morphological measure equivalent to the size of the cell. The blue curves were found significantly different from the green curves by the Morphologi G3 software.

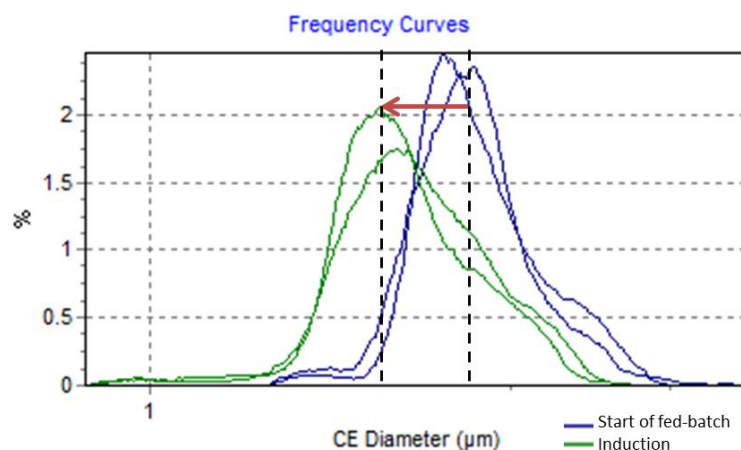


Figure III-37. Morphological analysis of samples taken in fed-batch mode and induction phase of cultures BR02 and BR03. The red arrow shows the shift on the average circle equivalent diameter (CE diameter, μm).

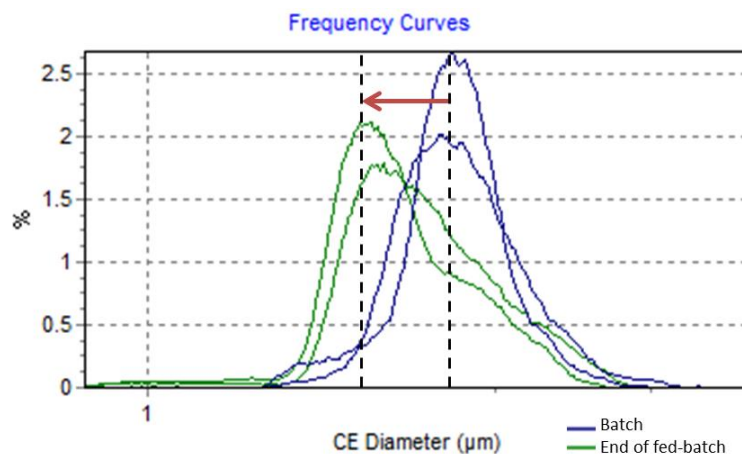


Figure III-38. Morphological analysis of samples taken in batch mode and fed-batch mode of cultures BR04 and BR05. The red arrow shows the shift on the average circle equivalent diameter (CE diameter, μm).

The CE diameter is higher for cells in batch mode and beginning of fed-batch mode (cells grown at maximum specific growth rate), and decreased for cells grown with glucose limitation at 0.4 h^{-1} and lower specific growth rate (end of fed batch mode and induction phase). This confirms the hypothesis proposed in shake-flask cultures were the change in shape of the microorganism was controlled by the specific growth rate.

Besides these results, we also looked at the effect of temperature during the induction of the protein. There was no significant effect on the shape of the microorganism (Figure III-39).

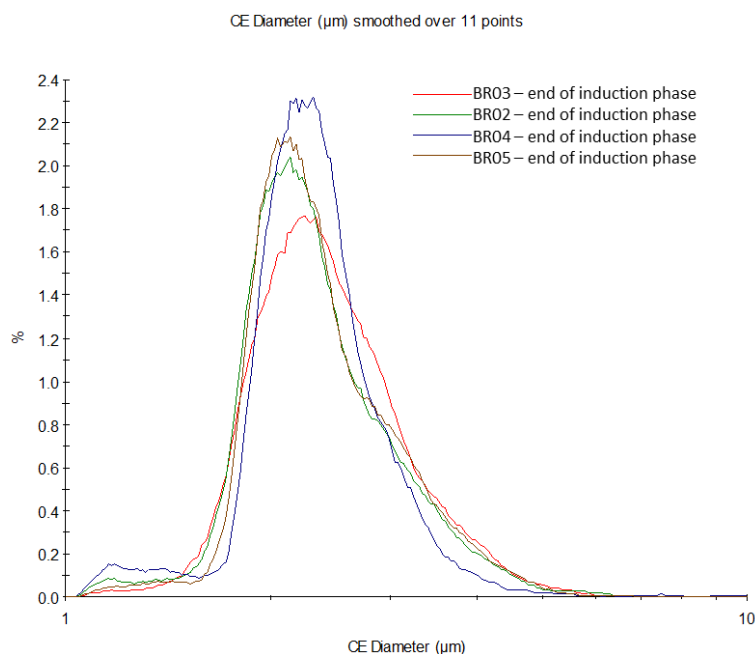


Figure III-39. Frequency curve of the samples of cultures BR02 – BR05 during the induction phase.

It can be concluded that the change in size and shape of the microorganism is only function of the addition of the IPTG pulse and the specific growth rate controlled by glucose limitation, and that the temperature of the culture does not play a role in the morphology of the *Escherichia coli* WK6 strains.

III.2.3.3. Acetic acid

The production of acetic acid occurs naturally in the batch culture, where glucose is in excess in the medium [182]. The chemical reaction occurring in the culture is defined by Eq. (III-2), §III.1.2.4.

In our cultures, as expected, acetic acid is only produced in the batch phase, at 0.8 g/L in average. This acetic acid is consumed in the fed-batch mode when glucose is limited. In the batch mode, the yield of acetic acid on biomass ($Y_{Ac/S}$) was about 0.29 g/g in average for all cultures (Table III-18) and consistent with the values reported in the literature of 0.3 g/g [86].

Culture	$Y_{Ac/S}$ [Cmol/Cmol] and [g/g]	$Y_{Ac/X}$ [Cmol/Cmol]	$Y_{Ac/X}$ [g/g]
BR01 – WK6	0.085 ± 0.004	0.198 ± 0.011	0.237 ± 0.014
BR02 – CH10-12	0.093 ± 0.002	0.285 ± 0.010	0.342 ± 0.012
BR03 – CH10-12	0.086 ± 0.001	0.206 ± 0.007	0.248 ± 0.008
BR04 – CH10-12	0.093 ± 0.004	0.165 ± 0.011	0.198 ± 0.014
BR05 – CH10-12	0.103 ± 0.004	0.259 ± 0.018	0.311 ± 0.021
BR06 – CH10-12	0.148 ± 0.012	0.392 ± 0.037	0.471 ± 0.044
BR07 – CH10-12	0.214 ± 0.023	0.385 ± 0.043	0.463 ± 0.052
BR08 – NbF12-10 NN	0.070 ± 0.004	0.042 ± 0.013	0.170 ± 0.015
BR09 – WK6	0.062 ± 0.004	0.123 ± 0.009	0.147 ± 0.011

Table III-18. Yield of acetic acid on glucose ($Y_{Ac/S}$) and on biomass ($Y_{Ac/X}$) for the batch mode. Cultures BR01 – BR09 grown in MM at pH 6.8, 37°C.

Other organic acids (lactate, succinate, and pyruvate) were not found in the supernatant, either during batch mode or fed-batch mode.

III.2.3.4. Citric acid

Citric acid is present in the culture medium (§II.3.2.2) as a chelating compound and it was quantified by HPLC (§II.6.5). The quantification of the citric acid was made only to check its constant concentration in the cultures. Citric acid is not metabolized by the *Escherichia coli* but it is present in the TCA cycle [129]. Despite this, for all cultures, the mass of the citric acid decreased during the culture, this consumption starts at the fed-batch mode and is enhanced during the induction phase (Figure III-40).

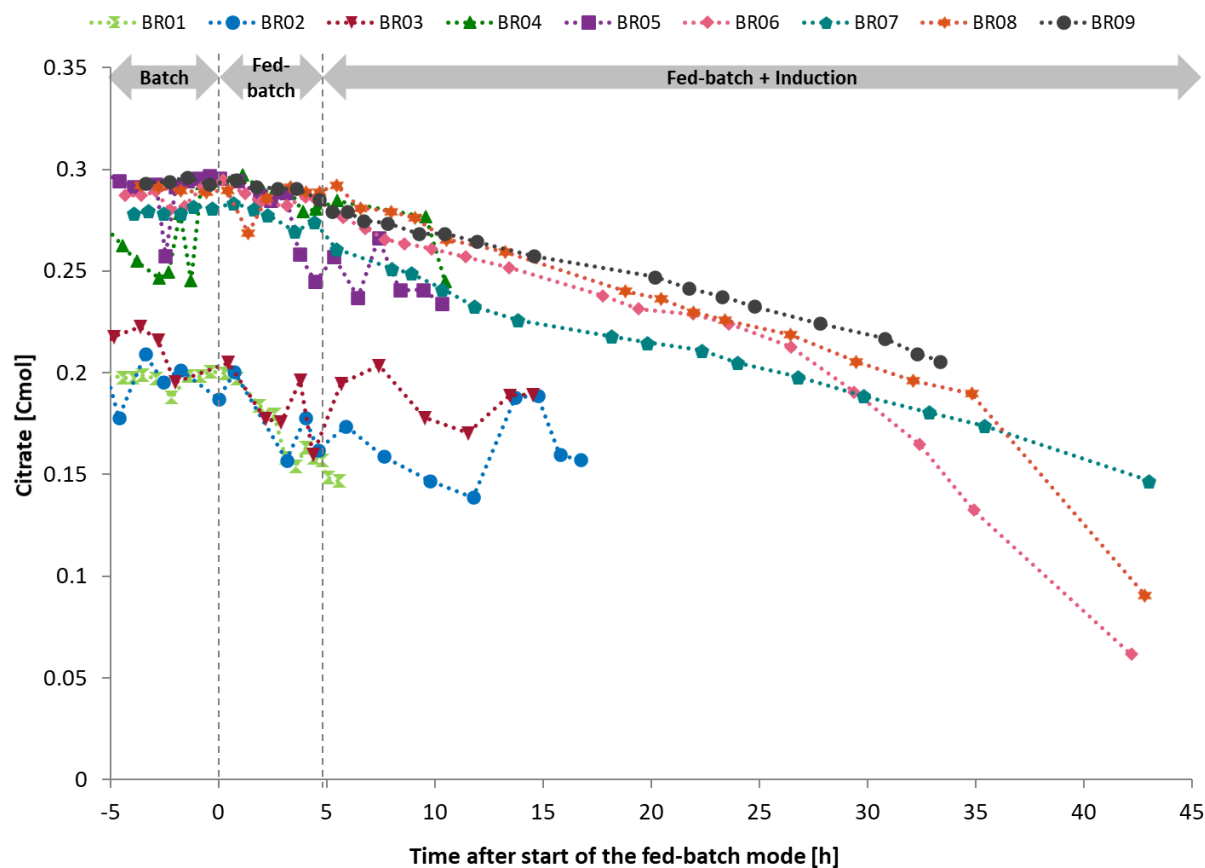


Figure III-40. Evolution of citric acid in cultures BR01 to BR09. The dotted lines show the approximate change of operating condition.

The utilization of the citrate by the *Escherichia coli* WK6 strains is not encoded in the strain genome nor in the recombinant plasmid. Ramchuran and colleagues [211] found a similar evolution citric acid of a recombinant strain of *E. coli* during protein production. They hypothesized that the mineral medium had a nutritional deficiency, from which the citric acid was being used in the TCA cycle to produce energy and the amino acids needed to synthesize the recombinant protein.

The consumption of citric is noted not only for the recombinant strains, but also for the reference strain when IPTG was added to the culture. It could be possible that the IPTG permeates the membrane of the microorganism, and citrate enters the system to produce energy through the TCA cycle, hence the high maintenance coefficient found during the induction phase. IPTG is known to weaken integrity of the outer membrane of the microorganism [85]. To verify this hypothesis, a culture induced with lactose, instead of IPTG, could be made.

III.2.3.5. Gas analysis

The gases carbon dioxide and oxygen were analyzed as described in §II.5.2. The evolution of the production or consumption of both gases seems to follow the same pace than the biomass, with a slope discontinuity between every change of operating condition (Figure III-41, Figure III-42).

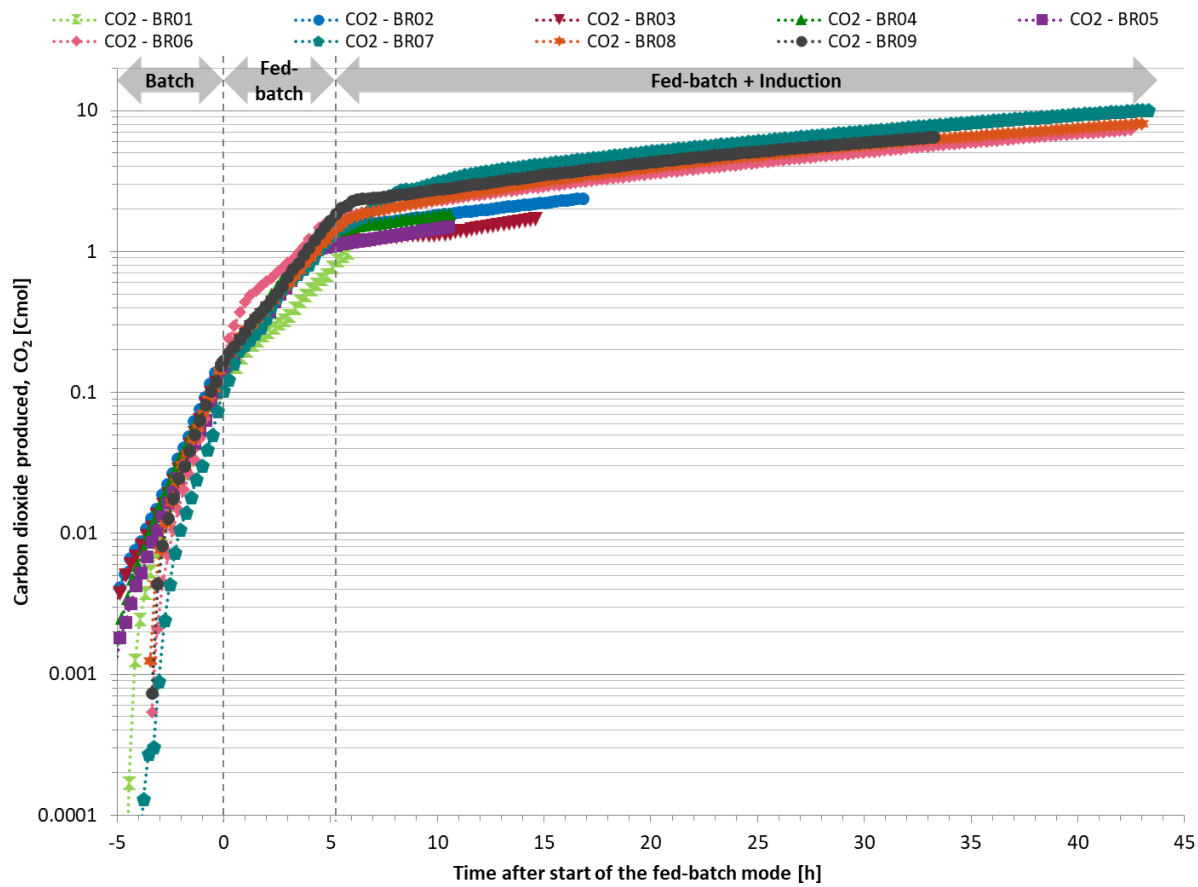


Figure III-41. Evolution of carbon dioxide production in cultures BR01 – BR09. The dotted lines show the approximate change of operating mode.

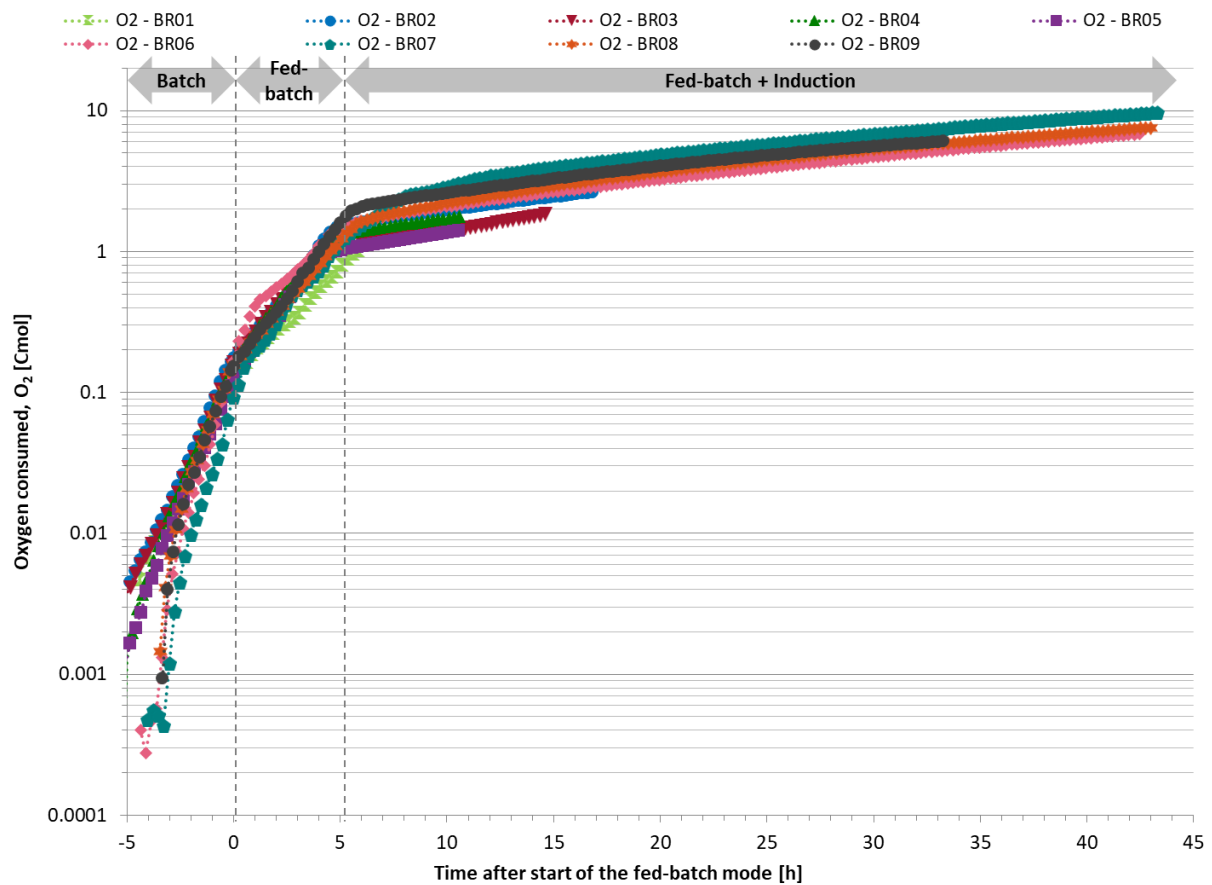


Figure III-42. Evolution of oxygen consumption in cultures BR01 – BR09. The dotted lines show the approximate change of operating mode.

The average yield of carbon dioxide on glucose, $Y_{CO_2/S}$, can be calculated for each operating condition. It was in average 0.4 Cmol/Cmol for the batch and fed-batch mode. During the induction phase, the yield was in average 0.6 Cmol/Cmol for the short induction duration cultures and over 0.8 Cmol/Cmol for the culture of long induction duration, which could be explained by the maintenance of the microorganism (Figure III-43).

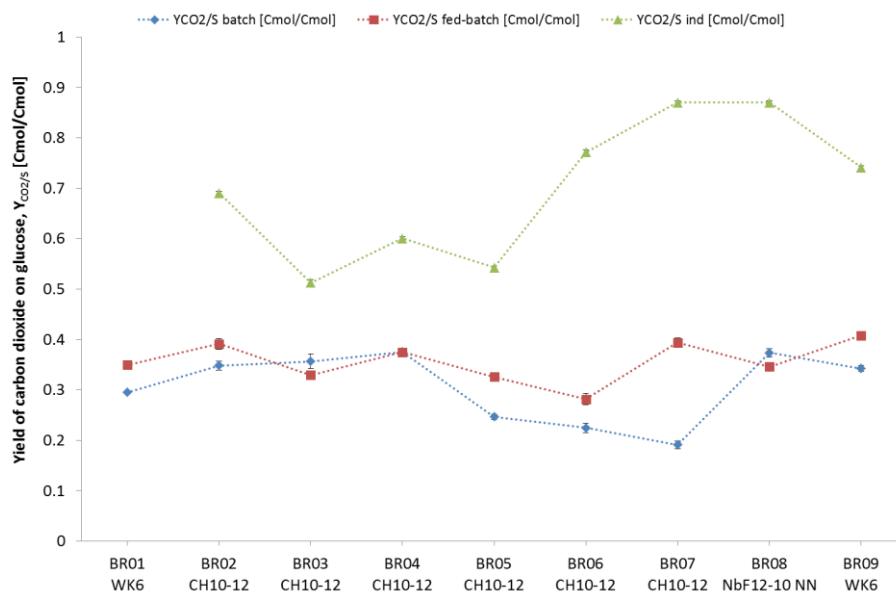


Figure III-43. Average yield of carbon dioxide on glucose ($Y_{CO_2/S}$) on each operating condition. Cultures BR01 – BR02 cultured in MM, 37°C, pH 6.8.

The induction phase caused an increase in the molar yield of carbon dioxide ($Y_{CO_2/S}$, Figure III-43) and coincidentally, the molar yield of biomass ($Y_{X/S}$, Figure III-35) decreased during the same phase. A hypothesis to explain this phenomenon is the shift of the metabolism caused by the protein expression, also known as metabolic burden.

The metabolic burden is defined as the stress of the microorganism to maintain the vector during protein expression [79]. The induction of the vector with IPTG starts the protein production machinery in the microorganism, increasing the metabolic needs to replicate the vector and inevitably reduce the biomass production [75]. The replication of the vector and the production of internal metabolites needed for the production of the nanobody increased the production of carbon dioxide during the production phase. The metabolic burden can explain the change of the molar yield of the recombinant strains CH10-12 (BR02 – BR07) and NbF12-10 NN (BR08), but not for the reference strain WK6 (BR09).

The reference strain WK6 (BR09) displayed similar average molar yields of carbon dioxide ($Y_{CO_2/S} = 0.74$) and biomass ($Y_{X/S} = 0.21$) during the induction phase, as for the other strains. There is no vector for protein expression in the reference strain that could explain a metabolic burden in the microorganism. It is possible, however, that the addition of the IPTG to the culture medium induced a metabolic stress. It has been proven that the addition of IPTG to non-transformed strains causes a variety of stress responses: synthesis of heat proteins, inhibition of proteins present during exponential growth, degradation of pathways and production of proteases [85]. Therefore, the metabolic burden can be directly linked to the maintenance metabolism identified in §III.2.3.2.2.

The yield of oxygen on biomass ($Y_{O_2/X}$) is parameter that can be influenced by oxygen transport and oxygen transport conditions [175]. It changed from about 0.5 g/g in the batch and fed-batch mode to about 0.7 g/g in the short induction time cultures, and over 2 g/g for the long induction time cultures (Figure III-44). This increase in the oxygen consumption could be explained by the increase of the maintenance metabolism, where glucose is oxidized into carbon dioxide with low biomass production.

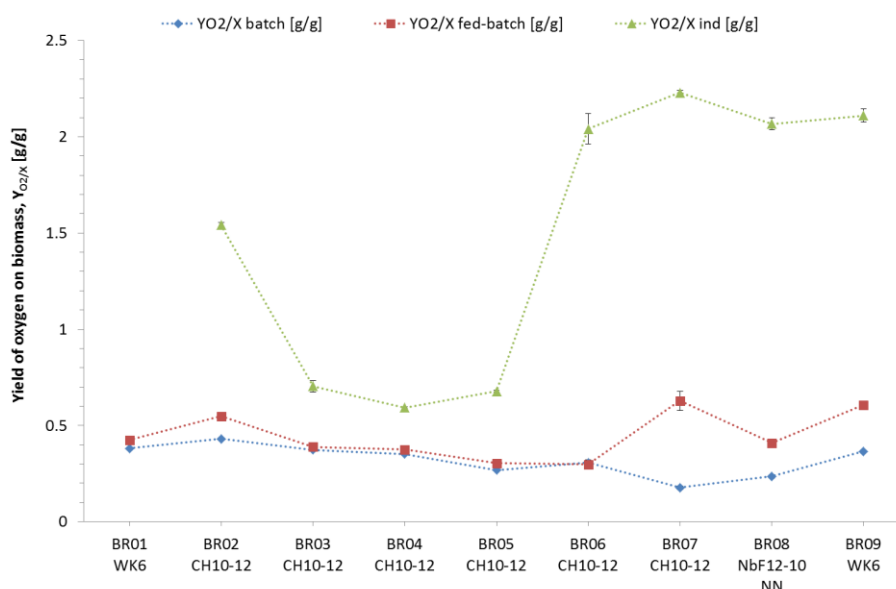


Figure III-44. Average yield of oxygen on biomass ($Y_{O_2/X}$) on each operating condition. Cultures BR01 – BR02 cultured in MM, 37°C, pH 6.8.

The rates of oxygen and carbon dioxide were calculated as explained in §II.8.1.2. Its evolution is shown in Figure III-45 and Figure III-46 for the short induction duration cultures, and in Figure III-47, and Figure III-48 for the long induction duration cultures. For each culture, the carbon dioxide production rate and the oxygen consumption rate are equivalent. In culture BR03, the problems of

the glucose feed can be clearly identified by the decrease in the carbon dioxide production and oxygen consumption rate.

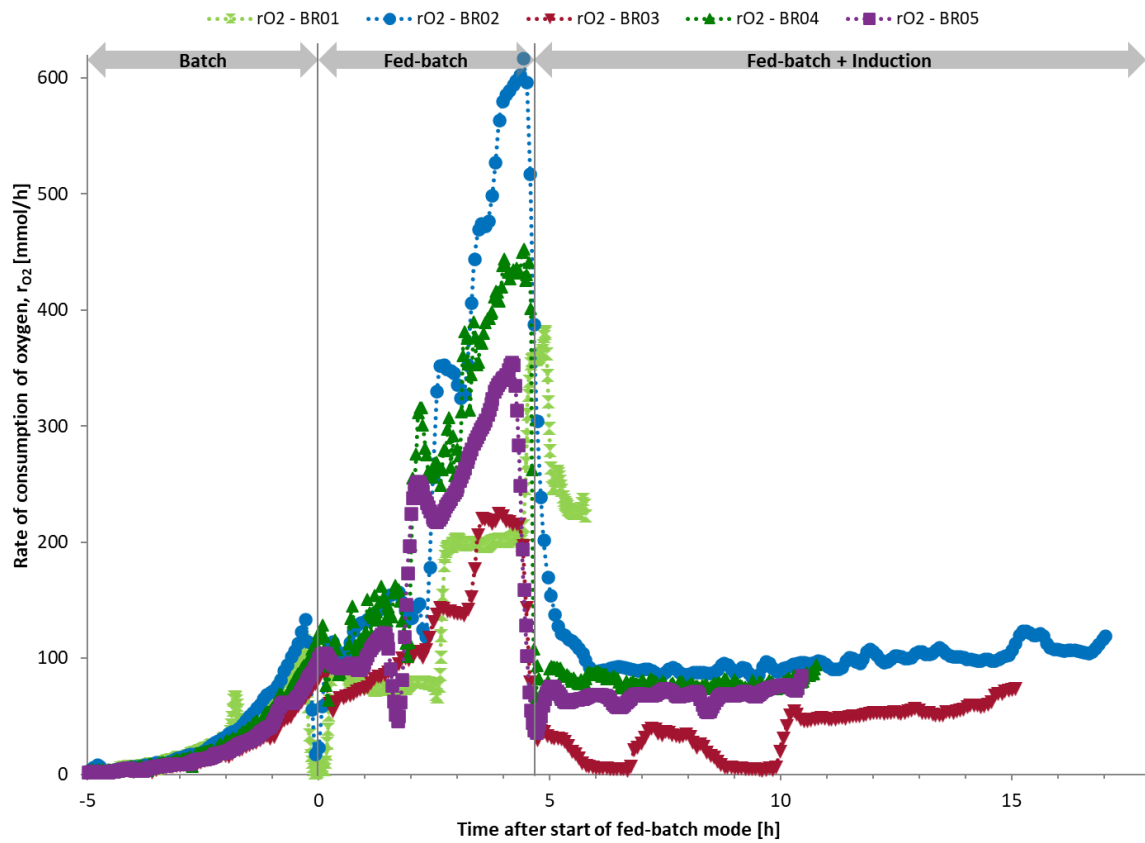


Figure III-45. Rate of consumption of oxygen in cultures BR01 to BR05.

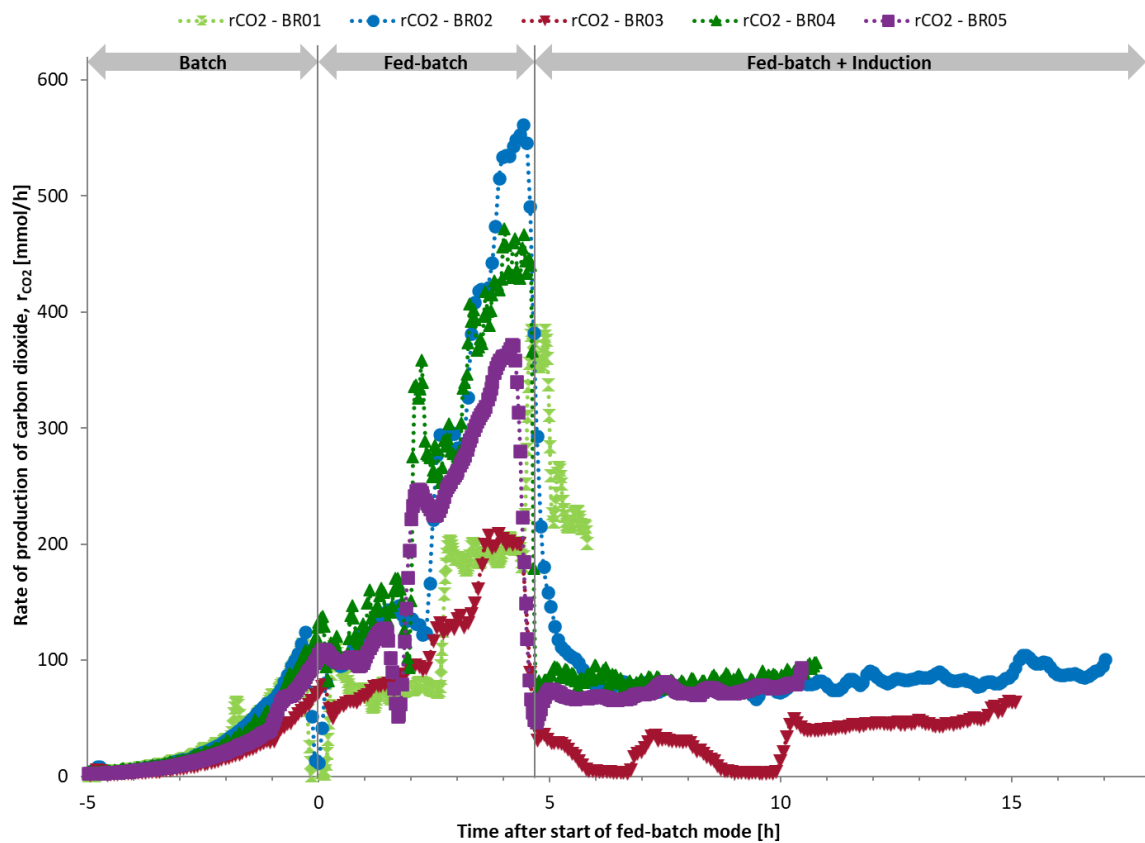


Figure III-46. Rate of production of carbon dioxide in cultures BR06 to BR09.

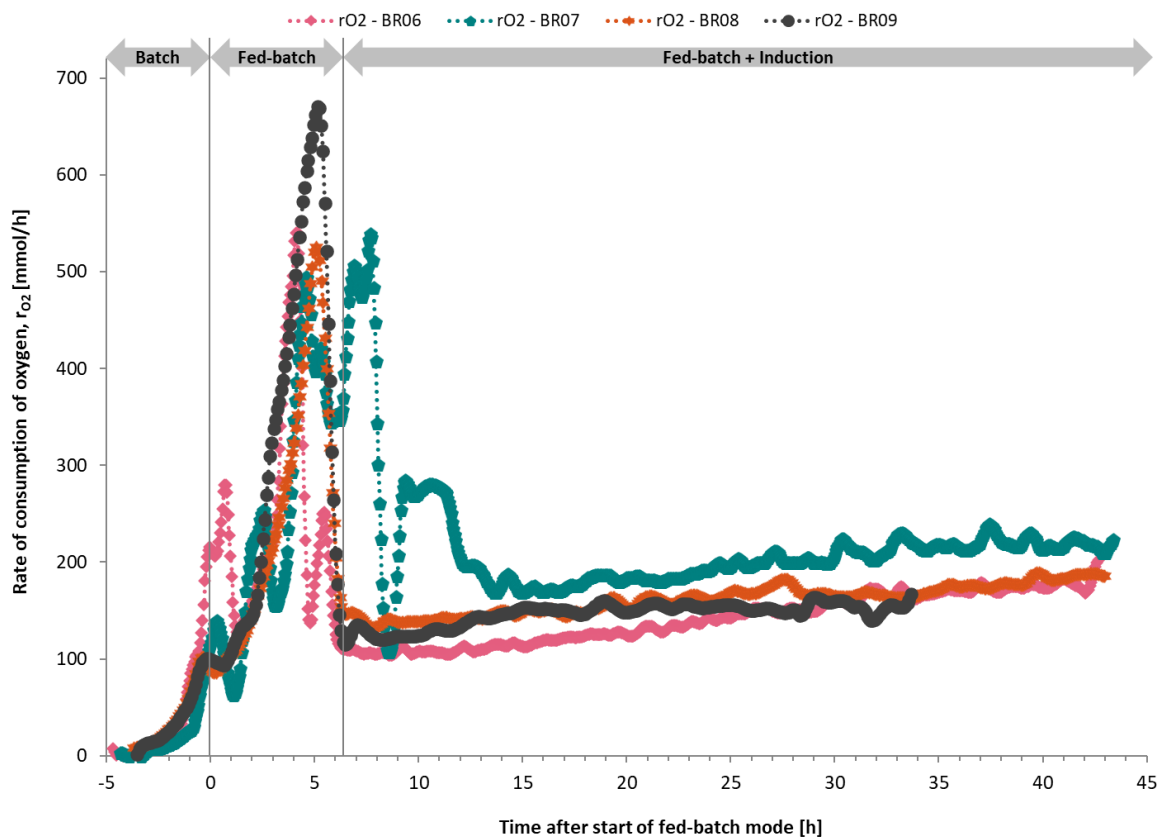


Figure III-47. Rate of consumption of oxygen in cultures BR07 to BR09.

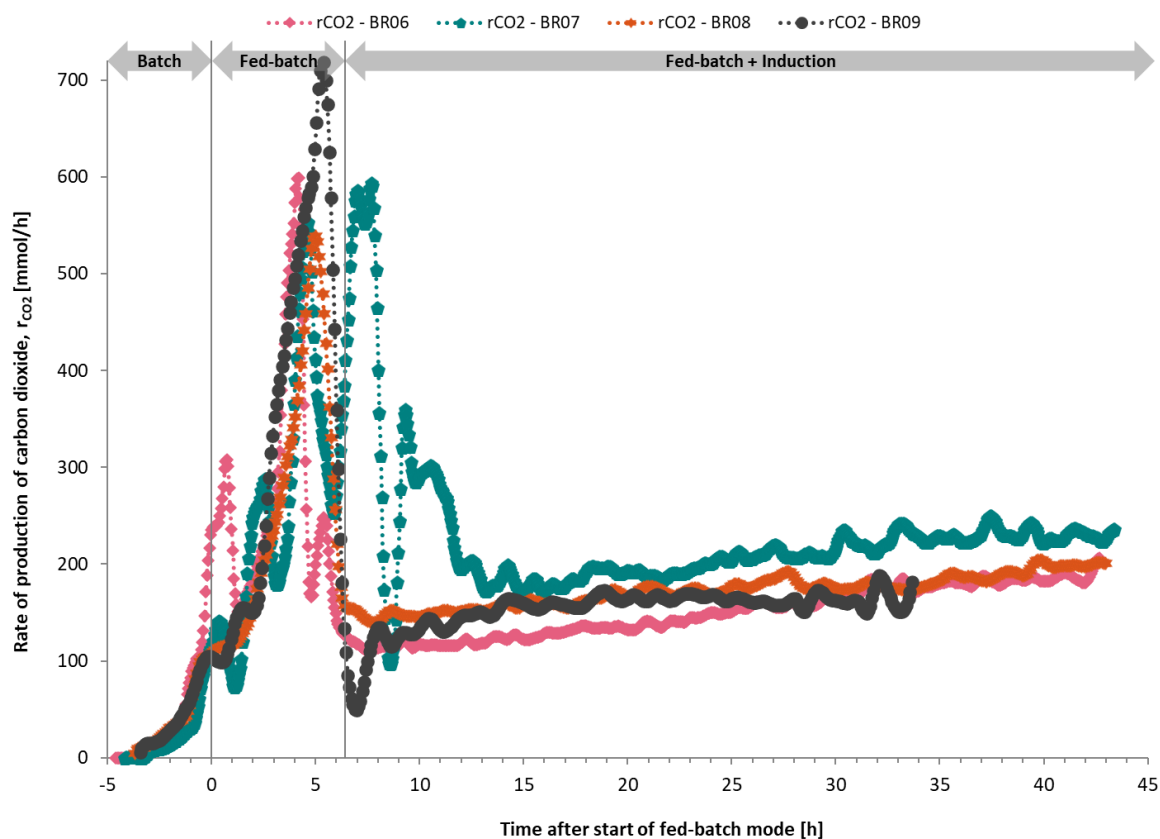


Figure III-48. Rate of production of carbon dioxide in cultures BR 06 to BR09.

III.2.3.6. Respiratory coefficient

The respiratory coefficient or respiratory quotient (RQ) is the ratio of the instantaneous production of carbon dioxide (r_{CO_2}) to the instantaneous consumption of oxygen (r_{O_2}). The RQ can change if there is a shift in the metabolism in which the production of carbon dioxide increases or if the rate of consumption of oxygen decreases; it is also an index of the organic matter being oxidized in respiration [212]. At the start of the culture the measure of carbon dioxide is not very accurate due to the low biomass titer in the bioreactor and the low aeration rates imposed, but over 1.5 g cdw/L the accuracy increased.

In the culture BR01, where there was no induction phase, the RQ was close to 1. In the case of the cultures with short induction times BR02 to BR05, the RQ was close to 1 in the batch and fed-batch modes for all cultures. A RQ close to 1 is expected with the utilization of only glucose as carbon source and the low acetate production (<1 g/L) during these two operation modes. During the induction phase, the RQ for cultures BR02 and BR03 decreased to about 0.85 but remained close to 1 for cultures BR04 and BR05 (Figure III-49).

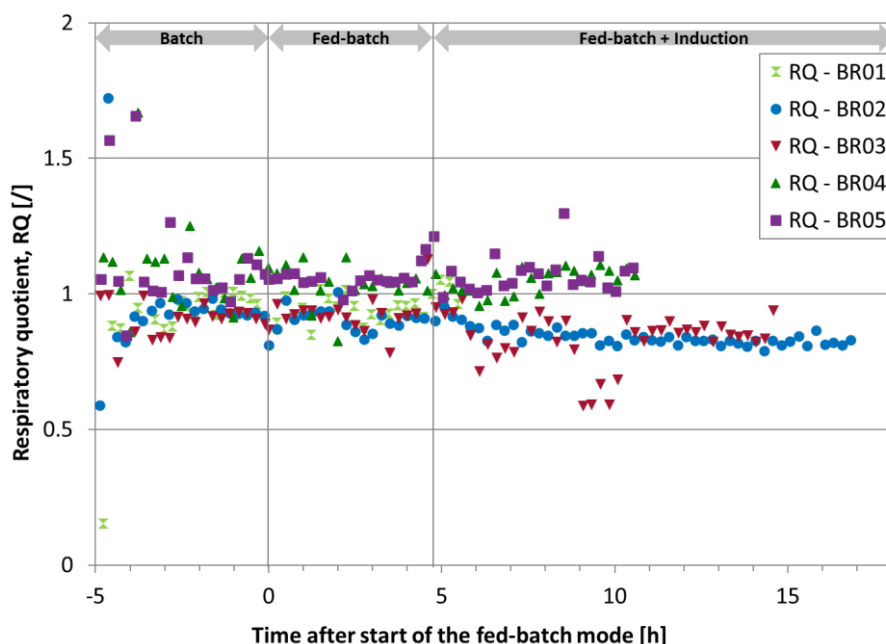


Figure III-49. Respiratory quotient (RQ) for cultures BR01 – BR05.

For the long induction duration cultures BR06 to BR09, the RQ was about 1.1 for the batch and fed-batch mode and decreased to about 1.05 for the induction phase (Figure III-50).

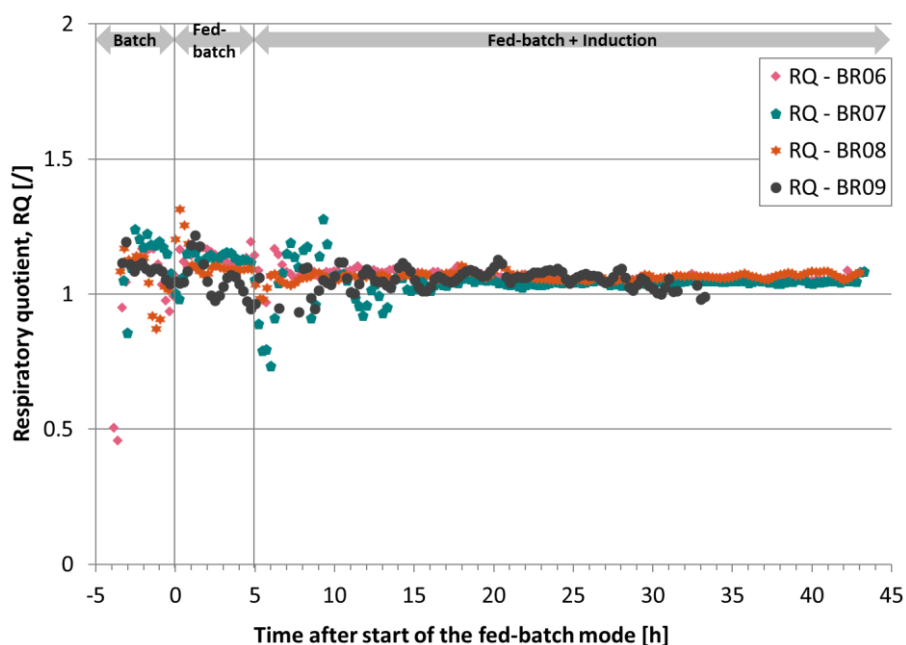


Figure III-50. Respiratory quotient (RQ) for cultures BR06 – BR09.

There is no detectable effect of the nanobody expression in the respiratory coefficient, RQ. In protein production, a RQ close to 0.8 is expected due to the degree of reduction of the protein (about 3.5) [212]. The amount of protein produced was almost negligible compared to the biomass production (>35 g cdw/L), hence the protein production had no effect on RQ. The addition of the inducer (IPTG) to the culture BR09, did not produced a change in the respiratory coefficient of the reference strain. Finally, the temperature of the different cultures during the induction phase had no effect on the RQ.

III.2.4. Nanobody

The production of the nanobody CH10-12 was studied at different temperatures in two series of cultures of *Escherichia coli* CH10-12, first in the cultures BR02 – BR05 with short induction duration and secondly in BR06 and BR07 with long induction duration. The production of the nanobody NbF12-10 was tested in a culture of *Escherichia coli* NbF12-10 NN induced at 29°C. As negative control, *Escherichia coli* WK6 was induced at 29°C with a pulse of 1 mM IPTG.

The purification of the nanobody from the periplasmic proteins is described in §II.7. The quantification of the nanobody was made as described in Appendix 2.

III.2.4.1. Short induction duration cultures (1st series)

Cultures of *Escherichia coli* CH10-12 (BR02 – BR05) were induced for protein expression and cultured after induction at different temperature for up to 12 h. The production of the nanobody CH10-12 increased over time, reaching a final concentration of 2.3 mg/L of culture for BR02 and BR03 (Figure III-51), and 0.4 and 0.2 mg/L of culture, for cultures BR04 and BR05, respectively.

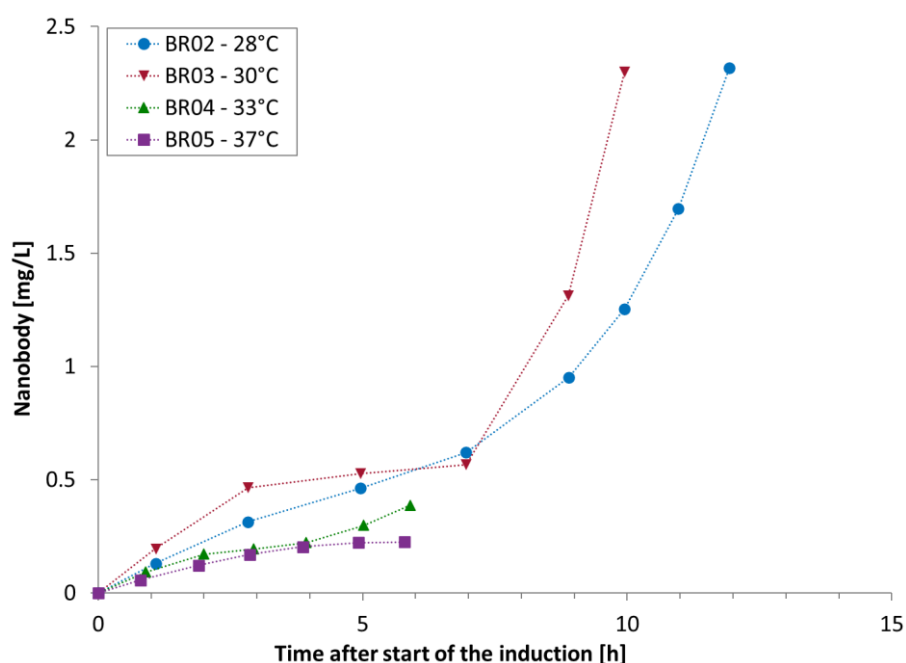


Figure III-51. Evolution of the concentration of the nanobody CH10-12 in cultures BR02 – BR05.

In terms of overall production, the culture BR03, induced at 30°C, obtained the highest titer after 10 h of induction (2.3 mg/L, Figure III-51), which is about two-fold the concentration achieved after 10 h of induction in BR02 at 28°C (1.2 mg/L). Cultures BR04 and BR05 induced at higher temperatures produced the lowest titers almost at the same rate (Figure III-51) and almost equivalent to half of the production in BR02 and BR03 at lower temperatures at the same induction time.

The specific production rate of the nanobody for the BR02 and BR03 show an exponential-like tendency (Figure III-52). For cultures BR04 and BR05 the protein concentration was almost constant which indicates the low productivity due to the high temperatures, although the tendency of the specific production rate is the same than for the cultures BR02 and BR03.

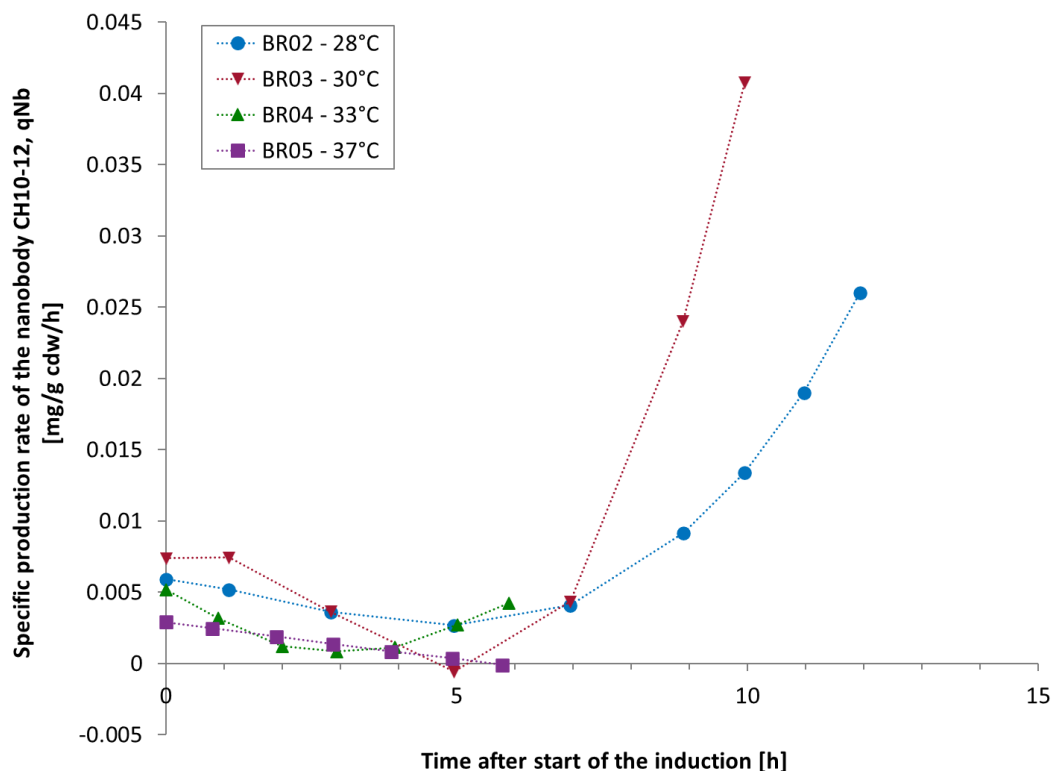


Figure III-52. Specific production rate of the nanobody CH10-12 in cultures BR02 to BR05. Induction made with a pulse of 1 mM of IPTG.

Despite the early stopping of cultures BR04, the results of nanobody productivity, suggests that the optimal temperatures to produce the nanobody were 28°C and 30°C with a final titer of 2.3 mg/L culture after, respectively, 10 h and 12 h of induction. The highest volumetric productivity and specific productivity was found at 30°C (0.0408 mg/g cdw/h and 0.23 mg/L/h).

Some questions arise from the evolution of the cultures BR02 and BR03: 1) if longer induction duration were used, would productivity keep increasing, will it arrive to a plateau or produced protein would be consumed? 2) For cultures BR04 and BR05, the induction time was not enough to fully activate the protein production machinery? Would longer induction times increase the productivity of the strain?

III.2.4.2. Long induction duration cultures (2nd series)

In order to see if the trend of the nanobody specific production rate in the cultures BR02, BR03 and BR04 was always ascending (Figure III-52), cultures BR06 and BR07 were induced over a longer period of time at 29°C and 32°C, respectively.

The nanobody final titers of cultures BR06 and BR07 reached a maximum of 1.4 and 0.7 mg/L of culture, respectively (Figure III-53). The increase on the induction duration had no effect on the concentration of the nanobody, as was expected for culture BR06 with a temperature of induction of 29°C.

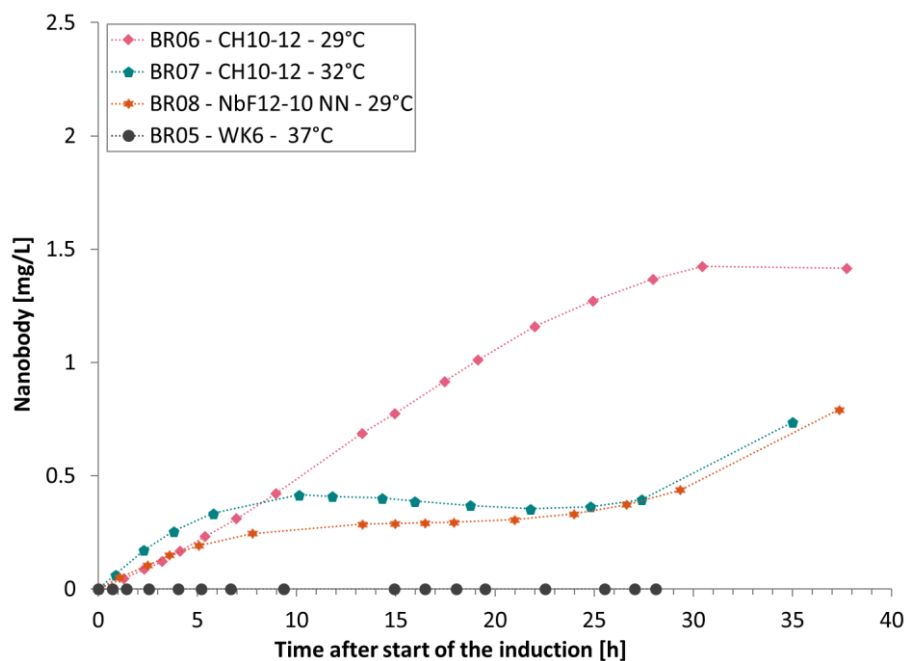


Figure III-53. Evolution of the concentration of the nanobody in cultures BR06 to BR09.

It could be seen that in culture BR06 the production of the nanobody seems to reach a plateau after 25 h of induction at 1.4 mg/L of culture. In the case of the cultures BR07 and BR08, the culture seems to arrive at a plateau after 10 h of induction and remain constant at about 0.4 and 0.3 mg/L of culture, respectively. In these last cultures, the production of the nanobody seems to restart after 28 h of induction, about 18 h after arriving to the plateau.

At an induction temperature of 29°C and after 37 h of induction, the strain *E. coli* CH10-12 produced 80% more nanobody than the strain *E. coli* NbF12-10 NN. In shake-flask cultures, the difference in nanobody production between the two strains was one order of magnitude (§III.1.3). The controlled conditions in the bioreactor cultures allowed an improvement in the production of nanobody NbF12-10 for the clone *E. coli* NbF12-10 NN, and similar to those found for the nanobody CH10-12.

In the case of the culture of *E. coli* WK6 (BR09) induced at 29°C, no nanobody was found after the purification of periplasmic extract, as expected for the negative control (Figure III-53).

The specific production rate of the nanobodies was one order of magnitude lower than the cultures of short induction duration (Figure III-54).

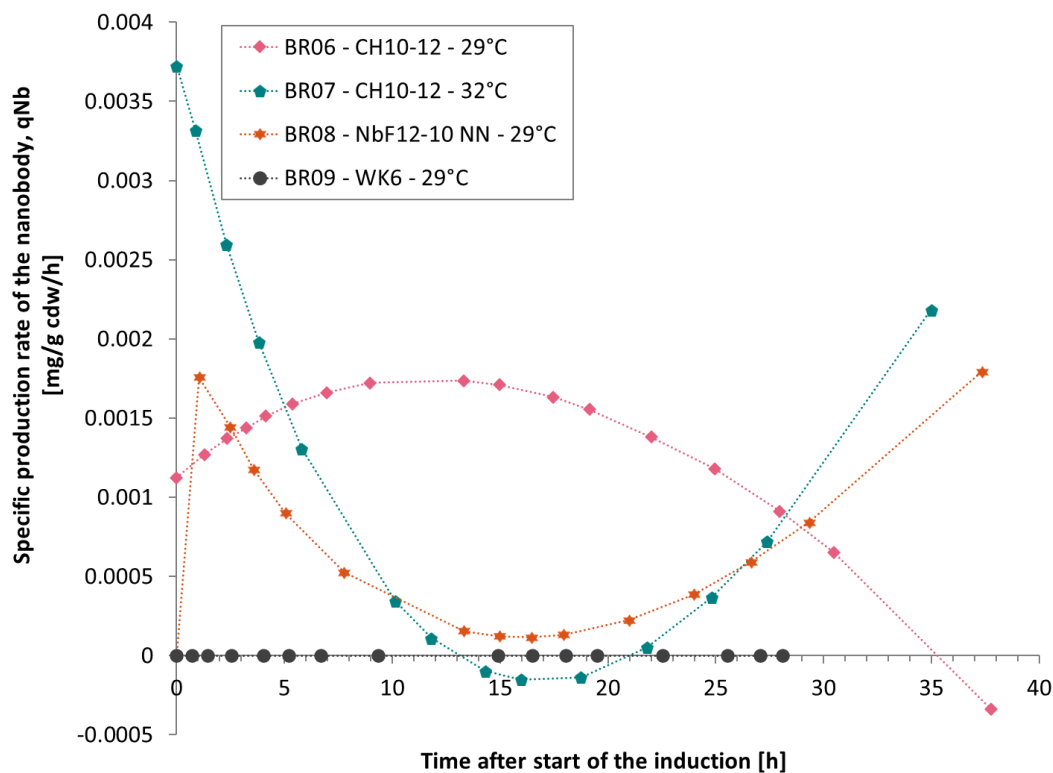


Figure III-54. Specific production rate of the nanobodies CH10-12 and NbF12-10 in cultures BR06 to BR09. Induction made with a pulse of 1 mM of IPTG

The nanobodies CH10-12 and NbF12-10 were only found in the periplasmic space of the microorganism. This was checked by the purification of 30 mL of supernatant from cultures BR02 to BR08. The electrophoresis gels show an absence of specific proteins throughout the protein induction (Figure III-55). It was concluded that the production of the protein of interest is only done inside the cell (periplasm) and it is not or only slightly excreted towards the culture medium.

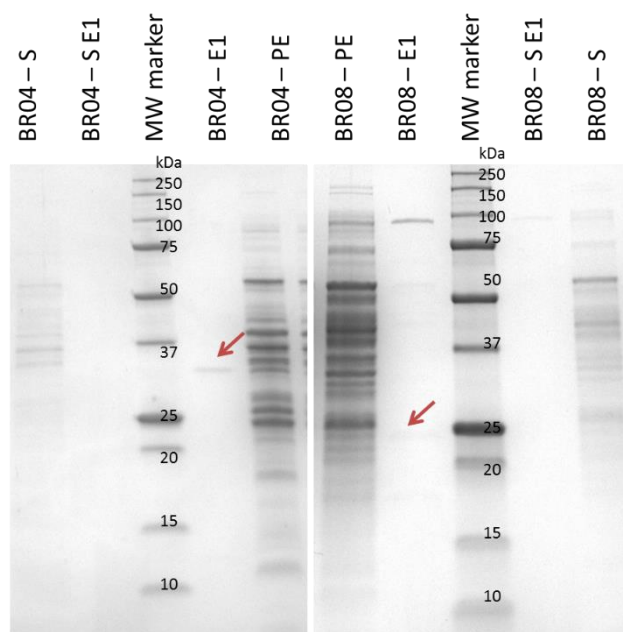


Figure III-55. SDS-PAGE gels of cultures BR04 and BR08. S: supernatant, S E1: first eluate of purification of supernatant, E1: first eluate of purification of periplasmic extract, PE: periplasmic extract. The red arrows show the presence of the nanobody.

III.2.4.3. Secondary proteins

In addition to the nanobody CH10-12 (31 kDa) and NbF12-10 (29 kDa) produced in cultures BR02 to BR08, two other bands were found in the electrophoresis gels, corresponding to a molecular weight of 11 kDa and 84 kDa (Figure III-56). These two bands were also found in the culture BR09 of the *E. coli* WK6 strain.

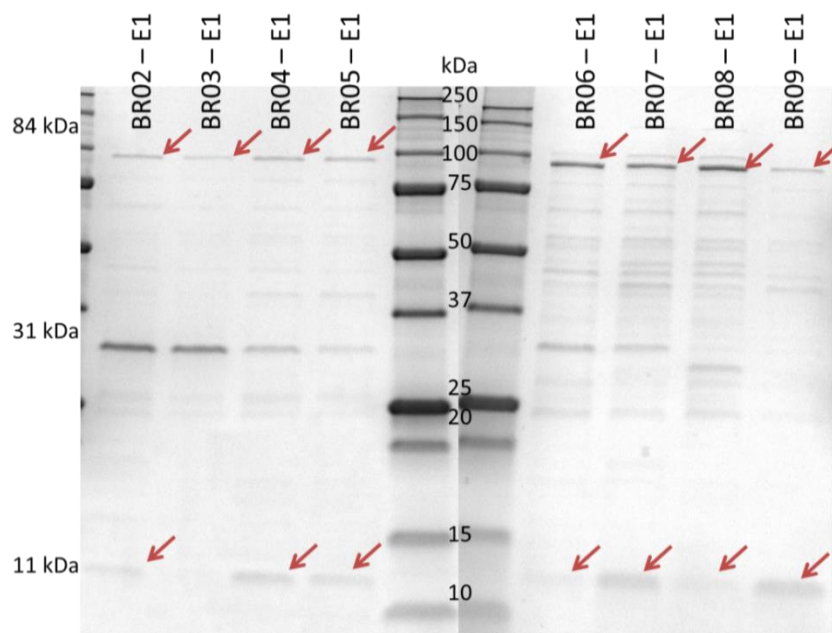


Figure III-56. SDS-PAGE gel of the first eluate of the last sample of cultures BR02 to BR09.

The purification of Nanobody is done by affinity chromatography (IMAC) as described in §II.7.2. The affinity between nickel and histidine ensures that only specific proteins (those with His₆-tag) are retained in the column. The three washes of eluent (PBS) after the incubation of the affinity matrix and the periplasmic extract are made to eliminate all the non-specific proteins of the matrix and of the column. Each wash of the column between the flow-through and the eluted fraction was checked by Nanodrop until an absorbance of 0 AU and by SDS-PAGE, where no proteins were found at the third wash (data not shown).

The evolution of the unknown proteins of 11 kDa, 84 kDa and the nanobody CH10-12 is given in Figure III-57. In the cultures with short induction duration (BR02 – BR05) the production of proteins at 11 kDa and 84 kDa was higher at higher temperatures (33°C and 37°C) than at low temperatures. In the longer induction duration cultures (BR06 and BR07), the production of the 84 kDa protein increases close to 20 h after protein expression, when the production of the Nanobody stops (plateau phase, Figure III-53). The protein of 11 kDa had the highest production at 32°C in culture BR07.

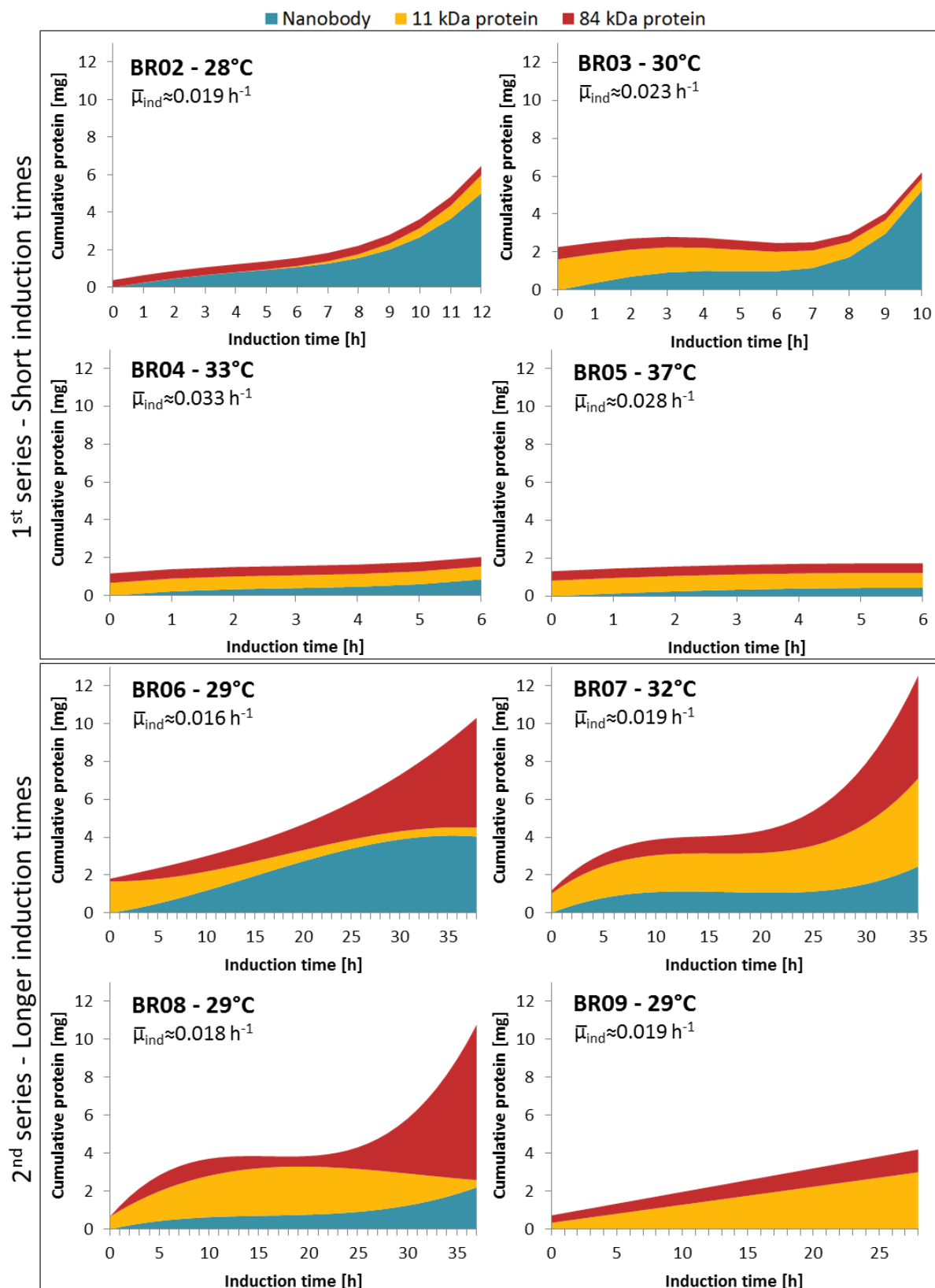


Figure III-57. Graphical comparison of nanobody CH10-12, NbF12-10 and secondary proteins found in the cultures BR02 – BR09. *Escherichia coli* CH10-12, NbF12-10 NN and WK6 grown in MM at 37°C, pH 6.8, induction at about 25 g cdw/L with 1 mM IPTG and change of temperature as specified in the image.

The culture BR03 had the lowest production of secondary proteins (30°C), accounting for 18% of the total protein production after 10 h of induction, followed by the culture BR02 (28°C) with 23% of

secondary proteins produced after 12 h of induction. The cultures at high induction temperatures 33°C and 37°C produced a total of 60% and 74% of secondary proteins, respectively, after 6 h of induction. The secondary proteins in the long induction duration cultures were 60% and 80% for cultures BR06 and BR07, respectively.

The production of the protein at 11 kDa was more important at high temperatures (32°C – 37°C), ranging from 37% to 45% of the total protein production. The protein of 84 kDa had its highest production during the long induction time cultures, at 56% and 43% for cultures BR06 and BR07, respectively. The nature of these proteins can only be found by a Western blot analysis.

III.2.4.4. Discussion

The metabolic burden or metabolic load can be defined as the load imposed to the microorganism by the expression of a foreign protein [85]. In the literature, this burden can be explained by three main points:

1. The induction phase conditions: temperature of induction, duration of the induction phase and imposed specific growth rate during induction in fed-batch mode.
2. The nature of the inducer: IPTG concentration in the medium (mM), specific IPTG concentration (mmol/g cdw), and the use of lactose as inducer.
3. The culture medium used during the induction phase.

The conditions of the culture during recombinant protein expression, mainly temperature, are the most studied in the literature [72], [85], [90]. As it was discussed in §1.5.1.6, lower temperatures of induction are favorable for recombinant protein production. The duo temperature-duration of the protein induction phase is still a trial-and-error process. In the case of bioreactor cultures, the common practice is to achieve a high biomass concentration before making the protein expression, in order to have a high protein productivity. Acetate production is known to hinder the production of protein [72]. Using glucose as carbon source, the specific growth rates must be kept lower than a critical rate to avoid the production of acetate and increase protein production.

The concentration of the inducer in the culture during the induction phase is known to increase the metabolic burden due to the overexpression of recombinant proteins [85]. The IPTG, used for the expression of the *lac* promoter and production of recombinant proteins (§1.5.1.2), can be used from 0.005 mM to 5 mM, with 1 mM being the most common. Recently, a Spanish team studied the specific concentration of IPTG (mmol/g cdw) and found the optimal concentration for the production of recombinant enzyme in *E. coli* during fed-batch cultures in defined minimal medium [144], [145], [148], [213].

The composition of the culture media used during protein expression is not as studied as the previous two points. Since most of the recombinant proteins reported in the literature are made in rich medium in shake-flask, nutritional limitation is not an issue in most cases (§1.5.1.5). In the case of protein expression in bigger proportions, such as a bioreactor, the use of a defined minimal medium is more adequate in economic terms. The use of defined minimal medium in a recombinant strain could, however, cause a nutritional limitation due to the higher needs of the strain during protein expression. The composition of defined minimal medium has been studied, for example, to predict shortages of intracellular metabolites in recombinant strains of *E. coli* [214].

The nanobody CH10-12 concentration achieved in cultures BR02 – BR08 were compared with the literature (Figure III-58). The reported literature titers of recombinant nanobodies with neutralizing effects against scorpion neurotoxins vary from 0.5 to 3.75 mg/L of culture with induction times ranging from 16 h to 24 h.

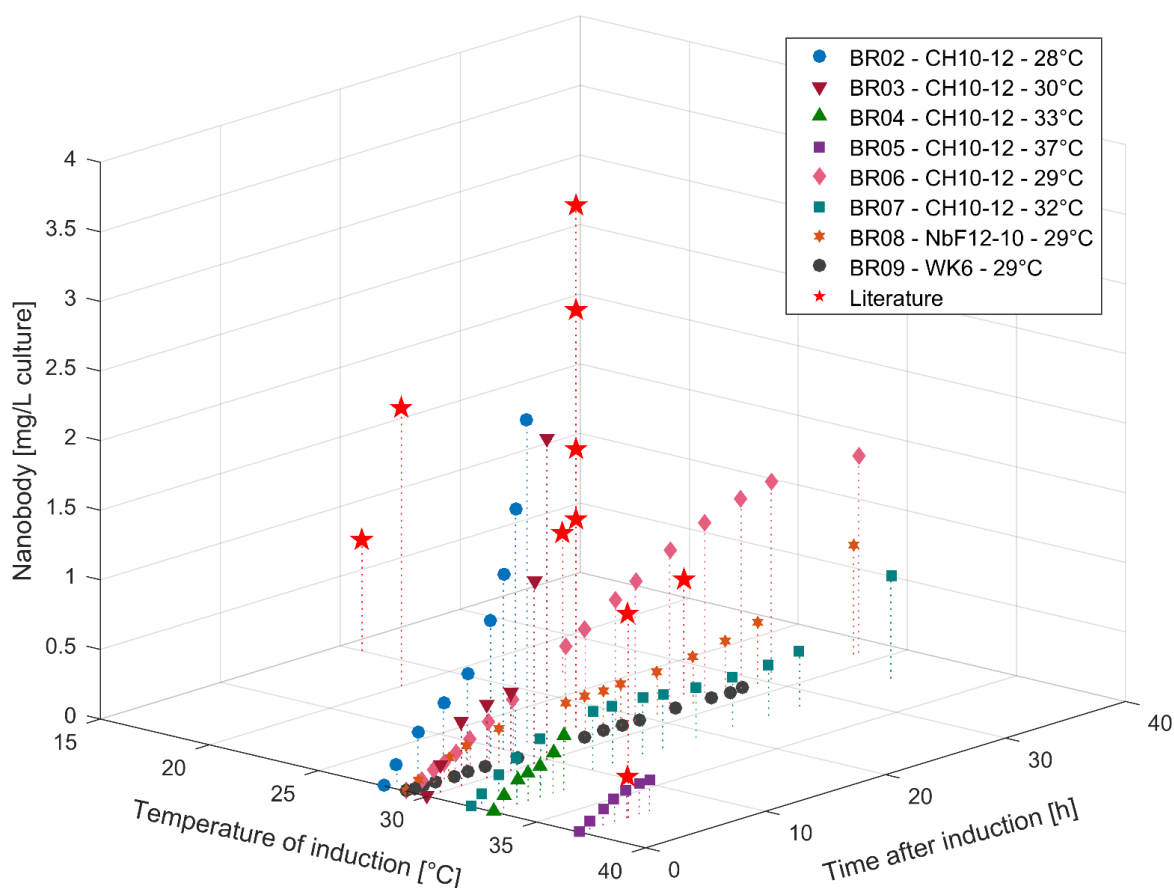


Figure III-58. Nanobody production in cultures BR02 – BR08 and comparison with the literature.

In the cultures BR02 and BR03, a titer of 2.3 mg/L culture was reached, comparable to those published in the literature (Table III-19). The production of recombinant nanobodies produced in the periplasmic space of *E. coli* strains has mostly been reported in shake-flask scale and rich medium and quantified at the end of the culture (Table III-19). Only the works of Kraïem show the production of nanobodies in defined mineral medium and bioreactor, and only final titer was reported [164], [165].

The expression of the protein in the literature was made over a long period of time (16 – 25 h) and low temperatures (16 – 28°C), and only Kraïem studied the effect of a high temperatures (37°C) in short induction duration [164], [165]. Information about the production of the biomass is not available and the specific yields could not be calculated, except for the data of Kraïem.

Strain	Culture media	Concentration, mg/L	Volumetric productivity, mg/L/h	Antibody	Duration [h] – T [°C]	$\bar{\mu}_{ind}$ [h ⁻¹]	Ref.
<i>E. coli</i> WK6	MM	2.32	0.193	31 kDa CH10-12	12 h – 28°C	0.019	This work
<i>E. coli</i> WK6	MM	2.3	0.230	31 kDa CH10-12	10 h – 30°C	0.023	This work
<i>E. coli</i> WK6	MM	0.39	0.065	31 kDa CH10-12	6 h – 33°C	0.033	This work
<i>E. coli</i> WK6	MM	0.23	0.038	31 kDa CH10-12	6 h – 37°C	0.028	This work
<i>E. coli</i> WK6	MM	1.41	0.037	31 kDa CH10-12	38 h – 29°C	0.016	This work

Strain	Culture media	Concentration, mg/L	Volumetric productivity, mg/L/h	Antibody	Duration [h] – T [°C]	$\bar{\mu}_{ind}$ [h ⁻¹]	Ref.
<i>E. coli</i> WK6	MM	0.68	0.019	31 kDa CH10-12	35 h – 32°C	0.019	This work
<i>E. coli</i> WK6	MM	0.79	0.021	29 kDa NbF12-10	37 h – 29°C	0.018	This work
<i>E. coli</i> HB215 1	2xYT	0.5 – 0.8	0.025 – 0.040	50 kDa scFv-scFv	20 h – 16°C	N. A.	[123]
<i>E. coli</i> TOPP2	2xYT	1	0.042	48 kDa chFab-BCF2	24 h – 23°C	N. A.	[101]
<i>E. coli</i> HB215 1	2xYT	1 – 2	0.063 – 0.125	29 kDa scFv 9C2	16 h – 20°C	N. A.	[124]
<i>E. coli</i> WK6	TB	1.5	0.094	78.5 kDa HCAb	16 h – 28°C	N. A.	[163]
<i>E. coli</i> WK6	TB	2	0.125	29 kDa NbF12-10	16 h – 28°C	N. A.	[163]
<i>E. coli</i> WK6	TB	2	0.125	14 kDa Nb12	16 h – 28°C	N. A.	[121]
<i>E. coli</i> WK6	TB	3	0.188	14 kDa NbAah1'22	16 h – 28°C	N. A.	[163]
<i>E. coli</i> WK6	TB	3.75	0.234	29 kDa NbF12-10	16 h – 28°C	N. A.	[4]
<i>E. coli</i> WK6	MM	0.3	0.075	29 kDa NbF12-10	4 h – 37°C	0.2	[164], [165]
<i>E. coli</i> WK6	MM	0.83	0.033	31 kDa CH10-12	25 h – 28°C	0.05	[164], [165]
<i>E. coli</i> WK6	MM	1.47	0.368	31 kDa CH10-12	4 h – 37°C	0.12	[164], [165]

Table III-19. Antibodies with neutralizing effects against scorpion neurotoxins. N. A.: not available.

In terms of the volumetric productivity, the culture BR03, induced at 30°C, had the highest productivity among most of the values of the literature, meaning that the production was faster in the cultures in the bioreactor. Longer induction durations were not favorable for the production of the nanobody CH10-12, as a final volume productivity of 0.037 mg/L/h, at 29°C and 37 h of induction, contrasted with 0.23 mg/L/h, at 30°C and 10 h of induction.

According to our findings, the temperature plays an important role in the production of the nanobody, with the highest titers attained at the lower temperatures (<30°C). These results contrasted with the findings of Kraïem, that found higher titers and volumetric productivities of nanobody at higher temperatures [164], [165]. The difference could be explained by the average specific growth rate during the induction phase, Kraïem worked at a rate of 0.12 h⁻¹ for the cultures at 37°C, whereas we worked at an average of 0.03 h⁻¹ (Table III-15). Some studies have suggested that the productivity of a recombinant protein can be increased with high specific growth rates ($\mu > 0.09$ h⁻¹) in order to reduce the metabolic burden [215], [216].

As a method to reduce the metabolic burden in recombinant strains, several authors have reported the use of an inducer concentration lower than 1 mM IPTG [85], [135], [144], [145], [148], [209], [217]. Moreover, the optimal concentration of IPTG used to express the recombinant protein is highly dependent on the microbial system [85].

For *Escherichia coli* BL21 (DE3) strains, several authors have studied the concentration of inducer for maximal protein expression [135], [148], [217]. Dynamically increasing the concentration of IPTG in the feed medium, Schmideder and colleagues [135] found that with an optimal concentration of 100 μM IPTG they could obtain 8 g/L of the photoactivatable mCherry (PAmCherry) recombinant protein, compared to 7 g/L obtained at 1 mM IPTG. Dela Coletta and colleagues [217] made a design of experiments in shake-flask cultures to determine the optimal IPTG concentration for the production of the recombinant protein CFP10. The optimal IPTG concentration was 0.12 mM, obtained from a linear analysis of the data of cultures induced from 0.016 to 0.184 mM IPTG. Calleja and colleagues [148] designed a model to predict protein production using inducer concentrations from 70 to 100 μM IPTG.

For *Escherichia coli* M15, derived from the K12 strain, a concentration as low as 10 μM IPTG have been used for complete induction of the *lac* promoter [144]. Ruiz and colleagues [144], [145] tested the concentration of inducer in fed-batch cultures, where the inducer was added in the feed solution and ranged from 0.4 to 3 μmol IPTG/g cdw. The optimal concentration of inducer was 1 μM IPTG/g cdw, reaching 8 g/L of His₆-tagged rhamnulose 1-phosphate aldolase (RhuA) enzyme.

In the cultures BR02 to BR05, the IPTG/biomass ratio was between 45 μmol IPTG/g cdw at the start of the induction phase and 30 μmol IPTG/g cdw at the end of protein expression. In the cultures BR06 to BR09, the ratio at the start and end of the protein expression phase was between 35 and 20 μmol /g cdw, respectively. These conditions comply with those used in shake-flask cultures (§III.1.3), and are, at least, 10-fold higher than the ratio used for other recombinant *E. coli* strains.

Other method to reduce the metabolic burden is to use a different inducer, such as lactose [85], [209], [211]. In addition to be used as an inducer, lactose will provide a different carbon source to the medium and reduce the stress caused by the IPTG. However, the genetic background of the strain must be studied before making any changes to ensure that lactose is correctly metabolized to allolactose and the induction can take place [85].

The metabolic burden can also be reduced by inducing the protein expression at low temperatures (25°C – 30°C), where protein solubility is higher [90]. Low temperatures also allow the correct formation of disulfide bridges in the oxidative environment of the periplasm [80], [81]. In the case of the cultures BR02 to BR05, the effect of the temperature on the metabolic burden can be clearly seen by the increase of protein concentration at low temperatures (Figure III-59). Although this same phenomenon can be observed for cultures BR06 to BR08, the final production was not comparable between the two series.

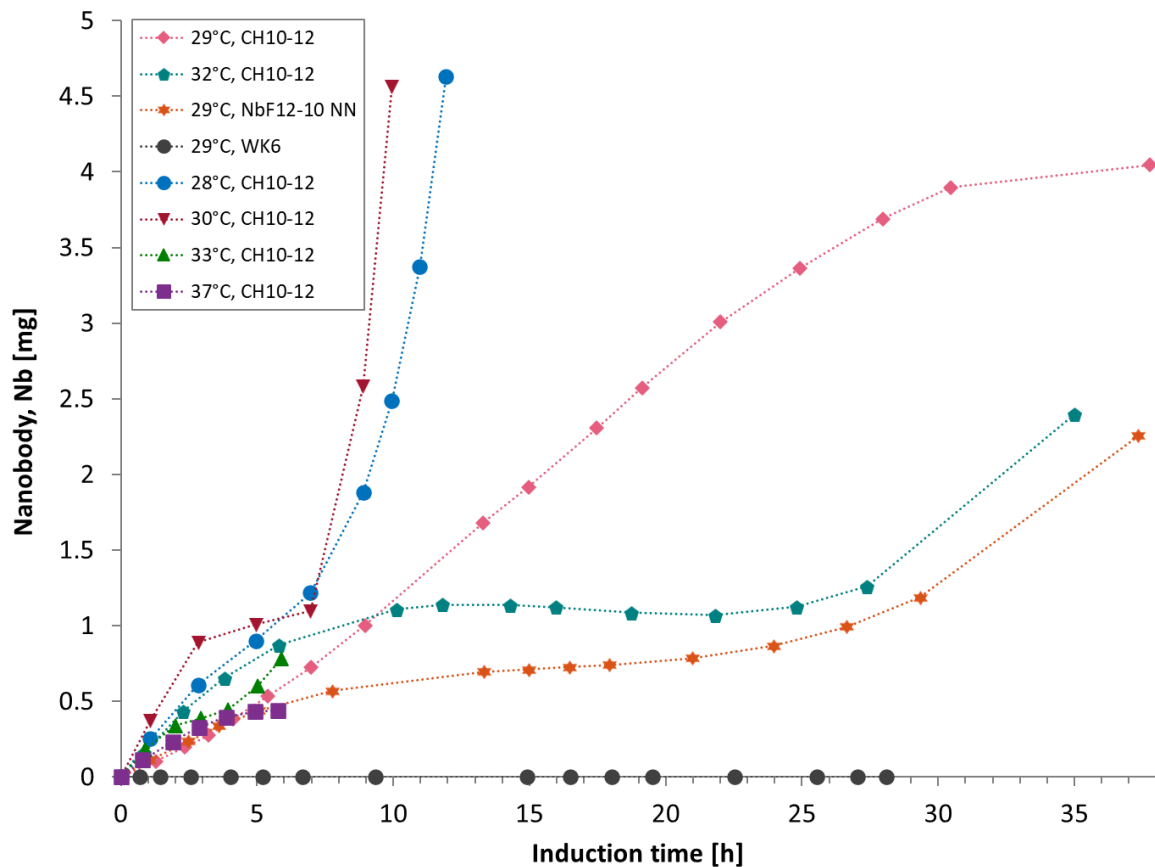


Figure III-59. Production of nanobodies CH10-12 and NbF12-10 in cultures BR02 to BR09.

None of the cultures were repeated due to the large amount of data processed for each cultures and the long purification processes needed for the quantification of the nanobodies. A high amount of time was put into the quantification methods of the nanobody by Nanodrop, Bradford assay and quantification by densitometry. The latter was the subject of an article published in *MicrobiologyOpen* [172].

The specific productivity of the nanobody, q_{Nb} , was plotted in function of the specific growth rate, μ , in cultures BR02 to BR08 (Figure III-60). The specific growth rates during induction varied from 0.06 to 0.005 h^{-1} (Table III-15).

Ramchuran and colleagues [211] ran fed-batch experiments of recombinant xylanase produced in *Escherichia coli* BR21 (DE3). They supplemented the glucose feed solution with citric acid, malic acid, succinic acid or cysteine. During protein expression, the citric acid was exhausted, as well as the malic acid in the supplemented cultures. The culture supplemented with cysteine had a higher final biomass concentration. With the consumption of citric acid, they concluded that the TCA cycle was used as a proxy to obtain the protein precursors for further biosynthesis.

Our results are consistent with those found by Ramchuran and colleagues [211]. The low specific growth rates, the high maintenance metabolism and the consumption of the citric acid during protein expression indicate a deficiency of the nutrients needed by the host microorganism to produce the recombinant nanobody in the cultures with longer induction times.

The origin of the secondary proteins found in the cultures (Figure III-57) can be explained by two hypotheses: 1) the bands are non-specific proteins with similar affinity to the histidine; 2) the bands are specific proteins (aggregates) or degradation products.

The first hypothesis proposes the production of unknown proteins within the cell, which potentially have an affinity similar to that of the histidine. Bacterial cellular proteins of the host microorganism can be produced during protein expression as building blocks for the production of the nanobody [218]. In the case of the culture BR09, the reference culture, host cell proteins or other proteins could have been produced due to the effect of the inducer IPTG as a stress response [85], [111], [210]. The production of these unknown proteins could be explained by the effect of the maintenance of the microorganism (§III.2.3.2.2) and the low biomass yields obtained during the induction phase (§III.2.3.2.2).

The second hypothesis proposes the aggregation and/or deterioration of the nanobody during protein expression. The degradation of the nanobody CH10-12 into a protein of 11 kDa can be explained by the high temperatures of induction (32°C – 37°C), when the protein is found in larger quantities. Proteolytic degradation is known to happen in the host cells during the expression of recombinant proteins [85]. Low temperatures (25°C – 30°C) will decrease the metabolic burden of the protein expression and reduce the proteolysis inside the host cell. The effect of the temperature can be clearly seen in Figure III-57, where the quantity of the protein at 11 kDa at 32°C was 4 mg, 10-times higher than the protein produced at 29°C in cultures BR07 and BR06, respectively.

High induction temperatures can also affect the aggregation of the recombinant proteins. Protein aggregates consist usually in partially folded proteins. They are favored by high temperatures due to the temperature dependence of hydrophobic interactions [90]. Low production temperatures will reduce the rate of production and, consequently, will favor the production of correctly folded proteins [219]–[221]. In addition to the expression of the protein at lower temperatures, the use of molecular chaperones can be used to avoid the protein aggregation or to reverse the aggregation in the inclusion bodies [90], [222].

The protein at 84 kDa is about 3-times the molecular weight of the nanobody CH10-12 (31 kDa). Assuming that the protein is aggregated due to high temperatures, the formation of an irreversible aggregate form of nanobody can be proposed. Protein aggregates are usually dimers or tetramers of the nanobody, and formed over 30°C [223]. There is evidence that due to the folding mechanisms of recombinant strains, new proteins aggregate while old proteins remain correctly folded [219].

The imbalance between reversible and irreversible reactions of protein expression can be proposed. The protein of 84 kDa seems to increase during protein expression in the longer induction cultures. The protein of 11 kDa could be a degradation product of either the nanobody or the aggregate form. It has been reported that some aggregates could be consumed after long induction times, as a reaction to the stringent response due to low specific growth rates [85], [224].

For both hypotheses, the origin of the secondary proteins could only be tested by a western blot analysis on the eluates of the purification of long induction duration cultures. Unfortunately, this analysis could not be done during this doctoral project due to a technical problem in the freezer chamber where the samples were stored in May 2019 that resulted in the total loss of these samples prepared for the Pasteur Institute of Tunis (Tunisia).

The presence of the His₆-tag would indicate that these secondary proteins are degradation products or protein aggregates. If the proteins do not contain the His₆-tag, the most possible explanation is that they are host cell proteins produced during the recombinant protein expression and due to the effect of the inducer.

III.2.5. Conclusion

The cultures in bioreactor showed a high repeatability with the fed-batch strategy used. Oxygen transfer was kept at optimal conditions ($pO_2 > 15\%$) in most of the cultures and incidents were minimal. The volumetric mass transfer coefficient, k_{La} , during biotic conditions was constant when the agitation and aeration rates were the same in all cultures. The biological enhancement factor, E , was at about 25 during the induction phase, one order of magnitude higher than the values of the literature.

The correlation coefficient of biomass and optical density was equal to 2 g cdw/AU for all cultures, and consistent with the values obtained in our shake-flask cultures. The maximum specific growth rate, μ_{max} , was 0.8 h⁻¹ for the reference strain and the recombinant strains at pH 6.8 and 37°C.

In batch and fed-batch modes, the yield of biomass on glucose, $Y_{X/S}$, was in average 0.4 Cmol/Cmol for all strains. In the induction phase $Y_{X/S}$ varied from 0.3 to 0.5 g/g in the short induction duration cultures, and 0.2 g/g in the long induction duration cultures.

During batch mode, acetic acid was produced due to the excess of glucose. The yield of acetate on glucose, $Y_{Ac/S}$, was 0.29 g/g for all cultures. During the long induction duration cultures, citrate was apparently and unexpectedly consumed.

The yield of carbon dioxide on glucose, $Y_{CO_2/S}$, in batch and fed-batch modes was 0.4 Cmol/Cmol for all cultures. In the induction phase, it increased from 0.6 to 0.8 Cmol/Cmol for the short induction duration cultures and the long induction duration cultures, respectively. The respiratory quotient, RQ, remained constant at 1 for all cultures during all culture's phases.

The maintenance coefficient was obtained with a linear analysis between the specific glucose consumption rate and the specific growth rate, and equal to 0.048 g/g/h for *E. coli* WK6 and 0.03 g/g/h for the recombinant strains CH10-12 and NbF12-10 NN.

The nanobodies CH10-12 and NbF12-10 were only found in the periplasmic space, and no protein was quantified in the growth medium (supernatant). The nanobody was not found on the reference culture of *Escherichia coli* WK6 induced at 29°C.

Nanobody concentration decreased with an increase on the induction temperature. In the short induction duration cultures, the cultures induced at 28°C and 30°C reached the same final titer (2.3 mg/L) at 12 h and 10 h of induction. The cultures induced at 33°C and 37°C produced at 0.4 and 0.23 mg/L after 6 h of induction.

The cultures of long-induction-duration did not produce higher titers than the short induction time cultures, despite having almost the same average specific growth rate (0.02 h⁻¹). The culture of *E. coli* CH10-12 induced at 29°C reached a plateau after 25 h of induction, at 1.4 mg/L. The culture of *E. coli* CH10-12 induced at 32°C and of *E. coli* NbF12-10 NN induced at 29°C reached a plateau after 10 h of induction, at about 0.4 mg/L and a final titer of 0.7 mg/L was achieved after 35 h and 37h, respectively.

The metabolic burden due to the protein expression in the induction phase was proposed as the reason behind the low productivity in the long induction duration cultures. The metabolic load due to the presence of the inducer during the long induction duration (>30 h) hindered the biomass production and could have also been responsible for the low nanobody productivity. The concentration of inducer to biomass (IPTG/g cdw) varied from 20 to 40 $\mu\text{mol/g cdw}$, 20-fold higher than for other recombinant strains.

The low specific growth rate (0.02 h^{-1}) during the induction phase could have also produced a stringent response in the microorganism and add more metabolic load to the presence of the inducer. It was also found a higher maintenance metabolism during the induction phase of all induced strains.

The consumption of the citrate during induction and its almost depletion could indicate a nutritional limitation in the culture medium for the production of the nanobody. The high maintenance metabolism during the induction phase, the low biomass production and high carbon dioxide production could indicate that the strain is producing the intracellular metabolites needed to produce the recombinant nanobody.

Unknown proteins were found on the purified eluates by IMAC, with an apparent molecular weight of 11 kDa and 84 kDa, approximately. The protein of 84 kDa, with about 3-fold the molecular weight of the nanobody (31 kDa), could be a protein aggregate, whereas the protein of 11 kDa could have been a degradation product of the nanobody.

The production of the protein of 11 kDa was higher at higher temperatures, suggesting a degradation of the recombinant nanobody due to proteolytic degradation. The production of the protein of 84 kDa was higher in the long induction time cultures; this could be due to the metabolic burden of the inducer due to the overexpression of the protein.

III.3. Kinetic model

The recombinant nanobodies CH10-12 and NbF12-10 were used to establish a kinetic model of the as function of the temperature of induction and the specific growth rate. The cultures BR02 to BR08, up to 13 h of production duration, were used to determine the kinetic parameters of the model using MALTAB®.

The kinetic model proposed was a Luedeking-Piret kinetics [179], [225], with a modification to include a function of the temperature in an Arrhenius-type kinetic [226].

III.3.1. Kinetic models for recombinant proteins

The production of recombinant proteins has been mathematically modeled in shake-flask and bioreactor cultures. There are two main type of models used to describe the production: segregated models and non-segregated models.

In the segregated models, it is assumed that the cells are heterogeneous, integrating a probability of plasmid loss in the model of the recombinant strain [130]. The cells are then usually segregated into at least two populations: plasmid-bearing cells and non-plasmid-bearing cells. Plasmid-bearing cells are those that can produce the recombinant protein, while the non-plasmid-bearing cells are those that have lost the recombinant plasmid [130], [225].

The segregated kinetic models often describe the specific growth rate as function of the plasmid-bearing cells (X^+), the non-plasmid-bearing cells (X^-), culturable cells (X_n) and/or concentration of the substrate (S) and inducer (IPTG) (III-15) [118], [129], [130], [225].

$$\mu = f(X^+, X^-, X_n, S, IPTG) \quad (\text{III-15})$$

The disadvantage of the segregated models relies on the identification of the plasmid-bearing cells. For each sample of the culture, the identification is made by biomolecular analyses of the RNA of the strain [118], [129] or by counting biomass colonies [225]. These kinds of analyses take a lot of time, which in our bioreactor cultures could not be assured.

On the other hand, the non-segregated models describe the cell as a homogeneous population [214]. These models can provide an accurate and robust description of the macroscopic phenomena taking place in the induction phase [145]. Most of the articles found in the literature review (§1.4) make use of a non-segregated kinetic model to describe and/or control the production process of recombinant proteins.

The biomass in the bioreactor is often modeled to have a controlled biomass growth and/or to reduce the quantity of acetate produced by controlling the substrate feed and the specific growth rate [88], [227].

Depending on the nature of the recombinant protein, protein inhibition can play an important role in the production process. If the recombinant protein is toxic or if it is produced as inclusion bodies or in the periplasmic space of the cell, it may induce some kind of inhibition when produced in large quantities inside the cell [91], [228]. The inhibition factor is then added to the protein kinetics as the concentration of the recombinant protein.

Temperature is seldom represented in the kinetic models, either because it is not changed or because the model described only the production phase. The temperature of the process can be integrated in the model when the recombinant strain is induced by a temperature change [93], [138] or if the temperature of production is different than the temperature of the optimal growth [93], [136].

Finally, the recombinant protein kinetics can be represented by a Luedeking-Piret kinetics (III-16), which includes a factor dependent of the protein production rate (α) and one dependent on the biomass in the culture (β) [91], [95], [138], [179].

$$r_p = \alpha * r_x + \beta * X \quad (\text{III-16})$$

III.3.2. Temperature effect in specific productivity of the nanobody production

In our bioreactor cultures, the characteristic change between cultures was the temperature during the production phase. Therefore, the kinetic model developed for the cultures focused on the effect of the induction temperature in the specific productivity of the nanobody (q_p).

We decided to use a modified form of the Luedeking-Piret kinetics to describe the specific production rate of the nanobody in terms of a parameter coupled with the specific growth rate and one independent of the specific growth rate (II-40). The independent parameter was then described as two temperature-dependent parameters and one parameter independent of the specific growth rate and the temperature (II-41).

The temperature-dependent parameters were inspired on an Arrhenius-type kinetics, with two kinetic factors describing the energy of activation and deactivation of the production of the recombinant nanobody as function of the temperature.

The parameters of the specific production rate of the nanobody kinetics are shown in equations (III-17) and (III-18). The estimated parameters were calibrated and the model was validated with an independent set of data (data of the culture BR03, Figure III-61).

$$q_{Nb} = -3.35 * \mu_{ind} + \beta \quad (\text{III-17})$$

$$\beta = 0.57 * e^{-\frac{34.55}{T}} - 2.52 * e^{-\frac{30.67}{T}} + 0.76 \quad (\text{III-18})$$

Figure III-61 shows the effect of the temperature on the metabolic burden, where the specific production rate of the nanobody increases at low temperatures. Furthermore, it is shown that the highest nanobody productivity was obtained when the specific growth rates of induction were small.

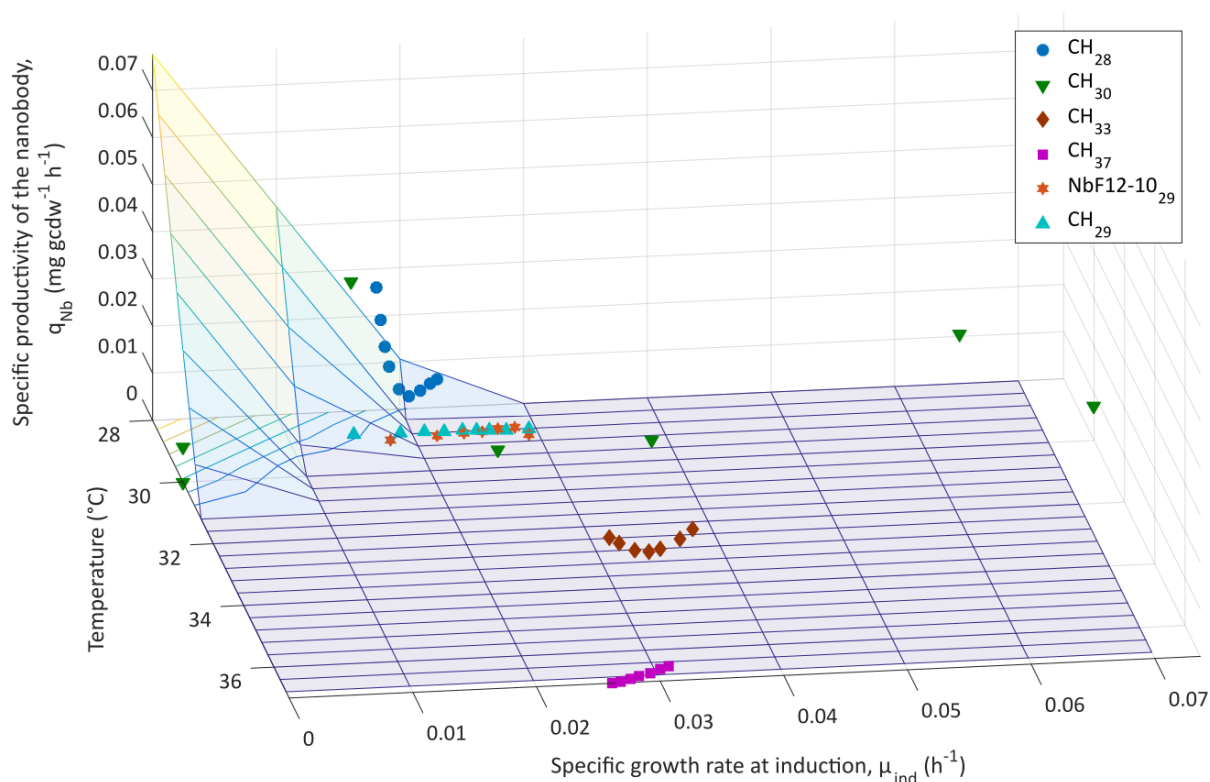


Figure III-61. Simulation of the kinetics for specific production rate of the nanobody.

The kinetic parameters were estimated for the specific production rate of the nanobody, which showed that the higher periplasmic production of the nanobody was made at low induction

temperatures. The production of the nanobodies could be tested at a temperature lower than 28°C or at lower specific growth rates to validate the model. The effect of the temperature on the production rate of recombinant proteins has not yet been modeled, highlighting the originality of the kinetic model presented in this research.

III.3.3. Conclusion

According to the kinetic model and the results found in §III.2.4, the temperature plays a key role in the production of the nanobody, with the highest production attained at the lowest temperatures during the induction phase. Lower induction temperatures (28°C and 30°C) attained the highest amounts of nanobody CH10-12 (4.6 mg Nb), and its production decreased along with the increase of induction temperature to 33°C and 37°C (0.78 and 0.44 mg Nb).

To improve the model, the production of the nanobodies at temperatures lower than 28°C could be tested to assess the effect of the Arrhenius-type kinetics on the nanobody production. The cultures could be made at specific growth rates between 0.05 h⁻¹ and 0.01 h⁻¹ to stay within the window of data of the cultures BR02 to BR08.

A proposition of a scientific article has been proposed for the description of the kinetic model. The article entitled “Effect of temperature on the production of a recombinant antivenom in fed-batch mode” will be submitted to Applied Microbiology and Biotechnology (Springer) in the fourth quarter of 2020. The full revised article can be found in Appendix 3.

The secondary proteins (§III.2.4.3, 11 kDa and 84 kDa) can be modeled using the same kinetic model once its origin is determined. This could help increase the purity of the recombinant nanobodies.

The inhibition of the biomass growth by the production of the nanobodies needs to be further investigated. The toxicity of the recombinant nanobodies produced in the periplasmic space could determine a maximum threshold of the achievable recombinant nanobody in the bioreactor cultures. Finally, further research is needed to investigate the neutralizing activity of the nanobodies CH10-12 and NbF12-10 by different *in vivo/in vitro* analyses.

CONCLUSIONS AND PERSPECTIVES

Scorpion stings are a serious health problem in tropical and subtropical zones around the globe. The most common treatment for scorpion stings is serotherapy, which uses antibodies or fragments of antibodies to target the 7 kDa neurotoxins present in the scorpion venom. The antivenoms are derived from equine plasma, and are available in low quantities at a high price for the health system due to the unavailability of the scorpion venom and the costly purification process of the 50 kDa antibody fragments [5].

Lately nanobodies, small fragments of camelid antibodies, have been proven to neutralize scorpion toxins [5], [163]. Furthermore, the production of recombinant therapeutic molecules in *Escherichia coli* is a common practice in the biopharmaceutical industry [77]. Then, the periplasmic production of the nanobodies has been studied in shake-flasks induced by synthetic IPTG under the control of the *lac* promoter [50]. The reported final concentration is low (< 4 mg/L [4]), and high cell density cultures have not been studied.

During this PhD project, the conditions to produce bispecific nanobodies were studied. The nanobodies CH10-12 and NbF12-10 with neutralizing effects against the neurotoxins of the *Androctonus australis Hector* scorpion species were produced in shake-flask and bioreactor cultures. The recombinant strains producing the nanobodies CH10-12 and NbF12-10 were *Escherichia coli* CH10-12 and the clones of *Escherichia coli* NbF12-10 (NN and NO). All the strains were prepared by the Laboratoire des Venins et Molécules Thérapeutiques of the Pasteur Institute of Tunis (LVMT-IPT, Tunis, Tunisia), and the strain of *Escherichia coli* WK6 was used as reference.

The strain screening in shake-flask cultures showed the adaptability of the recombinant *E. coli* strains to a rich medium (terrific broth, TB) and to a defined minimal medium (MM). From the four strains tested, only the recombinant clone NbF12-10 NO was unable to grow in MM. In TB medium, all strains had an average specific growth rate of over 0.4 h^{-1} . The maximum specific growth rate of the strains WK6 and CH10-12 grown in MM was the same (0.6 h^{-1}), and it was 30% lower for the strain NbF12-10 NN (0.2 h^{-1}). In the MM shake-flask cultures, the yields of biomass on glucose, $Y_{X/S}$, was 0.4 g/g for all strains, whereas the yield of acetic acid on glucose, $Y_{Ac/S}$, was between 0.06 and 0.14 g/g .

The inability of the clone NbF12-10 NO to grow in MM and the low specific growth rate of the clone NbF12-10 NN in MM in shake-flask cultures, could point out the longer adaptation needed for the strain to the culture medium.

The production of nanobody was tested in strains CH10-12 and NbF12-10 NN grown in TB with an induction at 28°C for 24 h. The release of periplasmic proteins through the permeation of the outer membrane was optimized in shake-flask cultures. The method improved by 300% the release of the periplasmic proteins in both strains. This study shows that the strain CH10-12 produced 20-fold more nanobody than the strain NbF12-10 under the same conditions of induction, temperature and osmotic shock (1.58 mg/L vs 0.08 mg/L).

The size of the microorganism was studied in shake-flask cultures and bioreactor cultures. On shake-flask cultures it was shown that it changed slightly during induction phase of cultures of *E. coli* CH10-12. The circle equivalent diameter (CE diameter) during the induction phase decreased 10% to 30%, compared to non-induced cultures at 37°C and 28°C . In bioreactor cultures of *E. coli* CH10-12, the CE diameter was 20% greater during batch mode than during fed-batch mode. During the induction phase, the CE diameter was almost constant for all cultures, regarding of the temperature of the induction phase. This suggests that the change in the cell size was mainly due to the specific growth rate of the microorganism, and independent of the protein induction or the temperature of production.

The quantification of the nanobody, particularly for the bioreactor cultures, was a studied during this thesis. The unknown concentration of nanobody was below the lower limit of detection of the

Nanodrop (0.1 mg/mL) in the purified samples by IMAC. For the Bradford assay, the samples were diluted in trial-and-error effort to quantify the protein within the limits of detection of the method, without success.

In the SDS-PAGE gels however, the band of the nanobody was clearly visible and incrementing with the time of the induction, as it was expected. In order to quantify the nanobody within the gel, a protocol of image processing was proposed. Optimal image processing was found at background subtraction with a size of the rolling ball of 250 pixels. The peak area of each protein was obtained by the uncalibrated optical density profile of each lane of the gel. BSA, CA, and OV were used to quantify the bands of the molecular weight marker. The nanobody was accurately quantified using the band of 50 kDa of the molecular weight marker as reference for 750 ng of recombinant protein. This was the subject of a published article in *MicrobiologyOpen* [172].

For the bioreactor cultures, high repeatability was found during batch and fed-batch modes. During batch mode, the maximum specific growth rate was 0.8 h^{-1} for all cultures at 37°C , pH 6.8, $p\text{O}_2 > 15\%$, 10 g Glc/L, MM. The yield of acetate on glucose, $Y_{Ac/S}$, was 0.29 g/g for all cultures in batch mode, and, it was completely consumed after a couple of hours after the start of the fed-batch mode.

The oxygen transfer in the cultures was assured by a defined strategy of aeration and agitation duos per operating mode. This assured a production of biomass and nanobody in strict aerobic conditions ($p\text{O}_2 > 15\%$) and the volumetric mass transfer coefficient, k_{La} , could be compared under the same conditions for all cultures. The k_{La} under biological conditions was, in average, one order of magnitude greater than the k_{La} under abiotic conditions. The biological enhancement factor, E , could be calculated and compared for all cultures, and varied from 5 to 40. The respiratory quotient, RQ , remained constant for all cultures at an average value of 1, despite the production of the nanobody during the induction phase.

In batch and fed-batch mode, the yields of biomass on glucose, $Y_{X/S}$, and the yield of carbon dioxide on glucose, $Y_{\text{CO}_2/S}$, were both 0.45 Cmol/Cmol for all cultures. During the induction phase, $Y_{X/S}$ decreased to 0.2 Cmol/Cmol, while $Y_{\text{CO}_2/S}$ increased up to 0.8 Cmol/Cmol. This indicates a change in the strain metabolism due to the nanobody production.

The maintenance metabolism was particularly high during the induction phase, as it can be appreciated by the increase in the production of carbon dioxide ($Y_{\text{CO}_2/S} = 0.45 \rightarrow 0.8 \text{ Cmol/Cmol}$) and the reduced production of biomass ($Y_{X/S} = 0.45 \rightarrow 0.2 \text{ Cmol/Cmol}$).

The fed-batch mode allowed achieving high biomass concentrations (25 – 30 g cdw/L) before protein expression with the consumption of the acetate produced during batch mode. The nanobodies CH10-12 ad NbF12-10 were expressed in MM medium. A residual carbon flux was set constant at 4 g Glc/h to avoid nutritional limitation during the production of the nanobody, the residual specific growth rate was in average 0.02 h^{-1} for all strains.

The effect of the temperature in the production of the nanobody was unmistakable in the cultures induced between 28°C and 37°C . Lower temperatures (28°C and 30°C) attained the highest titers of nanobody CH10-12 (2.3 mg/L), and its concentration decreased concomitantly with the increase of temperature to 33°C and 37°C (0.4 mg/L and 0.2 mg/L). Since low induction temperatures decrease the metabolic burden of the recombinant strain, these findings were consistent with the literature [85].

In the cultures where the induction phase was over 35 h, the productivity was lower than the cultures of short induction duration (<12 h). The production of the nanobodies seemed to reach a plateau after a time. Final titers of 1.4 mg/L and 0.4 mg/L were obtained for cultures of *E. coli* CH10-12 induced at 29°C and 32°C , respectively. The culture of *E. coli* NbF12-10 NN induced at 29°C reached a final titer of 0.7 mg/L after 35 h of induction.

The low nanobody concentrations obtained in the long-induction-duration cultures could be explained by the metabolic burden of the induced plasmid [85]. Despite the low temperature of production (29°C), the culture BR06 reached a plateau after 25 h of induction, and the cultures BR07 (32°C) and BR08 (29°C) reached a plateau after only 10 h of induction.

During the induction phase, the citrate present in the culture medium was consumed in the long induction duration cultures. The apparent consumption of the citrate in the cultures of long induction duration indicated the stimulation of the TCA-cycle of the microorganism. The permeation of the membrane due to the long exposure of the strain to the IPTG could be a possibility that explain the internalization of the citrate and further consumption. This phenomenon was found in the production of other recombinant proteins [211]. The hypothesis proposed was that the citrate was used to synthesize the intracellular metabolites needed to produce the recombinant nanobody.

The metabolic burden could have been enhanced by the low specific growth rate (0.02 h^{-1}) during the induction phase. Low titers of substrate in the culture medium cause a stringent response in the recombinant strains, which could produce unwanted intracellular proteins.

The long induction duration (>30 h) could have also been responsible for the high metabolic load due to the long exposure of the microorganism with IPTG. This inducer is a non-metabolized compound that activates the recombinant plasmid to produce the nanobody, but it is also known to hinder biomass production at high inducer concentrations [85]. The optimal inducer concentration is system-dependent and, in bioreactor cultures, it could be controlled by the biomass concentration ($0.4 - 3 \mu\text{mol IPTG/g cdw}$) to reduce the metabolic burden [144], [145], [148]. The induced cultures had an inducer-biomass concentration of 20 to $40 \mu\text{mol IPTG/g cdw}$, 10-fold higher than the used for other recombinant *E. coli* strains, but consistent with the shake-flask cultures of recombinant nanobodies.

The production of unknown proteins in the purified samples of nanobody could be a response of the strain to the low specific growth rate and the long exposure time to the inducer. The protein of low molecular weight (11 kDa) could be a degradation product of the nanobody caused by a high temperature (proteolytic degradation). The high molecular weight protein (84 kDa) could be a trimer of the nanobody produced as a response to an inadequate medium composition and the low specific growth rate.

Finally, due to the high repeatability of the cultures, a mathematical model was proposed and tested on the data of cultures of the strain *Escherichia coli* CH10-12. The model was a modified Luedeking-Piret kinetic with Arrhenius-like kinetic parameters. The hypothesis of thermo-dependency of the recombinant nanobody production was confirmed by the model, which showed that the highest production was obtained at the lowest temperature (28°C). The model was compared with the culture of the strain *Escherichia coli* NbF12-10 NN, which showed the same tendency than the cultures of *E. coli* CH10-12. The description of the model and its findings will be submitted in the form of an article to Applied Microbiology and Biotechnology (Appendix 3.).

As perspectives of this doctoral project, further analysis on the nanobody CH10-12 could be made. The nanobody CH10-12 is the humanized form of the nanobody NbF12-10, created with the same neurotoxins Aahl' and AahlII of the *Androctonus australis hector* scorpion. An analysis of bioactivity of the nanobody CH10-12 needs to be performed against the neurotoxins and/or the venom of the *Androctonus australis hector* scorpion.

Western blot analyses need to be made in order to elucidate the origin of the secondary proteins found in the purification steps of the nanobody (11 kDa and 84 kDa). The hypotheses proposed of the aggregation of the nanobody during long induction times and the proteolytic degradation of the

nanobody due to high temperatures will help to improve the induction conditions at which the nanobody production is better.

Experiments at lower temperatures (<28°C) should be made to further validate the kinetic model presented in this research. The secondary proteins could be as well modeled once its origin is determined, and to increase the purity of the recombinant nanobodies CH10-12 and NbF12-10 in the cultures.

The relationship between the nanobody productivity and the metabolic burden due to inducer concentrations, long induction durations or low specific growth rates could be tested in a series of extra experiments. Induction phase could be carried over with a high specific growth rate (0.3 h^{-1}) to quickly achieve a high biomass concentration and reduce the metabolic burden due to the long exposure to the inducer. The use of lactose as inducer of protein expression can also be explored.

Finally, the hypothesis of the deficiency of nutrients in the defined minimal medium could be tested with an experiment where citrate is added continuously during the fed-batch mode to maintain a constant titer during all the induction phase.

REFERENCES

- [1] D. Warrell, J.-M. Gutierrez, and A. Padilla, "Rabies and envenomings : a neglected public health issue : report of a Consultative Meeting.," Geneva, Switzerland, 2007.
- [2] K. Deffar, H. Shi, L. Li, X. Wang, and X. Zhu, "Nanobodies - the new concept in antibody engineering," *African J. Biotechnol.*, vol. 8, no. 12, pp. 2645–2652, 2009.
- [3] A. O. Carmo *et al.*, "Evolution of alternative methodologies of scorpion antivenoms production," *Toxicon*, vol. 97, pp. 64–74, Apr. 2015.
- [4] I. Hmila *et al.*, "A bispecific nanobody to provide full protection against lethal scorpion envenoming," *FASEB J.*, vol. 24, no. 9, pp. 3479–3489, Sep. 2010.
- [5] E. Alirahimi *et al.*, "Nanobodies as novel therapeutic agents in envenomation," *Biochim. Biophys. Acta - Gen. Subj.*, vol. 1862, no. 12, pp. 2955–2965, Dec. 2018.
- [6] J.-P. Chippaux and M. Goyffon, "Epidemiology of scorpionism: A global appraisal," *Acta Trop.*, vol. 107, no. 2, pp. 71–79, Aug. 2008.
- [7] J.-P. Chippaux, "Emerging options for the management of scorpion stings," *Drug Des. Devel. Ther.*, vol. 6, p. 165, Jul. 2012.
- [8] R. Dehghani and M. G. Arani, "Scorpion sting prevention and treatment in ancient Iran," *J. Tradit. Complement. Med.*, vol. 5, no. 2, pp. 75–80, Apr. 2015.
- [9] M. S. V. Santos *et al.*, "Clinical and Epidemiological Aspects of Scorpionism in the World: A Systematic Review," *Wilderness Environ. Med.*, vol. 27, no. 4, pp. 504–518, Dec. 2016.
- [10] M. Goyffon, "Le scorpionisme," *Rev. Française des Lab.*, vol. 2002, no. 342, pp. 41–48, Apr. 2002.
- [11] M. Ismail, "Treatment of the scorpion envenoming syndrome: 12-years experience with serotherapy," *Int. J. Antimicrob. Agents*, vol. 21, no. 2, pp. 170–174, Feb. 2003.
- [12] A. Al-Asmari, R. A. Manthiri, N. Abdo, F. A. Al-Duaiji, and H. A. Khan, "Saudi medicinal plants for the treatment of scorpion sting envenomation," *Saudi J. Biol. Sci.*, vol. 24, no. 6, pp. 1204–1211, Sep. 2017.
- [13] M. Dehesa-Dávila and L. D. Possani, "Scorpionism and serotherapy in Mexico," *Toxicon*, vol. 32, no. 9, pp. 1015–1018, Sep. 1994.
- [14] Secretaría de Salud de México, "Programa de Acción Específico: Prevención y Control de la Intoxicación por Picadura de Alacrán," Mexico City, 2014.
- [15] V. M. Granja Bermúdez, R. Martínez Zúñiga, and P. Chico Aldama, "Tratamiento del alacranismo y costos," *Alergia, Asma e Inmunomolgía Pediátricas*, vol. 8, no. 4, pp. 113–117, 1999.
- [16] A. Carboney and C. E. Jasso Villazul, "Manual de Procedimientos Estandarizados para la Vigilancia Epidemiológica de la Intoxicación por Picadura de Alacrán," Mexico City, 2012.
- [17] A. M. Queiroz *et al.*, "Severity of Scorpion Stings in the Western Brazilian Amazon: A Case-Control Study," *PLoS One*, vol. 10, no. 6, p. e0128819, Jun. 2015.
- [18] R. Dehghani and B. Fathi, "Scorpion sting in Iran: A review," *Toxicon*, vol. 60, no. 5, pp. 919–933, Oct. 2012.
- [19] M. B. Pucca, F. N. Oliveira, E. F. Schwartz, E. C. Arantes, and R. M. Lira-da-Silva, "Scorpionism and Dangerous Species of Brazil," in *Scorpion Venoms*, Toxinology., Dordrecht: Springer Netherlands, 2015, pp. 299–324.
- [20] G. D'Suze *et al.*, "Scorpionism and Dangerous Species of Venezuela," in *Toxinology*, Dordrecht: Springer Netherlands, 2013, pp. 1–23.
- [21] M. Ismail, "The scorpion envenoming syndrome," *Toxicon*, vol. 33, no. 7, pp. 825–858, Jul. 1995.
- [22] N. Mansour, "Delai et caracteristiques de la prise en charge des piqués par scorpion dans la region de Sidi-Bouزيد," *Arch. Inst. Pasteur Tunis*, vol. 78, no. 1/2/3/4, pp. 25–31, 2001.
- [23] Y. Laid, R. Oudjehane, and K. Bachiri, "Envenimation scorpionique: Rapport Annuel sur la situation epidemiologique en Algérie," El Biar, Algeria, 2012.

- [24] D. Hammoudi and F. Laraba, "Application du test ELISA pour la quantification du venin d'*Androctonus australis hector* dans les sérums de personnes et de rats envenimés avant et après immunothérapie," *Bull. la Société Pathol. Exot.*, vol. 96, no. 4, pp. 297–301, 2003.
- [25] H. Hellal *et al.*, "Données épidémiologiques sur l'envenimation scorpionique en Algérie," *Bull. la Société Pathol. Exot.*, vol. 105, no. 3, pp. 189–193, Aug. 2012.
- [26] A. Benslimane *et al.*, "Scorpion envenomation and serotherapy in Morocco.," *Am. J. Trop. Med. Hyg.*, vol. 62, no. 2, pp. 277–283, Feb. 2000.
- [27] M. Goyffon and C. Guette, "Scorpions dangereux du Niger," *Bull. la Société Pathol. Exot.*, vol. 98, no. 4, pp. 293–295, 2005.
- [28] M. Ismail, "The treatment of the scorpion envenoming syndrome: The Saudi experience with serotherapy," *Toxicon*, vol. 32, no. 9, pp. 1019–1026, Sep. 1994.
- [29] E. El Aminn and R. Berair, "Piqûres de scorpion chez l'enfant. Expérience saoudienne," *Arch. Pédiatrie*, vol. 2, no. 8, pp. 766–773, Aug. 1995.
- [30] M. H. Pipelzadeh, A. Jalali, M. Taraz, R. Pourabbas, and A. Zaremirakabadi, "An epidemiological and a clinical study on scorpionism by the Iranian scorpion *Hemiscorpius lepturus*," *Toxicon*, vol. 50, no. 7, pp. 984–992, Dec. 2007.
- [31] J. Nejati, E. Mozafari, A. Saghafipour, and M. Kiyani, "Scorpion fauna and epidemiological aspects of scorpionism in southeastern Iran," *Asian Pac. J. Trop. Biomed.*, vol. 4, no. Suppl 1, pp. S217–S221, May 2014.
- [32] A. Tarasiuk, S. Menascu, and S. Sofer, "Antivenom serotherapy and volume resuscitation partially improve peripheral organ ischemia in dogs injected with scorpion venom," *Toxicon*, vol. 42, no. 1, pp. 73–77, Jul. 2003.
- [33] J. Barona, R. Otero, and V. Núñez, "Aspectos toxicológicos e inmunoquímicos del veneno del escorpión *Tityus pachyurus* Pocock de Colombia: capacidad neutralizante de antivenenos producidos en Latinoamérica.," *Biomédica*, vol. 24, no. 1, p. 42, Mar. 2004.
- [34] P. Bailey and J. Wilce, "Venom as a source of useful biologically active molecules," *Emerg. Med. Australas.*, vol. 13, no. 1, pp. 28–36, Mar. 2001.
- [35] M. W. Pennington, A. Czerwinski, and R. S. Norton, "Peptide therapeutics from venom: Current status and potential," *Bioorganic Med. Chem.*, vol. 26, no. 10, pp. 2738–2758, 2018.
- [36] A. Lakowitz, T. Godard, R. Biedendieck, and R. Krull, "Mini review: Recombinant production of tailored bio-pharmaceuticals in different *Bacillus* strains and future perspectives," *Eur. J. Pharm. Biopharm.*, vol. 126, pp. 27–39, May 2018.
- [37] S. Steeland, R. E. Vandembroucke, and C. Libert, "Nanobodies as therapeutics: big opportunities for small antibodies," *Drug Discov. Today*, vol. 21, no. 7, pp. 1076–1113, Jul. 2016.
- [38] M. Arbabi-Ghahroudi, "Camelid Single-Domain Antibodies: Historical Perspective and Future Outlook," *Front. Immunol.*, vol. 8, no. NOV, pp. 1–8, Nov. 2017.
- [39] O. Spadiut, S. Capone, F. Krainer, A. Glieder, and C. Herwig, "Microbials for the production of monoclonal antibodies and antibody fragments," *Trends Biotechnol.*, vol. 32, no. 1, pp. 54–60, Jan. 2014.
- [40] N. K. Tripathi, "Production and Purification of Recombinant Proteins from *Escherichia coli*," *ChemBioEng Rev.*, vol. 3, no. 3, pp. 116–133, Jun. 2016.
- [41] T. Schirrmann, L. Al-Halabi, S. Dübel, and M. Hust, "Production systems for recombinant antibodies.," *Front. Biosci.*, vol. 13, no. 6, pp. 4576–94, May 2008.
- [42] A. de Marco, "Strategies for successful recombinant expression of disulfide bond-dependent proteins in *Escherichia coli*," *Microb. Cell Fact.*, vol. 8, no. 1, p. 26, 2009.
- [43] P. A. Marichal-Gallardo and M. M. Álvarez, "State-of-the-art in downstream processing of monoclonal antibodies: Process trends in design and validation," *Biotechnol. Prog.*, vol. 28, no. 4, pp. 899–916, Jul. 2012.
- [44] E. A. Blackstone and J. P. Fuhr, "The economics of biosimilars," *Am. Heal. Drug Benefits*, vol. 6, no. 8, pp. 469–477, 2013.

- [45] E. P. Armstrong, M. Bakall, G. H. Skrepnek, and L. V. Boyer, "Is scorpion antivenom cost-effective as marketed in the United States?," *Toxicon*, vol. 76, pp. 394–398, Dec. 2013.
- [46] J.-P. Chippaux, M. H. Akaffou, B. K. Allali, M. Dosso, A. Massougbodji, and B. Barraviera, "The 6th international conference on envenomation by Snakebites and Scorpion Stings in Africa: a crucial step for the management of envenomation," *J. Venom. Anim. Toxins Incl. Trop. Dis.*, vol. 22, no. 1, p. 11, Dec. 2016.
- [47] F. Abroug, S. ElAtrous, S. Nouria, H. Haguiga, N. Touzi, and S. Bouchoucha, "Serotherapy in scorpion envenomation: a randomised controlled trial," *Lancet*, vol. 354, no. 9182, pp. 906–909, Sep. 1999.
- [48] V. A. Prieto Ramos, "Panorama de la intoxicación por picadura de alacrán en la Jurisdicción Sanitaria número 3, Zitacuaro Michoacán," *Rev. Especializada en Ciencias la Salud*, vol. 7, no. 1, pp. 16–22, 2004.
- [49] C. A. M. De Davila, M. Parra, A. Fuenmayor, N. Salgar, Z. Gonzalez, and D. F. Davila, "Scorpion envenomation in Merida, Venezuela," *Toxicon*, vol. 35, no. 9, pp. 1459–1462, Sep. 1997.
- [50] A. Laustsen, M. Solà, E. Jappe, S. Oscoz, L. Lauridsen, and M. Engmark, "Biotechnological Trends in Spider and Scorpion Antivenom Development," *Toxins (Basel)*, vol. 8, no. 8, p. 226, Jul. 2016.
- [51] S. Sofer, E. Shahak, and M. Gueron, "Scorpion envenomation and antivenom therapy," *J. Pediatr.*, vol. 124, no. 6, pp. 973–978, Jun. 1994.
- [52] H. S. Bawaskar and P. H. Bawaskar, "Scorpion sting: a review of 121 cases," *J. Wilderness Med.*, vol. 2, no. 3, pp. 164–174, Aug. 1991.
- [53] Instituto Bioclon, "Highlights for prescribing information: ANASCORP," 2017. [Online]. Available: http://www.anascorp-us.com/resources/Package_Insert.pdf. [Accessed: 18-Jun-2019].
- [54] Instituto Bioclón, "Faboterapia." UNAM, Mexico City, p. 16, 2014.
- [55] N. . Rezende, C. F. . Amaral, and L. Freire-Maia, "Immunotherapy for scorpion envenoming in Brazil," *Toxicon*, vol. 36, no. 11, pp. 1507–1513, Nov. 1998.
- [56] S. R. Q. Sperb, "Soro antiescorpiônico - Modelo de Bula." Instituto Butantan, Sao Paulo, Brazil, p. 7, 2017.
- [57] H. Scannone, "Suero antiescorpiónico." Universidad Central de Venezuela, Caracas, Venezuela.
- [58] F. Chgoury *et al.*, "Effectiveness of the Androctonus Australis Hector Nanobody Nbf12-10 Antivenom to Neutralize Significantly the Toxic Effect and Tissue Damage Provoked by Fraction of Androctonus mauretanicus (Morocco) Scorpion Venom," *Biochem. Pharmacol. Open Access*, vol. 04, no. 03, pp. 4–11, 2015.
- [59] G. Hassanzadeh-Ghassabeh, N. Devoogdt, P. De Pauw, C. Vincke, and S. Muyldermans, "Nanobodies and their potential applications," *Nanomedicine*, vol. 8, no. 6, pp. 1013–1026, 2013.
- [60] S. K. Gupta and P. Shukla, "Microbial platform technology for recombinant antibody fragment production: A review," *Crit. Rev. Microbiol.*, vol. 43, no. 1, pp. 31–42, Jan. 2017.
- [61] L. Jank, C. Pinto-Espinoza, Y. Duan, F. Koch-Nolte, T. Magnus, and B. Rissiek, "Current Approaches and Future Perspectives for Nanobodies in Stroke Diagnostic and Therapy," *Antibodies*, vol. 8, no. 1, p. 5, Jan. 2019.
- [62] J. Helma, M. C. Cardoso, S. Muyldermans, and H. Leonhardt, "Nanobodies and recombinant binders in cell biology," *J. Cell Biol.*, vol. 209, no. 5, pp. 633–644, Jun. 2015.
- [63] S. Muyldermans, "Nanobodies: Natural Single-Domain Antibodies," *Annu. Rev. Biochem.*, vol. 82, no. 1, pp. 775–797, Jun. 2013.
- [64] L. Alvarenga *et al.*, "Engineering Venom's Toxin-Neutralizing Antibody Fragments and Its Therapeutic Potential," *Toxins (Basel)*, vol. 6, no. 8, pp. 2541–2567, Aug. 2014.
- [65] D. M. Candido and S. Lucas, "Maintenance of scorpions of the genus Tityus Koch (Scorpiones, Buthidae) for venom obtention at Instituto Butantan, São Paulo, Brazil," *J. Venom. Anim.*

- Toxins Incl. Trop. Dis.*, vol. 10, no. 1, pp. 86–97, 2004.
- [66] S. Tobassum, H. M. Tahir, M. T. Zahid, Q. A. Gardner, and M. M. Ahsan, “Effect of Milking Method, Diet, and Temperature on Venom Production in Scorpions,” *J. Insect Sci.*, vol. 18, no. 4, pp. 1–7, Jul. 2018.
- [67] O. Ozkan, S. Adigüzel, C. Ates, I. Bozyigit, and A. Filazi, “Optimization of antiscorpion venom production,” *J. Venom. Anim. Toxins Incl. Trop. Dis.*, vol. 12, no. 3, pp. 390–399, 2006.
- [68] C. M. Nuebling and D. J. Williams, “Guidelines for the production, control and regulation of snake antivenom immunoglobulins,” 2016.
- [69] J.-P. Chippaux and M. Goyffon, “Venoms, antivenoms and immunotherapy,” *Toxicon*, vol. 36, no. 6, pp. 823–846, Jun. 1998.
- [70] M. Kuhlmann and A. Covic, “The protein science of biosimilars,” *Nephrol. Dial. Transplant.*, vol. 21, no. Supplement 5, pp. v4–v8, Oct. 2006.
- [71] E. Pardon *et al.*, “A general protocol for the generation of Nanobodies for structural biology,” *Nat. Protoc.*, vol. 9, no. 3, pp. 674–93, Mar. 2014.
- [72] L. Yee and H. W. Blanch, “Recombinant protein expression in high cell density fed-batch cultures of *Escherichia coli*,” *Biotechnology. (N. Y.)*, vol. 10, no. 12, pp. 1550–6, Dec. 1992.
- [73] M. Arbabi-Ghahroudi, J. Tanha, and R. MacKenzie, “Prokaryotic expression of antibodies,” *Cancer Metastasis Rev.*, vol. 24, no. 4, pp. 501–519, Dec. 2005.
- [74] T. De Meyer, S. Muyltermans, and A. Depicker, “Nanobody-based products as research and diagnostic tools,” *Trends Biotechnol.*, vol. 32, no. 5, pp. 263–270, 2014.
- [75] C.-J. Huang, H. Lin, and X. Yang, “Industrial production of recombinant therapeutics in *Escherichia coli* and its recent advancements,” *J. Ind. Microbiol. Biotechnol.*, vol. 39, no. 3, pp. 383–399, Mar. 2012.
- [76] B. V. Ayyar, S. Arora, and S. S. Ravi, “Optimizing antibody expression: The nuts and bolts,” *Methods*, vol. 116, pp. 51–62, Mar. 2017.
- [77] K. Graumann and A. Premstaller, “Manufacturing of recombinant therapeutic proteins in microbial systems,” *Biotechnol. J.*, vol. 1, no. 2, pp. 164–186, Feb. 2006.
- [78] S. K. Gupta and P. Shukla, “Sophisticated Cloning, Fermentation, and Purification Technologies for an Enhanced Therapeutic Protein Production: A Review,” *Front. Pharmacol.*, vol. 8, no. Jul, pp. 1–17, Jul. 2017.
- [79] T. W. Overton, “Recombinant protein production in bacterial hosts,” *Drug Discov. Today*, vol. 19, no. 5, pp. 590–601, May 2014.
- [80] M. A. Blight, C. Chervaux, and I. B. Holland, “Protein secretion pathway in *Escherichia coli*,” *Curr. Opin. Biotechnol.*, vol. 5, no. 5, pp. 468–74, Oct. 1994.
- [81] F. J. M. Mergulhão, D. K. Summers, and G. A. Monteiro, “Recombinant protein secretion in *Escherichia coli*,” *Biotechnol. Adv.*, vol. 23, no. 3, pp. 177–202, May 2005.
- [82] S. S. J. Leong and W. N. Chen, “Preparing recombinant single chain antibodies,” *Chem. Eng. Sci.*, vol. 63, no. 6, pp. 1401–1414, Mar. 2008.
- [83] F. Baneyx and M. Mujacic, “Recombinant protein folding and misfolding in *Escherichia coli*,” *Nat. Biotechnol.*, vol. 22, no. 11, pp. 1399–1408, 2004.
- [84] A. Skerra and A. Pluckthun, “Assembly of a functional immunoglobulin Fv fragment in *Escherichia coli*,” *Science (80-.)*, vol. 240, no. 4855, pp. 1038–1041, May 1988.
- [85] R. S. Donovan, C. W. Robinson, and B. R. Glick, “Review: Optimizing inducer and culture conditions for expression of foreign proteins under the control of the lac promoter,” *J. Ind. Microbiol.*, vol. 16, no. 3, pp. 145–154, Mar. 1996.
- [86] R. J. Carvalho, J. Cabrera-Crespo, M. M. Tanizaki, and V. M. Gonçalves, “Development of production and purification processes of recombinant fragment of pneumococcal surface protein A in *Escherichia coli* using different carbon sources and chromatography sequences,” *Appl. Microbiol. Biotechnol.*, vol. 94, no. 3, pp. 683–694, 2012.
- [87] B. J. Hoffman, J. A. Broadwater, P. Johnson, J. Harper, B. G. Fox, and W. R. Kenealy, “Lactose fed-batch overexpression of recombinant metalloproteins in *Escherichia coli* BL21(DE3):

- Process control yielding high levels of metal-incorporated, soluble protein," *Protein Expression and Purification*, vol. 6, no. 5, pp. 646–654, 1995.
- [88] A. C. L. Horta *et al.*, "On-line monitoring of biomass concentration based on a capacitance sensor: Assessing the methodology for different bacteria and yeast high cell density fed-batch cultures," *Brazilian J. Chem. Eng.*, vol. 32, no. 4, pp. 821–829, 2015.
- [89] B. V. Kilikian, I. D. Suárez, C. W. Liria, and A. K. Gombert, "Process strategies to improve heterologous protein production in *Escherichia coli* under lactose or IPTG induction," *Process Biochem.*, vol. 35, no. 9, pp. 1019–1025, 2000.
- [90] G. L. Rosano and E. A. Ceccarelli, "Recombinant protein expression in *Escherichia coli*: Advances and challenges," *Front. Microbiol.*, vol. 5, no. APR, pp. 1–17, Apr. 2014.
- [91] M. Nadri, I. Trezzani, H. Hammouri, P. Dhurjati, R. Longin, and J. Lieto, "Modeling and observer design for recombinant *Escherichia coli* strain," *Bioprocess Biosyst. Eng.*, vol. 28, no. 4, pp. 217–225, 2006.
- [92] M. P. DeLisa, J. Li, G. Rao, W. a Weigand, and W. E. Bentley, "Monitoring GFP-operon fusion protein expression during high cell density cultivation of *Escherichia coli* using an on-line optical sensor.," *Biotechnol. Bioeng.*, vol. 65, pp. 54–64, 1999.
- [93] A. Cockshott and I. Bogle, "Modelling the effects of glucose feeding on a recombinant *E-coli* fermentation," *Bioprocess Eng.*, vol. 20, pp. 83–90, 1999.
- [94] G. Korte, U. Rinas, H.-A. Kracke-Helm, and K. Schügerl, "Structured model for cell growth and enzyme production by recombinant *Escherichia coli*," *Appl. Microbiol. Biotechnol.*, vol. 35, no. 2, pp. 185-188., May 1991.
- [95] X. Hua *et al.*, "Kinetics of High Cell Density Fed-batch Culture of Recombinant *Escherichia coli* Producing Human-like Collagen," *Chinese J. Chem. Eng.*, vol. 14, no. 2, pp. 242–247, Apr. 2006.
- [96] J. Boldrini-França *et al.*, "Expression of a new serine protease from *Crotalus durissus collilineatus* venom in *Pichia pastoris* and functional comparison with the native enzyme," *Appl. Microbiol. Biotechnol.*, vol. 99, no. 23, pp. 9971–9986, 2015.
- [97] A. O. O'Reilly, A. R. Cole, J. L. S. Lopes, A. Lampert, and B. A. Wallace, "Chaperone-mediated native folding of a β -scorpion toxin in the periplasm of *Escherichia coli*," *Biochim. Biophys. Acta - Gen. Subj.*, vol. 1840, no. 1, pp. 10–15, 2014.
- [98] O. H. P. Ramos, A. K. Carmona, and H. S. Selistre-de-Araujo, "Expression, refolding, and in vitro activation of a recombinant snake venom pro-metalloprotease," *Protein Expr. Purif.*, vol. 28, no. 1, pp. 34–41, 2003.
- [99] A. M. Morgon *et al.*, "Expression and immunological cross-reactivity of LALP3, a novel astacin-like metalloprotease from brown spider (*Loxosceles intermedia*) venom," *Biochimie*, vol. 128–129, pp. 8–19, 2016.
- [100] Z. Le, X. Li, P. Yuan, P. Liu, and C. Huang, "Orthogonal optimization of prokaryotic expression of a natural snake venom phospholipase A2 inhibitor from *Sinonatrix annularis*," *Toxicon*, vol. 108, pp. 264–271, 2015.
- [101] B. Selisko, G. Cosío, C. García, B. Becerril, L. D. Possani, and E. Horjales, "Bacterial expression, purification and functional characterization of a recombinant chimeric Fab derived from murine mAb BCF2 that neutralizes the venom of the scorpion *Centruroides noxius hoffmanni*," *Toxicon*, vol. 43, no. 1, pp. 43–51, 2004.
- [102] T. M. Johnson, M. W. Quick, T. T. Sakai, and N. R. Krishna, "Expression of functional recombinant scorpion beta-neurotoxin C_{ss} II in *E. coli*," *Peptides*, vol. 21, no. 6, pp. 767–72, 2000.
- [103] J. H. Shao *et al.*, "Cloning, expression, and pharmacological activity of BmK AS, an active peptide from scorpion *Buthus martensii* Karsch," *Biotechnol. Lett.*, vol. 30, no. 1, pp. 23–29, 2008.
- [104] Y. F. Liu *et al.*, "Expression of an antitumor-analgesic peptide from the venom of Chinese scorpion *Buthus martensii* karsch in *Escherichia coli*," *Protein Expr. Purif.*, vol. 27, no. 2, pp.

- 253–258, 2003.
- [105] M. Turkov *et al.*, “In vitro folding and functional analysis of an anti-insect selective scorpion depressant neurotoxin produced in *Escherichia coli*,” *Protein Expr. Purif.*, vol. 10, no. 1, pp. 123–131, 1997.
- [106] P. Cao *et al.*, “Expression and purification of an antitumor-analgesic peptide from the venom of *Mesobuthus martensii* Karsch by small ubiquitin-related modifier fusion in *Escherichia coli*,” *Biotechnol. Prog.*, vol. 26, no. 5, pp. 1240–1244, 2010.
- [107] T. Han *et al.*, “A novel expression vector for the improved solubility of recombinant scorpion venom in *Escherichia coli*,” *Biochem. Biophys. Res. Commun.*, vol. 482, no. 1, pp. 120–125, 2017.
- [108] P. G. Roberto *et al.*, “Cloning and expression of an acidic platelet aggregation inhibitor phospholipase A2 cDNA from *Bothrops jararacussu* venom gland,” *Protein Expr. Purif.*, vol. 37, no. 1, pp. 102–108, 2004.
- [109] R. J. Ward, A. H. C. De Oliveira, R. K. Bortoleto, J. C. Rosa, V. M. Faça, and L. J. Greene, “Refolding and purification of bothropstoxin-I, a Lys49-phospholipase A2 homologue, expressed as inclusion bodies in *Escherichia coli*,” *Protein Expr. Purif.*, vol. 21, no. 1, pp. 134–140, 2001.
- [110] S. Banerjee, E. V. Curto, M. Beckman, G. B. Brown, J. Zhong, and N. R. Krishna, “Expression of functional scorpion neurotoxin Lqq-V in *E. coli*,” *Peptides*, vol. 27, no. 1, pp. 49–54, 2006.
- [111] A. L. Tscheliessnig, J. Konrath, R. Bates, and A. Jungbauer, “Host cell protein analysis in therapeutic protein bioprocessing - methods and applications,” *Biotechnol. J.*, vol. 8, no. 6, pp. 655–670, Jun. 2013.
- [112] S. Hamilton, J. Odili, M. D. Pacifico, G. D. Wilson, and J. M. Kupsch, “Effect of imidazole on the solubility of a his-tagged antibody fragment,” *Hybrid. Hybridomics*, vol. 22, no. 6, pp. 347–355, 2003.
- [113] J. E. Cantu-Bustos *et al.*, “Expression and purification of recombinant proteins in *Escherichia coli* tagged with the metal-binding protein CusF,” *Protein Expr. Purif.*, vol. 121, pp. 61–65, 2016.
- [114] C. Legros *et al.*, “Use of fusion protein constructs to generate potent immunotherapy and protection against scorpion toxins,” *Vaccine*, vol. 20, no. 5–6, pp. 934–942, Dec. 2001.
- [115] T. Dudler *et al.*, “High-level expression in *Escherichia coli* and rapid purification of enzymatically active honey bee venom phospholipase A2,” *Biochim. Biophys. Acta*, vol. 1165, no. 2, pp. 201–210, 1992.
- [116] K. Tokugawa, T. Ishii, K. Nakamura, H. Masaki, and T. Uozumi, “A model system for the continuous production of a heterologous protein using a novel secretion promoting factor which operates in *Escherichia coli*,” *J. Biotechnol.*, vol. 37, no. 1, pp. 33–37, Sep. 1994.
- [117] S. Kischnick *et al.*, “Bacterial fermentation of recombinant major wasp allergen Antigen 5 using oxygen limiting growth conditions improves yield and quality of inclusion bodies,” *Protein Expr. Purif.*, vol. 47, no. 2, pp. 621–628, 2006.
- [118] M. A. Palaiomylitou, K. A. Matis, A. I. Zouboulis, and D. A. Kyriakidis, “A kinetic model describing cell growth and production of highly active, recombinant ice nucleation protein in *Escherichia coli*,” *Biotechnol. Bioeng.*, vol. 78, no. 3, pp. 321–332, 2002.
- [119] Y. P. Khasa, A. Khushoo, and K. J. Mukherjee, “Enhancing toxic protein expression in *Escherichia coli* fed-batch culture using kinetic parameters: Human granulocyte-macrophage colony-stimulating factor as a model system,” *J. Biosci. Bioeng.*, vol. 115, no. 3, pp. 291–297, 2013.
- [120] K. E. Conrath *et al.*, “Beta-lactamase inhibitors derived from single-domain antibody fragments elicited in the camelidae,” *Antimicrob. Agents Chemother.*, vol. 45, no. 10, pp. 2807–12, Oct. 2001.
- [121] M. Darvish, M. Behdani, M. A. Shokrgozar, K. Pooshang-Bagheri, and D. Shahbazzadeh, “Development of protective agent against *Hottentotta saulcyi* venom using camelid single-

- domain antibody," *Mol. Immunol.*, vol. 68, no. 2, pp. 412–420, 2015.
- [122] C. Legros, E. Feyfant, F. Sampieri, H. Rochat, P. E. Bougis, and M. F. Martin-Eauclaire, "Influence of a NH₂-terminal extension on the activity of KTX2, a K⁺ channel blocker purified from *Androctonus australis* scorpion venom," *FEBS Lett.*, vol. 417, no. 1, pp. 123–129, 1997.
- [123] N. Aubrey, C. Devaux, P. Y. Sizaret, H. Rochat, M. Goyffon, and P. Billiald, "Design and evaluation of a diabody to improve protection against a potent scorpion neurotoxin," *Cell. Mol. Life Sci.*, vol. 60, no. 3, pp. 617–628, 2003.
- [124] C. Devaux, E. Moreau, M. Goyffon, H. Rochat, and P. Billiald, "Construction and functional evaluation of a single-chain antibody fragment that neutralizes toxin Aahl from the venom of the scorpion *Androctonus australis* hector," *Eur. J. Biochem.*, vol. 268, no. 3, pp. 694–702, 2001.
- [125] P. Billiald, G. Motta, and D. J. Vaux, "Production of a functional anti-scorpion hemocyanin scFv in *Escherichia coli*," *Arch. Biochem. Biophys.*, vol. 317, no. 2, pp. 429–438, 1995.
- [126] S. Vemula, R. Thunuguntla, A. Dedaniya, S. Kokkiligadda, C. Palle, and S. R. Ronda, "Improved production and characterization of recombinant human granulocyte colony stimulating factor from *E. coli* under optimized downstream processes," *Protein Expr. Purif.*, vol. 108, pp. 62–72, 2015.
- [127] G. Ravi, K. Ella, and M. Lakshmi Narasu, "Development of pilot scale production process and characterization of a recombinant multiepitope malarial vaccine candidate FALVAC-1A expressed in *Escherichia coli*," *Protein Expr. Purif.*, vol. 61, no. 1, pp. 57–64, 2008.
- [128] C.-K. Kim, J.-H. Choi, S.-B. Lee, S.-M. Lee, and J.-W. Oh, "Expression and Purification of Recombinant Human Granulocyte Colony-Stimulating Factor in Fed-Batch Culture of *Escherichia coli*," *Appl. Biochem. Biotechnol.*, vol. 172, no. 5, pp. 2425–2435, 2014.
- [129] E. Toksoy Öner, B. Kirdar, Z. I. Önsan, and K. Ö. Ülgen, "Modeling of the induced expression for high-level production of a foreign protein by recombinant *E. coli* under the control of the T7 phage promoter," *Process Biochem.*, vol. 39, no. 3, pp. 315–323, 2003.
- [130] N. Nancib, R. Mosrati, and J. Boudrant, "Modelling of batch fermentation of a recombinant *Escherichia coli* producing glyceraldehyde-3-phosphate dehydrogenase on a complex selective medium," *Chem. Eng. J.*, vol. 52, no. 2, 1993.
- [131] F. Miao and D. S. Kompala, "Overexpression of cloned genes using recombinant *Escherichia coli* regulated by a T7 promoter: I. Batch cultures and kinetic modeling," *Biotechnol. Bioeng.*, vol. 40, no. 7, pp. 787–796, 1992.
- [132] F. Miao and D. S. Kompala, "Overexpression of cloned genes using recombinant *Escherichia coli* regulated by a t7 promoter .2. 2-Stage continuous cultures and model simulations," *Biotechnol. Bioeng.*, vol. 42 (1), pp. 74–80, 1993.
- [133] D. M., C. H., W. W., V. J., R. G., and B. W., "Generic model control of induced protein expression in high cell density cultivation of *Escherichia coli* using on-line GFP-fusion monitoring," *Bioprocess Biosyst. Eng.*, vol. 24, no. 2, pp. 83–91, 2001.
- [134] M. Kangwa, V. Yelemene, A. N. Polat, K. D. D. Gorrepati, M. Grasselli, and M. Fernández-Lahore, "High-level fed-batch fermentative expression of an engineered *Staphylococcal* protein A based ligand in *E. coli*: purification and characterization," *AMB Express*, vol. 5, no. 1, p. 70, Dec. 2015.
- [135] A. Schmideder, J. H. Cremer, and D. Weuster-Botz, "Parallel steady state studies on a milliliter scale accelerate fed-batch bioprocess design for recombinant protein production with *Escherichia coli*," *Biotechnol. Prog.*, vol. 32, no. 6, pp. 1426–1435, 2016.
- [136] D. Levisauskas, V. Galvanauskas, S. Henrich, K. Wilhelm, N. Volk, and A. Lübbert, "Model-based optimization of viral capsid protein production in fed-batch culture of recombinant *Escherichia coli*," *Bioprocess Biosyst. Eng.*, vol. 25, no. 4, pp. 255–262, 2003.
- [137] K.-M. Lee, C.-H. Rhee, C.-K. Kang, and J.-H. Kim, "Statistical medium formulation and process modeling by mixture design of experiment for peptide overexpression in recombinant *Escherichia coli*," *Appl. Biochem. Biotechnol.*, vol. 135, no. 1, pp. 81–110, Oct. 2006.

- [138] E. Franco-Lara, V. Galvanauskas, N. Volk, and A. Lübbert, "Model-Based Optimization of the Cultivation Process for Recombinant Virus Capsid Proteins in *E. coli*," *IFAC Proc. Vol.*, vol. 34, no. 5, pp. 299–303, 2001.
- [139] L. F. Vallejo *et al.*, "Renaturation and purification of bone morphogenetic protein-2 produced as inclusion bodies in high-cell-density cultures of recombinant *Escherichia coli*," *J. Biotechnol.*, vol. 94, no. 2, pp. 185–194, 2002.
- [140] X. M. Yang, "Optimization of a cultivation process for recombinant protein production by *Escherichia coli*," *J. Biotechnol.*, vol. 23, no. 3, pp. 271–289, 1992.
- [141] C. Sieblist, M. Jenzsch, M. Pohlscheidt, and A. Lübbert, "Insights into large-scale cell-culture reactors: I. Liquid mixing and oxygen supply," *Biotechnol. J.*, vol. 6, no. 12, pp. 1532–1546, 2011.
- [142] M. N. Baeshen *et al.*, "Production of Biopharmaceuticals in *E. coli*: Current Scenario and Future Perspectives," *J. Microbiol. Biotechnol.*, vol. 25, no. 7, pp. 953–962, Jul. 2015.
- [143] A. de Marco, "Recombinant antibody production evolves into multiple options aimed at yielding reagents suitable for application-specific needs," *Microb. Cell Fact.*, vol. 14, no. 1, p. 125, Dec. 2015.
- [144] J. Ruiz *et al.*, "Alternative production process strategies in *E. coli* improving protein quality and downstream yields," *Process Biochem.*, vol. 44, no. 9, pp. 1039–1045, Sep. 2009.
- [145] J. Ruiz, G. González, C. de Mas, and J. López-Santín, "A semiempirical model to control the production of a recombinant aldolase in high cell density cultures of *Escherichia coli*," *Biochem. Eng. J.*, vol. 55, no. 2, pp. 82–91, 2011.
- [146] M. Jenzsch, R. Simutis, and A. Luebbert, "Generic model control of the specific growth rate in recombinant *Escherichia coli* cultivations," *J. Biotechnol.*, vol. 122, no. 4, pp. 483–493, 2006.
- [147] A. C. L. Horta *et al.*, "Intensification of high cell-density cultivations of rE. coli for production of *S. pneumoniae* antigenic surface protein, PspA3, using model-based adaptive control," *Bioprocess Biosyst. Eng.*, vol. 35, no. 8, pp. 1269–1280, 2012.
- [148] D. Calleja, J. Kavanagh, C. de Mas, and J. López-Santín, "Simulation and prediction of protein production in fed-batch *E. coli* cultures: An engineering approach," *Biotechnol. Bioeng.*, vol. 113, no. 4, pp. 772–782, 2016.
- [149] F. Garcia-Ochoa and E. Gomez, "Bioreactor scale-up and oxygen transfer rate in microbial processes: An overview," *Biotechnol. Adv.*, vol. 27, no. 2, pp. 153–176, 2009.
- [150] M. Suntravat, Y. Jia, S. E. Lucena, E. E. Sánchez, and J. C. Pérez, "cDNA cloning of a snake venom metalloproteinase from the eastern diamondback rattlesnake (*Crotalus adamanteus*), and the expression of its disintegrin domain with anti-platelet effects," *Toxicon*, vol. 64, pp. 43–54, 2013.
- [151] T. K. S. Kumar *et al.*, "Cloning, direct expression, and purification of a snake venom cardiotoxin in *Escherichia coli*," *Biochem. Biophys. Res. Commun.*, vol. 219, no. 2, pp. 450–456, 1996.
- [152] K. Sun *et al.*, "Expression, purification and characterization of a novel recombinant SVTLE, r-agkihpin-2, from *Gloydius halys* Pallas venom gland in *Escherichia coli*," *Protein Expr. Purif.*, vol. 136, pp. 7–13, 2017.
- [153] R. Nian, L. Tan, and W. S. Choe, "Polyethyleneimine-mediated chemical extraction of cytoplasmic his-tagged inclusion body proteins from *Escherichia coli*," *Biotechnol. Prog.*, vol. 24, no. 2, pp. 417–425, 2008.
- [154] B. Gao *et al.*, "Expression and secretion of functional recombinant μ O-conotoxin MrVIB-His-tag in *Escherichia coli*," *Toxicon*, vol. 72, pp. 81–89, Sep. 2013.
- [155] B. Bouhaouala-Zahar *et al.*, "A recombinant insect-specific alpha-toxin of *Buthus occitanus tunetanus* scorpion confers protection against homologous mammal Ttoxins," *Eur. J. Biochem.*, vol. 238, no. 3, pp. 653–660, 1996.
- [156] B. Bouhaouala-Zahar *et al.*, "A chimeric scorpion α -toxin displays de novo electrophysiological properties similar to those of α -like toxins," *Eur. J. Biochem.*, vol. 269, no. 12, pp. 2831–2841,

- 2002.
- [157] J. M. Jiménez-Vargas, V. Quintero-Hernández, L. González-Morales, E. Ortiz, and L. D. Possani, "Design and expression of recombinant toxins from Mexican scorpions of the genus *Centruroides* for production of antivenoms," *Toxicon*, vol. 128, pp. 5–14, Mar. 2017.
- [158] S. Z. Pang *et al.*, "Expression of a gene encoding a scorpion insectotoxin peptide in yeast, bacteria and plants," *Gene*, vol. 116, no. 2, pp. 165–172, 1992.
- [159] Y. J. Fu, B. F. Chai, W. Wang, H. Zhi, L. T. Yin, and A. H. Liang, "Expression and purification of the BmK Mm2 neurotoxin from the scorpion *Buthus martensii* Karsch and its biological activity test," *Protein Expr. Purif.*, vol. 38, no. 1, pp. 45–50, 2004.
- [160] G. Hariprasad *et al.*, "Group III PLA2 from the scorpion, *Mesobuthus tamulus*: Cloning and recombinant expression in *E. coli*," *Electron. J. Biotechnol.*, vol. 12, no. 3, 2009.
- [161] M. A. Tekook *et al.*, "Gene construction, expression and functional testing of an inotropic peptide from the venom of the black scorpion *Hottentotta judaicus*," *Toxicon*, vol. 60, no. 8, pp. 1415–1427, 2012.
- [162] F. Olvera *et al.*, "An efficient approach to clone and express active Neopladine 2, an anticancer peptide from *Tityus discrepans* scorpion venom," *Process Biochem.*, vol. 51, no. 5, pp. 624–631, 2016.
- [163] I. Hmila *et al.*, "VHH, bivalent domains and chimeric Heavy chain-only antibodies with high neutralizing efficacy for scorpion toxin Aahl'," *Mol. Immunol.*, vol. 45, no. 14, pp. 3847–3856, Aug. 2008.
- [164] H. Kraïem *et al.*, "Expression of the recombinant NbF12-10 and its chimeric antibody format in *Escherichia Coli*: investigation of fed-batch bioprocess on minimal media," in *Second Mediterranean Congress on Biotechnology*, 2019.
- [165] H. Kraïem, "Développement de méthodes de contrôle-qualité pour deux facteurs de croissance et un fragment d'anticorps: «Mise au point et optimisation de tests immuno-biochimiques et fonctionnelles in vivo et in vitro»,» Institut Pasteur de Tunis, Unimed Laboratories, Institut National de Sciences Appliquées et de Technologie, 2018.
- [166] K. D. Tartof and C. A. Hobbs, "Improved Media for Growing Plasmid and Cosmid Clones," *Bethesda Res. Lab. Focus*, vol. 9, no. 12, 1987.
- [167] Y. Manon, "Etude de milieux de culture complexes et évolutifs par développement de mesures physiques en ligne," Institut National des Sciences Appliquées, 2012.
- [168] R. C. Weast, *Handbook of Chemistry & Physics*, 57th ed. CRC Press, 1977.
- [169] H. C. Neu and L. A. Heppel, "The release of enzymes from *Escherichia coli* by osmotic shock and during the formation of spheroplasts.," *J. Biol. Chem.*, vol. 240, no. 9, pp. 3685–92, Sep. 1965.
- [170] J. A. Bornhorst and J. J. Falke, "Purification of proteins using polyhistidine affinity tags.," *Methods Enzymol.*, vol. 326, no. 18, pp. 245–54, 2000.
- [171] M. M. Bradford, "A rapid and sensitive method for the quantitation of microgram quantities of protein utilizing the principle of protein-dye binding," *Anal. Biochem.*, vol. 72, no. 1–2, pp. 248–254, May 1976.
- [172] S. M. Alonso Villela, H. Kraïem, B. Bouhaouala-Zahar, C. Bideaux, C. A. Aceves Lara, and L. Fillaudeau, "A protocol for recombinant protein quantification by densitometry," *Microbiologyopen*, no. in press, 2020.
- [173] R. Sander, "Compilation of Henry's law constants (version 4.0) for water as solvent," *Atmos. Chem. Phys.*, vol. 15, no. 8, pp. 4399–4981, 2015.
- [174] A. Savitzky and M. J. E. Golay, "Smoothing and Differentiation of Data by Simplified Least Squares Procedures.," *Anal. Chem.*, vol. 36, no. 8, pp. 1627–1639, Jul. 1964.
- [175] F. Garcia-Ochoa, E. Gomez, V. E. Santos, and J. C. Merchuk, "Oxygen uptake rate in microbial processes: An overview," *Biochem. Eng. J.*, vol. 49, no. 3, pp. 289–307, 2010.
- [176] F. Garcia-Ochoa and E. Gomez, "Prediction of gas-liquid mass transfer coefficient in sparged stirred tank bioreactors," *Biotechnol. Bioeng.*, vol. 92, no. 6, pp. 761–772, Dec. 2005.

- [177] A. Donoso-Bravo, J. Mailier, C. Martin, J. Rodríguez, C. A. Aceves-Lara, and A. Vande Wouwer, "Model selection, identification and validation in anaerobic digestion: A review," *Water Res.*, vol. 45, no. 17, pp. 5347–5364, Nov. 2011.
- [178] D. Summers, "The kinetics of plasmid loss," *Trends Biotechnol.*, vol. 9, no. 1, pp. 273–278, Jan. 1991.
- [179] A. Bin Ariff, R. Nelofer, R. N. Z. R. A. Rahman, and M. Basri, "Kinetics and modelling of batch fermentation for the production of organic solvent tolerant and thermostable lipase by recombinant *E. coli*," *Turkish J. Biochem.*, vol. 40, no. 4, pp. 298–309, 2015.
- [180] E. Theodosiou, O. Frick, B. Bühler, and A. Schmid, "Metabolic network capacity of *Escherichia coli* for Krebs cycle-dependent proline hydroxylation," *Microb. Cell Fact.*, vol. 14, no. 1, p. 108, 2015.
- [181] J.-L. Uribelarrea, "Travaux pratiques de Fermentation," Toulouse, France.
- [182] L. Yee and H. W. Blanch, "Recombinant trypsin production in high cell density fed-batch cultures in *Escherichia coli*," *Biotechnol. Bioeng.*, vol. 41, no. 8, pp. 781–790, Apr. 1993.
- [183] P. Kumar and A. Libchaber, "Pressure and temperature dependence of growth and morphology of *Escherichia coli*: experiments and stochastic model," *Biophys. J.*, vol. 105, no. 3, pp. 783–793, 2013.
- [184] T. L. Philichi and M. K. Stenstrom, "Effects of dissolved oxygen lag on oxygen transfer estimation probe parameter," *Water Environ. Fed.*, vol. 61, no. 1, pp. 83–86, 2009.
- [185] J. Koizumi and S. Aiba, "Reassessment of the Dynamic k_La Method," *Biotechnol. Bioeng.*, vol. 26, pp. 1131–1133, 1984.
- [186] J. C. Merchuk, S. Yona, M. H. Siegel, and A. Ben Zvi, "On the first-order approximation to the response of dissolved oxygen electrodes for dynamic k_La estimation," *Biotechnol. Bioeng.*, vol. 35, no. 11, pp. 1161–1163, May 1990.
- [187] L. A. Tribe, C. L. Briens, and A. Margaritis, "Determination of the volumetric mass transfer coefficient ($k(L)a$) using the dynamic 'gas out-gas in' method: Analysis of errors caused by dissolved oxygen probes.," *Biotechnol. Bioeng.*, vol. 46, no. 4, pp. 388–392, 1995.
- [188] P. Juárez and J. Orejas, "Oxygen transfer in a stirred reactor in laboratory scale," *Lat. Am. Appl. Res.*, vol. 31, no. 5, pp. 433–439, 2001.
- [189] S. Suresh, V. C. Srivastava, and I. M. Mishra, "Techniques for oxygen transfer measurement in bioreactors: A review," *J. Chem. Technol. Biotechnol.*, vol. 84, no. 8, pp. 1091–1103, 2009.
- [190] J. Kane, "Measuring k_La for Better Bioreactor Performance," *BioProcess International*, no. 10(3), pp. 46–49, 2012.
- [191] J. J. Orgill, H. K. Atiyeh, M. Devarapalli, J. R. Phillips, R. S. Lewis, and R. L. Huhnke, "A comparison of mass transfer coefficients between trickle-bed, hollow fiber membrane and stirred tank reactors," *Bioresour. Technol.*, vol. 133, pp. 340–346, 2013.
- [192] T. Moucha, F. J. Rejl, M. Kordač, and L. Labík, "Mass transfer characteristics of multiple-impeller fermenters for their design and scale-up," *Biochem. Eng. J.*, vol. 69, pp. 17–27, 2012.
- [193] S. M. Alonso Villela, "Oxygen transfer limitation in bioreactor," Toulouse, France, 2016.
- [194] M. Urrea Navarro, "YARROWIA LIPOLOTYCA CULTIVATION IN BIOREACTOR : INVESTIGATION OF BIOREACTOR PERFORMANCES (TRANSFER LIMITATIONS) AND STUDY OF MYCELIAL TRANSITION INDUCED BY pH," 2013.
- [195] K. Van't Riet, "Review of Measuring Methods and Results in Nonviscous Gas-Liquid Mass Transfer in Stirred Vessels," *Ind. Eng. Chem. Process Des. Dev.*, vol. 18, no. 3, pp. 357–364, Jul. 1979.
- [196] C. M. Cooper, G. A. Fernstrom, and S. A. Miller, "Performance of Agitated Gas-Liquid Contactors," *Ind. Eng. Chem.*, vol. 36, no. 6, pp. 504–509, Jun. 1944.
- [197] F. Scargiali, A. Busciglio, F. Grisafi, and A. Brucato, "Simplified dynamic pressure method for k_La measurement in aerated bioreactors," *Biochem. Eng. J.*, vol. 49, no. 2, pp. 165–172, 2010.
- [198] A. C. Badino, M. C. R. Facciotti, and W. Schmidell, "Volumetric oxygen transfer coefficients

- (kLa) in batch cultivations involving non-Newtonian broths," *Biochem. Eng. J.*, vol. 8, no. 2, pp. 111–119, 2001.
- [199] M. M. Buffo, L. J. Corrêa, M. N. Esperança, A. J. G. Cruz, C. S. Farinas, and A. C. Badino, "Influence of dual-impeller type and configuration on oxygen transfer, power consumption, and shear rate in a stirred tank bioreactor," *Biochem. Eng. J.*, vol. 114, pp. 130–139, 2016.
- [200] T. Moucha, V. Linek, and E. Prokopová, "Gas hold-up, mixing time and gas-liquid volumetric mass transfer coefficient of various multiple-impeller configurations: Rushton turbine, pitched blade and techmix impeller and their combinations," *Chem. Eng. Sci.*, vol. 58, no. 9, pp. 1839–1846, 2003.
- [201] M. Nocentini, D. Fajner, G. Pasquali, and F. Magelli, "Gas-liquid mass transfer and holdup in vessels stirred with multiple Rushton turbines: water and water-glycerol solutions," *Ind. Eng. Chem. Res.*, vol. 32, no. 1, pp. 19–26, Jan. 1993.
- [202] M. Fyferling, "Transfert d'oxygène en conditions de culture microbienne intensive," Institut National des sciences Appliquées de Toulouse, 2007.
- [203] J. Cescut, C. Jouve-Molina, and J.-L. Uribelarrea, "Accumulation d'acylglycérols par des espèces levuriennes à usage carburant aéronautique : physiologie et performances de procédés," 2009.
- [204] H. Kraiem, L. Ben Gaïda, Y. Manon, D. Anne-Archard, and L. Fillaudeau, "IMPACT OF CELL PHYSIOLOGY AND DENSITIES DURING OXIDATIVE AXENIC CULTURES OF YARROWIA LIPOLYTICA ON PHYSICO-CHEMICAL PROPERTIES OF BROTH." p. 4, 2011.
- [205] S. Sunya, "Dynamique de la réponse physiologique d'Escherichia coli à des perturbations maîtrisées de son environnement : vers le développement de nouveaux outils de changement d'échelle," INSA Toulouse, 2012.
- [206] G. Goma, R. Moletta, and M. Novak, "Comments on the 'Maintenance coefficient' changes during alcohol fermentation," *Biotechnol. Lett.*, vol. 1, no. 10, pp. 415–420, Oct. 1979.
- [207] P. van Bodegom, "Microbial Maintenance: A Critical Review on Its Quantification," *Microb. Ecol.*, vol. 53, no. 4, pp. 513–523, May 2007.
- [208] S. B. McGrew and M. F. Mallette, "ENERGY OF MAINTENANCE IN ESCHERICHIA COLI.," *J. Bacteriol.*, vol. 83, no. 4, pp. 844–50, Apr. 1962.
- [209] L. Andersson, S. Yang, P. Neubauer, and S. O. Enfors, "Impact of plasmid presence and induction on cellular responses in fed batch cultures of Escherichia coli.," *J. Biotechnol.*, vol. 46, no. 3, pp. 255–63, May 1996.
- [210] M. Kosinski, U. Rinas, and J. Bailey, "Isopropyl-beta-d-thiogalactopyranoside influences the metabolism of Escherichia coli," *Appl. Microbiol. Biotechnol.*, vol. 36, no. 6, pp. 844–50, Mar. 1992.
- [211] S. O. Ramchuran, O. Holst, and E. N. Karlsson, "Effect of postinduction nutrient feed composition and use of lactose as inducer during production of thermostable xylanase in Escherichia coli glucose-limited fed-batch cultivations," *J. Biosci. Bioeng.*, vol. 99, no. 5, pp. 477–484, May 2005.
- [212] V. Romero-Kutzner, T. T. Packard, E. Berdalet, S. O. Roy, J. P. Gagné, and M. Gómez, "Respiration quotient variability: Bacterial evidence," *Mar. Ecol. Prog. Ser.*, vol. 519, no. 2013, pp. 47–59, 2015.
- [213] D. Calleja Martínez, "Modeling bioreactors for the production of recombinant proteins in high-cell density cultures of Escherichia coli," Universitat Autònoma de Barcelona, 2014.
- [214] S. Harcum, "Structured model to predict intracellular amino acid shortages during recombinant protein overexpression in E. coli.," *J. Biotechnol.*, vol. 93, no. 3, pp. 189–202, 2002.
- [215] D. Ehgartner, P. Sagmeister, T. Langemann, A. Meitz, W. Lubitz, and C. Herwig, "A novel method to recover inclusion body protein from recombinant E. coli fed-batch processes based on phage ΦX174-derived lysis protein E," *Appl. Microbiol. Biotechnol.*, vol. 101, no. 14, pp. 5603–5614, 2017.

- [216] M. Boström, K. Markland, A. M. Sandén, M. Hedhammar, S. Hober, and G. Larsson, "Effect of substrate feed rate on recombinant protein secretion, degradation and inclusion body formation in *Escherichia coli*," *Appl. Microbiol. Biotechnol.*, vol. 68, no. 1, pp. 82–90, 2005.
- [217] L. Dela Coletta Troiano Araújo *et al.*, "Process parameters optimization to produce the recombinant protein CFP10 for the diagnosis of tuberculosis," *Protein Expr. Purif.*, vol. 154, no. July 2018, pp. 118–125, 2019.
- [218] P. Malakar and K. V. Venkatesh, "Effect of substrate and IPTG concentrations on the burden to growth of *Escherichia coli* on glycerol due to the expression of Lac proteins," *Appl. Microbiol. Biotechnol.*, vol. 93, no. 6, pp. 2543–2549, 2012.
- [219] A. I. Gragerov, E. S. Martin, M. A. Krupenko, M. V. Kashlev, and V. G. Nikiforov, "Protein aggregation and inclusion body formation in *Escherichia coli* rpoH mutant defective in heat shock protein induction.," *FEBS Lett.*, vol. 291, no. 2, pp. 222–4, Oct. 1991.
- [220] J. Klein and P. Dhurjati, "Protein aggregation kinetics in an *Escherichia coli* strain overexpressing a *Salmonella typhimurium* CheY mutant gene.," *Appl. Environ. Microbiol.*, vol. 61, no. 4, pp. 1220–5, Apr. 1995.
- [221] G. Calloni, S. Zoffoli, M. Stefani, C. M. Dobson, and F. Chiti, "Investigating the Effects of Mutations on Protein Aggregation in the Cell," *J. Biol. Chem.*, vol. 280, no. 11, pp. 10607–10613, Mar. 2005.
- [222] C. Schlieker, B. Bukau, and A. Mogk, "Prevention and reversion of protein aggregation by molecular chaperones in the *E. coli* cytosol: implications for their applicability in biotechnology.," *J. Biotechnol.*, vol. 96, no. 1, pp. 13–21, Jun. 2002.
- [223] R. Ben Abderrazek *et al.*, "Development of Cys38 knock-out and humanized version of NbAahII10 nanobody with improved neutralization of AahII Scorpion toxin," *Protein Eng. Des. Sel.*, vol. 24, no. 9, pp. 727–735, Sep. 2011.
- [224] U. I. Baig, B. J. Bhadbhade, D. Mariyam, and M. G. Watve, "Protein Aggregation in *E. coli*: Short Term and Long Term Effects of Nutrient Density," *PLoS One*, vol. 9, no. 9, p. e107445, Sep. 2014.
- [225] Z. Y. Zheng, S. J. Yao, and D. Q. Lin, "Using a kinetic model that considers cell segregation to optimize hEGF expression in fed-batch cultures of recombinant *Escherichia coli*," *Bioprocess Biosyst. Eng.*, vol. 27, no. 3, pp. 143–152, 2005.
- [226] E. Amillastre, C.-A. Aceves-Lara, J.-L. Uribelarrea, S. Alfenore, and S. E. Guillouet, "Dynamic model of temperature impact on cell viability and major product formation during fed-batch and continuous ethanolic fermentation in *Saccharomyces cerevisiae*," *Bioresour. Technol.*, vol. 117, pp. 242–250, Aug. 2012.
- [227] I. Rocha and E. C. Ferreira, *Model-Based Adaptive Control of Acetate Concentration During the Production of Recombinant Proteins With E. Coli*, vol. 35, no. 1. IFAC, 2002.
- [228] M. J. Betenbaugh and P. Dhurjati, "A comparison of mathematical model predictions to experimental measurements for growth and recombinant protein production in induced cultures of *Escherichia coli*," *Biotechnol. Bioeng.*, vol. 36, no. 2, pp. 124–134, 1990.
- [229] S. M. Alonso Villela, H. Kraïem, B. Bouhaouala-Zahar, C. Bideaux, C. A. Aceves Lara, and L. Fillaudeau, "A protocol for recombinant protein quantification by densitometry," *Microbiologyopen*, p. e1027, Apr. 2020.

APPENDIX 1. EXTENDED ABSTRACT IN FRENCH

Les piqûres de scorpion constituent un grave problème de santé dans les zones tropicales et subtropicales du globe. Le traitement le plus courant des piqûres de scorpion est la sérothérapie, qui utilise des anticorps ou des fragments d'anticorps pour cibler les neurotoxines de 7 kDa présentes dans le venin de scorpion. Les antivenins sont dérivés du plasma équin et sont disponibles en faibles quantités à un prix élevé pour le système de santé en raison de l'indisponibilité du venin de scorpion et du processus de purification coûteux des fragments d'anticorps de 50 kDa ¹.

Récemment, il a été prouvé que les nanocorps (nanobody), des petits fragments d'anticorps de camélidés, neutralisent les toxines de scorpion ^{1,2}. La production de molécules thérapeutiques recombinantes dans *Escherichia coli* est une pratique courante dans l'industrie biopharmaceutique ³. La production périplasmique des nanocorps a été étudiée dans des fioles erlenmeyer induits par l'IPTG synthétique sous le contrôle du promoteur *lac* ⁴. Le rendement rapporté est faible (< 4 mg/L ⁵), et les cultures en bioréacteur et à haute densité cellulaire n'ont pas été étudiées.

Au cours de ce projet de doctorat, les conditions de production de nanocorps bispécifiques ont été étudiées. Les nanocorps CH10-12 et NbF12-10, ayant des effets neutralisants contre les neurotoxines de l'espèce de scorpion *Androctonus australis hector* ont été produits dans des cultures en fioles Erlenmeyer et en bioréacteurs. Les souches recombinantes produisant les nanocorps CH10-12 et NbF12-10 étaient *Escherichia coli* CH10-12 et les clones d'*Escherichia coli* NbF12-10 (NN et NO). Toutes les souches ont été préparées par le Laboratoire des Venins et Molécules Thérapeutiques de l'Institut Pasteur de Tunis (LVMT-IPT, Tunis, Tunisie), et la souche d'*Escherichia coli* WK6 a été utilisée comme référence.

Le criblage des souches dans des cultures en fioles Erlenmeyer agitées a montré l'adaptabilité des souches recombinantes d'*E. coli* à un milieu riche (terrific broth, TB) et à un milieu minimal défini (MM). Parmi les quatre souches testées, seul le clone recombinant NbF12-10 NO n'a pas pu être cultivé dans le milieu minimum. Dans le milieu TB, toutes les souches avaient un taux de croissance spécifique moyen de plus de 0,4 h⁻¹ (Table 1-1). Le taux de croissance spécifique maximal des souches WK6 et CH10-12 cultivées dans le MM était le même (0,6 h⁻¹), mais il était inférieur de 30% pour la souche NbF12-10 NN (0,2 h⁻¹). Dans les cultures en fioles Erlenmeyer agitées en MM, le rendement de la biomasse sur le glucose, $Y_{X/S}$, était de 0,4 g/g pour toutes les souches, tandis que le rendement de l'acide acétique sur le glucose, $Y_{Ac/S}$, était compris entre 0,06 et 0,14 g/g.

Souche	Terrific Broth (TB)			Milieu minimum (MM)		
	DO	Filtre	Eppendorf	DO	Filtre	Eppendorf
<i>E. coli</i> WK6	0.65 ± 0.05	0.64 ± 0.04	0.64 ± 0.05	0.66 ± 0.02	0.66 ± 0.06	0.70 ± 0.08
<i>E. coli</i> CH10-12	0.49 ± 0.01	0.49 ± 0.04	0.41 ± 0.01	0.63 ± 0.02	0.66 ± 0.04	0.61 ± 0.05
<i>E. coli</i> NbF12-10 NN	0.59 ± 0.08	0.52 ± 0.01	0.47 ± 0.01	0.26 ± 0.03	0.15 ± 0.08	0.20 ± 0.16
<i>E. coli</i> NbF12-10 NO	0.44 ± 0.01	0.41 ± 0.05	0.43 ± 0.01	/	/	/

Table 1-1. Taux de croissance moyen en milieu riche (TB) et maximum en milieu minimum (MM)

L'incapacité du clone NbF12-10 NO à se développer dans le MM et le faible taux de croissance spécifique du clone NbF12-10 NN dans le MM pourraient mettre en évidence la détérioration du plasmide pHEN6/NbF12-10 ou une insertion inadéquate dans les cellules compétentes.

La production de nanobodies a été testée dans des souches CH10-12 et NbF12-10 NN cultivées dans TB avec une induction à 28°C pendant 24 h en erlenmeyer. La libération de protéines périplasmiques par la perméation de la membrane extérieure a été optimisée dans des cultures en fioles erlenmeyer. La méthode a amélioré de 300% la libération des protéines périplasmiques dans les deux souches (Figure 1-1). Cette étude montre que la souche CH10-12 a produit 20 fois plus de nanobody que la souche NbF12-10 dans les mêmes conditions d'induction, de température et de choc osmotique (1,58 mg/L contre 0,08 mg/L).

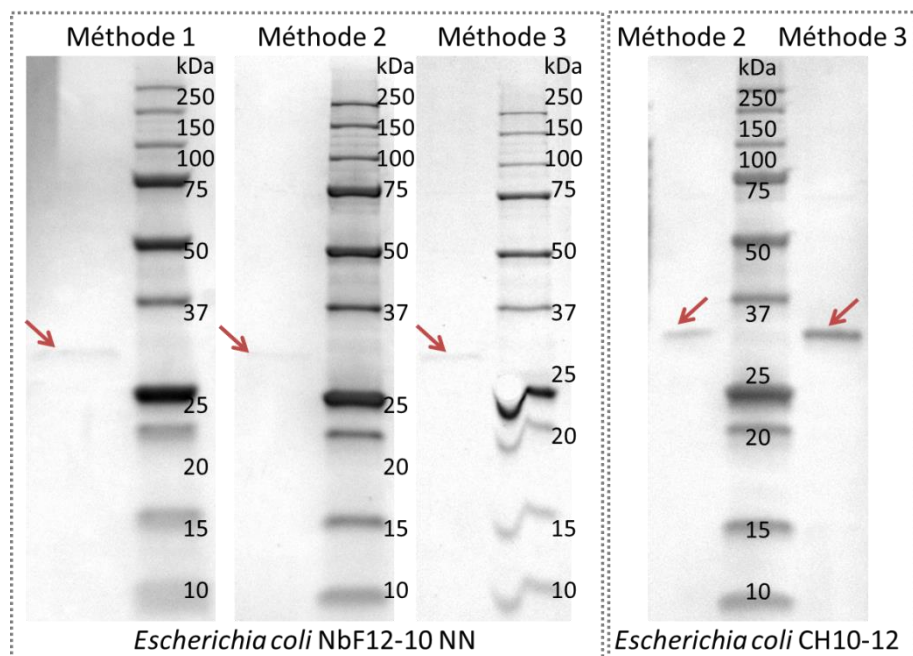


Figure 1-1. Expression du nanobody par différentes méthodes de choc osmotique. Les flèches rouges indiquent les bandes du nanobody NbF12-10 (29 kDa) et CH10-12 (31 kDa) du premier éluat du purification par IMAC en gels d'électrophorèse.

Méthode 1 : incubation en TES (Tris-HCl 200 mM, EDTA 0.5 mM, sucrose 500 mM) pendant 2 h et choc osmotique par addition du TES/4 pendant 2 h ; Méthode 2 : incubation en TES pendant 6 h et choc osmotique par addition du TES/4 pendant 12 h ; Méthode 3 : incubation dans du TES et choc osmotique par addition d'eau distillée froide pendant 2 h. Le marqueur de poids moléculaire utilisé a été le Precision Plus Protein Unstained Protein Standards (Bio-rad, USA).

La taille du microorganisme a été étudiée et il a été démontré qu'elle changeait légèrement lors de l'induction de cultures d'*E. coli* CH10-12 en Erlenmeyer agités. Le diamètre de cercle équivalent (diamètre CE) pendant la phase d'induction a diminué de 10 à 30%, par rapport aux cultures non induites à 37°C et 28°C. Dans les cultures d'*E. coli* CH10-12 en bioréacteur, le diamètre de CE était 20% plus élevé en mode discontinu (batch) qu'en mode discontinu alimenté (fed-batch). Pendant la phase d'induction, le diamètre de CE était presque constant pour toutes les cultures, dans toutes les températures d'induction. Cela suggère que le changement de la taille des cellules était principalement dû au taux de croissance spécifique du micro-organisme, et indépendant de l'induction de la protéine. Le paramètre morphologique ne peut être considéré comme un indicateur ou marqueur de l'induction.

La quantification du nanobody, en particulier pour les cultures en bioréacteur, a été étudiée au cours de cette thèse. La concentration inconnue du nanobody était inférieure à la limite inférieure de détection de la Nanodrop (0,1 mg/mL) dans les échantillons purifiés par l'IMAC. Pour l'essai Bradford, les échantillons ont été dilués par essais et erreurs afin de quantifier la protéine dans les limites de détection de la méthode.

Dans les gels SDS-PAGE, cependant, la bande du nanobody était clairement visible et s'incrémentait avec le temps de l'induction, comme attendu. Afin de quantifier le nanobody dans le gel, un protocole de traitement d'image a été proposé. Le traitement optimal des images repose sur la soustraction du bruit de fond, le contrôle de la sursaturation et en éliminant les variations spatiales de l'intensité du fond par la méthode de « rolling ball » d'une dimension de 250 pixels. La surface de pic de chaque protéine a été obtenue par le profil de densité optique non calibré de chaque puits du gel (Figure 1-2A et Figure 1-2B). BSA, CA et OV ont été utilisés pour quantifier les bandes du marqueur de poids moléculaire. Le nanobody a été quantifié avec précision en utilisant la bande de 50 kDa du marqueur de poids moléculaire comme référence pour 750 ng de protéine recombinante (Figure 1-2C et Figure 1-2D). Ce développement méthodologique a fait l'objet d'un article publié dans *MicrobiologyOpen* ⁶.

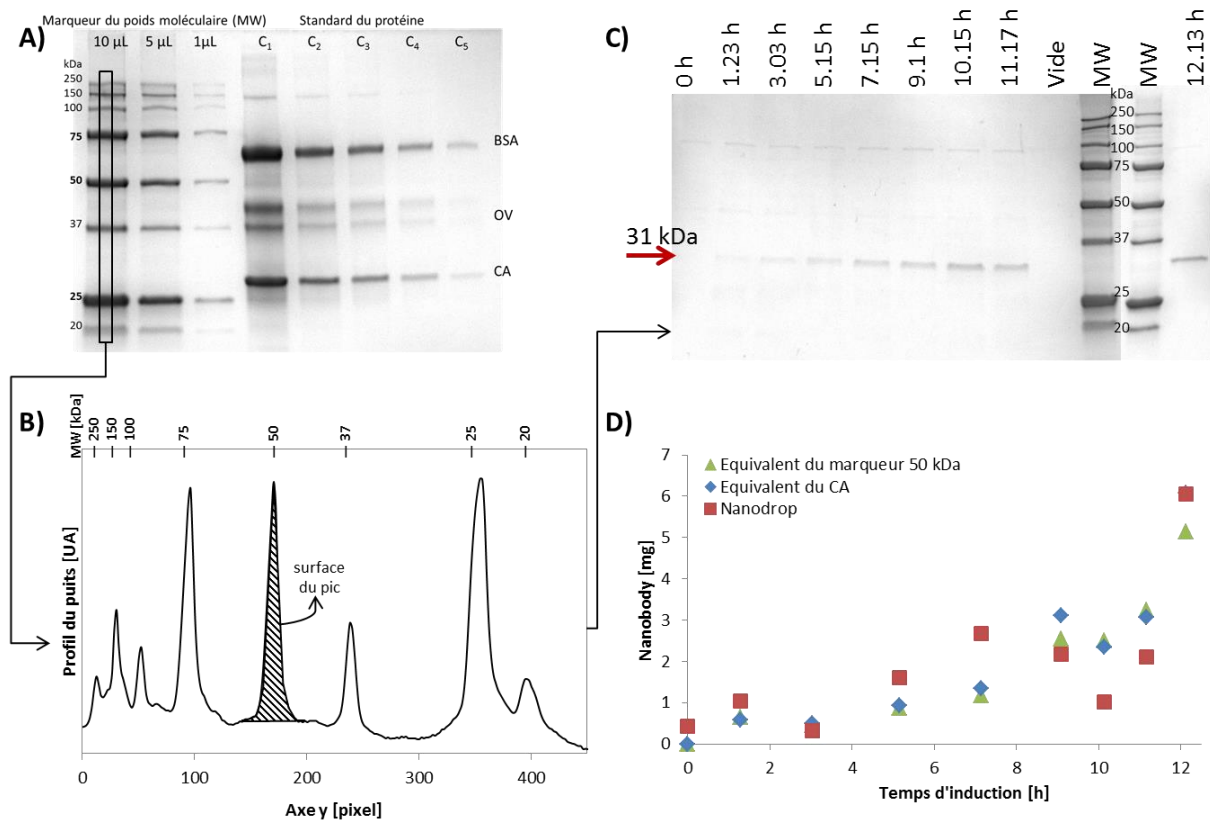


Figure 1-2. Méthodologie de traitement d'images des gels d'électrophorèse. A) Image du gel d'électrophorèse utilisé pour les analyses. BSA : albumine de sérum bovin, OV : ovalbumine, CA : anhydrase carbonique, MW : marqueur du poids moléculaire. B) Profil du puits et détermination de la surface du pic. C) Identification du nanobody CH10-12 en gels d'électrophorèse. La flèche rouge indique la bande du nanobody à un poids moléculaire apparent du 31 kDa. D) Comparaison de la quantification du nanobody par densitométrie et nanodrop.

Pour les cultures en bioréacteur, une grande répétabilité a été trouvée en mode batch et fed-batch. En mode batch, le taux de croissance spécifique maximal était de $0,8 \text{ h}^{-1}$ pour toutes les cultures à 37°C , pH 6,8, $p\text{O}_2 > 15\%$, 10 g Glc/L , MM (Table 1-2). Le rendement d'acétate sur glucose, $Y_{Ac/S}$, était de $0,29 \text{ g/g}$ pour toutes les cultures en mode batch, et, après le début du mode fed-batch, il était complètement consommé après quelques heures.

Culture	$\mu_{\max} [\text{h}^{-1}]$	$\mu_{\text{fix}} [\text{h}^{-1}]$	$\mu_{\text{ind}} \text{ max} \rightarrow \text{min} [\text{h}^{-1}]$	Température d'induction $[\text{C}^\circ]$	Temps d'induction [h]
BR01 – WK6	0.85 ± 0.02	0.52 to 0.13	/	/	/
BR02 – CH10-12	0.70 ± 0.04	0.38 ± 0.02	$0.023 \rightarrow 0.018$	28	12
BR03 – CH10-12	0.67 ± 0.02	0.40 ± 0.03	$0.074 \rightarrow 0.014$	30	10
BR04 – CH10-12	0.85 ± 0.03	0.43 ± 0.03	$0.048 \rightarrow 0.022$	33	6
BR05 – CH10-12	0.85 ± 0.03	0.45 ± 0.03	$0.031 \rightarrow 0.003$	37	6
BR06 – CH10-12	0.85 ± 0.02	0.44 ± 0.02	$0.029 \rightarrow 0.002$	29	38
BR07 – CH10-12	0.78 ± 0.03	0.37 ± 0.01	$0.025 \rightarrow 0.013$	32	35
BR08 – NbF12-10 NN	0.87 ± 0.02	0.39 ± 0.01	$0.029 \rightarrow 0.008$	29	37
BR09 – WK6	0.81 ± 0.01	0.35 ± 0.03	$0.033 \rightarrow 0.001$	29	28

Table 1-2. Taux de croissance moyen en conditions opératoires : batch (μ_{\max}), fed-batch (μ_{fix}) et induction ($\mu_{\text{induction}}$).

Le transfert d'oxygène dans les cultures a été étudié avec une méthodologie unique imposant des couples (aération, agitation) identiques pour toutes les cultures. Cela a permis d'assurer une production dans des conditions aérobies strictes ($p\text{O}_2 > 15\%$) et le coefficient de transfert de masse volumétrique, $k_L a$, a pu être comparé dans les mêmes conditions pour toutes les cultures. Le $k_L a$ en conditions biotiques était, en moyenne, supérieur d'un ordre de grandeur au $k_L a$ en conditions

abiotiques. Le facteur d'accélération biologique, E , a pu être calculé et comparé pour toutes les cultures, et a varié de 5 à 40. Le quotient respiratoire, QR , est resté constant pour toutes les cultures à une valeur moyenne de 1, malgré la production du nanobody pendant la phase d'induction.

En mode batch et fed-batch, les rendements de la biomasse sur le glucose, $Y_{X/S}$, et le rendement du dioxyde de carbone sur le glucose, $Y_{CO_2/S}$, étaient tous deux de 0,45 Cmol/Cmol pour toutes les cultures. Pendant la phase d'induction, $Y_{X/S}$ a diminué à 0,2 Cmol/Cmol, tandis que $Y_{CO_2/S}$ a augmenté jusqu'à 0,8 Cmol/Cmol.

Le mode fed-batch a permis d'atteindre des concentrations de biomasse élevées (25 - 30 g cdw/L) avant l'expression des protéines avec la consommation de l'acétate produit pendant le mode batch. Les nanobodies CH10-12 et NbF12-10 ont été exprimés en milieu MM. Un flux de carbone résiduel a été fixé à 4 g Glc/h pour éviter toute limitation nutritionnelle, le taux de croissance spécifique résiduel était en moyenne de 0,02 h⁻¹ pour toutes les souches.

Le métabolisme de maintenance était particulièrement élevé pendant la phase d'induction, car il peut être apprécié par l'augmentation de la production de dioxyde de carbone ($Y_{CO_2/S} = 0,45 \rightarrow 0,8$ Cmol/Cmol) et la production réduite de biomasse ($Y_{X/S} = 0,45 \rightarrow 0,2$ Cmol/Cmol).

L'effet de la température dans la production du nanobody a été démontré par les cultures induites entre 28°C et 37°C (Figure 1-3). Des températures plus basses (28°C et 30°C) ont permis d'atteindre les titres les plus élevés de nanobody CH10-12 (2,3 mg/L), et sa production a diminué en même temps que l'augmentation de la température à 33°C et 37°C (0,4 mg/L et 0,2 mg/L). Comme les basses températures d'induction diminuent la charge métabolique de la souche recombinante, ces résultats sont conformes à la littérature ⁷.

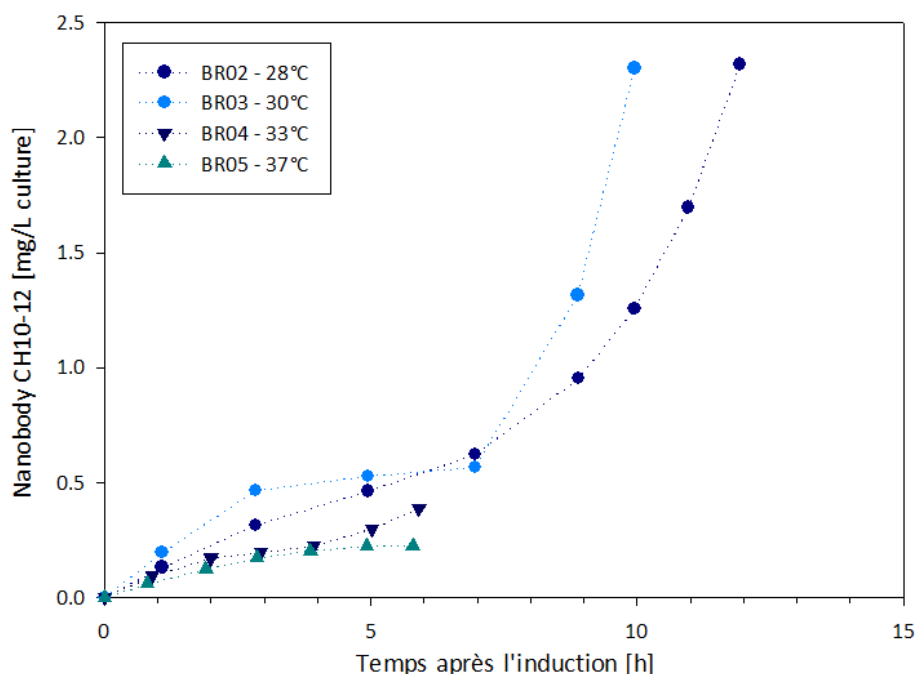


Figure 1-3. Production du nanobody CH10-12 par de court temps d'induction.

Dans les cultures où la phase d'induction était supérieure à 35 h, la productivité était inférieure à celle des cultures à courte durée d'induction (<12 h). La production de nanobody semblait atteindre un plateau au bout d'un certain temps (Figure 1-4). Des titres finaux de 1,4 mg/L et 0,4 mg/L ont été obtenus pour des cultures d'*E. coli* CH10-12 induites à 29°C et 32°C, respectivement. La culture d'*E. coli* NbF12-10 NN induite à 29°C a atteint un titre final de 0,7 mg/L après 35 h d'induction.

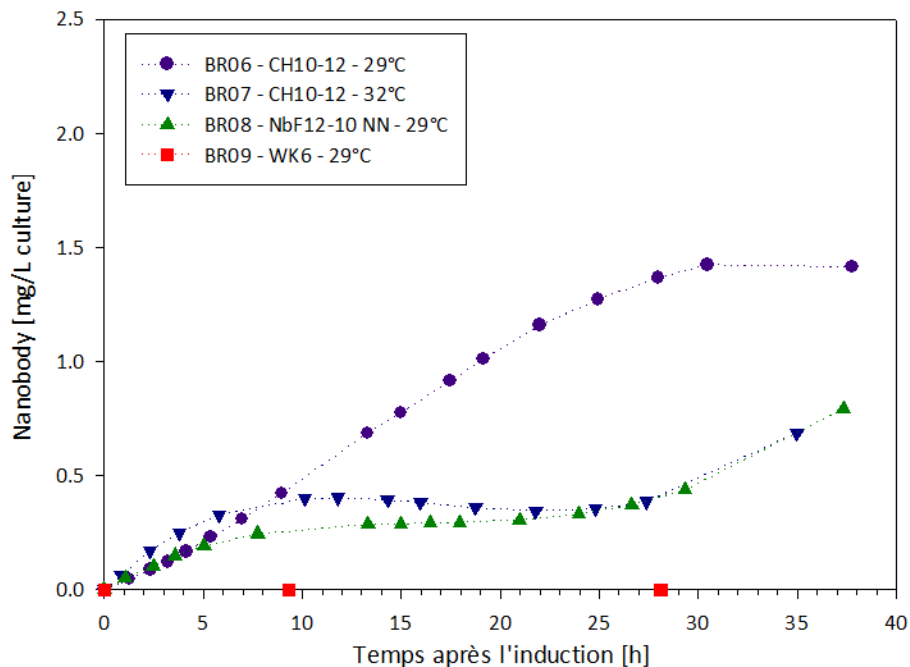


Figure 1-4. Production du nanobody CH10-12 et NbF12-10 en cultures de bioréacteur par de longs temps d'induction.

La faible productivité des cultures par de long temps d'induction pourrait s'expliquer par la charge métabolique du plasmide induit ⁷. Malgré la faible température de production (29°C), la culture BR06 a atteint un plateau après 25 heures d'induction, et les cultures BR07 (32°C) et BR08 (29°C) ont atteint un plateau après seulement 10 heures d'induction.

Pendant la phase d'induction, le citrate présent dans le milieu de culture a été consommé dans les cultures à longue durée d'induction. La consommation apparente du citrate dans les cultures à longue durée d'induction indiquait la stimulation du cycle des acides tricarboxyliques (TCA) du micro-organisme. Ce phénomène a été constaté dans la production d'autres protéines recombinantes ⁸. L'hypothèse proposée était que le citrate était utilisé pour synthétiser les métabolites intracellulaires nécessaires à la production du nanobody recombinant.

La charge métabolique aurait pu être augmentée par le faible taux de croissance spécifique ($0,02 \text{ h}^{-1}$) pendant la phase d'induction. De faibles concentrations de substrat dans le milieu de culture provoquent une augmentation de la charge métabolique chez les souches recombinantes, ce qui pourrait produire des protéines intracellulaires indésirables.

Le long temps d'induction (>30 h) pourrait également induire une charge métabolique élevée due à la longue exposition du micro-organisme à l'IPTG. Cet inducteur est un composé non métabolisé qui active le plasmide recombinant pour produire le nanobody, mais il est également connu pour entraver la production de biomasse à des concentrations élevées d'inducteur ⁹. La concentration optimale de l'inducteur dépend du système et, dans les cultures en bioréacteur, elle pourrait être contrôlée par la concentration de la biomasse ($0,4$ à $3 \mu\text{mol d'IPTG/g cdw}$) pour réduire la charge métabolique ¹⁰⁻¹². Les cultures induites avaient une concentration d'inducteur-biomasse de 20 à $40 \mu\text{mol IPTG/g cdw}$, soit 10 fois plus que celle utilisée pour les autres souches recombinantes d'*E. coli*.

La génération de protéines inconnues dans les échantillons purifiés de nanobody pourrait être une réponse de la souche au faible taux de croissance spécifique et à la longue durée d'exposition à l'inducteur. La protéine de faible poids moléculaire (11 kDa) pourrait être un produit de dégradation du nanobody causé par une température élevée (dégradation protéolytique). La protéine de haut poids moléculaire (84 kDa) pourrait être produite en réponse à une composition moyenne inadéquate et à un faible taux de croissance spécifique, concomitante avec la diminution du citrate dans le milieu de culture.

En raison de la grande répétabilité des cultures, un modèle mathématique a été proposé pour déterminer les conditions optimales de production de nanobody. Le modèle était une cinétique de Luedeking-Piret modifiée avec des paramètres cinétiques de type Arrhenius. L'hypothèse de la thermo-dépendance de la production de nanobodies recombinants a été confirmée par le modèle, qui a montré que la production la plus élevée était obtenue à la température la plus basse (28°C). Le modèle a été comparé à la culture de la souche *Escherichia coli* NbF12-10 NN, qui a montré la même tendance que les cultures de *E. coli* CH10-12.

En perspective à ce doctorat, plusieurs actions complémentaires et questions scientifiques peuvent être proposés. Premièrement, une analyse plus approfondie du nanobody CH10-12 pourrait être effectuée. Le nanobody CH10-12 est la forme humanisée de la nanobody NbF12-10, créée avec les mêmes neurotoxines Aahl' et AahlII du scorpion *Androctonus australis hector*. Une analyse de la bioactivité du nanobody CH10-12 doit être effectuée contre les neurotoxines et/ou le venin du scorpion *Androctonus australis hector*.

Des analyses par Western blot doivent être effectuées afin d'éclaircir l'origine des protéines secondaires trouvées dans les étapes de purification du nanobody (11 kDa et 84 kDa). Les hypothèses proposées de l'agrégation du nanobody pendant de longues périodes d'induction et de la dégradation protéolytique du nanobody due aux températures élevées permettront d'améliorer les conditions d'induction auxquelles la production du nanobody est meilleure.

Deuxièmement, la relation entre la productivité du nanobody et la charge métabolique due aux concentrations d'inducteurs, aux longs temps d'induction ou aux faibles taux de croissance spécifiques pourrait être testée dans une série d'expériences supplémentaires. La phase d'induction pourrait être prolongée avec un taux de croissance spécifique élevé (0,3 h⁻¹) pour atteindre rapidement une concentration élevée de biomasse et réduire la charge métabolique due à la longue exposition à l'inducteur. L'utilisation du lactose comme inducteur de l'expression des protéines peut également être explorée.

Finalement, la carence en nutriments dans le milieu minimal défini pourrait être testée par une expérience dans laquelle du citrate est ajouté en continu pendant le mode fed-batch pour maintenir un titre constant pendant toute la phase d'induction.

- (1) Alirahimi, E.; Kazemi-Lomedasht, F.; Shahbazzadeh, D.; Habibi-Anbouhi, M.; Hosseininejad Chafi, M.; Sotoudeh, N.; Ghaderi, H.; Muyldermans, S.; Behdani, M. Nanobodies as Novel Therapeutic Agents in Envenomation. *Biochim Biophys Acta - Gen Subj* 2018, 1862 (12), 2955–2965. <https://doi.org/10.1016/j.bbagen.2018.08.019>.
- (2) Hmila, I.; Abdallah R, B. A.-B.; Saerens, D.; Benlasfar, Z.; Conrath, K.; Ayeb, M. El; Muyldermans, S.; Bouhaouala-Zahar, B. VHH, Bivalent Domains and Chimeric Heavy Chain-Only Antibodies with High Neutralizing Efficacy for Scorpion Toxin Aahl'. *Mol Immunol* 2008, 45 (14), 3847–3856. <https://doi.org/10.1016/j.molimm.2008.04.011>.
- (3) Graumann, K.; Premstaller, A. Manufacturing of Recombinant Therapeutic Proteins in Microbial Systems. *Biotechnol J* 2006, 1 (2), 164–186. <https://doi.org/10.1002/biot.200500051>.
- (4) Laustsen, A.; Solà, M.; Jappe, E.; Oscoz, S.; Lauridsen, L.; Engmark, M. Biotechnological Trends in Spider and Scorpion Antivenom Development. *Toxins (Basel)* 2016, 8 (8), 226. <https://doi.org/10.3390/toxins8080226>.

- (5) Hmila, I.; Saerens, D.; Ben Abderrazek, R.; Vincke, C.; Abidi, N.; Benlasfar, Z.; Govaert, J.; El Ayeb, M.; Bouhaouala-Zahar, B.; Muyldermans, S. A Bispecific Nanobody to Provide Full Protection against Lethal Scorpion Envenoming. *FASEB J* 2010, 24 (9), 3479–3489. <https://doi.org/10.1096/fj.09-148213>.
- (6) Alonso Villela, S. M.; Kraïem, H.; Bouhaouala-Zahar, B.; Bideaux, C.; Aceves Lara, C. A.; Fillaudeau, L. A Protocol for Recombinant Protein Quantification by Densitometry. *Microbiologyopen* 2020, No. in press.
- (7) Donovan, R. S.; Robinson, C. W.; Glick, B. R. Review: Optimizing Inducer and Culture Conditions for Expression of Foreign Proteins under the Control of the Lac Promoter. *J Ind Microbiol* 1996, 16 (3), 145–154. <https://doi.org/10.1007/BF01569997>.
- (8) Ramchuran, S. O.; Holst, O.; Karlsson, E. N. Effect of Postinduction Nutrient Feed Composition and Use of Lactose as Inducer during Production of Thermostable Xylanase in *Escherichia Coli* Glucose-Limited Fed-Batch Cultivations. *J Biosci Bioeng* 2005, 99 (5), 477–484. <https://doi.org/10.1263/jbb.99.477>.
- (9) Baneyx, F.; Mujacic, M. Recombinant protein folding and misfolding in *Escherichia coli*. *Nat Biotechnol* 2004, 22 (11), 1399–1408.
- (10) Ruiz, J.; González, G.; de Mas, C.; López-Santín, J. A Semiempirical Model to Control the Production of a Recombinant Aldolase in High Cell Density Cultures of *Escherichia Coli*. *Biochem Eng J* 2011, 55 (2), 82–91. <https://doi.org/10.1016/j.bej.2011.03.001>.
- (11) Ruiz, J.; Pinsach, J.; Álvaro, G.; González, G.; de Mas, C.; Resina, D.; López-Santín, J. Alternative Production Process Strategies in *E. Coli* Improving Protein Quality and Downstream Yields. *Process Biochem* 2009, 44 (9), 1039–1045. <https://doi.org/10.1016/j.procbio.2009.05.007>.
- (12) Calleja, D.; Kavanagh, J.; de Mas, C.; López-Santín, J. Simulation and Prediction of Protein Production in Fed-Batch *E. Coli* Cultures: An Engineering Approach. *Biotechnol Bioeng* 2016, 113 (4), 772–782. <https://doi.org/10.1002/bit.25842>.

APPENDIX 2. PROTEIN QUANTIFICATION METHODOLOGY

During induction, the accurate quantification of proteins became a challenge. The quantification methods used, Bradford and Nanodrop, were not reliable due to the low quantity of protein produced. The Bradford assay produced non-exploitable results and the Nanodrop measures fell on the lower limits of detection of this equipment.

As an alternative method, a protocol of image analysis was proposed to quantify the protein from the SDS-PAGE gels. The protocol details the methodology used to quantify the recombinant nanobody using the band of 50 kDa in the molecular weight marker as a reference for 750 ng of recombinant protein in the gel. This protocol was accepted and published in MicrobiologyOpen (DOI: 10.1002/MBO3.1027, Impact factor of 2.738) [229]. The full article can be found here.



A protocol for recombinant protein quantification by densitometry

Susana María Alonso Villela¹ | Hazar Kraïem² | Balkiss Bouhaouala-Zahar^{2,3} | Carine Bideaux¹ | César Arturo Aceves Lara¹ | Luc Fillaudeau¹

¹TBI, CNRS, INRAE, INSA, Université de Toulouse, Toulouse, France

²Laboratoire des Venins et Molécules Thérapeutiques, Institut Pasteur de Tunis, Université Tunis El Manar, Tunis, Tunisia

³Faculté de Médecine de Tunis, Université Tunis El Manar, Tunis, Tunisia

Correspondence

Susana María Alonso Villela, TBI, CNRS, INRAE, INSA, Université de Toulouse, Toulouse, France.
Email: salonsovillela@gmail.com

Funding information

Consejo Nacional de Ciencia y Tecnología, Grant/Award Number: 461347

Correspondence

Susana María Alonso Villela, TBI, CNRS, INRAE, INSA, Université de Toulouse, Toulouse, France.
Email: salonsovillela@gmail.com

Funding information

Consejo Nacional de Ciencia y Tecnología, Grant/Award Number: 461347

Abstract

The protein purity is generally checked using SDS-PAGE, where densitometry could be used to quantify the protein bands. In literature, few studies have been reported using image analysis for the quantification of protein in SDS-PAGE: that is, imaged with Stain-Free™ technology. This study presents a protocol of image analysis for electrophoresis gels that allows the quantification of unknown proteins using the molecular weight markers as protein standards. *Escherichia coli* WK6/pHEN6 encoding the bispecific nanobody CH10-12 engineered by the Pasteur Institute of Tunisia was cultured in a bioreactor and induced with isopropyl β-D-1-thiogalactopyranoside (IPTG) at 28°C for 12 hr. Periplasmic proteins extracted by osmotic shock were purified by immobilized metal affinity chromatography (IMAC). Images of the SDS-PAGE gels were analyzed using ImageJ, and the lane profiles were obtained in grayscale and uncalibrated optical density. Protein load and peak area were linearly correlated, and optimal image processing was then performed by background subtraction using the rolling ball algorithm with radius size 250 pixels. No brightness and contrast adjustment was applied. The production of the nanobody CH10-12 was obtained through electrophoresis gels that allows the quantification of unknown proteins using the molecular weight markers as protein standards. *Escherichia coli* WK6/pHEN6 encoding the bispecific nanobody CH10-12 engineered by the Pasteur Institute of Tunisia was cultured in a bioreactor and induced with isopropyl β-D-1-thiogalactopyranoside (IPTG) at 28°C for 12 hr. Periplasmic proteins extracted by osmotic shock were purified by immobilized metal affinity chromatography (IMAC). Images of the SDS-PAGE gels were analyzed using ImageJ, and the lane profiles were obtained in grayscale and uncalibrated optical density. Protein load and peak area were linearly correlated, and optimal image processing was then performed by background subtraction using the rolling ball algorithm with radius size 250 pixels. No brightness and contrast adjustment was applied. The production of the nanobody CH10-12 was obtained through a fed-batch strategy and quantified using the band of 50 kDa in the marker as reference for 750 ng of recombinant protein. The molecular weight marker was used as a sole protein standard for protein quantification in SDS-PAGE gel images.

KEYWORDS

densitometry, image analysis, nanobody production, protein quantitation, SDS-PAGE

1 | INTRODUCTION

Escherichia coli is a well-known microorganism used as a workhorse in the production of recombinant therapeutic molecules, such as antibodies and antibody fragments (Graumann & Premstaller, 2006). Lately, nanobodies, small fragments of camelid antibodies, have been proven to neutralize scorpion toxins (Alirahimi et al., 2018; Hmila et al., 2008). The periplasmic

production of these nanobodies has been studied in shake flasks induced by synthetic IPTG under the control of the *lac* promoter (Laustsen et al., 2016).

The nanobodies are normally obtained after purification of periplasmic proteins using IMAC (Pardon et al., 2014). The identification and quantification of these nanobodies are of the utmost importance during the purification steps. SDS-PAGE is used to check and characterize the purified recombinant proteins, and colorimetric and

This is an open access article under the terms of the Creative Commons Attribution License, which permits use, distribution and reproduction in any medium, provided the original work is properly cited.

© 2020 The Authors. *MicrobiologyOpen* published by John Wiley & Sons Ltd.

ultraviolet absorption methods are used to quantify them (Bradford, 1976; Stoscheck, 1990).

The semiquantification of protein load in the gel is made through a nonstandardized methodology, using densitometry in SDS-PAGE and Western blot assays (Gassmann, Grenacher, Rohde, & Vogel, 2009). The use of external protein standards of known concentration is commonly used for the quantification of the electrophoresis-based separated samples (Holzmüller & Kulozik, 2016; Rehbein & Schwalbe, 2015; Vincent, Cunningham, Stephens, Halayko, & Fisher, 1997). Stain-Free™ technology by Bio-rad (USA) has been applied by Holzmüller and Kulozik (2016) and Gürtler et al. (2013), in which the ultraviolet fluorescence of the protein of interest was used as the quantifying parameter of the unknown samples.

Image analysis by densitometry is made using the profiles of the lanes and calibrated to a known standard (Cromey, 2010; Srový & Hodný, 1991). The peak area is the signal used in most densitometry analysis (Gassmann et al., 2009; Gorr & Vogel, 2015; Rehbein & Schwalbe, 2015), and the peak maximum intensity has been utilized in the quantification of proteins in Western blots imaged by fluorescence (Gürtler et al., 2013; Holzmüller & Kulozik, 2016). The volume of the peak is not commonly considered (Vincent et al., 1997) since the correlations obtained often yield inaccurate protein load estimation (Gassmann et al., 2009).

In the present work, a new protocol of image analysis for electrophoresis gels is reported. The protocol describes the quantification of protein in the bands of SDS-PAGE gels. The unknown proteins are quantified with commercially available protein standards: bovine serum albumin (BSA), carbonic anhydrase (CA), and ovalbumin (OV), and molecular weight markers of known concentration. The molecular weight marker is then used as a sole protein standard for protein quantification and molecular weight estimation. The protocol was applied to the quantification of the periplasmic production of a recombinant nanobody that neutralizes specific toxins in the scorpion venom.

2 | MATERIALS AND METHODS

2.1 | Nanobody protein

Experiments were conducted with *Escherichia coli* K12/WK6 (Δ (lac-pro), galE, strA, nal; F' lacI^q Z Δ M15, pro+) harboring pHEN6 plasmid

(derived from pBR322) encoding the chimeric format of the bispecific nanobody VHH10-VHHF12 (called CH10-12), retrieved from the combinatorial libraries. The strain was engineered by the Pasteur Institute of Tunisia (Kraiem, 2018). The nanobody CH10-12 has an estimated molecular weight of 31 kDa, and it neutralizes the toxins present in the groups Aahl' and Aahl of the *Androctonus australis* hector scorpion venom (Hmila et al., 2010).

Cultures were performed in a 5 L bioreactor (Figure 1), Biostat B-DCU (Sartorius) using glucose as a carbon source in 1.5 L of minimal mineral culture medium (Sunya, Delvigne, UribeArrea, Molina-Jouve, & Gorret, 2012). The batch phase was conducted at 37°C, and at the depletion of the 10 g/L of initial glucose, a fed-batch mode was applied with an exponential feed of a glucose solution at 300 g/L, imposing a specific growth rate of $\mu = 0.38$ per hour.

Residual glucose and organic acids were quantified by HPLC (Aminex column HPX-87H, Bio-rad). Biomass cell dry weight was determined by a gravimetric method using preweighted microcentrifuge tubes (Eppendorf).

Protein expression was induced at 23 g cdw/L with 1 mM of isopropyl β -D-1-thiogalactopyranoside (IPTG, Sigma-Aldrich) at 28°C for 12 hr. At induction, the glucose feed rate was set to 4.5 g/hr of glucose imposing a $\mu \leq 0.03$ per hour.

Samples of 25 ml of the cell suspension were taken every 2 hr, and cells were harvested by centrifugation at 8,228 g and 4°C for 8 min. Cells were suspended in 1.8 ml ice-cold TES buffer (200 mM Tris pH 8.0, 0.5 mM EDTA pH 8.0, 0.5 M Sucrose) and incubated at 4°C for 2 hr under agitation at 350 rpm in a Thermomixer comfort (Eppendorf). The osmotic shock was performed adding 3.2 ml of cold water to the cell suspension and incubated at 4°C for 2 hr under agitation at 350 rpm in a Thermomixer comfort (Eppendorf; Neu & Heppel, 1965). After the addition of 46 μ l of MgCl₂ 2 M (Sigma-Aldrich), the cell suspension was centrifuged at 8,228 g and 4°C for 30 min and the periplasmic extract was recovered (Pardon et al., 2014).

Periplasmic proteins were purified by immobilized metal affinity chromatography (IMAC) using His-Select Nickel Affinity Gel (Sigma-Aldrich). The nanobody protein was eluted from the column with phosphate-buffered saline (PBS) and 250 mM Imidazole (Sigma-Aldrich), pH 7.54. Six elute fractions, of 1 ml each, were obtained and stored at 4°C (Figure 1).

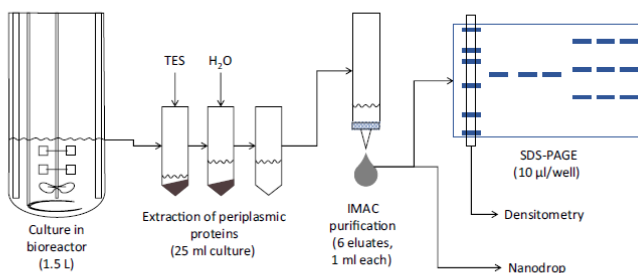


FIGURE 1 Experimental setup and purification steps of the nanobody CH10-12

2.2 | Protein standards

Three proteins were used as standards: Bovine serum albumin (BSA, Sigma-Aldrich) lyophilized powder for gel electrophoresis with a molecular weight of 66 kDa; albumin from chicken egg white or ovalbumin (OV, Sigma-Aldrich) lyophilized powder for gel electrophoresis with a molecular weight of 45 kDa, and carbonic anhydrase from bovine erythrocytes (CA, Sigma-Aldrich) lyophilized powder for enzyme analysis with a molecular weight of 30 kDa.

The BSA is a cheap, well-known protein commonly used in protein quantification (Bradford, 1976). The ovalbumin (OV) and the carbonic anhydrase (CA) have a molecular weight close to that of the protein of interest.

A standard of each protein was prepared. The absorbance of each solution was measured in a Nanodrop spectrophotometer 1.000 (Thermo Fisher Scientific) at a wavelength of 280 nm. The Beer–Lambert law was used for the calculation of the final protein concentration of each solution using the percent extinction coefficient ($\epsilon_{1\%}^{1\text{cm}}$) of each protein for a wavelength of 280 nm (Equation 1).

$$C = \frac{A_{280}}{\epsilon_{1\%}^{1\text{cm}}} \quad (1)$$

Concentrations for BSA, CA, and OV were 8.9, 9.1, and 5.9 mg/ml respectively. A mixture of the proteins was prepared by combining 100 μl of each protein standard in a microcentrifuge tube (Eppendorf) for a final concentration of 3 mg/ml for BSA and CA, and 2 mg/ml for OV. Successive dilutions were made from this protein mixture, and five concentrations were prepared, of approximately, 0.01, 0.03, 0.06, 0.1, and 0.3 mg/ml per protein mixture. All protein standards were stored in aliquots at -20°C until use.

For the SDS-PAGE, the ready-to-use Precision Plus Protein Unstained Protein Standards (Bio-rad) were used as molecular weight markers. The marker contains ten recombinant protein bands of 250, 150, 100, 75, 50, 37, 25, 20, 15, and 10 kDa.

According to the manufacturer, the protein bands of 75, 50, and 25 kDa are reference markers within the molecular weight marker, as they have three times the intensity of the other bands. Similarly, for a 10 μl lane of molecular weight marker, the band of 50 kDa has 750 ng of protein, and the bands of 20 and 100 kDa have 150 ng of protein, each. The nature of the recombinant proteins in the molecular weight marker is not described by the manufacturer.

2.3 | SDS-PAGE

Protein samples were diluted at a ratio 1:1 with Laemmli 2 \times buffer solution (Bio-rad) with 5% 2-mercaptoethanol (Sigma-Aldrich) as a denaturing agent and heated in a water bath at 90°C for 10 min.

Protein samples of 10 μl were poured in the wells of an Any kD Mini-Protean TGX Stain-Free™ Precast gel (Bio-rad). The molecular weight marker was loaded in three wells at 10, 5, and 1 μl without dilution in Laemmli buffer (Figure 2a).

Tetra cell (Bio-rad) using TGX running buffer (Bio-rad). Gels were washed with distilled water and stained with Instant Blue (Expedeon) for 1 hr.

Gels were imaged in a Molecular Imager ChemiDoc XRS System (170-8070, Bio-rad) under white light epi-illumination. Images were saved as a TIFF file with a size of 16-bit and a resolution of $1,392 \times 1,040$ pixels.

2.4 | ImageJ

Images were analyzed using ImageJ (NIH), a public domain program from the National Institutes of Health that allows image processing. Images were cropped to $1,070 \times 774$ pixels to zoom into the gel, equivalent to $0.1493 \text{ pixel}/\mu\text{m}$.

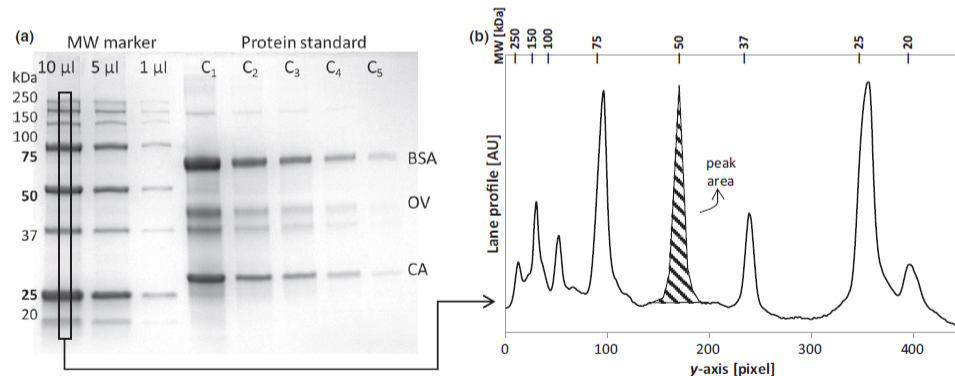


FIGURE 2 Qualitative analysis made on the gels. (a) Image of the SDS-PAGE used for the tests. (b) Lane profile and peak area determination

2.5 | Brightness and contrast adjustments

Brightness and contrast adjustments were made using the automatic function of the program which oversaturates the pixels outside an automatically selected grayscale range. The adjustment is made using the histogram of the image.

2.6 | Background subtraction

The function for background subtraction in ImageJ is based on the rolling ball algorithm of Sternberg (Sternberg, 1983). The algorithm simulates a spherical ball passing under the 3D profile of the optical density of the image. Increasing the size of the rolling ball radius decreases the background subtracted. This function is applied to the entire image. The rolling ball radius size was set to 50, 150, and 250 pixels for the analysis of data processing.

2.7 | Oversaturation

For each analysis, the oversaturation of the maximal and minimal values of the grayscale was calculated from the histogram of gray values. For 16-bit images, the histogram represents the results of 256 bins over the range of the grayscale values of the selected image. The oversaturation over black and white, maximal and minimal values, respectively, was made using the smallest and highest bin on the histogram of the entire image.

2.8 | Densitometry

The Gel Analyzer tool of ImageJ was used to determine the profiles of each lane of the gels. The size of the lane selection tool was 16 pixels wide (Figure 2a), equivalent to 30% of the total width of the well as suggested by Gassmann et al. (2009). The lanes were always positioned at the center of the gel lane.

The profiles of the lanes were represented as the average of the grayscale values or the uncalibrated optical density along a one-pixel-height horizontal lane.

The calculation of the uncalibrated optical density uses an 8-bit copy of the 16-bit original image, and the grayscale values of the image are used according to Equation 2.

$$\text{Uncalibrated OD} = \log_{10} \left(\frac{255}{\text{pixel value}} \right) \quad (2)$$

From the profile of the lanes, the area of the peaks was created manually, drawing a straight line across the baseline of the profile (Figure 2b).

3 | RESULTS AND DISCUSSION

3.1 | Optimal image processing with BSA as protein standard

With the objective of simultaneously determining the molecular weight and the protein load of the nanobody band on an SDS-PAGE gel, the optimal image processing was identified using the BSA.

The oversaturation and the smoothness of the profiles were used as parameters for the selection of the optimal image modification. Of the seven tests performed, one was used as a control (automatic brightness and contrast adjustment and no background subtraction), and three different values of the background subtraction function (50, 150 and 250 pixels) were done using or not the automatic brightness and contrast adjustment. In Table 1, the tests performed to the raw image are displayed, with the results on the oversaturation on the maximal (over black) and minimal (over white) bin value.

The protein load was correlated with the peak area of the protein in the densitometry profile (Figure 2b). The peak area is the signal used in most densitometry analysis (Gassmann et al., 2009; Gorr & Vogel, 2015; Rehbein & Schwalbe, 2015), and the peak maximum

TABLE 1 Tests performed for the image manipulation selection

Test on BSA	1	2	3	4	5	6	7
Brightness and contrast correction	Auto	Auto	Auto	N. A.	N. A.	N. A.	Auto
Rolling ball radius [pixel]	N. A.	50	150	50	150	250	250
Oversaturation over black [%]	0.19	0.00	0.04	0.00	0.00	0.00	0.00
Oversaturation over white [%]	0.01	20.05	10.8	18.34	10.33	6.56	6.29
Flattened peaks at high protein load	Yes	Yes	Yes	No	No	No	Yes
R ² for grayscale profile [/]	.822	.852	.896	.935	.917	.872	.879
p-Value for grayscale profile [/]	.013	.009	.004	.002	.003	.006	.006
R ² for OD profile [/]	.993	.950	.974	.995	.992	.984	.975
p-Value for OD profile [/]	2.28E-04	9.43E-04	2.54E-04	7.90E-06	2.44E-05	9.57E-05	2.29E-04

Note: Brightness and contrast adjustments were made with the automatic function. The background subtraction was made using the rolling ball radius at the given size. Flattened peaks found in both optical density and grayscale profiles. R² and p-values were calculated for the BSA.

Abbreviation: N. A.: not applied.

intensity has been used in the quantification of proteins in Western blots imaged by fluorescence (Gürtler et al., 2013; Holzmüller & Kulozik, 2016). The volume of the peak is not commonly used (Vincent et al., 1997) since the correlations obtained often yield inaccurate protein load estimation (Gassmann et al., 2009).

The protein load (P, ng) in the well was calculated for each concentration (C, mg/ml) of the protein standard in the volume (V, mL) of 10 µl of sample diluted in Laemmli buffer (Equation 3).

$$P = C * V * (1/2) \quad (3)$$

The results show that at high protein load, the grayscale and uncalibrated optical density profiles arrived at saturation levels when the brightness and contrast were adjusted. This led to profiles with plateaus at the top of the peaks in both profiles losing information of protein quantitation.

The oversaturation of white pixels increased when the radius of the background subtraction was reduced, according to the rolling ball algorithm. Conversely, the automatic correction of brightness and contrast decreased the oversaturation of white pixels between 5% and 10%. Oversaturation is a result of overprocessing the image that leads to a loss of information in the image (Cromey, 2010).

The grayscale profiles and the uncalibrated optical density profiles were compared by performing linear regression analysis between the BSA load and the peak area. The coefficients of determination and p-values of each linear regression are shown in Table 1. The correlation of peak area with protein load using uncalibrated optical density profiles showed a better fit (p -value $< 1 \times 10^{-4}$, $R^2 > .97$) than the ones of the grayscale intensity.

The optimal data treatment chosen was Test 6, with background subtraction at the size of the rolling ball of 250 pixels and no adjustment of brightness and contrast. This image processing protected the integrity of the data without losing important information. The uncalibrated optical density profiles were used for the linear regression analysis of the BSA, CA, and OV, and the correlations established had a good fit (p -value $< 1 \times 10^{-4}$, $R^2 > .98$, Table 2).

The difference in the slopes of the correlations could be attributed to the protein-Coomassie dye bond. The Coomassie stain binds primarily to basic amino acids such as arginine, histidine, and lysine, and to a lesser extent, to tryptophan and phenylalanine (Congdon, Muth, & Splittgerber, 1993; Stoscheck, 1990; Tal, Silberstein, & Nusser, 1985). The combined weight of these amino acids in the proteins is 22.41% mol/mol, 20.69% mol/mol, and

16.84% mol/mol for BSA, CA, and OV, respectively (<https://www.uniprot.org>, <https://web.expasy.org/protparam>). Unfortunately, a correlation between the molar content of those amino acids and molar slopes could not be found.

The fluorescence of tryptophan residues under UV-light has been used for the quantification of proteins in SDS-PAGE using Stain-Free™ technology (Bio-rad; Holzmüller & Kulozik, 2016). Protein quantitation was possible for proteins containing up to 5.25% mol/mol of relative tryptophan.

3.2 | Quantification of molecular weight marker bands

According to the manufacturer (Bio-rad), the ratio of intensities between the three reference bands (75, 50, and 25 kDa) and the seven other bands of the molecular weight marker should be 3, but it was not the case in this analysis. The ratio ranged from 2 to 3.4 using the maximum intensity of the peaks and from 4.8 to 17 using the peak area along the three molecular weight lanes (10, 5, and 1 µl, Figure 2a).

Using the information of protein load per band (Bio-rad) for the bands of 100, 50, and 20 kDa, and the different loads in the SDS-PAGE gel (10, 5, and 1 µl), the amount of protein per band was positively correlated with the peak area using Microsoft Excel 2010 (Microsoft Company; p -value $< .001$, $R^2 > .98$, Table 2). Ranging from 2.058 to 7.524 pixel*AU/ng, the difference in the slopes of each molecular weight marker could be explained from their composition in amino acids. Unfortunately, this piece of information was not provided by the manufacturer (Bio-rad).

The migration of the molecular weight marker on the gel could also explain the big difference in the slopes. The choice of gel, buffer, and running conditions of electrophoresis can modify slightly the migration of the bands. In the case of the Any kD Mini-Protean TGX Stain-Free™ Precast gels (Bio-rad) used in these experiments, the gel gives a maximum resolution to proteins below 75 kDa, which is optimum for the nanobody CH10-12 with a molecular weight of 31 kDa.

3.3 | Quantification of an unknown protein

The quantification of an unknown protein could be made using the correlations established earlier for either the protein standards:

TABLE 2 Regression analysis for bovine serum albumin (BSA), carbonic anhydrase (CA), and ovalbumin (OV) and molecular weight markers

Protein	BSA	CA	OV	100 kDa	50 kDa	20 kDa
Slope [(pixel*AU)/ng]	4.032	3.749	2.375	2.058	3.193	7.524
σ [(pixel*AU)/ng]	0.257	0.185	0.046	0.176	0.064	0.380
R^2 [/]	.984	.99	.998	.986	.999	.995
p -Value [/]	9.57E-05	3.49E-05	8.62E-07	7.26E-03	3.98E-04	2.54E-03

Note: Equation was established as $A = \text{slope} * P$. A: peak area, P: protein load.

BSA, CA, and OV, or the molecular weight markers: 100, 50, and 20 kDa. The choice depends on the type of molecule to be quantified, in this case, the nanobody CH10-12 with a molecular weight of 31 kDa.

The unknown concentration of a nanobody protein expression was obtained from 7 SDS-PAGE gels stained with Instant Blue and analyzed by ImageJ with background subtraction (Figure 3a). The molecular weight marker was electrophoresed with the nanobody samples, and only the first two eluates were electrophoresed and quantified by densitometry. The concentrations of the purified nanobody were recalculated from the eluates of purification steps to the concentration in the culture (Figure 1).

The peak of 50 kDa in each gel was used as a reference for 750 ng, and linear regression with the intercept in zero was recalculated for the quantification of the nanobody. For comparative purposes, the correlation for CA was used to quantify the nanobody. The protein in the bands of the gel ranged from 33 to 258 ng per band for the molecular weight marker correlation and from 36 to 217 ng with the CA, corresponding respectively to concentration from 0.235 to 2.571 mg/L of culture and from 0.255 to 3.038 mg/L of culture.

The quantification of the protein bands using the CA correlation gives values on average 17% larger than using the correlation for the

50 kDa molecular weight marker. The use of one or the other can be used since the slopes are not significantly different.

The quantification by densitometry was compared with the nanodrop quantification of the samples (Figure 3b). The difference between the densitometry and nanodrop measures is due to the low concentration of protein in the samples, which falls in the lower limit of detection (0.1 mg/ml in the eluted fraction).

It has been reported a method of documentation and quantification of electrophoresis gel, using a series of diluted protein standards of known concentration electrophoresed with unknown samples (Rehbein & Schwalbe, 2015). The disadvantage is that at least one protein standard of known concentration must be used and electrophoresed with the samples in order to do the quantification.

In the present study, a protocol of optimum image processing in ImageJ was identified with the use of protein standards: BSA, CA, and OV. The linearity of the optical density profile versus protein load was tested in the protein standards and in the molecular weight markers. The molecular weight markers used in SDS-PAGE were electrophoresed with the nanobody CH10-12 samples and used to quantify the protein load, as well as to determine the molecular weight of the sample. This reduces the material costs related to the use of multiple protein standards and polyacrylamide gels.

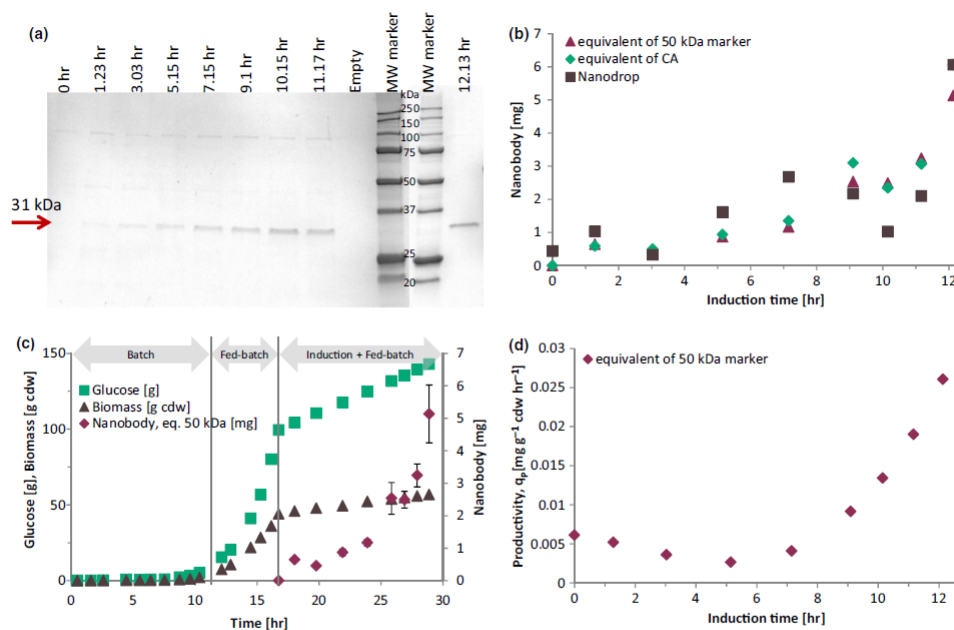


FIGURE 3 Quantification of a nanobody in SDS-PAGE using densitometry. (a) Nanobody identification in SDS-PAGE during protein expression. (b) Comparison between quantification using densitometry and nanodrop. (c) Nanobody production strategy during microbial culture of strain *E. coli* WK6/CH10-12. (d) Productivity of the nanobody from ImageJ measures

3.4 | Monitoring of nanobody production

The evolution of the periplasmic production of the nanobody CH10-12 during protein expression in a fed-batch bioreactor is represented in Figure 3c. During biomass production in the batch phase, the specific growth rate reached a maximum specific growth rate of 0.71 per hour. During the fed-batch phase of biomass production, an average μ of 0.38 per hour was obtained with the exponential glucose feed. The nanobody was produced only after induction with IPTG (Figure 3c), and biomass growth was linear, with an average μ of 0.02 per hour.

The metabolic needs of the coupled production of the nanobody CH10-12 and biomass were satisfied with the fed-batch after induction, which has not been reported yet. The final titer of the nanobody CH10-12 was 3.04 mg/L in a fed-batch culture, which yield a total of 6.06 mg of nanobody CH10-12. The maximum instantaneous productivity was obtained at the end of the culture with 0.026 mg/(g cdw*hr), and the average productivity was 0.0088 mg/(g cdw*hr; Figure 3d).

4 | CONCLUDING REMARKS

This study has presented a protocol for image processing and protein quantification in electrophoresed gels. The densitometric analysis of protein standards of known concentrations (BSA, CA, and OV) and molecular weight marker bands (100, 50, and 20 kDa) was discussed for the quantification of unknown proteins in SDS-PAGE gels. The protein band of 50 kDa in the molecular weight marker was used for the quantification of a nanobody during protein expression in a bioreactor.

The evolution of the periplasmic expression of the nanobody CH10-12 was obtained in fed-batch culture, with a maximum productivity of 0.026 mg/(g cdw*hr) after 12 hr of induction.

The optimum image processing was obtained by background subtraction with a rolling ball size of 250 pixels without brightness and contrast adjustment. The uncalibrated optical density was used for the correlation between protein load and peak area. The advantage of this methodology is the use of the molecular weight marker for the quantification of the protein in SDS-PAGE gels without the use of additional protein standards.

ACKNOWLEDGMENTS

Susana María Alonso Villela is grateful to the National Council of Science and Technology (CONACYT, Mexico) for the doctoral scholarship grant No. 461347.

CONFLICT OF INTEREST

None declared.

AUTHOR CONTRIBUTION

Susana María Alonso Villela: Conceptualization (equal); Formal analysis (equal); Methodology (equal); Writing-original draft

(equal); Writing-review & editing (equal). Hazar Kraïem: Writing-review & editing (equal). Balkiss Bouhaouala-Zahar: Formal analysis (equal); Writing-review & editing (equal). Carine Bideaux: Writing-review & editing (equal). César Arturo Aceves Lara: Supervision (equal); Writing-review & editing (equal). Luc Fillaudeau: Formal analysis (equal); Supervision (equal); Writing-review & editing (equal).


DATA AVAILABILITY STATEMENT

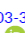
All data generated or analyzed during this study are included in this published article.

ORCID

Susana María Alonso Villela  <https://orcid.org/0000-0001-8290-1635>

Hazar Kraïem  <https://orcid.org/0000-0002-8180-0573>

Balkiss Bouhaouala-Zahar  <https://orcid.org/0000-0003-3147-245X>

Carine Bideaux  <https://orcid.org/0000-0002-9830-5093>

REFERENCES

- Alirahimi, E., Kazemi-Lomedasht, F., Shahbazzadeh, D., Habibi-Anbouhi, M., Hosseininejad Chafi, M., Sotoudeh, N., ... Behdani, M. (2018). Nanobodies as novel therapeutic agents in envenomation. *Biochimica Et Biophysica Acta (BBA) - General Subjects*, 1862(12), 2955–2965. <https://doi.org/10.1016/j.bbagen.2018.08.019>
- Bradford, M. M. (1976). A rapid and sensitive method for the quantitation of microgram quantities of protein utilizing the principle of protein-dye binding. *Analytical Biochemistry*, 72(1–2), 248–254. [https://doi.org/10.1016/0003-2697\(76\)90527-3](https://doi.org/10.1016/0003-2697(76)90527-3)
- Congdon, R. W., Muth, G. W., & Splittgerber, A. G. (1993). The binding interaction of Coomassie blue with proteins. *Analytical Biochemistry*, 213(2), 407–413. <https://doi.org/10.1006/abio.1993.1439>
- Cromey, D. W. (2010). Avoiding twisted pixels: Ethical guidelines for the appropriate use and manipulation of scientific digital images. *Science and Engineering Ethics*, 16(4), 639–667. <https://doi.org/10.1007/s11948-010-9201-y>
- Gassmann, M., Grenacher, B., Rohde, B., & Vogel, J. (2009). Quantifying Western blots: Pitfalls of densitometry. *Electrophoresis*, 30(11), 1845–1855. <https://doi.org/10.1002/elps.200800720>
- Gorr, T. A., & Vogel, J. (2015). Western blotting revisited: Critical appraisal of underappreciated technical issues. *Proteomics - Clinical Applications*, 9(3–4), 396–405. <https://doi.org/10.1002/prca.201400118>
- Graumann, K., & Premstaller, A. (2006). Manufacturing of recombinant therapeutic proteins in microbial systems. *Biotechnology Journal*, 1(2), 164–186. <https://doi.org/10.1002/biot.200500051>
- Gürtler, A., Kunz, N., Gomolka, M., Hornhardt, S., Friedl, A. A., McDonald, K., ... Posch, A. (2013). Stain-Free technology as a normalization tool in Western blot analysis. *Analytical Biochemistry*, 433(2), 105–111. <https://doi.org/10.1016/j.jab.2012.10.010>
- Hmila, I., Abdallah R, B.-B., Saerens, D., Benlasfar, Z., Conrath, K., Ayeb, M. E., ... Bouhaouala-Zahar, B. (2008). VHH, bivalent domains and chimeric Heavy chain-only antibodies with high neutralizing efficacy for scorpion toxin Aahl. *Molecular Immunology*, 45(14), 3847–3856. <https://doi.org/10.1016/j.molimm.2008.04.011>
- Hmila, I., Saerens, D., Ben Abderrazek, R., Vincke, C., Abidi, N., Benlasfar, Z., ... Muyldermans, S. (2010). A bispecific nanobody to provide full protection against lethal scorpion envenoming. *The FASEB Journal*, 24(9), 3479–3489. <https://doi.org/10.1096/fj.09-148213>

- Holzmueller, W., & Kulozik, U. (2016). Protein quantification by means of a stain-free SDS-PAGE technology without the need for analytical standards: Verification and validation of the method. *Journal of Food Composition and Analysis*, 48, 128–134. <https://doi.org/10.1016/j.jfca.2016.03.003>
- Kraiem, H. (2018). *Développement de méthodes de contrôle-qualité pour deux facteurs de croissance et un fragment d'anticorps : «Mise au point et optimisation de tests immuno-biochimiques et fonctionnelles in vivo et in vitro»*. PhD thesis (in French), Institut National de Sciences Appliquées et de Technologie and Université de Carthage.
- Laustsen, A., Solà, M., Jappe, E., Oscoz, S., Lauridsen, L., & Engmark, M. (2016). Biotechnological trends in spider and scorpion antivenom development. *Toxins*, 8(8), 226. <https://doi.org/10.3390/toxins8080226>
- Neu, H. C., & Heppel, L. A. (1965). The release of enzymes from *Escherichia coli* by osmotic shock and during the formation of spheroplasts. *The Journal of Biological Chemistry*, 240(9), 3685–3692.
- Pardon, E., Laeremans, T., Triest, S., Rasmussen, S. G. F., Wohlkönig, A., Ruf, A., ... Steyaert, J. (2014). A general protocol for the generation of nanobodies for structural biology. *Nature Protocols*, 9(3), 674–693. <https://doi.org/10.1038/nprot.2014.039>
- Rehbein, P., & Schwalbe, H. (2015). Integrated protocol for reliable and fast quantification and documentation of electrophoresis gels. *Protein Expression and Purification*, 110, 1–6. <https://doi.org/10.1016/j.pep.2014.12.006>
- Sternberg, S. R. (1983). Biomedical image processing. *Computer*, 16(1), 22–34. <https://doi.org/10.1109/MC.1983.1654163>
- Stoscheck, C. M. (1990). Quantitation of protein. *Methods in Enzymology*, 182(C), 50–68. [https://doi.org/10.1016/0076-6879\(90\)82008-P](https://doi.org/10.1016/0076-6879(90)82008-P)
- Sunya, S., Delvigne, F., Uribelarrea, J.-L., Molina-Jouve, C., & Gorret, N. (2012). Comparison of the transient responses of *Escherichia coli* to a glucose pulse of various intensities. *Applied Microbiology and Biotechnology*, 95(4), 1021–1034. <https://doi.org/10.1007/s00253-012-3938-y>
- Syrový, I., & Hodný, Z. (1991). Staining and quantification of proteins separated by polyacrylamide gel electrophoresis. *Journal of Chromatography B: Biomedical Sciences and Applications*, 569(1–2), 175–196. [https://doi.org/10.1016/0378-4347\(91\)80229-6](https://doi.org/10.1016/0378-4347(91)80229-6)
- Tal, M., Silberstein, A., & Nusser, E. (1985). Why does Coomassie Brilliant Blue R interact differently with different proteins? A partial answer. *The Journal of Biological Chemistry*, 260(18), 9976–9980.
- Vincent, S. G., Cunningham, P. R., Stephens, N. L., Halayko, A. J., & Fisher, J. T. (1997). Quantitative densitometry of proteins stained with coomassie blue using a Hewlett Packard Scanjet scanner and Scanplot software. *Electrophoresis*, 18(1), 67–71. <https://doi.org/10.1002/elps.1150180114>

How to cite this article: Alonso Villela SM, Kraiem H, Bouhaouala-Zahar B, Bideaux C, Aceves Lara CA, Fillaudeau L. A protocol for recombinant protein quantification by densitometry. *MicrobiologyOpen*. 2020;00:e1027. <https://doi.org/10.1002/mbo3.1027>

APPENDIX 3. KINETIC MODEL OF RECOMBINANT NANOBODIES

The kinetic model for the production of the recombinant nanobodies CH10-12 and NbF12-10 is presented in this section as the proposition of an article. The article titled “Effect of temperature on the production of a recombinant antivenom in fed-batch mode” will be submitted to Applied Microbiology and Biotechnology (Springer) in the fourth quarter of 2020.

Effect of temperature on the production of a recombinant antivenom in fed-batch mode

Susana María Alonso Villela¹ (ORCID0000-0001-8290-1635)

Hazar Kraiem² (ORCID 0000-0002-8180-0573)

Balkiss Bouhaouala-Zahar^{2,3} (ORCID 0000-0003-3147-245X)

Carine Bideaux¹ (ORCID 0000-0002-9830-5093)

César Arturo Aceves Lara¹

Luc Fillaudeau¹

¹ TBI, Université de Toulouse, CNRS, INRAE, INSA, Toulouse, France

² Laboratoire des Venins et Molécules Thérapeutiques, Institut Pasteur de Tunis, Université de Tunis El Manar, Tunisia

³ Faculté de Médecine de Tunis, Université de Tunis El Manar, Tunisia

Abstract

In the pharmaceutical industry, nanobodies show promising properties for its application in serotherapy targeting the highly diffusible scorpion toxins. The production of recombinant nanobodies in *Escherichia coli* has been widely studied in shake flask cultures in rich medium. However, there are no studies of nanobody production in defined minimal medium and the effect of the induction temperature on the production kinetics.

In this work, the effect of the temperature during the expression of the chimeric bispecific nanobody form CH10-12 was studied in bioreactor cultures of *E. coli*. High biomass concentrations (25 g cdw/L) were achieved in fed-batch mode and the expression of the nanobody CH10-12 was induced at temperatures 28, 29, 30, 33 and 37°C with a residual glucose constant feed. For the bispecific form NbF12-10, the induction was performed at 29°C.

Nanobody production in the strain CH10-12 was higher at 28°C and 30°C, reaching 4.6 mg of nanobody after 10 h and 12 h of induction. At 29°C, the strains CH10-12 and NbF12-10 produced only 1.68 and 0.64 mg of nanobody, respectively, after 13 h of induction. The specific productivity of the nanobodies was modeled as a function of the temperature and the specific growth rates. Experimental results confirm that low temperatures increase the productivity of the nanobody.

Keywords: nanobody, recombinant antivenom, induction temperature, fed-batch strategy, productivity kinetics, *Escherichia coli*

Key points

- Nanobodies with scorpion antivenom activity produced using two recombinant strains.
- Nanobodies production was achieved in fed-batch cultures at different induction temperatures.
- Low induction temperatures result in high volumetric productivities of the nanobody CH10-12.

Introduction

Scorpion stings are a serious public health problem in tropical and subtropical countries (Warrell et al. 2007). The most common treatment for scorpion stings is serotherapy. Serotherapy uses antibodies or fragments of antibodies to target the neurotoxins in the scorpion venom. Neurotoxins with low molecular weight, of about 7 kDa, promptly diffuse and block the Na⁺, K⁺ ionic channels in excitable cells.

Most of the scorpion antivenoms in the market consist of fragments F(ab)₂' of equine antibodies with a size of about 100 kDa. However, an insufficient potency of these antibodies as antidote has been reported. Alternatively, nanobodies (V_HH), fragments of camelid antibodies that enable better tissue penetration with a lower molecular weight (15 kDa), have been retrieved (Deffar et al. 2009; Bouhaouala-Zahar et al. 2011; Hmila et al. 2012). Nanobodies have the higher neutralization ability than conventional antibody fragments or full antibodies and have easy-folding mechanisms (Alirahimi et al. 2018). Defined as next-generation therapeutics, nanobodies are the best candidates to produce bispecific antibodies (Deffar et al. 2009; Bouhaouala-Zahar et al. 2011).

The production of fully matured scorpion antibodies can be possible by genetic engineering (Hmila et al. 2008; Abderrazek et al. 2009), to produce high quantities in a short period of time during high cell density cultures (> 25 g cdw/L) (Yee and Blanch 1992). Its production in microbial hosts is a tool frequently used in the pharmaceutical industry to increase antiserum production (Carmo et al. 2015).

Escherichia coli is the preferred host as microbial expression systems due to its high ability to be metabolically modified to obtain overproducer strains (Gupta and Shukla 2017). The *E. coli* strain is recognized by drug regulatory authorities for the production of recombinant proteins (Overton 2014). Its production in the periplasmic space allows the formation of the disulfide bonds in the protein and cytoplasmic proteins require renaturation process during the purification steps (Muyldermans 2013; De Meyer et al. 2014).

There are three main critical factors influencing the production of recombinant proteins in *E. coli* strains: 1) the temperature during the induction, coupled with the duration of the induction, especially for the strains harboring the T7 system controlled by the addition of an inducer to the culture medium (Donovan et al. 1996); 2) the concentration of the inducer (Dvorak et al. 2015); and 3) the availability of oxygen in the culture medium, which could have a negative impact on the stability of the recombinant plasmid (Tomazetto et al. 2007), however, aerobic cultures are shown to produce higher quantities of recombinant proteins when cultured in high cellular densities (Huang et al. 2012). In bioreactor, concentrations of oxygen higher than 40% ensure a high cell density culture while minimizing the production of organic acids, such as acetic acid which inhibits biomass growth (Yee and Blanch 1992).

Recombinant antibody fragments have been proven effective as neutralizing agents against different venoms from the scorpions *Androctonus australis Hector* (Devaux et al. 2001; Aubrey et al. 2003; Hmila et al. 2010), *Centruroides noxius* (Selisko et al. 2004), and *Hottentotta saulcyi* (Darvish et al. 2015), and expressed as single-chain variable fragment (scFv) or single-domain camelid antibody (V_HH). Notably, the bispecific nanobody NbF12-10 displayed high neutralizing abilities against the whole venom of the *Androctonus australis Hector* scorpion (Benabderrazek et al., 2009; Hmila et al.,

2010), even at the preclinical level (Hmila et al. 2012), and showed cross-reactivity when challenged with the *Androctonus mauretanicus* scorpion venom (Chgoury et al. 2015), proving promising properties as new therapeutic antivenom for treatment of the North African scorpion stings. Recently, the humanized and chimeric form of the NbF12-10, namely CH10-12 having human conserved framework regions (FRs), have been generated and characterized for reaching the biopharmaceutical requirements. The produced and purified CH10-12 chimeric nanobody displays high neutralizing capacity against lethal effect of the whole toxic fraction of the scorpion venom (unpublished data).

The production of all the scorpion antibodies investigated as today is in shake-flask scale cultured in rich medium with low biomass concentrations (Devaux et al. 2001; Aubrey et al. 2003; Selisko et al. 2004; Darvish et al. 2015). The couple of temperature and duration of the induction are not studied, and only two main conditions have been used: 28°C – 16 h and 37°C – 4 h. The expression on the periplasm of the cell seems to be the best way to produce antibodies or nanobodies and accomplish active biomolecules (Hmila et al. 2008; Abderrazek et al. 2009). The production of neutralizing-venom antibodies has not been studied at bioreactor scale and further research is needed to increase the production yields in the host *Escherichia coli*.

The maximum reported titer is low (< 4 mg/L) (Hmila et al. 2010), biomass production is not reported, and the production in high cell density cultures has not been studied. Production conditions (induction temperature and duration) are still a trial-and-error issue and nanobody production kinetics has not been addressed. The productivity of recombinant proteins is usually modeled as Monod or Luedeking-Piret kinetics (Zheng et al. 2005; Ariff et al. 2015), and rarely modeled as a function of the temperature in an Arrhenius-type kinetic (Amillastre et al. 2012).

In this work, the effect of temperature in the production of the recombinant bispecific nanobody CH10-12 in *E. coli* WK6 was studied in bioreactor scale. The production strategy allowed the production of biomass in fed-batch mode and the expression of nanobody under a residual glucose feed at induction temperatures of 28, 29, 30, 33, and 37°C. The production conditions were applied to the production of the nanobody NbF12-10 and the reference strain WK6. The production rate of the nanobodies CH10-12 and NbF12-10 was modeled as an Arrhenius-type kinetics and its parameters were estimated.

Materials and methods

Bacterial strain

The recombinant strains used were *Escherichia coli* K12/WK6 { Δ (lac-pro), galE, strA, nal; F' lacIq Z Δ M15, pro+} with pHEN6 (derived from pBR322) coding for bispecific antibody fragments V_HHF12-V_HH10 (called NbF12-10) (Hmila et al. 2010) and its chimeric bispecific form VHH10-VHHF12 (called CH10-12) (Kraïem 2018), both engineered from the dromedary VHH library rescued clones. The *Escherichia coli* K12/WK6 wild strain was used as reference for the growth kinetics analysis and comparison to recombinant strains. Stock cultures of each strain were stored in 30% glycerol at -80°C.

The nanobodies CH10-12 and NbF12-10 produced in the periplasmic space as the soluble format were hexa-histidine tagged proteins (His₆-tag). The expression was induced under the *lac* promoter and the strain is ampicillin resistant.

Culture media

The starting culture was prepared by streaking a LB agar plate (yeast extract, 5 g/L; tryptone, 10 g/L; NaCl, 10 g/L; ampicillin, 100 µg/mL; agar, 15 g/L) with a drop of thawed glycerol stock culture and incubated overnight at 37°C. Then, one single colony of the LB agar plate was inoculated in 15 mL of

LB medium (yeast extract, 5 g/L; tryptone, 10 g/L; NaCl, 10 g/L) supplemented with, 100 µg/mL of ampicillin in a 100 mL baffled shake-flask, and cultured overnight at 37°C at 120 rpm.

A defined minimal medium (MM) was used for the inoculum and the batch mode culture. The MM consisted in citric acid, 6 g/L; (NH₄)₂HPO₄, 8 g/L; K₂HPO₄, 8 g/L; Na₂HPO₄·12H₂O, 5.046 g/L; NH₄Cl, 0.13 g/L; (NH₄)₂SO₄, 0.75 g/L. The culture medium was supplemented with 1 mL per liter of medium of each trace element solution 1000-fold concentrated (MnSO₄·H₂O, 20 g/L; Na₂MoO₄·2H₂O, 4 g/L; CoCl₂·6H₂O, 8 g/L; CuCl₂·2H₂O, 2 g/L; ZnSO₄·7H₂O, 4 g/L; H₃BO₃, 1 g/L; MgSO₄·7H₂O, 500 g/L; CaCl₂·2H₂O, 40 g/L; FeSO₄·7H₂O (pH 2), 40 g/L, thiamine, 10 g/L) (Sunya et al. 2012). The pH was adjusted to 6.8 with 28% ammonium solution before autoclaving at 121°C for 20 min. Ampicillin was added at a final concentration of 100 µg/mL, and glucose at a final concentration of 5 g/L and 10 g/L for the inoculum and the batch mode, respectively.

The inoculum of the bioreactor was prepared by adding a 1 mL of the LB pre-culture to 100 mL of MM in a 1 L baffled shake-flask and cultured overnight at 37°C at 120 rpm.

The feed solution used during the fed-batch mode consisted in: glucose, 300 g/L; H₃PO₄ (85%), 0.96 mL/L, K₂HPO₄, 3.2 g/L; Na₂HPO₄·12H₂O, 0.39 g/L; MgSO₄·7H₂O, 2 g/L; CaCl₂·2H₂O, 0.16 g/L; FeSO₄·7H₂O, 0.16 g/L; ZnSO₄·7H₂O, 0.03 g/L. The already defined trace elements solution 1000-fold concentrated were added at the following ratios: MnSO₄·H₂O, 0.45 mL/L; Na₂MoO₄·2H₂O, 0.24 mL/L; CoCl₂·6H₂O, 0.19 mL/L; CuCl₂·2H₂O, 1.37 mL/L; H₃BO₃, 0.98 mL/L; thiamine, 3.42 mL/L. Thiamine was added to the feed solution before fed-batch mode was started.

All chemicals and reagents had the highest analytical grade available and were obtained from Sigma-Aldrich (USA).

Culture conditions and experimental strategy

Cultures were conducted in a Biostat® B-DCU (Sartorius) of 5 L of working volume (Figure 3-1). The bioreactor is fully instrumented with sensors of dissolved oxygen, pH, temperature, and pressure, and equipped with two six-flat-blade Rushton turbines and a three-blade marine impeller. The control and monitoring of these parameters were made by the BioPAT® MFCS (Sartorius) acquisition system.

Temperature was set at 37°C for the batch and fed-batch modes. Temperature and duration after induction were set to 28°C-12h, 29°C-13h, 30°C-10h, 33°C-6h, and 37°C-4h. The pH was maintained at 6.8 by the addition of a solution of 14% w/v ammonia. Antifoam (100% polypropylene glycol P2000) was supplemented as needed. The expression of soluble periplasmic nanobodies was induced with IPTG (isopropyl β-D-1-thiogalactopyranoside), added to the bioreactor in a pulse of 1 mM when biomass reached approximately 25 g cdw/L. To maintain strict aerobic conditions, agitation and air flow were adjusted to increase the transfer of oxygen in the bioreactor when the dissolved oxygen was close to 15%. Four conditions of agitation and air flow were chosen: 500 rpm – 1 NL/min for batch mode; 1000 rpm – 2 NL/min, and 1500 rpm – 3 NL/min for fed-batch mode; 1500 rpm – 1 NL/min for induction phase. Each condition allows a time window of 2 to 4 h of culture in which the dissolved oxygen is kept over 15%.

The glucose feeding was controlled using the acquisition system (BIOPAT® MFCS/win 2.1, Sartorius) with a previously calibrated peristaltic pump (102R, 5-50 rpm, Watson Marlow). At depletion of the initial 10 g/L of glucose of the batch phase, an exponential glucose feed was started equivalent to a specific growth rate (μ) of 0.38 h⁻¹. During the induction phase, a constant feed was set, equivalent to 4 g/h of glucose. Inlet and outlet gas were analyzed with a gas analyzer (INNOVA 1313, Lumasense Technologies) for carbon dioxide and oxygen by photoacoustic spectroscopy and magneto acoustic spectroscopy, respectively.

Biomass quantification

The spectroscopic absorbance of the cell culture was measured with a spectrophotometer (Biochrom Libra S4) at a wavelength of 600 nm using High precision cells (2 mm optic path cell, Hellma Analytics). Cell culture was diluted with a Microlab 500 (Hamilton) diluter to keep the absorbance under 0.5 AU. The catalytic biomass was evaluated through measurements of cell dry weight by gravimetric method with pre-weighted filters (0.2 μm , polyamide, Sartolon, Sartorius) and micro centrifuge tubes (1.5 mL, Eppendorf). A 5 to 10 mL of cell culture was filtered on the pre-weighted filters. A 1.4 mL of cell culture was put in the pre-weighted micro centrifuge tube and spun down at 12 000 g for 5 min; the cell residue was washed thrice with distilled water. Both, filters, and micro centrifuge tubes, were put to dry in an oven at 60°C and 266 mbar for 4 days. Difference of weight of the filter and micro centrifuge tube was used for the calculation of cell dry weight.

Glucose and organic acids

The residual glucose and organic acids concentrations in the supernatant were quantified by a high-performance liquid chromatography coupled with a photodiode array (UV) and a refractive index (RI) detector (Waters Alliance 2690 HPLC, Waters 996 PDA detector, Waters 2414 RI detector). The retention of glucose and organic acids was made using a column Aminex HPX-87H (Biorad). The mobile phase of the HPLC was a filtered solution of 5 mM H_2SO_4 in deionized water (18.2 M Ω) and using 0.22 μm filter (Sartorius). The temperature of the column was set to 50°C. The PDA was set at 210 nm and the RI used the mobile phase as reference. Each analysis took 10 μL of sample and was run for 30 min at a rate of 0.5 mL/min. Residual glucose was detected in a range from 0.5 to 50 g/L \pm 0.01 g/L in the RI detector, and organic acids were detected from 0.1 to 10 g/L \pm 0.01 g/L in the RI detector and the UV detector. Additionally, the residual glucose in the cell culture was measured with an enzymatic analyzer (YSI Model 2700, Yellow Springs Instruments Life Sciences), and detected within a range of 0.1 to 2.5 g/L \pm 0.05 g/L.

Nanobody extraction, purification, and quantification

The periplasmic nanobodies were extracted by osmotic shock (Neu and Heppel 1965) and loaded on a His-Select column (IMAC). After washing with PBS, the His-tagged nanobodies were eluted with 250 mM imidazole (pH 7.4) (Hmila et al. 2010; Pardon et al. 2014). The purity of the eluted nanobody was checked by denaturing SDS-PAGE, according to Biorad specifications. Nanobody quantification was made by absorbance at 280 nm (Nanodrop, Thermo-Fischer) and densitometry on SDS-PAGE gels (Alonso Vilella et al. 2020).

Kinetic model and parameter estimation

The kinetics of the specific production rate of the nanobody were established mathematically to study the effect of the temperature. A modified Luedeking-Piret kinetics described the specific production rate of the nanobody, dependent on the specific growth rate and a decoupling factor as a function of the temperature in an Arrhenius-like kinetics as follows:

$$q_{Nb} = -\alpha * \mu_{ind} + \beta \quad (1)$$

Where:

$$\beta = \gamma_1 * e^{-Ea_1/T} - \gamma_2 * e^{-Ea_2/T} + \sigma \quad (2)$$

With q_{Nb} as the specific productivity rate of the nanobody (mg Nb/(g cdw*h)), μ_{ind} as the specific growth rate at induction (h^{-1}), α as the growth associated parameter (mg Nb/g cdw) and β as the non-growth associated parameter (mg Nb/(g cdw*h)), β as function of the temperature with γ_1 and γ_2 as the pre-exponential constants (mg Nb/(g cdw*h)), Ea_1 and Ea_2 as the activation and inactivation energy for the nanobody production ($^{\circ}\text{C}$), respectively, and σ as the non-temperature associated parameter (mg Nb/(g cdw*h)).

All parameters were estimated using the function *fmincon* of MATLAB® software (MATLAB® R2019, MathWorks) and the model was validated with the experimental data of the strain CH10-12 at 30°C. The objective function used to minimize the sum of the least squares (Donoso-Bravo et al. 2011) was defined as follows:

$$J(\varphi) = 10 * \min \sum_{i=1}^N \left(\frac{(y_{exp} - y_{model})}{\max(y_{exp})} \right)^2 \quad (3)$$

Results

The bioreactor cultures were performed to study different conditions of the expression of the nanobodies CH10-12 and NbF12-10 expression: duration of the induction and induction temperature. Firstly, the yields of biomass, acetic acid, carbon dioxide, and nanobody were determined through mass and energy balances. Secondly, the effect of the induction temperature during the protein expression was studied. The strain CH10-12 was cultured at 37°C, and then induced in a range from 28°C to 37°C with different induction duration and a specific feeding strategy to maintain a residual growth. Finally, the production rate of the nanobody was modeled as a modified Arrhenius kinetics.

Culture overview

Culture evolution

Six cultures were carried out at different induction temperatures (Table 3-1) to investigate the effects of induction temperature on nanobodies production. All the cultures consisted of three phases: a batch phase used to identify the maximum specific growth rate, followed by a fed-batch phase used to obtain high cell densities, continued by an induction phase to produce the nanobodies.

The evolution of one representative culture (CH₃₃) is shown in Figure 3-2. All cultures followed the same layout as the culture CH₃₃. During the batch mode, dissolved oxygen concentration was kept over 15%. Acetate was produced at a maximum of 1.2 g, and in average 7 g cdw of biomass was produced from 14.5 g of glucose. During the fed-batch mode, an exponential feed equivalent to a specific growth rate (μ) of 0.38 h⁻¹ was successfully applied without accumulation of glucose. The acetate was consumed during the first hours of the fed-batch mode, and dissolved oxygen was kept over 15%. About 50 g cdw of biomass were produced at the end of the fed-batch mode. The induction phase lasted between 6 h and 13 h, depending on the culture. The dissolved oxygen was always kept over 55% during the induction phase, without accumulation of glucose nor acetate production. For all cultures, the glucose feed was assured by a constant feed equivalent to 4 g/h of glucose, except for the culture CH₃₀. The culture CH₃₀ had problems with the pump feeding, which led to two starvation zones between 1 to 2 h and 3.5 to 5 h after the start of the induction, where glucose was not fed, and the dissolved oxygen increased to 100%. Once the feed was restarted at a rate of 5 g/h, dissolved oxygen decreased to a value about 65%. Citric acid concentration remained constant during all the cultures, and other organic acids (lactate, succinate, pyruvate) were not found on the supernatant, in either operating mode.

For each culture sample, substrate or metabolite masses produced or consumed were calculated considering the variation of volume in the bioreactor. Production and consumption rates were calculated using polynomial regression. The mass carbon and degree of reduction (redox) balances were calculated in the final points from the raw data of the cultures. The carbon and the redox balances at the final points were 95 ± 6% and 92 ± 6%, respectively for all cultures.

Specific growth rates and yields

The correlation coefficient between biomass cell dry weight and optical density was determined along all the culture modes and it was equivalent to 1.94 ± 0.04 g cdw/AU. All cultures showed high repeatability using the strategies defined for the oxygen transfer and glucose feed. The maximum specific growth rates were determined for batch mode and the average specific growth rates were determined in fed-batch mode and the induction phase.

The average maximum specific growth rate was 0.79 ± 0.08 h⁻¹ for all strains and cultures under the optimal controlled conditions: 37°C, pH 6.8, >15% dissolved oxygen. During the fed-batch mode the average specific growth rate was 0.40 ± 0.03 h⁻¹ for all cultures, which was consistent with the specific growth rate of 0.38 h⁻¹ imposed by the feed of glucose. During the induction phase of the cultures, the specific growth rate decreased from 0.040 ± 0.017 h⁻¹ to 0.021 ± 0.005 h⁻¹ due to the constant substrate flow rate (Table 3-1).

The evolution of the yield of biomass on glucose reflects the carbon utilization during the cultures. These yields were calculated for each operating condition as the slope on the representation of biomass produced versus consumed glucose. The yield, $Y_{X/S}$, was around 0.44 ± 0.05 g/g and 0.48 ± 0.07 g/g, for batch mode and fed-batch mode, respectively (Table 3-1).

The production of acetic acid is made naturally in the batch phase, where glucose is in excess in the medium (Yee and Blanch 1993). The yield of acetic acid on biomass ($Y_{Ac/X}$) during the batch mode was about 0.22 ± 0.07 g/g cdw in average for all cultures.

The average yield of carbon dioxide on glucose, $Y_{CO_2/S}$, was calculated for each operating condition. It was in average 0.51 ± 0.04 g CO₂/g Glc for the batch and fed-batch mode for all cultures. During the induction phase, the yield increases and was in average 0.97 ± 0.18 g CO₂/g Glc.

Maintenance coefficient

The maintenance of a microorganism includes several complex phenomena, physiological and non-growth associated, and can be defined as the consumption of apparently non-finalized substrate (Goma et al. 1979; van Bodegom 2007). The maintenance coefficient can be obtained using the Pirt equation (Pirt 1965), as defined by:

$$\frac{1}{Y_{X/S}} = \frac{m}{\mu} + \frac{1}{Y_{X/S}^{Growth}} \quad (19)$$

With $Y_{X/S}$ the apparent yield of biomass on glucose in g cdw /g Glc, m the maintenance coefficient in g Glc/g cdw/h, μ the specific growth rate in h⁻¹, and $Y_{X/S}^{Growth}$ the theoretical limit yield of biomass on glucose in g Glc/g cdw.

The maintenance coefficient was 0.0149 ± 0.0064 g Glc/g cdw/h for strain CH10-12 as average of the four cultures, and 0.0254 ± 0.0048 and 0.0408 ± 0.0068 g Glc/g cdw/h for strains NbF12-10, and WK6, respectively.

Nanobody production and temperature effect

The production of the nanobody CH10-12 was studied in cultures of *Escherichia coli* CH10-12 induced at different temperatures for up to 13 h. The production of the nanobody NbF12-10 was tested in a culture of *Escherichia coli* NbF12-10 induced at 29°C for 13 h. As a negative control, *Escherichia coli* WK6 was induced at 29°C for 9 h. The nanobodies CH10-12 and NbF12-10 were checked in the periplasmic space of the microorganism and not quantifiable in the supernatant (data not shown).

The production of the protein increased over time achieving the maximum production at the end of the culture (Figure 3-3a). The nanobody CH10-12 reached a final production of 4.6 mg Nb in cultures

CH₂₈ and CH₃₀ after 12 h and 10 h of induction, respectively. In cultures CH₃₃ and CH₃₇, the production was 0.78 and 0.44 mg of nanobody (Nb), respectively.

For the cultures induced at 29°C, the culture CH₂₉ reached a final production of 1.68 mg Nb after 13 h of induction (Figure 3-3b). The culture NbF12-10₂₉ reached a final production of 0.7 mg Nb. In the case of the culture of WK₂₉, no nanobody was found after the purification of periplasmic extract, as expected for the negative control.

In all cultures, after 10 h of induction, the culture CH₃₀ obtained the highest production of nanobody CH10-12 (4.6 mg Nb), which is about two-fold the quantity achieved in culture CH₂₈ (2.48 mg Nb), about four-fold the quantity achieved in culture CH₂₉ (1.18 mg Nb) and over seven-fold the quantity obtained for the nanobody NbF12-10 in culture NbF12-10₂₉ (0.64 mg Nb).

Discussion

Specific growth rates and yields

The maximum specific growth rate during the batch phase and the average specific growth rate during the fed-batch mode were 0.8 h⁻¹ and 0.4 h⁻¹, respectively, for all strains at pH 6.8 and 37°C.

The yield of biomass on glucose ($Y_{X/S}$) during batch mode of 0.44 g/g was within the range of the values found in other recombinant strains of *Escherichia coli*. Between 0.38 g/g to 0.47 g/g are routinely obtained in defined minimal medium in batch mode (Yee and Blanch 1993; Calleja et al. 2016). The yield of acetic acid on biomass was also consistent with the values reported in the literature of 0.3 g/g (Carvalho et al. 2012). During the fed-batch mode, the yield of biomass was 0.48 g/g and similar to values of 0.42 g/g to 0.51 g/g found in the literature for fed-batch cultures (Hua et al. 2006; Sunya 2012). Notably, the recombinant strain of *E. coli* DPD2085 grown in a continuous culture with our same defined minimal medium (MM) showed a yield of 0.42 g/g (Sunya 2012). During the induction phase, the yield of biomass on glucose, $Y_{X/S}$, was slightly lower than in batch and fed-batch modes and varied from 0.22 to 0.53 g/g depending on the culture operating conditions. The inhibition of the biomass growth by the production of the nanobodies during the induction phase needs further investigation.

Maintenance coefficient

The maintenance coefficient values obtained for the three *E. coli* strains were consistent with those found in the literature for the *E. coli* strains BL21, RV304, and K12 of 0.024 (Levisauskas et al. 2003), 0.03 (Cockshott and Bogle 1999), and 0.06 g Glc/g cdw/h, respectively (Çalik et al. 2004).

A hypothesis of thermo-dependency of the maintenance coefficient was checked at the low specific growth rates for cultures of *Escherichia coli* CH10-12, but no relationship between maintenance coefficient and temperature was found (data not shown).

During the nanobody production, it is expected to see a shift on the metabolism, which would cause the glucose to be converted to either the recombinant nanobody or carbon dioxide. During this phase, glucose was mostly utilized in the energy of maintenance instead than to produce biomass, this is defined as metabolic burden (Overton 2014).

The induction of the vector with IPTG starts the protein production machinery in the microorganism, increasing the metabolic needs to replicate the vector and, inevitably, reduce the biomass production (Huang et al. 2012). The induction phase caused an increase of ATP requirement and therefore in the yield of carbon dioxide ($Y_{CO_2/S}$).

For the reference strain, *E. coli* WK6, the addition of the IPTG to the culture medium could have induced a metabolic stress. Some studies have shown that the induction of non-recombinant strains with IPTG results in a variety of stress responses in the cell (production of heat-shock-like proteins and proteases, degradation of metabolic pathways) (Kosinski et al. 1992; Donovan et al. 1996). The

metabolic burden can be identified by the switch of the flux of glucose from the production of biomass to the production of energy of maintenance and other metabolites.

Nanobody production and temperature effect

In this study, the bispecific nanobodies CH10-12 and NbF12-10 were expressed in defined minimal medium (MM) during high cell density cultures (40 g cdw/L) of *E. coli*. The induction of the nanobody CH10-12 was made at ca 50 g cdw of biomass and temperature was adjusted from 28°C to 37°C and checked in the periplasmic compartment.

Nanobody production

The cultures CH₃₃ and CH₃₇ induced at higher temperatures produced the lowest quantities of nanobody almost at the same rate, and equivalent to half of the production in cultures CH₂₈ and CH₃₀ induced at lower temperatures with the same duration of the induction of 6 h (0.78 mg Nb and 0.44 mg Nb for CH₃₃ and CH₃₇ against 1 mg Nb for CH₂₈ and CH₃₀, Figure 3-3a). The induction temperature, lower than the optimal temperature of *E. coli* (37°C), is a useful tool to regulate the gene expression of potentially toxic recombinant proteins. Low induction temperatures increase the solubility of the recombinant proteins and reduce the formation of inclusion bodies due to the slower rate of protein synthesis (Jhamb and Sahoo 2012). Low temperatures can also reduce the stress of the cell, by reducing the rate of protein aggregation and hydrophobic interactions between the polypeptides produced. Correctly folded proteins can be then obtained by lowering the induction temperature, which involves the reduction of the cellular growth and allows a slower accumulation of the recombinant protein.

The accumulation of the nanobody CH10-12 in the periplasmic space seems to be a little toxic to the recombinant bacterial strain. This toxicity could be responsible for the decrease on the specific growth rate during the induction phase, and not only due to the regulation of the induction temperature or the glucose feed during the production phase (Shin et al. 1997; Salema et al. 2013).

Lower induction temperatures produced the higher quantities of nanobody CH10-12. Through empirical observation, the induction temperature of 29°C was chosen as a temperature in-between the induction temperatures of cultures CH₂₈ and CH₃₀. The culture CH₂₉ produced the nanobody in an almost linear manner, and in lower quantity than the cultures CH₂₈ and CH₃₀ (Figure 3-3b). The production of the nanobody NbF12-10 seems to reach a plateau after 8 h of induction and remain almost constant at about 0.6 mg Nb.

It could be assumed that the protein expression machinery in the strain is slightly divergent at different temperatures. This could correspond to the metabolic adaptation of the *E. coli* strain as a function of the strength of the induction and would indicate that the induction duration is not optimized for the nanobody production, despite the activation of the *lac* promoter with IPTG.

According to our findings, the temperature plays a key role in the production of the nanobody, with the highest production attained at the lowest temperatures during the induction phase. Lower induction temperatures (28°C and 30°C) attained the highest amounts of nanobody CH10-12 (4.6 mg Nb), and its production decreased along with the increase of induction temperature to 33°C and 37°C (0.78 and 0.44 mg Nb).

Comparison with the literature

The titers of the nanobodies CH10-12 and NbF12-10 produced in the cultures were compared with the literature (Figure 3-4). The reported literature titers of recombinant antibodies with neutralizing activity against scorpion neurotoxins vary from 0.5 to 3.75 mg/L of culture; the expression of the proteins was made over a long period of time (16 – 25 h) and, mostly, at low temperatures (16 – 28°C).

In our cultures of *E. coli* CH10-12 a final titer of 2.3 mg/L culture was reached for the cultures CH₂₈ and CH₃₀, achieved after 10 h and 12 h of induction, and comparable to those published in the literature (Table 3-2). The production of recombinant nanobodies produced in the periplasmic space of *E. coli* strains has mostly been reported in shake-flask scale and rich medium (Terrific Broth, TB (Tartof and Hobbs 1987)) and quantified only at the end of the culture. Information about the production of the biomass is not available for the cultures made in shake-flask scale and the specific yields and rates could not be calculated.

In the case of the cultures of *E. coli* CH10-12, the positive effect of the temperature on the metabolic burden is shown by the increase of productivity at lower temperatures. In terms of the volumetric productivity, the culture CH₃₀ had the highest productivity among most of the values of the literature, 0.23 mg/L/h and only surpassed by the works of Kraïem (Kraïem 2018; Kraïem et al. 2019) and Hmila et al. (Hmila et al. 2010) that obtained 0.234 mg/L/h and 0.368 mg/L/h, respectively.

The conditions of the culture during recombinant protein expression, mainly temperature, are the most studied in the literature (Yee and Blanch 1992; Donovan et al. 1996; Rosano and Ceccarelli 2014). The metabolic burden can be reduced by inducing the protein expression at low temperatures (25°C – 30°C), where protein solubility is higher (Rosano and Ceccarelli 2014). Low induction temperatures also allow the correct formation of disulfide bridges in the oxidative environment of the periplasm (Blight et al. 1994; Mergulhão et al. 2005).

The concentration of the inducer in the culture during the induction phase also increases the metabolic burden due to the overexpression of recombinant proteins (Donovan et al. 1996). The IPTG, used for the expression of the *lac* promoter, can be used from 0.005 mM to 5 mM, with 1 mM being the most common (Donovan et al. 1996).

As a method to reduce the metabolic burden in recombinant strains, several authors have reported the use of an inducer concentration lower than 1 mM IPTG in fed-batch bioreactor cultures (Donovan et al. 1996; Andersson et al. 1996; Ruiz et al. 2009; Ruiz et al. 2011; Calleja et al. 2016; Schmideder et al. 2016; Dela Coletta Troiano Araújo et al. 2019). The optimal concentration of IPTG is highly dependent on the microbial system (Donovan et al. 1996). For *Escherichia coli* BL21 (DE3) strains, several authors have found that the concentration of inducer for maximal protein expression was 100 µM IPTG (Calleja et al. 2016; Schmideder et al. 2016; Dela Coletta Troiano Araújo et al. 2019). For *Escherichia coli* M15, derived from the K12 strain, a concentration as low as 10 µM IPTG was used for complete induction of the *lac* promoter in fed-batch cultures (Ruiz et al. 2009).

Recently, the specific concentration of IPTG (mmol/g cdw) has been used as a factor to determine maximal protein expression in fed-batch cultures in defined minimal medium (Ruiz et al. 2009; Ruiz et al. 2011; Calleja Martínez 2014; Calleja et al. 2016). Specific inducer concentrations as low as 1 µmol IPTG/g cdw have been used to fully induce recombinant *E. coli* strains, ranging from 0.4 to 6 mmol IPTG/g cdw (Ruiz et al. 2009; Ruiz et al. 2011).

The concentration of IPTG used in our experiments was the same of those used in shake-flask cultures, estimated at 125 µmol IPTG/ g cdw (Hmila et al. 2010; Pardon et al. 2014). In our cultures of *E. coli* CH10-12, *E. coli* NbF12-10 and *E. coli* WK6, the IPTG/biomass ratio was between 45 µmol IPTG/g cdw at the start of the induction phase and 30 µmol IPTG/g cdw at the end of protein expression. This was, at least, 10-fold higher than the ratio used for other recombinant *E. coli* strains cultured in bioreactors (Ruiz et al. 2009; Ruiz et al. 2011; Calleja et al. 2016). The ratio of inducer to plasmid-bearing cells could be another parameter to indicate the strength of the protein expression (Miao and Kompala 1993).

Another method to reduce the metabolic burden is to use lactose as an inducer (Donovan et al. 1996; Andersson et al. 1996; Ramchuran et al. 2005). In addition to be used as an inducer, the lactose will provide a different carbon source to the medium and reduce the stress caused by the IPTG. However, the genetic background of the strain must be studied before making any changes to

ensure that lactose is correctly metabolized to allolactose and the lac promoter is fully activated (Donovan et al. 1996).

In terms of the activity of the nanobodies CH10-12 and NbF12-10, further research is needed to investigate their neutralizing activity by different injection routes *in vivo/in vitro* analyses.

Temperature effect in specific productivity of the nanobody production

The parameters of the specific production rate of the nanobody kinetics for the equations (1) and (2) are shown in equations (5) and (6). The estimated parameters were evaluated in their respective equations, compared with the experimental data of the strain *E. coli* CH10-12 (Figure 3-5).

$$q_{Nb} = -3.35 * \mu_{ind} + \beta \quad (5)$$

$$\beta = 0.57 * e^{-\frac{34.55}{T}} - 2.52 * e^{-\frac{30.67}{T}} + 0.76 \quad (6)$$

Figure 3-5 shows the effect of the temperature on the metabolic burden, where the specific production rate of the nanobody increases at low temperatures. Furthermore, it is shown that the highest nanobody productivity was obtained when the specific growth rates of induction were small.

The models found in the literature use the growth-dependent Luedeking-Piret equation to estimate the production of proteins (Aucoin et al. 2006; Hua et al. 2006; Ariff et al. 2015). The protein concentration is often included in the kinetic model, and accounts as a growth-inhibiting parameter due to the toxicity of the protein produced (Bettenbaugh and Dhurjati 1990; Palaomyliou et al. 2002; Levisauskas et al. 2003; Jenzsch et al. 2006; Nadri et al. 2006). The effect of the temperature on the production rate of recombinant proteins has not been modeled, highlighting the originality of the kinetic model presented in this study.

The kinetic parameters were estimated for the specific production rate of the nanobody, which showed that the higher periplasmic production of the nanobody was made at low induction temperatures. The production of the nanobodies could be tested at a temperature lower than 28°C or at lower specific growth rates to validate the model.

Author's contributions

Conceptualization: SMAV, BBZ, LF, CAAL. Formal analysis: SMAV, HK, BBZ, CB, CAAL, LF. Investigation: SMAV. Software: SMAV, CAAL. Supervision: LF, CAAL. Writing – original draft preparation: SMAV. Writing – editing review: SMAV, HK, BBZ, CB, CAAL, LF.

Declarations

Availability of data and material

All data generated or analyzed during this study are included in this published article.

Conflicts of interest

The authors declare that they have no conflict of interest.

Ethical approval

This article does not contain any studies with human participants or animals performed by any of the authors.

Funding

Susana María Alonso Villela is grateful to the National Council of Science and Technology (CONACYT, Mexico) for the doctoral scholarship No. 461347.

References

- Abderrazek R Ben, Hmila I, Vincke C, Benlasfar Z, Pellis M, Dabbek H, Saerens D, El Ayeb M, Muyltermans S, Bouhaouala-Zahar B (2009) Identification of potent nanobodies to neutralize the most poisonous polypeptide from scorpion venom. *Biochem J* 424:263–272
- Alirahimi E, Kazemi-Lomedasht F, Shahbazzadeh D, Habibi-Anbouhi M, Hosseininejad Chafi M, Sotoudeh N, Ghaderi H, Muyltermans S, Behdani M (2018) Nanobodies as novel therapeutic agents in envenomation. *Biochim Biophys Acta - Gen Subj* 1862:2955–2965
- Alonso Villela SM, Kraïem H, Bouhaouala-Zahar B, Bideaux C, Aceves Lara CA, Fillaudeau L (2020) A protocol for recombinant protein quantification by densitometry. *Microbiologyopen* 9:1175–1182
- Amillastre E, Aceves-Lara C-A, Uribelarrea J-L, Alfenore S, Guillouet SE (2012) Dynamic model of temperature impact on cell viability and major product formation during fed-batch and continuous ethanolic fermentation in *Saccharomyces cerevisiae*. *Bioresour Technol* 117:242–250
- Andersson L, Yang S, Neubauer P, Enfors SO (1996) Impact of plasmid presence and induction on cellular responses in fed batch cultures of *Escherichia coli*. *J Biotechnol* 46:255–263
- Ariff A Bin, Nelofer R, Rahman RNZRA, Basri M (2015) Kinetics and modelling of batch fermentation for the production of organic solvent tolerant and thermostable lipase by recombinant *E. coli*. *Turkish J Biochem* 40:298–309
- Aubrey N, Devaux C, Sizaret PY, Rochat H, Goyffon M, Billiald P (2003) Design and evaluation of a diabody to improve protection against a potent scorpion neurotoxin. *Cell Mol Life Sci* 60:617–628
- Aucoin MG, McMurray-Beaulieu V, Poulin F, Boivin EB, Chen J, Ardelean FM, Cloutier M, Choi YJ, Miguez CB, Jolicoeur M (2006) Identifying conditions for inducible protein production in *E. coli*: combining a fed-batch and multiple induction approach. *Microb Cell Fact* 5:27
- Betenbaugh MJ, Dhurjati P (1990) A comparison of mathematical model predictions to experimental measurements for growth and recombinant protein production in induced cultures of *Escherichia coli*. *Biotechnol Bioeng* 36:124–134
- Blight MA, Chervaux C, Holland IB (1994) Protein secretion pathway in *Escherichia coli*. *Curr Opin Biotechnol* 5:468–474
- Bouhaouala-Zahar B, Ben Abderrazek R, Hmila I, Abidi N, Muyltermans S, El Ayeb M (2011) Immunological aspects of scorpion toxins: current status and perspectives. *Inflamm Allergy Drug Targets* 10:358–368
- Çalik P, Yilgör P, Ayhan P, Demir AS (2004) Oxygen transfer effects on recombinant benzaldehyde lyase production. *Chem Eng Sci* 59:5075–5083
- Calleja D, Kavanagh J, de Mas C, López-Santín J (2016) Simulation and prediction of protein production in fed-batch *E. coli* cultures: An engineering approach. *Biotechnol Bioeng* 113:772–782
- Calleja Martínez D (2014) Modeling bioreactors for the production of recombinant proteins in high-cell density cultures of *Escherichia coli*. Dissertation, Universitat Autònoma de Barcelona
- Carmo AO, Chatzaki M, Horta CCR, Magalhães BF, Oliveira-Mendes BBR, Chávez-Olórtegui C, Kalapothakis E (2015) Evolution of alternative methodologies of scorpion antivenoms production. *Toxicon* 97:64–74
- Carvalho RJ, Cabrera-Crespo J, Tanizaki MM, Gonçalves VM (2012) Development of production and purification processes of recombinant fragment of pneumococcal surface protein A in *Escherichia coli* using different carbon sources and chromatography sequences. *Appl Microbiol Biotechnol* 94:683–694
- Chgoury F, Benabderrazek R, Tounsi H, Oukkache N, Hmila I, Boubaker S, Ayeb M, Saïle R, Ghalim N, Bouhaouala-Zahar B (2015) Effectiveness of the *Androctonus australis Hector* nanobody Nbf12-10 antivenom to neutralize significantly the toxic effect and tissue damage provoked by fraction

- of *Androctonus mauretanicus* (Morocco) scorpion venom. *Biochem Pharmacol Open Access* 04:4–11
- Cockshott A, Bogle I (1999) Modelling the effects of glucose feeding on a recombinant *E. coli* fermentation. *Bioprocess Eng* 20:83–90
- Darvish M, Behdani M, Shokrgozar MA, Pooshang-Bagheri K, Shahbazzadeh D (2015) Development of protective agent against *Hottentotta saulcyi* venom using camelid single-domain antibody. *Mol Immunol* 68:412–420
- De Meyer T, Muyldermans S, Depicker A (2014) Nanobody-based products as research and diagnostic tools. *Trends Biotechnol* 32:263–270
- Deffar K, Shi H, Li L, Wang X, Zhu X (2009) Nanobodies - the new concept in antibody engineering. *African J Biotechnol* 8:2645–2652
- Dela Coletta Troiano Araújo L, Wibrantz M, Rodríguez-Fernández DE, Karp SG, Talevi AC, Maltempo de Souza E, Soccol CR, Thomaz-Soccol V (2019) Process parameters optimization to produce the recombinant protein CFP10 for the diagnosis of tuberculosis. *Protein Expr Purif* 154:118–125
- Devaux C, Moreau E, Goyffon M, Rochat H, Billiald P (2001) Construction and functional evaluation of a single-chain antibody fragment that neutralizes toxin Aahl from the venom of the scorpion *Androctonus australis hector*. *Eur J Biochem* 268:694–702
- Donoso-Bravo A, Mailier J, Martin C, Rodríguez J, Aceves-Lara CA, Wouwer A Vande (2011) Model selection, identification and validation in anaerobic digestion: A review. *Water Res* 45:5347–5364
- Donovan RS, Robinson CW, Glick BR (1996) Review: Optimizing inducer and culture conditions for expression of foreign proteins under the control of the lac promoter. *J Ind Microbiol* 16:145–154
- Dvorak P, Chrast L, Nikel PI, Fedr R, Soucek K, Sedlackova M, Chaloupkova R, Lorenzo V, Prokop Z, Damborsky J (2015) Exacerbation of substrate toxicity by IPTG in *Escherichia coli* BL21(DE3) carrying a synthetic metabolic pathway. *Microb Cell Fact* 14:1–15
- Goma G, Moletta R, Novak M (1979) Comments on the “Maintenance coefficient” changes during alcohol fermentation. *Biotechnol Lett* 1:415–420
- Gupta SK, Shukla P (2017) Microbial platform technology for recombinant antibody fragment production: A review. *Crit Rev Microbiol* 43:31–42
- Hmila I, Abdallah R BA-B, Saerens D, Benlasfar Z, Conrath K, Ayeb M El, Muyldermans S, Bouhaouala-Zahar B (2008) VHH, bivalent domains and chimeric heavy chain-only antibodies with high neutralizing efficacy for scorpion toxin Aahl'. *Mol Immunol* 45:3847–3856
- Hmila I, Cosyns B, Tounsi H, Roosens B, Cavelliers V, Abderrazek R Ben, Boubaker S, Muyldermans S, El Ayeb M, Bouhaouala-Zahar B, Lahoutte T (2012) Pre-clinical studies of toxin-specific nanobodies: evidence of in vivo efficacy to prevent fatal disturbances provoked by scorpion envenoming. *Toxicol Appl Pharmacol* 264:222–231
- Hmila I, Saerens D, Ben Abderrazek R, Vincke C, Abidi N, Benlasfar Z, Govaert J, El Ayeb M, Bouhaouala-Zahar B, Muyldermans S (2010) A bispecific nanobody to provide full protection against lethal scorpion envenoming. *FASEB J* 24:3479–3489
- Hua X, Fan D, Luo Y, Zhang X, Shi H, Mi Y, Ma X, Shang L, Zhao G (2006) Kinetics of high cell density fed-batch culture of recombinant *Escherichia coli* producing human-like collagen. *Chinese J Chem Eng* 14:242–247
- Huang C-J, Lin H, Yang X (2012) Industrial production of recombinant therapeutics in *Escherichia coli* and its recent advancements. *J Ind Microbiol Biotechnol* 39:383–399
- Jenzsch M, Simutis R, Luebbert A (2006) Generic model control of the specific growth rate in recombinant *Escherichia coli* cultivations. *J Biotechnol* 122:483–493
- Jhamb K, Sahoo DK (2012) Production of soluble recombinant proteins in *Escherichia coli*: effects of process conditions and chaperone co-expression on cell growth and production of xylanase. *Bioresour Technol* 123:135–143

- Kosinski M, Rinas U, Bailey J (1992) Isopropyl-beta-d-thiogalactopyranoside influences the metabolism of *Escherichia coli*. *Appl Microbiol Biotechnol* 36:844–850
- Kraïem H (2018) Développement de méthodes de contrôle-qualité pour deux facteurs de croissance et un fragment d'anticorps : «Mise au point et optimisation de tests immuno-biochimiques et fonctionnelles in vivo et in vitro». Dissertation, Institut Pasteur de Tunis, Unimed Laboratories, Institut National de Sciences Appliquées et de Technologie
- Kraïem H, Manon Y, Hmila I, Ben Abderrazek R, Alonso Villela SM, Luc F, Bouhaouala-Zahar B (2019) Expression of the recombinant NbF12-10 and its chimeric antibody format in *Escherichia coli*: investigation of fed-batch bioprocess on minimal media. In: Second Mediterranean Congress on Biotechnology. Hammamet, Tunisia
- Levisauskas D, Galvanauskas V, Henrich S, Wilhelm K, Volk N, Lübbert A (2003) Model-based optimization of viral capsid protein production in fed-batch culture of recombinant *Escherichia coli*. *Bioprocess Biosyst Eng* 25:255–262
- Mergulhão FJM, Summers DK, Monteiro GA (2005) Recombinant protein secretion in *Escherichia coli*. *Biotechnol Adv* 23:177–202
- Miao F, Kompala DS (1993) Overexpression of cloned genes using recombinant *Escherichia coli* regulated by a t7 promoter .2. 2-Stage continuous cultures and model simulations. *Biotechnol Bioeng* 42 (1):74–80
- Muyldermans S (2013) Nanobodies: Natural Single-Domain Antibodies. *Annu Rev Biochem* 82:775–797
- Nadri M, Trezzani I, Hammouri H, Dhurjati P, Longin R, Lieto J (2006) Modeling and observer design for recombinant *Escherichia coli* strain. *Bioprocess Biosyst Eng* 28:217–225
- Neu HC, Heppel LA (1965) The release of enzymes from *Escherichia coli* by osmotic shock and during the formation of spheroplasts. *J Biol Chem* 240:3685–3692
- Overton TW (2014) Recombinant protein production in bacterial hosts. *Drug Discov Today* 19:590–601
- Palaomylytou MA, Matis KA, Zouboulis AI, Kyriakidis DA (2002) A kinetic model describing cell growth and production of highly active, recombinant ice nucleation protein in *Escherichia coli*. *Biotechnol Bioeng* 78:321–332
- Pardon E, Laeremans T, Triest S, Rasmussen SGF, Wohlkönig A, Ruf A, Muyldermans S, Hol WGJ, Kobilka BK, Steyaert J (2014) A general protocol for the generation of Nanobodies for structural biology. *Nat Protoc* 9:674–693
- Pirt SJ (1965) The maintenance energy of bacteria in growing cultures. *Proceedings Biol Sci* 163:224–231
- Ramchuran SO, Holst O, Karlsson EN (2005) Effect of postinduction nutrient feed composition and use of lactose as inducer during production of thermostable xylanase in *Escherichia coli* glucose-limited fed-batch cultivations. *J Biosci Bioeng* 99:477–484
- Rosano GL, Ceccarelli EA (2014) Recombinant protein expression in *Escherichia coli*: Advances and challenges. *Front Microbiol* 5:1–17
- Ruiz J, González G, de Mas C, López-Santín J (2011) A semiempirical model to control the production of a recombinant aldolase in high cell density cultures of *Escherichia coli*. *Biochem Eng J* 55:82–91
- Ruiz J, Pinsach J, Álvaro G, González G, de Mas C, Resina D, López-Santín J (2009) Alternative production process strategies in *E. coli* improving protein quality and downstream yields. *Process Biochem* 44:1039–1045
- Salema V, Marín E, Martínez-Arteaga R, Ruano-Gallego D, Fraile S, Margolles Y, Teira X, Gutierrez C, Bodelón G, Fernández LÁ (2013) Selection of single domain antibodies from immune libraries displayed on the surface of *E. coli* cells with two β -domains of opposite topologies. *PLoS One* 8:1–18

- Schmideder A, Cremer JH, Weuster-Botz D (2016) Parallel steady state studies on a milliliter scale accelerate fed-batch bioprocess design for recombinant protein production with *Escherichia coli*. *Biotechnol Prog* 32:1426–1435
- Selisko B, Cosío G, García C, Becerril B, Possani LD, Horjales E (2004) Bacterial expression, purification and functional characterization of a recombinant chimeric Fab derived from murine mAb BCF2 that neutralizes the venom of the scorpion *Centruroides noxius hoffmann*. *Toxicon* 43:43–51
- Shin CS, Hong MS, Bae CS, Lee J (1997) Enhanced production of human mini-proinsulin in fed-batch cultures at high cell density of *Escherichia coli* BL21(DE3)[pET-3aT2M2]. *Biotechnol Prog* 13:249–257
- Sunya S (2012) Dynamique de la réponse physiologique d'*Escherichia coli* à des perturbations maîtrisées de son environnement : vers le développement de nouveaux outils de changement d'échelle. Dissertation, INSA Toulouse
- Sunya S, Delvigne F, Uribe Larrea J-L, Molina-Jouve C, Gorret N (2012) Comparison of the transient responses of *Escherichia coli* to a glucose pulse of various intensities. *Appl Microbiol Biotechnol* 95:1021–1034
- Tartof KD, Hobbs CA (1987) Improved media for growing plasmid and cosmid Clones. *Bethesda Res Lab Focus* 9:
- Tomazetto G, Mulinari F, Stanisçuaski F, Settembrini B, Carlini CR, Ayub MAZ (2007) Expression kinetics and plasmid stability of recombinant *E. coli* encoding urease-derived peptide with bioinsecticide activity. *Enzyme Microb Technol* 41:821–827
- van Bodegom P (2007) Microbial maintenance: A critical review on its quantification. *Microb Ecol* 53:513–523
- Warrell D, Gutierrez J-M, Padilla A (2007) Rabies and envenomings: a neglected public health issue: report of a Consultative Meeting. Geneva, Switzerland
- Yee L, Blanch HW (1993) Recombinant trypsin production in high cell density fed-batch cultures in *Escherichia coli*. *Biotechnol Bioeng* 41:781–790
- Yee L, Blanch HW (1992) Recombinant protein expression in high cell density fed-batch cultures of *Escherichia coli*. *Biotechnology (N Y)* 10:1550–1556
- Zheng ZY, Yao SJ, Lin DQ (2005) Using a kinetic model that considers cell segregation to optimize hEGF expression in fed-batch cultures of recombinant *Escherichia coli*. *Bioprocess Biosyst Eng* 27:143–152

Figures

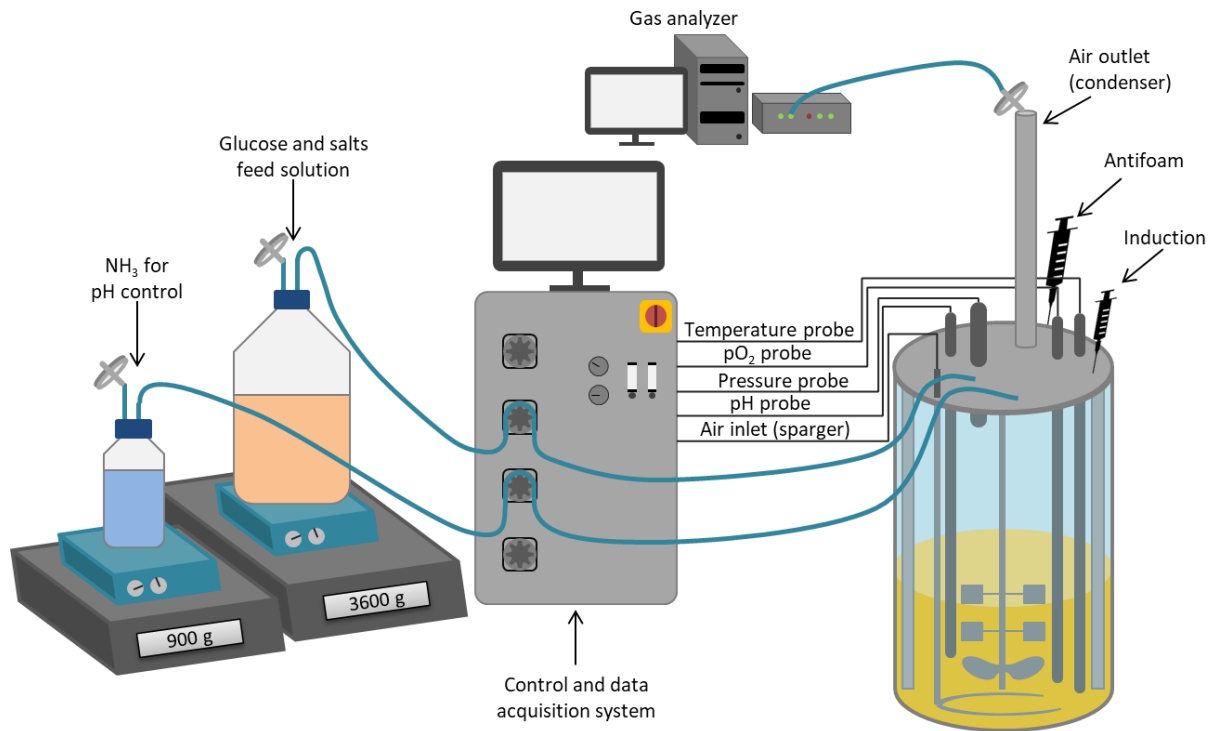


Figure 3-1. Schematic of the experimental set-up used in fed-batch cultures in 5 L bioreactor.

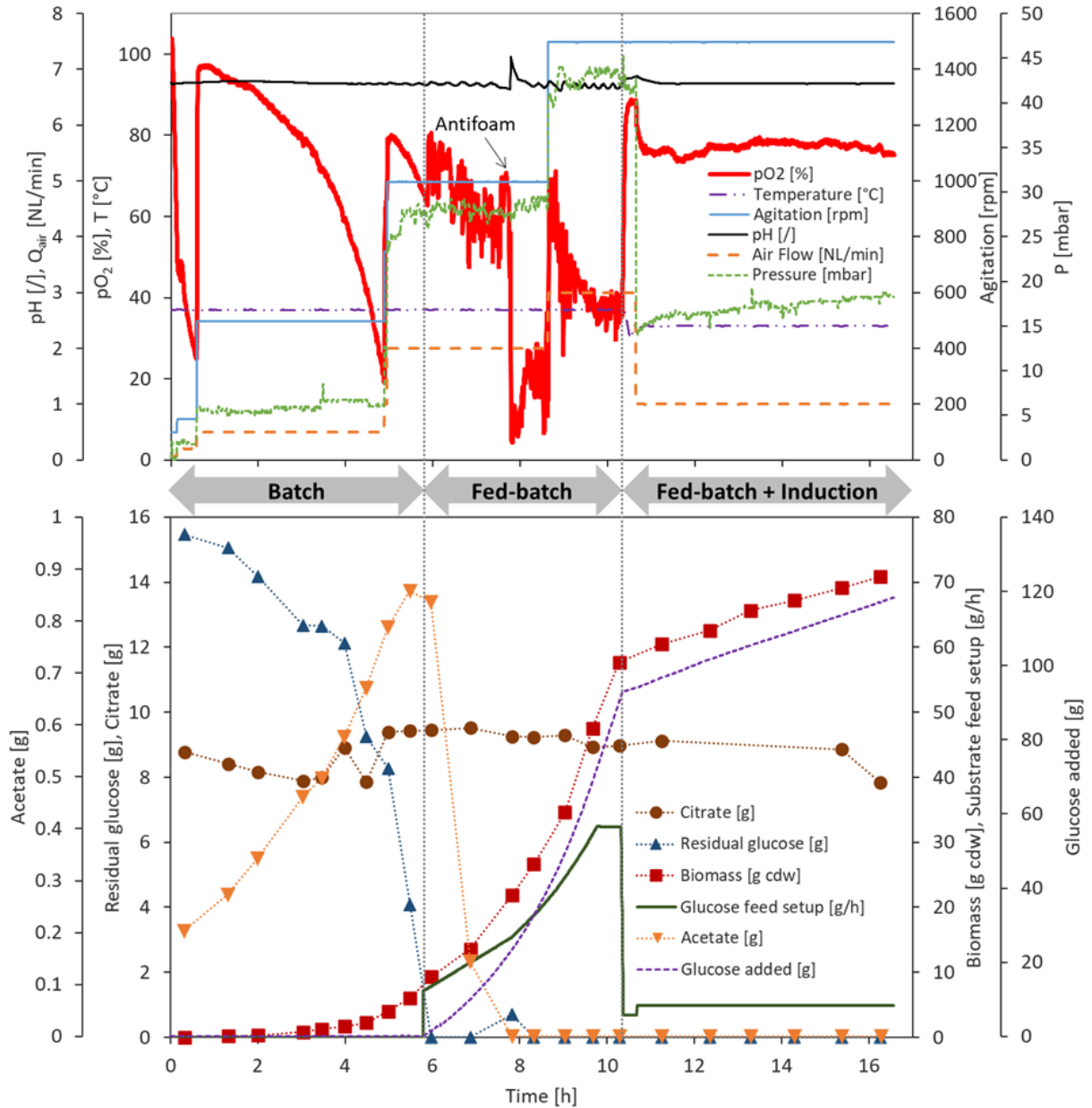


Figure 3-2. Physico-chemical parameters, operating conditions, and biological parameters of the culture of *Escherichia coli* CH10-12 grown in MM, pH 6.8, 37°C, induced at 33°C for 6 h. The dotted lines depict the change in the operating mode.

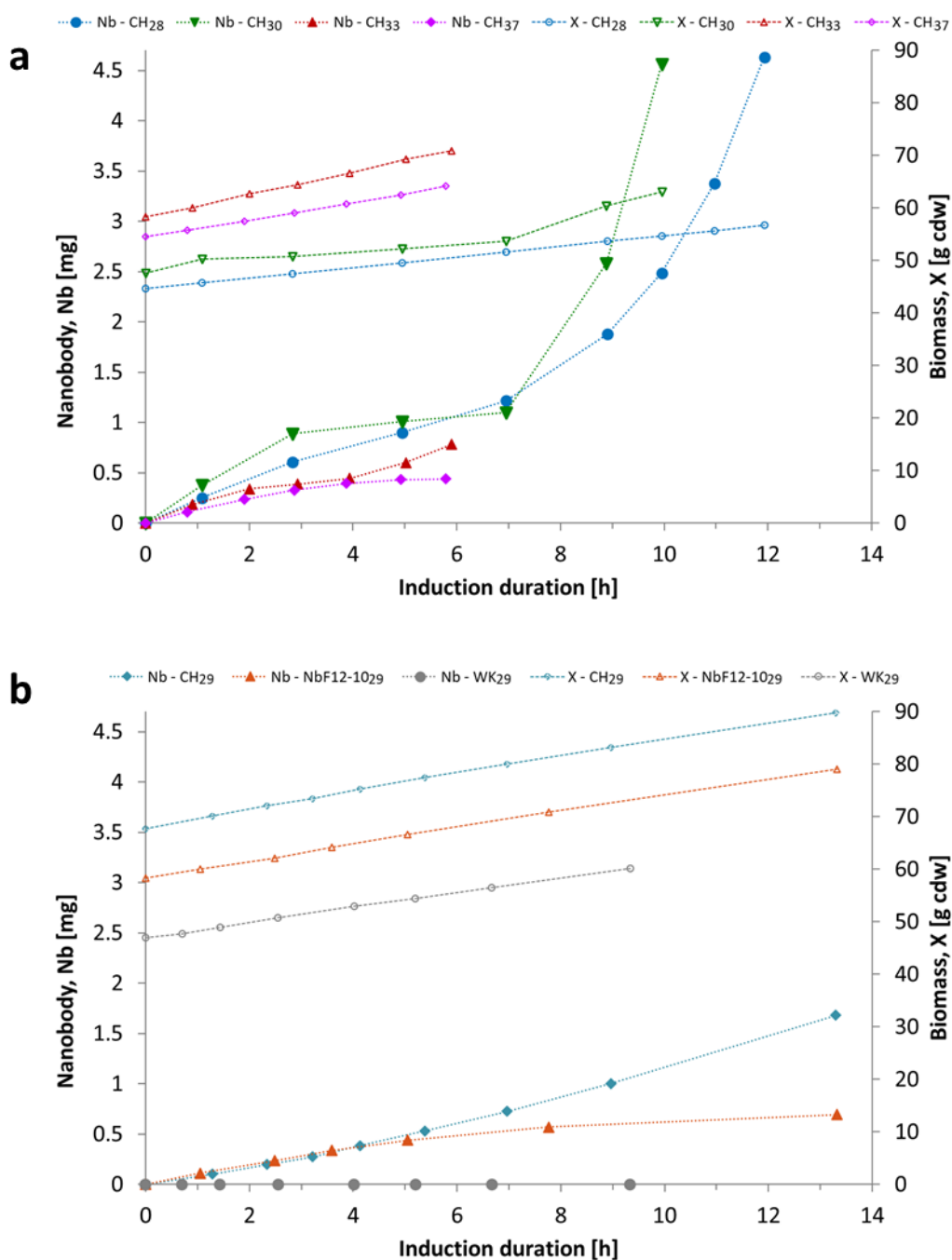


Figure 3-3. Evaluation of the temperature and duration of the induction during the production of biomass and recombinant nanobodies. (a) Production of biomass and recombinant nanobody CH10-12 at an induction temperature of 28°C, 30°C, 33°C and 37°C. (b) Production of biomass and recombinant nanobodies CH10-12 and NbF12-10, and the reference strain *E. coli* WK6 at an induction temperature of 29°C. All cultures were grown at 37°C with glucose as carbon source in defined minimal medium and induced at different temperatures.

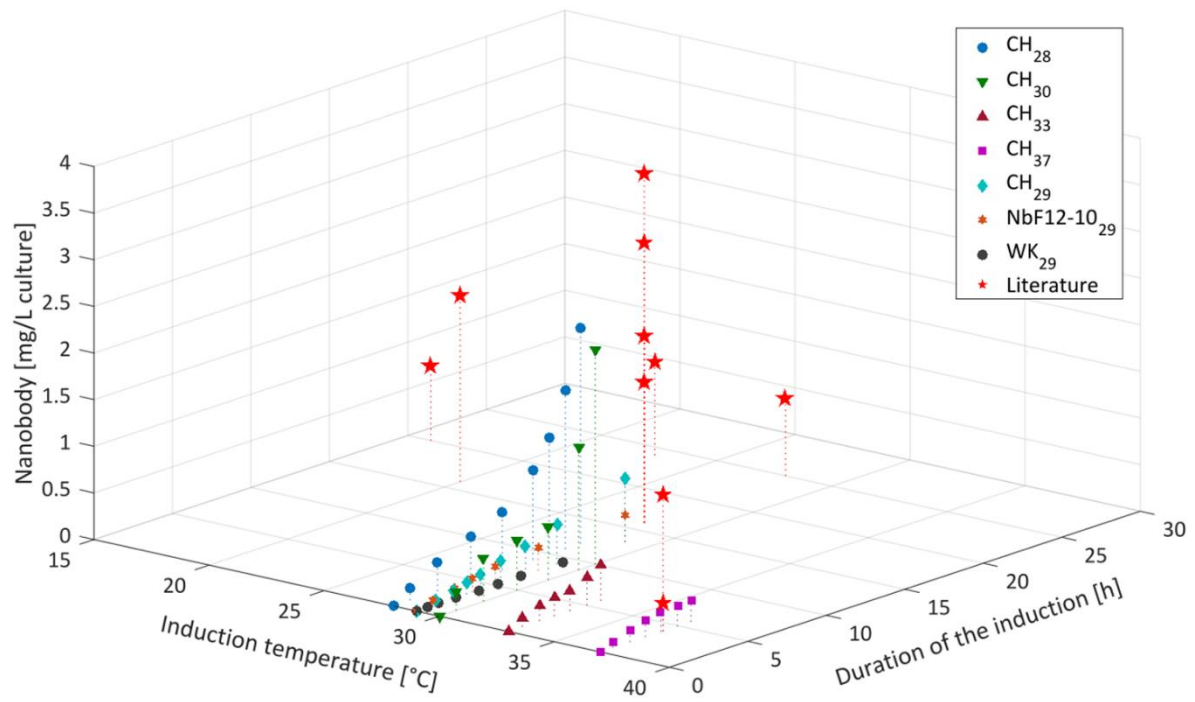


Figure 3-4. Comparison of the recombinant nanobodies CH10-12 and NbF12-10 in bioreactor cultures and the literature.

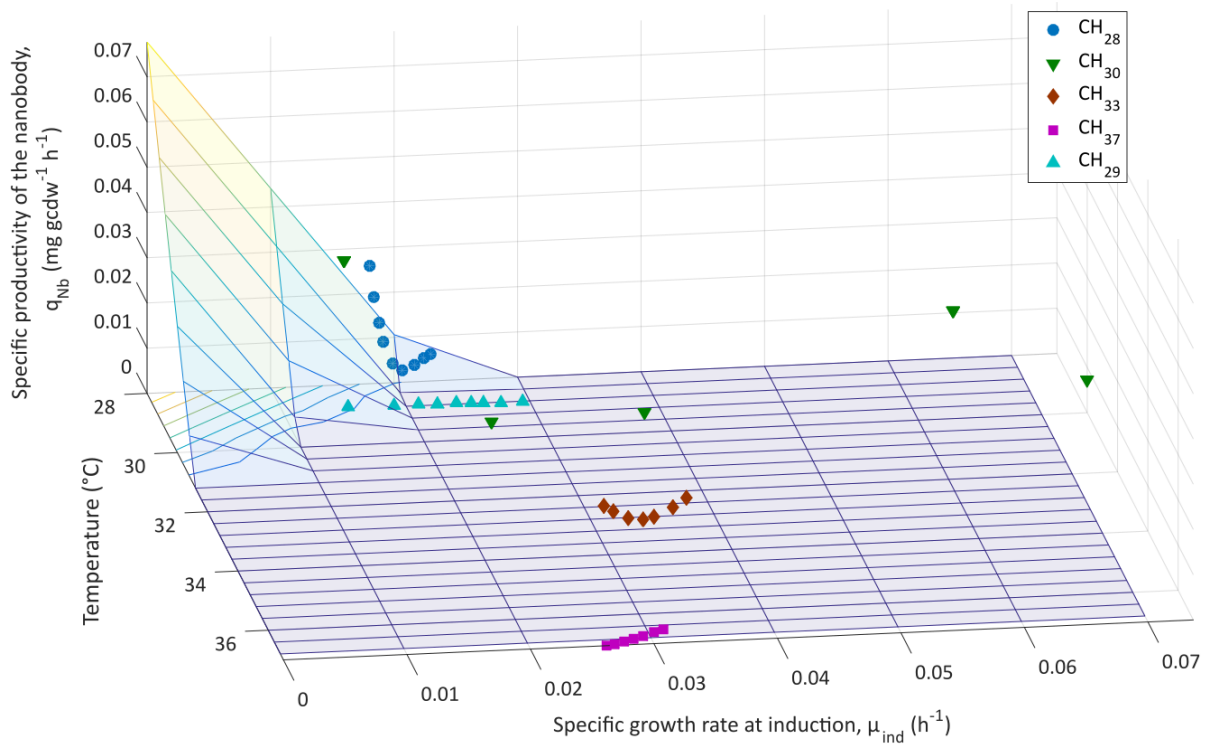


Figure 3-5. Simulation of the kinetics for specific production rate of the nanobody using a growth- and temperature-dependent Luedeking-Piret kinetic model.

Tables

Table 3-1. Average specific growth rates (μ) and average biomass yield on glucose ($Y_{X/S}$) on each culture.

ID culture	<i>E. coli</i> strain	Batch mode		Fed-batch mode		Induction			
		μ_{\max} [h ⁻¹]	$Y_{X/S}$ [g/g]	μ_{fix} [h ⁻¹]	$Y_{X/S}$ [g/g]	μ_{ind} max→min [h ⁻¹]	$Y_{X/S}$ [g/g]	T [°C]	Induction duration [h]
CH ₂₈	CH10-12	0.70	0.45	0.38	0.44	0.023 → 0.018	0.29	28	12
CH ₃₀	CH10-12	0.67	0.47	0.40	0.52	0.074 → 0.014	0.44	30	10
CH ₃₃	CH10-12	0.85	0.40	0.43	0.52	0.048 → 0.031	0.53	33	6
CH ₃₇	CH10-12	0.85	0.42	0.45	0.58	0.031 → 0.026	0.42	37	6
CH ₂₉	CH10-12	0.85	0.39	0.44	0.47	0.029 → 0.015	0.29	29	13
NbF12-10 ₂₉	NbF12-10	0.87	0.39	0.39	0.44	0.029 → 0.018	0.26	29	13
WK ₂₉	WK6	0.81	0.44	0.35	0.37	0.033 → 0.022	0.22	29	9

Table 3-2. Yield and productivity of antivenom antibodies. $\bar{\mu}_{ind}$: average specific growth rate at induction, MM: defined minimal medium, 2xYT: yeast extract and tryptone medium, TB: terrific broth, N. A.: not available.

<i>E. coli</i> strain	Antibody	Culture media	Concentration, mg/L	Volumetric productivity, mg/L/h	Duration [h] – T [°C]	$\bar{\mu}_{ind}$ [h ⁻¹]	Reference
CH10-12	31 kDa CH10-12	MM	2.32	0.193	12 h –28°C	0.019	This work
CH10-12	31 kDa CH10-12	MM	0.69	0.052	13 h – 29°C	0.023	This work
CH10-12	31 kDa CH10-12	MM	2.3	0.230	10 h – 30°C	0.023	This work
CH10-12	31 kDa CH10-12	MM	0.39	0.065	6 h –33°C	0.033	This work
CH10-12	31 kDa CH10-12	MM	0.23	0.038	6 h –37°C	0.028	This work
CH10-12	31 kDa CH10-12	MM	0.83	0.033	25 h – 28°C	0.05	[164], [165]
CH10-12	31 kDa CH10-12	MM	1.47	0.368	4 h – 37°C	0.12	[164], [165]
HB2151	50 kDa scFv-scFv	2xYT	0.8	0.040	20 h – 16°C	N. A.	[123]
HB2151	29 kDa scFv 9C2	2xYT	2	0.125	16 h – 20°C	N. A.	[124]
NbF12-10	29 kDa NbF12-10	MM	0.28	0.021	13 h – 29°C	0.024	This work
NbF12-10	29 kDa NbF12-10	MM	0.3	0.075	4 h – 37°C	0.2	[164], [165]
NbF12-10	29 kDa NbF12-10	TB	3.75	0.234	16 h – 28°C	N. A.	[4]
TOPP2	48 kDa chFab- BCF2	2xYT	1	0.042	24 h – 23°C	N. A.	[101]
WK6	78.5 kDa V _H H22-Fc HCAb	TB	1.5	0.094	16 h – 28°C	N. A.	[163]
WK6	29 kDa bivalent NbAahI'2 2	TB	2	0.125	16 h – 28°C	N. A.	(Hmila et al., 2008)
WK6	14 kDa Nb12	TB	2	0.125	16 h – 28°C	N. A.	[121]
WK6	14 kDa NbAahI'2 2	TB	3	0.188	16 h – 28°C	N. A.	[163]

Electronic supplementary material**ESM 1. SDS-PAGE analyses of the nanobodies after purification by IMAC**